Mechanistic insights in the autonomic modulation of ventricular arrhythmia



Dr Manish Kalla

Thesis submitted for the degree of Doctor of Philosophy

Department of Physiology, Anatomy and Genetics
Cardiovascular Medicine

Merton College

Michaelmas Term 2015

Dedicated to my grandfathers, Professor Govind Ram Purohit and Mr Sheo Dutt Kalla, who have always inspired me

Mechanistic insights in the autonomic modulation of ventricular arrhythmia

Abstract

Cardiovascular disease is the leading cause of mortality in the developed world with up to fifty percent of cases being due to sudden cardiac death. Changes in sympatho-vagal balance underpin many cardiovascular conditions including heart failure and myocardial infarction. Neuraxial modulation of the autonomic nervous system is an emerging therapy to prevent ventricular arrhythmias, the main cause of sudden cardiac death.

Chapter One reviews our current understanding of how the cardiac autonomic nervous system influences ventricular arrhythmogenesis. A particular focus was on the controversial role of cholinergic receptors and nitric oxide (NO) in parasympathetic protection from ventricular arrhythmias. Tetrahydrobiopterin (BH_4), a critical cofactor for both tyrosine hydroxylase and NO synthases, and the co-transmitter neuropeptide-Y (NPY) may also influence sympathetic triggering of ventricular arrhythmias. This leads to the specific aims of the thesis which were to determine the mechanisms of the cholinergic antifibrillatory effect, investigate the role of cotransmission in arrhythmogenesis and, the mechanistic role of BH4 in autonomic cardiovascular control.

Chapter Two detailed the experimental approach taken to investigate the hypotheses. A novel Langendorff heart preparation was developed with intact autonomic nerves to investigate how the stable analogue of acetylcholine, carbamylcholine (CCh) raises ventricular fibrillation threshold (VFT) and whether exogenous or endogenously released NPY lowers VFT. These actions are further investigated using optical mapping, dye free imaging of ventricular cell monolayers, immunohistochemistry, ELISA assays and measurements of NO metabolite production. To investigate the role of BH4 in the sympathetic control of the heart, an IRES-cre recombinase strategy was used to produce genomic deletion of *GCH1* (the gene encoding BH4) in sympathetic neurons. Biopterins and plasma catecholamines were measured using HPLC, and blood pressure and heart rate via tail cuff plethysmography.

Chapter 3 showed that CCh increased VFT, prolonged action potential duration and flattened the electrical restitution curve. This effect required stimulation of both muscarinic and nicotinic receptors and the generation of nNOS derived NO utilising a cGMP dependent pathway. These observations are in keeping with established evidence demonstrating the obligatory role of the muscarinic receptor and indicate that the role of NO is likely to be via modulation of cholinergic neurotransmission.

Chapter 4 studied the role of the sympathetic co-transmitter NPY. NPY has been shown to increase ventricular myocyte calcium dynamics. Plasma levels are also increased post myocardial infarction and during heart failure, and correlate with outcomes. Perfusion of NPY decreased VFT via a Y_1 receptor dependent mechanism and increased arrhythmic activity in myocyte monolayers. Direct sympathetic stimulation resulted in NPY release and remained pro-arrhythmic despite β-blockade, an effect that could be abolished by combined β-Y_1 receptor blockade. These observations indicated that NPY may be a novel, pro-arrhythmic trigger amenable to therapeutic pharmacological modulation.

Chapter 5 details the generation and phenotyping of two tissue specific *Gch1* knockout mouse models. Whilst one model failed to produce significant lowering of BH_4 in sympatho-adrenal tissue, the other did result in a marked neuro-motor phenotype. A biochemical rescue or alternative genomic modification approach would be required to study the cardiovascular phenotype of sympathetic *Gch1* deletion in more detail.

Chapter 6 is a concluding discussion summarising the main findings of the thesis, placing them in a clinical context and discussing avenues for further research.

Acknowledgements

First and foremost I would like to thank Professor David Paterson and Professor Keith Channon for their inspiring and supportive supervision. They have shown me the dedication and motivation needed to succeed in research and set the standards that I will aspire to throughout my career. A special thank you to Professor Neil Herring who has been a phenomenal mentor, teacher and, more importantly a friend.

I have had the opportunity to be part of two talented research teams who have taken the time to teach me how to be a scientist and offer guidance and support. I am immensely grateful to Dr Gil Bub, Dr Gillian Douglas, Dr Brent Ryan, Dr Guoliang Hao, Dr Rebecca Burton, Dr Dan Li, Dr Julia Shanks, Dr Mark Crabtree, Dr Jyoti Patel and Dr Eileen McNeill. A special mention must be made of Mr Ashley Hale, who has helped immensely and took the time to teach me all the techniques required.

A big thank you to fellow students Jay Lu, Hege Larsen, Goudarz Karimi, Lampson Fan, Surawee Chuiphichai, Emma Bardsley and Kun Liu for their friendship through the highs and lows of science. I wish them the best in their careers.

I am very grateful to the BHF Centre for Research Excellence for giving me the opportunity to be part of this inspirational research centre and to Merton College and the Department of Physiology, Anatomy & Genetics for supporting me generously with funding to present my work at meetings.

Lastly I must thank my family for supporting me through this endeavour. My parents have given me the foundations to achieve my goals. My parents in law, Kunal and Nisha have been immensely supportive and have always encouraged me to keep working hard. My biggest thanks are to the three girls in my life, my daughters Anaiya and Aarya and, my wife and best friend, Sunaina. They have provided humour and support at the perfect moments and I have a lot of time to make up to them. This thesis is as much their achievement as it is mine.

Publications associated with this thesis

Kalla M, Herring N, Paterson DJ. *Cardiac sympatho-vagal balance and ventricular arrhythmia.* Autonomic Neuroscience (2016) S1566 (epub ahead of print)

Kalla M, Chotalia M, Coughlan C, Hao G, Tomek J, Crabtree M, Bub G, Paterson DJ, Herring N (2016). *Protection against ventricular fibrillation via cholinergic receptor stimulation and the generation of nitric oxide*. The Journal of Physiology (2016) **14**: 3981-91

Abstracts and Presentations

Kalla M, Bub G, Burton R, Larsen H, Paterson DJ and Herring N (2015). *The sympathetic co-transmitter Neuropeptide Y is a novel pro-arrhythmic trigger even in the presence of maximal beta-blockade.*

Poster presentation: **International Society of Autonomic Neuroscience 2015,** Stressa, Italy. Autonomic Neuroscience: Basic and Clinical 192 (2015) 56–141

Kalla M, Bub G, Larsen H, Paterson DJ and Herring N (2015). *Cardiac symnpathetic nerve stimulation causes NPY release and is pro-arrhythmic independent of beta-receptors: role for the Y1 receptor*

Poster presentation: **Heart Rhythm Society Scientific Sessions 2015**, Boston, USA. Heart Rhythm (2015) **12:**5 S324

Kalla M, Bub G, Larsen H, Paterson DJ and Herring N (2014). *Beta-blockers do not block the pro-arrhythmic effect of high level stimulation: a role for Neuropeptide Y?*

Prize winning (Young Investigator) presentation at **British Heart Rhythm Society 2014**, Birmingham, UK

Poster presentation: ***Physoc 2014****, London. Proc Physiol Soc 31 (2014)*

Poster presentation: **European Society of Cardiology 2014**, Barcelona. European Heart Journal (2014) **35** (Abstract Supplement) 1147

Kalla M, Chotalia M, Coughan C, Hao G, Bub G, Paterson D and Herring N (2014). *The anti-fibrillatory effect of Carbamylcholine requires muscarinic and nicotinic receptor stimulation and the generation of NO.*

Poster presentation: **Physoc 2014**, London. Proc Physiol Soc 31 (2014)

Kalla M, Chotalia M, Coughlan C, Hao G, Paterson D and Herring N (2013). *Acetylcholine analogue mimics the protective effect of cardiac vagus nerve stimulation on ventricular fibrillation threshold*

Poster presentation: **IUPS (International Union of Physiological Sciences) 2013**, Birmingham, UK. Proc Physiol Soc 30 (2013)

Poster presentation: **European Society of Cardiology 2013**, Amsterdam. European Heart Journal (2013) **34** (Abstract Supplement), 1137–1212

Prizes

British Heart Rhythm Society Young Investigator Award (Basic Science) 2014

Peter Beaconsfield Prize 2014, Medical Sciences Division, University of Oxford

BHF Centre for Research Excellence Poster Prize 2013, University of Oxford

Statement of contribution to this thesis

The planning and design of the experimental work in this thesis was done with the support and guidance of my supervisors. The undertaking and analysis of data was my own work, while interpretation was done in conjunction with my supervisors. However, I would like to acknowledge the contributions of others to the work presented in this thesis.

Chapter 3

A proportion (25%) of the experiments were carried out under my direct supervision by two undergraduate medicine dissertation students; Mr Minesh Chotalia and Mr Charles Coughlan.

The optical mapping protocol was developed and optimised with the assistance of Dr Gil Bub (University Research Lecturer, University of Oxford) and analysed with software custom written by Dr Gil Bub and Mr Jakub Tomek (DPhil student).

Ozone chemiluminescence experiments for NO metabolites were performed with the assistance of Dr Mark Crabtree (BHF Intermediate Fellow, University of Oxford).

Chapter 4

The isolated heart with intact sympathetic innervation model was developed and optimised with Professor Neil Herring.

Dye-free imaging of myocyte monolayers was done in collaboration with Dr Rebecca Burton (University of Oxford)

Western immunoblotting and immunohistochemistry experiments were done in collaboration with Miss Hege Larsen (DPhil student) and Dr Rebecca Burton (University of Oxford).

Chapter 5

Mr Ashley Hale (Research Assistant, University of Oxford) and Dr Gillian Douglas (Post-doctoral scientist, University of Oxford) provided assistance with animal work and training in molecular techniques.

Catecholamine measurements were done in collaboration with Dr Brent Ryan (OPDC Career Development Fellow, University of Oxford).

Macrophage samples were kindly provided by Dr Eileen McNeill (Post-doctoral scientist, University of Oxford) and Mr Ashley Hale.

Motion analysis experiments were designed and analysed in collaboration with Dr Eric Tam (Post-doctoral scientist, University of Oxford)

Table of Contents

Chapter 1 General introduction 1
1.1 Clinical Perspectives 1
1.2 Cardiac sympatho-vagal imbalance 1
1.3 Current treatment strategies 4
1.4 The cardiac vagus and ventricular arrhythmia 5
1.5 Mechanisms of ventricular arrhythmias 8
1.6 The anti-fibrillatory effect of the cardiac vagus 14
1.6.1 Sympatho-vagal balance and accentuated antagonism 16
1.6.2 Tissue heterogeneity 17
1.6.3 Heart rate reduction 18
1.6.4 Direct effects of VNS on ventricular electrophysiology 22
1.7 Vagal nerve stimulation and the role of NO 23
1.8 Vagal innervation of the ventricle 26
1.10 The anti-arrhythmic effects of NO 30
1.10.1 NO mediated anti-arrhythmic effects - mechanisms 32
1.10.2 Ion channel regulation and electrophysiological effects 33
1.10.3 Cyclic GMP signalling pathways 37
1.10.4 Gap junction regulation 37
1.10.5 Oxidative stress and cell injury 37
1.10.6 NO and autonomic ganglia 38
1.11 Sympatho-vagal crosstalk 38
1.12 Transmitter release during sympathetic nerve stimulation ... 41
1.12.1 NA and ATP 41
1.12.2 Galanin and Neuropeptide Y 41
1.13 Tetrahydrobiopterin: a molecular component of autonomic regulation? 45
1.13.1 BH4 and vascular function 47
1.13.2 BH4 as a therapeutic tool 48
1.13.3 Cardiac role of BH4 49
1.13.4 BH4 and autonomic function 50
1.13.5 Models of BH4 deficiency and autonomic dysfunction 52
1.14 Integrated cardiac-neural axis and the hearts "little brain".. 53
1.15 Aims and objectives 57

Chapter 2 General Methods 59
2.1 Isolated Langendorff perfused heart 59
2.1.1 Historical context 59
2.1.2 Advantages of the Langendorff system 59
2.1.3 Species selection 60
2.2 Isolated heart apparatus 60
2.3 Anaesthesia and surgical dissection 62
2.3.1 Isolated Langendorff heart preparation 62
2.3.2 Isolated Langendorff heart with intact sympathetic innervation 63
2.4 Measurements 64
2.5 Electrical pacing 65

2.6 Arrhythmia induction and ventricular fibrillation threshold testing..... 66
2.6.1 VFT pacing protocols 67
2.6.2 Testing VFT 68
2.6.3 Ventricular arrhythmia scoring post ischaemia-reperfusion.....68
2.7 Whole heart electrophysiology..... 69
2.8 Contact (suction) electrode action potential recordings 69
2.9 Optical mapping..... 70
2.9.1 Photodetectors.....70
2.9.2 Illumination.....71
2.9.3 Lenses and filters 72
2.9.4 Potentiometric dyes.....72
2.9.5 Elimination of motion artefacts 73
2.9.6 Mechanical restraint.....73
2.9.7 Electro-mechanical uncouplers.....74
2.9.8 Dye loading in Langendorff perfused rat hearts 75
2.9.9 Image acquisition.....75
2.10 Dye free imaging of myocyte monolayers 76
2.10.1 Myocyte Isolation and Plating 76
2.10.2 Imaging 76
2.11 Measurement of NO metabolites 77
2.12 Measurement of neuropeptide Y by ELISA 78
2.13 Western blotting for NPY Y1 receptors on myocytes..... 78
2.14 Immunohistochemistry for Y1 receptor on ventricular myocytes..... 79
2.15 Genetic mouse models..... 79
2.15.1 Cre-Lox technology 80
2.15.2 The THcre $GCH^{f/f}$ mouse.....80
2.16 Mouse welfare..... 82
2.17 Tissue harvest protocol..... 83
2.17.1 Adrenal micro-dissection.....83
2.17.2 Stellate ganglia harvest 83
2.17.3 Midbrain dissection.....84
2.18 Genotyping transgenic mice 84
2.18.1 DNA extraction.....85
2.19 Polymerase Chain Reactions..... 85
2.20 Cell culture..... 89
2.20.1 Macrophage isolation from Tie2cre $GCH^{f/f}$ animals 89
2.20.2 sEND-1 cell culture.....90
2.21 RNA techniques..... 90
2.21.1 RNA extraction 90
2.21.2 Complementary DNA synthesis 91
2.21.3 Real time RT-PCR using Taqman® probes.....91
2.22 Determination of protein concentration using the BCA™ Protein Assay Kit..... 92
2.23 Western immnoblotting for GTPCH and TH..... 93
2.24 Measurement of biopterins: BH4, BH2 and biopterin..... 93
2.25 Measurement of plasma catecholamines..... 96

2.26 Non-invasive blood pressure recordings 96
2.27 Motion tracking 97
2.28 Statistics and data analysis 97
2.29 Chapter 2 Figures 99

Chapter 3 The cholinergic modulation of ventricular fibrillation threshold 110
3.1 Introduction 110
3.2 Methods 111
3.2.1 Animals 111
3.2.2 Langendorff perfused rat heart 111
3.2.3 Ventricular fibrillation threshold testing 112
3.2.4 Optical mapping of voltage 112
3.2.5 NOx chemiluminescence assay 113
3.2.6 Solutions and drugs 113
3.2.7 Statistical analysis 114
3.3 Results 115
3.3.1 Inclusion criteria 115
3.3.2 Protocol for testing VFT 115
3.3.3 The effect of CCh on haemodynamics and VFT 115
3.3.4 The effect of CCh on ventricular electrophysiology 116
3.3.5 Role of muscarinic receptor 117
3.3.6 Role of nitric oxide 118
3.3.7 The role of NO in mediating the anti-fibrillatory effect of CCh 118
3.3.8 Which NOS isoform is involved in this signaling cascasde? 119
3.3.9 Localisation of nNOS activity 121
3.3.10 Release of NO upon CCh perfusion 122
3.3.11 Autocrine versus paracrine effects of NO 123
3.4 Discussion 123
Role and source of NO as a cholinergic antiarrhythmic modulator 125
The antiarrhythmic action of muscarinic receptor stimulation 126
Limitations 128
Clinical significance 130
3.5 Chapter 3 Figures 132

Chapter 4 Neuropeptide Y and sympathetic modulation of ventricular fibrillation threshold 146
4.1 Introduction 146
4.2 Methods 147
4.2.1 Animals 147
4.2.2 Langendorff perfused heart 148
4.2.3 Langendorff perfused heart with intact sympathetic innervation 148
4.2.4 Ventricular fibrillation threshold testing 149
4.2.5 Dye free mapping of myocyte monolayers 150
4.2.6 Determination of coronary perfusate NPY levels by ELISA 152
4.2.7 Western blotting of ventricular lysates 153
4.2.8 Isolated ventricular myocyte immunohistochemistry 153
4.2.9 Determining the effect of NPY on ventricular arrhythmias post ischaemia-reperfusion 154
4.2.10 Solutions and drugs 154
4.2.11 Statistical analysis 155

4.3 Results 155
4.3.1 Inclusion criteria 155
4.3.2 Protocol for testing VFT 156
4.3.3 Effect of NPY perfusion on haemodynamics and VFT 156
4.3.4 Receptor dependency of the effect of NPY 157
4.3.5 Monolayer mapping 158
4.3.6 Confirmation of Y_1 receptor presence on ventricular myocytes 159
4.3.7 The sympathetic nerve innervated isolated rat heart model – effects of direct nerve stimulation 159
4.3.8 Direct SG stimulation and VFT 161
4.3.9 Validation of baseline data and β-blockade efficacy 161
4.3.10 Neuropeptide release during direct stellate ganglia stimulation 162
4.3.11 NPY increases ventricular arrhythmias in the context of ischaemia-reperfusion 163
4.4 Discussion 163
NPY is a novel, independent, pro-arrhythmic trigger 164
Mechanism of pro-arrhythmic action 165
Clinical implications 166
Limitations 168
Conclusions 169
Chapter 4 Figures 170

Chapter 5 Tetrahydrobiopterin and autonomic control of cardiovascular function 181
5.1 Introduction 181
5.2 Methods 185
5.2.1 Generation of the THcre $GCH^{f/f}$ and THiresGCH$^{f/f}$ mouse models 185
5.2.2 Genotyping $GCH^{f/f}$; cre loci 187
5.2.3 Determination of tissue BH4 and biopterin levels 187
5.2.4 Determination of catecholamine levels 188
5.2.5 Real time quantified RT-PCR 188
5.2.5 Measurement of heart rate and arterial blood pressure 189
5.2.6 Western immunoblotting 189
5.2.7 Motion analysis in the THiresGCH$^{f/f}$ model 190
5.2.8 Statistical analysis 191
5.3 Results 191
5.3.1 Generation of the THcre $GCH^{f/f}$ mouse 191
5.3.2 Genotyping animals from generation of THcreGCH$^{f/f}$ animals 191
5.3.3 Comparison of tissue biopterin levels in THcreGCH$^{f/f}$ animals and littermate controls 192
5.3.4 Comparison of plasma catecholamines levels in THcreGCH$^{f/f}$ animals and littermate controls 193
5.3.5 Comparison of blood pressure and heart rate in THcreGCH$^{f/f}$ animals and littermate controls 193
5.3.6 Inefficient gene excision by cre-recombinase in THcreGCH$^{f/f}$ animals 194
5.3.7 GTPCH protein expression was not decreased in THcreGCH$^{f/f}$ animals 195
5.3.8 Generation of the THiresGCH$^{f/f}$ model 195
5.3.9 TH ires-cre results in effective deletion from central and peripheral TH expressing cells 196
5.3.10 GTPCH protein expression was decreased in THiresGCH$^{f/f}$ animals 196
5.3.11 Comparison of tissue biopterin levels in THiresGCH$^{f/f}$ animals and littermate controls 197

5.3.12 Comparison of plasma catecholamine levels in THiresGCH$^{f/f}$ animals and littermate controls 197
5.3.12 Movement was significantly decreased in THiresGCH$^{f/f}$ animals compared to littermate controls 197
5.4 Discussion 198
Role of BH4 in neurological disease 202
Chapter 5 Figures 205
Chapter 6 Concluding discussion 216
6.1 Key findings from this thesis 217
6.2 The cholinergic autonomic modulation of ventricular arrhythmia 218
6.3 Sympathetic co-transmission and the pro-arrhythmic effect of sympathetic stimulation 223
6.4 Tetrahydrobiopterin and autonomic cardiovascular control 227
6.5 Concluding summary 229
References 231

Table of Figures

Figure 1.1 Dynamics of cardiac fibrillation 10
Figure 1.2 Proposed model of interaction between dynamic and fixed factors in determining VF risk 14
Figure 1.3 NO facilitates acetycholine release and vagal bradycardia 21
Figure 1.4 Schematic diagram of the anterior view of the heart with a summary of parasympathetic innervation 28
Figure 1.5 Putative mechanisms by which NO mediates protection against cardiac fibrillation 32
Figure 1.6 Electrophysiological effects of NO on (A) atrial and ventricular cells and (B) sino-atrial node currents which contribute to the action potential 34
Figure 1.7 Cardiac sympatho-vagal crosstalk 44
Figure 1.8 Tetrahydrobiopterin biosynthesis and metabolism 46
Figure 1.9 Enzyme cofactor activity of tetrahydrobiopterin 47
Figure 1.10 Schematic summary of proposed neural interactions encompassing central and peripheral autonomic control 56

Figure 2.1 Schematic of Langendorff apparatus for whole heart experiments 99
Figure 2.2 Photograph of Langendorff apparatus used for whole heart experiments 100
Figure 2.3 Photograph of typical experimental preparation 101
Figure 2.4 Photograph of an experiment of an isolated rat heart with intact sympathetic innervation 101
Figure 2.5 Raw data trace of measured physiologic parameters 102
Figure 2.6 Ventricular fibrillation threshold: control data 103
Figure 2.7 Ventricular fibrillation threshold testing 104
Figure 2.8 Schematic of optical mapping equipment 105
Figure 2.9 Optical mapping of whole hearts 106
Figure 2.10 Breeding protocol for generation of tissue specific GCH1 knockout mouse model 107
Figure 2.11 Optimisation of BH4 determination by HPLC in adrenal tissue 108
Figure 2.12 Catecholamine determination by HPLC in mouse plasma 109

Figure 3.1 Experimental raw data trace of CCh perfusion 132
Figure 3.2 Haemodynamic changes during perfusion of Carbamylcholine 200nM 133
Figure 3.3 Ventricular fibrillation threshold (VFT) is increased by Carbamylcholine 200nM 134
Figure 3.4 Optical mapping of ventricular repolarisation and electrical restitution during CCh perfusion 135
Figure 3.5 Haemodynamic and VFT changes during investigation of the effect of muscarinic receptor blockade with atropine during CCh perfusion 136
Figure 3.6 Haemodynamic changes during perfusion of sodium nitroprusside 10μM 137
Figure 3.7 Ventricular fibrillation threshold (VFT) is increased by sodium nitroprusside 10μM 138
Figure 3.8 Haemodynamic and VFT changes during investigation of the effect of NOS blockade and substrate restoration during perfusion with carbamylcholine 139
Figure 3.9 Haemodynamic and VFT changes during investigation of the effect of nNOS blockade with SMTC and substrate restoration during perfusion with carbamylcholine 140
Figure 3.10 Haemodynamic and VFT changes during investigation of the effect of nNOS blockade with AAAN during CCh perfusion 141
Figure 3.11 Haemodynamic and VFT changes during investigation of the effect of sGC blockade with ODQ during CCh perfusion 142
Figure 3.12 Haemodynamic and VFT changes during investigation of the effect of nicotinic receptor blockade with mecamylamine during CCh perfusion 143
Figure 3.13 Detection of NO release during CCh stimulation and the effect of nicotinic receptor blockade 144
Figure 3.14 Haemodynamic and VFT changes during perfusion of sodium nitroprusside 10μM and atropine 0.1μM 145

Figure 4.1 Experimental trace of neuropeptide Y (NPY) perfusion 170
Figure 4.2 Haemodynamic effects of neuropeptide Y perfusion 171
Figure 4.3 NPY lowers VFT independent of HR 172
Figure 4.4 NPY lowers VFT independent of heart rate via a Y_1 receptor dependent mechanism 173

Figure 4.5 NPY lowers VFT independent of heart rate via a Y_1 receptor dependent mechanism ___ *174*
Figure 4.6 NPY results in spontaneous wave activity in quiescent myocyte monolayers _____ *175*
Figure 4.7 NPY Y_1 receptor is present on cardiomyocytes _____ *176*
Figure 4.8 Direct stellate ganglia stimulation and haemodynamics _____ *177*
Figure 4.9 Direct stellate ganglia stimulation and VFT _____ *178*
Figure 4.10 The pro-arrhythmic effect of norepinephrine is abolished by beta-blockade _____ *179*
Figure 4.11 Direct stellate ganglia stimulation results in increased NPY levels in coronary perfusate _____ *179*
Figure 4.12 NPY increases the incidence of ventricular arrhythmias following ischaemia reperfusion _____ *180*

Figure 5.1 Generation and breeding of the THcreGCH$^{f/f}$ mouse _____ *205*
Figure 5.2 Confirmation of genotype in ear snip and target tissue _____ *206*
Figure 5.3 Comparison of tissue biopterin levels in THcreGCH$^{f/f}$ animals and littermate controls _ *207*
Figure 5.4 Comparison of plasma catecholamines levels in THcreGCH$^{f/f}$ animals and littermate controls _____ *208*
Figure 5.5 Non-invasive tail cuff plethysmography blood pressure and heart rate assessment in THcreGCH$^{f/f}$ animals and littermate controls _____ *209*
Figure 5.6 Assessment of efficiency of gene excision by qRT-PCR and PCR in THcreGCH$^{f/f}$ animals _____ *210*
Figure 5.7 GTPCH protein was not decreased in whole adrenal from THcreGCH$^{f/f}$ animals compared to littermate controls _____ *211*
Figure 5.8 Generation of the THiresGCH$^{f/f}$ mouse _____ *212*
Figure 5.9 Genomic deletion of GCH1 in target tissues from THiresGCH$^{f/f}$ animals _____ *213*
Figure 5.10 Decreased GTPCH protein expression in THiresGCH$^{f/f}$ animals _____ *213*
Figure 5.11 Comparison of tissue biopterin and plasma dopamine levels in THiresGCH$^{f/f}$ animals and littermate controls _____ *214*
Figure 5.12 Comparison of movement by motion tracking of THiresGCH$^{f/f}$ animals and littermate controls _____ *215*

Chapter 1 General introduction

1.1 Clinical Perspectives

Cardiovascular disease is the leading cause of morbidity and mortality in developed countries despite advances in medical and interventional therapies. Sudden cardiac death (SCD) caused by malignant ventricular arrhythmias including ventricular tachycardia (VT) and ventricular fibrillation (VF) account for over 70,000 deaths in the UK [1] and over 325,000 in the USA [2]. These mortality figures have persisted despite implementation of comprehensive emergency revascularisation strategies for acute myocardial infarction (primary percutaneous coronary interventions, PCI), device therapy for heart failure (HF) and broad-based, secondary prevention medications including β-blockers, angiotensin converting enzyme (ACE) inhibitors and statins. The mortality associated with ventricular arrhythmia can be treated either prophylactically in some high-risk groups or after aborted sudden cardiac death with the implantation of an implantable cardioverter defibrillator (ICD) [3-5]. Despite this, the morbidity and reduction in quality of life due to the burden of ventricular arrhythmia and shock therapy persists. Therefore, future therapies must aim to mechanistically target the underlying pathophysiologies that contribute to ventricular arrhythmia generation. This may be of particular relevance in patients with HF in whom the arrhythmic mortality is high [5].

1.2 Cardiac sympatho-vagal imbalance

A hallmark of cardiovascular disease including hypertension, myocardial infarction and HF is autonomic imbalance with a reduction in vagal tone and increase in sympathetic activity [6]. These observations have been seen in experimental models and replicated in large-scale human studies in the setting of HF and myocardial infarction.

Changes in autonomic tone have been shown to precede the development of left ventricular dysfunction. Ishise *et al.* [7] utilised a pacing mediated, tachycardia-induced cardiomyopathy model in dogs to study the time course of changes in autonomic function by measurement of heart rate variability and left ventricular contractility. In this experiment, mongrel dogs underwent implantation of a left ventricular (LV) micromanometer and LV epicardial electrodes for ECG recording and pacing. Following recovery, they were paced at 260bpm with serial measurements taken to determine changes in autonomic function. These included left ventricular pressure and power spectra of heart rate variability (HRV) at 4 time points within the first 14 days of rapid pacing and blood samples were taken for the measurement of noradrenaline (NA). This study elegantly demonstrated that changes in parasympathetic control of cardiac function preceded changes in sympathetic activation as evidence by a decline in the high frequency component of HRV during the asymptomatic early phase of tachycardia induced HF. These changes were in parallel with the decline in contractile function, while changes in plasma NA levels and the low frequency components of HRV occurred with worsening left ventricular diastolic function. Interestingly, the changes observed were reversed towards baseline values upon cessation of rapid pacing. These observations were also demonstrated by Motte *et al.* [8] in a similar rapid pacing induced canine HF model. However, this model employed a more gradual increase in heart rate by pacing in order to create a more realistic representation of the clinical course of chronic dilated cardiomyopathy and more accurately study the autonomic dysfunction in this context. With the onset of mild left ventricular dysfunction (systolic and diastolic), a major decrease in total R-R interval variability (RRI) and also the high frequency of RRI was seen, indicating early onset sympatho-vagal imbalance in heart failure. The findings in these models could potentially be

explained by the baseline power density of heart rate being in the high frequency parasympathetic mediated zone, reflecting the high vagal tone in the dogs at rest [8].

However, human studies have demonstrated a similar pattern of autonomic changes in patients with mild LV impairment [9]. This study of 42 patients examined whether peripheral sympathetic activity and baroreflex modulation assessed by microneurography are affected in HF, and if a different pattern was exhibited in HF of ischaemic or non-ischaemic aetiology. This study demonstrated an increase in plasma NA and peripheral sympathetic nerve traffic in HF patients compared with controls. No differences were seen between ischaemic and non-ischaemic HF patients. In addition, baroreflex control of heart rate (tested by blood pressure and microneurography during phenylephrine/nitroprusside drug infusions) was less effective in patients with HF, mimicking the data from the canine HF studies. Mechanistically these changes are thought to be linked to increased activity of arterial chemoreceptors [10] and sympathetic afferent fibres [11] with resulting increase in sympathetic efferent activity [12].

The relevance of these mechanistic and clinical observations studies was demonstrated by large clinical studies, which identified the relationship between impaired cardiac autonomic control and increased mortality as a result of malignant ventricular arrhythmias [13]. These studies also utilised HRV and baroreflex sensitivity (BRS) as markers of parasympathetic tone to avoid invasive measurements of vagal nerve activity. An early prospective study by La Rovere *et al.* [14] demonstrated that low BRS post myocardial infarction was associated with increased mortality, and the prognostic value of HRV and BRS in this population was further demonstrated in a

larger, multicentre, prospective study (ATRAMI) [15]. The UK-Heart investigators [16] tested a similar hypothesis in patients with HF and demonstrated that impaired HRV indicative of reduced parasympathetic tone were independently predictive of mortality. However, the utility of HRV and spectral analysis must also take into account non-neural mechanisms that contribute to HRV in HF and may therefore lead to overestimation of cardiac parasympathetic responsiveness in this patient group [17].

1.3 Current treatment strategies

The mainstays of current treatment for cardiovascular diseases such as hypertension, ischaemic heart disease and HF are pharmacological with drugs aimed at specific targets with each organ system treated in isolation. These strategies are supported by a wealth of large scale, randomised control trials demonstrating significant improvements in morbidity and mortality [18-23]. The key drug classes that influence the local autonomic influences on the heart include β-blockers and angiotensin converting enzyme (ACE) inhibitors. The rationale for β-blockers is based upon the clinical and prognostic significance of sympathetic over activity that is the hallmark of ischaemic heart disease and HF and its relationship to ventricular arrhythmia [6]. This increase in adrenergic stimulation leads to activation of cardiac β_1 adrenergic receptors (βAR) with resulting activation of adenylate cyclase, generation of cyclic adenosine monophosphate (cAMP) and an increase in intracellular Ca^{2+} via the L-type Ca^{2+} current (LTCC) via protein kinase A (PKA). Sarcoplasmic reticulum (SR) calcium loading is also increased by PKA-dependent phosphorylation of phospholamban (PLB) which removes its inhibition of the sarco/endoplasmic reticulum calcium ATPase (SERCA). Chronically β-adrenergic stimulation also has other transcriptional actions promoting hypertrophy and remodelling and in the kidneys promotes renin release and activation of the renin-angiotensin system (RAAS) [24]. Beta-blockers aim

to block this signalling cascade and trials such as CIBIS II [21] established their use in a large, multi-centre, double blind, randomised controlled trial in 2647 patients with New York Heart Association (NYHA) class III-IV HF and ejection fraction <35%. This trial was terminated early due to the significant mortality benefit seen in the bisoprolol group and also fewer sudden cardiac deaths. Results such as these have been replicated with other β-blockers such as metoprolol [22] and carvedilol [25].

ACE inhibitors target the generation of angiotensin II and therefore this underpins its central role as an anti-hypertensive [26]. Angiotensin II (AngII) is a potent vasoconstrictor via its direct action on vascular smooth muscle [27] and also interacts with the sympathetic nervous system peripherally and centrally to increase NA release [28] and vascular tone [29]. It also has a myriad of deleterious cellular effects including cell migration, proliferation and hypertrophy [30-34]. In the setting of HF, ACE inhibitors favourably alter haemodynamics by reducing afterload, preload and systolic wall stress [35-44] leading to a reduction in mortality seen in major clinical trials [18-20, 45, 46].

1.4 The cardiac vagus and ventricular arrhythmia

Despite the advances in emergency revascularisation and medical therapies for secondary prevention and HF, sudden cardiac death due to ventricular arrhythmia remains a significant clinical problem. Recent clinical studies have attempted to target the cardiac vagus directly with electrical vagus nerve stimulation (VNS) in order to improve outcomes in HF in keeping with the Ardell and Armour vision of an integrated central and cardiac physiological axis [47]. The first in man trial of VNS [48] was a small, proof of concept study which demonstrated an improvement in symptoms in patients treated with VNS, but the larger trials such as ANTHEM-HF [49]

and NECTAR-HF [50] have been disappointing in terms of echocardiographic and clinical end points. A larger, randomised clinical trial, INOVATE-HF [51] continues to recruit and data from this trial in which the electrophysiological stimulation of the vagus closely matches physiological vagal discharge is eagerly awaited. The end points of these studies focus on cardiac imaging and symptomatic improvements in patients with severe, medically refractory HF. However, of considerable mechanistic interest may be the potential role of VNS therapy in supressing ventricular arrhythmia. This can be achieved in preclinical models without significant bradycardia [52].

The anti-fibrillatory effect of the vagus was first reported by Einbrodt in 1859 [53] in canine experiments where VF induction during VNS was more difficult. A variety of experimental models have replicated this observation and some key studies will be discussed here. Early studies in the 1970's utilised canine models of coronary artery occlusion (CAO) as the trigger for the generation of ventricular arrhythmia. Using this model, several studies demonstrated that VNS interrupted the occurrence of ventricular arrhythmia during CAO [54-60]. However, Kent *et al.* [60] amongst others [58, 59] also demonstrated the anti-fibrillatory properties of VNS in the absence of ischaemia or structural heart disease. Their experiments also described a quantifiable approach to the assessment of inducibility of ventricular fibrillation by increasing the current delivered during a train of electrical pulses applied during the refractory period. The current at which VF was induced was defined as the ventricular fibrillation threshold (VFT). Using this approach, they were able to demonstrate an increase in VFT during VNS that was independent of heart rate. There followed a sequence of work which suggested that VNS was dependent upon the presence of sympathetic stimulation in

order for the anti-fibrillatory action to be demonstrated. Yoon *et al.* [59] also demonstrated a rise in VFT during VNS but this effect was lost in the presence of β-blockade (propranolol, a non-selective β-blocker). An elegant study [58] reinforced this observation by application of VNS after crushing the left stellate ganglion. Following stellate ganglia stimulation, VNS was anti-arrhythmic, however this effect was lost following crushing of the stellate ganglia.

The intensity of VNS also influences the anti-arrhythmic effect of VNS. Myers *et al.* [56] demonstrated that VNS was associated with an intensity dependent reduction in VF. Bilateral vagotomy and atropine perfusion in a feline model increased mortality after CAO, suggesting basal vagal tone was important in protection against ventricular arrhythmia [61]. In the setting of ischaemia-reperfusion, Zuanetti *et al.* [62] observed a reduction in ventricular arrhythmia with VNS, while vagotomy showed 55% arrhythmia occurrence compared to controls. Despite some conflicting data, the weight of evidence from these early, original studies is supportive of the anti-fibrillatory effect of VNS.

Perhaps the most compelling demonstration of the anti-fibrillatory effect of vagal tone and VNS has come from Peter Schwartz's lab, utilising a canine model of healed myocardial infarction at increased risk of malignant ventricular arrhythmia. Adult dogs were anaesthetised and underwent ligation of the left anterior descending coronary artery resulting in anterior myocardial infarction along with instrumentation for future studies. The animals were allowed to recover for one month resulting in surviving animals having a healed myocardial infarction. Animals were then subjected to increasing workload on a treadmill with concurrent circumflex occlusion

resulting in VF in 60% of animals [63, 64]. The animals which survived this trigger, demonstrated an ischaemia-induced decrease in heart rate, indicating vagal reflexes exert a protective influence. A subsequent study [65] analysed vagal tone in this preparation with muscarinic blockade. Atropine administration promoted ventricular arrhythmia with no evidence of arrhythmia during control experiments, and the presence of vagal reflexes correlated with BRS, another marker of parasympathetic activity. The final series of experiments in this model [66] used direct VNS before and during CAO. In the absence of VNS, 92% of animals developed VF, and post VNS this reduced to 10%, providing further support of the anti-fibrillatory effect of the vagus. The species variation in parasympathetic innervation and therefore resting vagal tone will influence these observations and may contribute to the significant vagal effects seen in the canine heart [67].

1.5 Mechanisms of ventricular arrhythmias

An understanding of the mechanisms responsible for the initiation and maintenance of VF is critical if effective treatment strategies are to be developed and studied, including the potential role of autonomic modulation. One of the principle mechanisms in the onset of arrhythmia is re-entry. Fibrillation occurs when an electrical wavebreak induces re-entry and leads to a sequence of new wavebreaks [68-70]. This wavebreak is affected by static and dynamic factors which increase or decrease the propensity for local wavebreak to result in re-entry and subsequent fibrillation. Static factors are predominantly anatomical (e.g. scar, fibrosis) caused by disease processes, leading to tissue heterogeneity and electrical remodelling that is fixed. Recent evidence has suggested dynamic factors function synergistically with tissue heterogeneity to create functional electrophysiological changes that destabilise

wave propagation. The critical determinants of dynamic stability include cellular membrane voltage (V_m) and intracellular calcium ($[Ca^{2+}]_i$).

Normal cardiac excitation can be viewed as an electrical wave encompassing depolarization (wavefront) and the upstroke and rapid repolarisation (waveback). These two regions of a wave do not meet as a wave propagates through normal tissue. In the setting of tissue or electrical heterogeneity, these two aspects of a wave may meet leading to wavebreak, and if this occurs in a spatially restricted fashion, wavebreak will occur with the potential for re-entry [68]. The mechanism of wavebreak leading to re-entry is thought to be localised wavebreak, leading to an increased curvature of an advancing wave, resulting in insufficient depolarising current with respect to the number of locally coupled unexcited cells. This slows conduction velocity, causing the wave to rotate around this point (source-sink mismatch) [71]. Anatomic re-entry occurs typically around regions of fixed scar, although recent experimental evidence also proposed functional re-entry or rotors may contribute to the development of rapid tachycardia [72, 73]. There remains controversy on the mechanisms that sustain fibrillation with the two principle hypotheses being multiple wavebreaks maintaining fibrillation [74] or mother rotors [75] driving fibrillation with functional conduction block occurring in distant regions. A unifying factor with these two conflicting mechanistic views is that the initial wavebreak is critical for the initiation of fibrillation. Figure 1.1 provides some experimental evidence of these mechanisms.

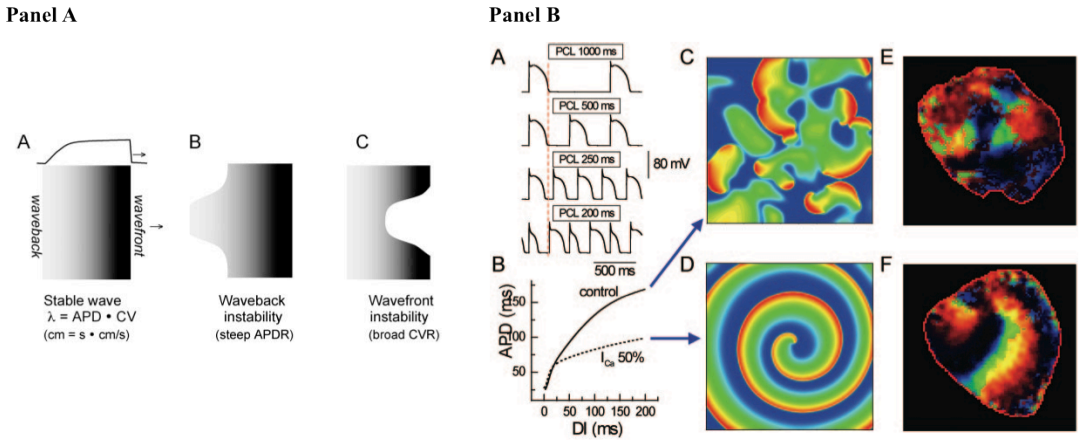


Figure 1.1 Dynamics of cardiac fibrillation

Panel A: Schematic representation of the cardiac impulse with a a wavefront (black) which corresponds the AP upstroke, and waveback **(**grey/white) representing repolarisation. **A** is a stable, uniform wave while **B** has waveback instability due to local APD prolongation and **C** has instability due to local CV slowing.
Panel B: Explores the critical issues of alternans and restitution relationship to complex or stable arrhythmia patterns. **A.** Increased pacing cycle length induces electrical alternans with marked variation in sequential APDs which lead to **B.** steep electrical restitution curves which can be flattened (less arrhythmic) by decreasing intracellular calcium. **C/D.** Homogenous 2D tissue with optical mapping demonstrating rotor/spinal activation patterns with steep and shallow restitution. **E/F.** Optical mapping of voltage in rabbit hearts showing a complex, multiple wavefront VF pattern (**E**) which converts to a more stable VT rotor pattern (**F**).
(APD: action potential duration, CV: conduction velocity, APDR: APD restitution, CVR: CV restitution, PCL: pacing cycle length, ms: milliseconds, VF: ventricular fibrillation, VT: ventricular tachycardia)
Adapted from Weiss et al. 2005

Tissue heterogeneity in the heart is a key determinant of the likelihood of fibrillation occurring. The disease processes themselves may increase potential triggers such as extrasystoles, while regional electrophysiological dispersion will make wavebreak more likely. A typical example of this is the border zone between normal and infarcted tissue [76]. The causes of heterogeneity are also multifactorial including infarction, fibrosis, structural remodelling or electrical remodelling due to genetic defects or changes in autonomic innervation. These changes contribute to wavebreak by several mechanisms. This includes regional differences in refractory period which can lead to regions of longer APD. Wavebreak will therefore occur if an advancing wave arrives before excitability in this region has recovered. Alternatively, regional

source-sink mismatch may occur due to anatomical structures such as papillary muscles [77] or temporal changes in excitability due to ischaemia or drugs [68].

Dynamic factors arise from changes in V_m and $[Ca^{2+}]_i$ resulting in alterations in APD and conduction velocity (CV). Membrane voltage changes influence APD restitution, CV restitution, cardiac memory and electrical currents. Changes in $[Ca^{2+}]_i$ include alternations in cycling dynamics and sarcoplasmic reticulum (SR) $[Ca^{2+}]_i$ release. As heart rate increases, APD shortens physiologically along with a greater shortening of diastole. Increased venous return and improved passive and active filling during increased heart rates acts to increase cardiac output during sympathetic stimulation. The relationship between the APD and the preceding DI can be plotted to generate an APD restitution curve. If the curve slope is steep (>1 in humans), small changes in DI lead to large changes in APD and wavelength. If these oscillations amplify, wavebreak ensues leading to fibrillatory wave patterns. This mechanistic model has been confirmed in tissue simulations [78-80] and experimentally [81-86]. Experimental studies [86] in which I_{Ca} was decreased by 50% resulted in a flatter restitution curve and prevented VF in a normal ventricle. While a steep APD curve influences repolarisation (waveback), Wu *et al.* [86] propose that that CV influences wavefront position and if related to preceding DI, can result in wavebreak. They used optical mapping of rabbit ventricles in the presence of D600 (Ca^{2+} channel blocker) to assess changes in VF patterns. In the absence of D600, VF was defined as type 1 (rapid, multi-wavelet pattern) and following high dose D600 (Na^+/Ca^{2+} channel blockade), type 2 VF (slow, coarse) was seen with optical activation suggestive of a stable mother rotor and distant fibrillatory conduction block. They propose that this observation may allow unification of the multi-wavelet hypothesis of Moe *et al.* [74]

with the rotor observations of Jalife [75, 87] amongst others. Clinically, this may correspond to type 1 VF seen in acute ischaemia with type 2 patterns being observed with increasing ischaemia and anatomic heterogeneity.

Weiss and colleagues [68] have made important observations regarding the utility of using restitution kinetics in isolation in order to predict the likelihood of wavebreak. This relates to short term cardiac memory which influences APD and pacing beyond that associated with preceding DI. The key determinants include ion currents with slow recovery kinetics (predominantly K^+ currents) and $[Ca^{2+}]_i$ cycling [88]. This differs from long term cardiac memory which is related to pacing induced changes in gene expression or post translational protein modification [68].

Therefore, restitution provides a useful metric of assessing arrhythmogenicity, and experimental studies have shown drugs that flatten the restitution curve can prevent VF [82, 84, 85, 89]. However, there are some key limitations. Pacing protocols themselves influence restitution curves and the slope does not always predict APD alternans [89], therefore they should be used as an approximation of dynamic changes that occur during arrhythmia [68]. In addition, APD alternans often precedes the initiation of fibrillation and is frequently attributed to $[Ca^{2+}]_i$ alternans rather than a steep APD restitution curve [69]. Abnormal Ca^{2+} cycling associated with the high sympathetic tone in HF or post-myocardial infarction may contribute to the generation of delayed after-depolarisations (DADs) and subsequent PVCs that may also trigger wavebreak [68, 69].

$[Ca^{2+}]_i$ cycling is a critical regulator of dynamic wave instability. Contractile activity in mammalian hearts is triggered by a small amount of Ca^{2+} entry via the LTCC

resulting in calcium induced calcium release (CICR) from the SR [90]. SR release of Ca^{2+} into the cytoplasm is via the ryanodine receptor (RyR_2), and reuptake is via the sarco/endoplasmic reticulum Ca-ATPase (SERCA) or transport into the extracellular space by the Na^{+}-Ca^{2+} exchanger (NCX). Under normal conditions, the $[Ca^{2+}]_i$ transient is closely coupled to V_m, however CICR may exhibit independent dynamics. Experimental evidence in support of this includes rapid pacing of isolated rabbit ventricular myocytes under AP clamp conditions [88] resulting in $[Ca^{2+}]_i$ alternans in the presence of a fixed V_m waveform. The SR can also release $[Ca^{2+}]_i$ independent of a trigger from the LTCC under conditions of Ca^{2+} overload [90] seen experimentally with rapid pacing or in disease models with increased sympathetic drive. Following release from the SR, $[Ca^{2+}]_i$ modifies APD through regulation of Ca-sensitive ion channels, including the LTCC, NCX, and Ca-activated non-selective and chloride currents [68]. An increase in $[Ca^{2+}]_i$ results in shortening of APD via inhibition of the LTCC, but can prolong the APD by enhancing inward current via the NCX. The balance between these effects can result in positive coupling with resulting APD prolongation, or negative coupling with APD shortening. Furthermore, the consequences of these current modifications influence SR calcium loading [90] resulting in a bidirectional coupling between V_m and $[Ca^{2+}]_i$. Under pathological conditions, $[Ca^{2+}]_i$ release may alter APD sufficiently to result in wavebreak as observed in experimental simulation [88]. Lastly, $[Ca^{2+}]_i$ cycling also affects APD restitution, as data described above demonstrates inhibition of LTCC by D600 results in marked flattening of the restitution curve and prevention of VF initiation.

In summary, the mechanisms underlying VF are complex and as yet, incompletely understood but rely on interaction between tissue heterogeneity and dynamic changes

in electrophysiology. This can be summarised in figure 1.2 below from Weiss *et al.*[68]. The normal heart lies in the white low vulnerable window zone, but if a rotor is induced, the probability of progressing to VF is high [91] due to wavebreak. Clinical data has shown that the patients with marked tissue heterogeneity are associated with physiological PVCs [92] but the rates of SCD are low as rotors are not induced. However, with disease progression, genetic abnormalities or autonomic changes, the influence of dynamic factors increases and wavebreak becomes more likely.

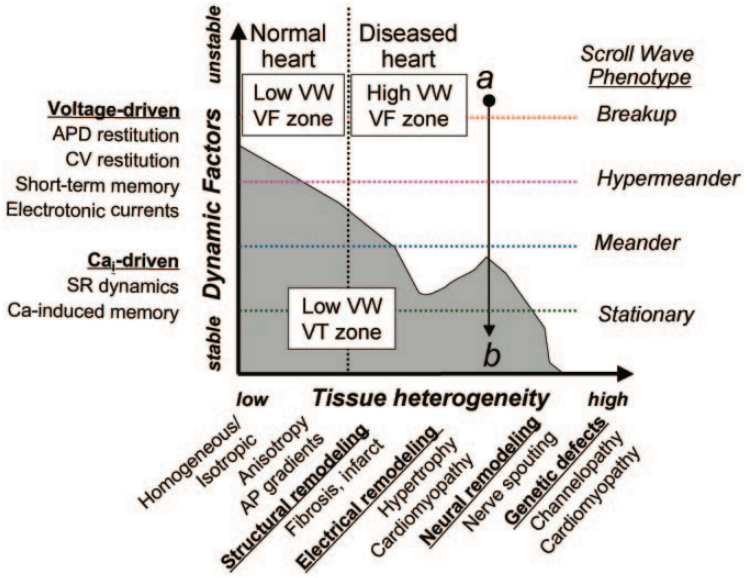


Figure 1.2 Proposed model of interaction between dynamic and fixed factors in determining VF risk

This panel is a hypothetical model of interaction of the multiple facets of dynamic and fixed variables that contribute to VF risk. Treatment goals would aim to reduce the impact of each of these variables to move patients from the high risk (point a) to low risk (b) zone (VW: vulnerable window, SR: sarcoplasmic reticulum)
Adapted from Weiss et al. 2005

1.6 The anti-fibrillatory effect of the cardiac vagus

The data above have provided clear evidence of the anti-fibrillatory properties of the vagus in animal models and human studies, confirming the protective influence of enhanced vagal tone. The mechanisms of VF have been explored *in vitro* and with

modelling studies and these observations allow discussion of the influence of VNS in modifying both the fixed and dynamic factors via direct and indirect routes.

The principle mechanisms are summarised in the table below and discussed in detail in the following section.

Mechanism	Effect on arrhythmogenicity	Effect of VNS
Electrical restitution	Increased slope (>1) results in APD heterogeneity in response to small changes in DI leading to increased risk of wavebreak and re-entry [93]	Flattens slope [94]
APD dispersion [95]	Sympathetic stimulation results in increased APD dispersion and increased arrhythmic risk (base>apex) [96]	VNS depresses sympathetic drive and therefore APD dispersion (accentuated antagonism) [98, 99]
		VNS increases APD, ERP and reduces VFT [94, 100]
	Gap junction remodeling due to HF leads to increased transmural APD dispersion [97]	VNS reverses reduction in Cx-43 expression [101]
Heart rate/ventricular refractoriness	Heart rate reduction has favourable effects in HF trials	VNS results in bradycardia
	Increased repolarisation phase reduces arrhythmic risk	VNS prolongs ventricular APD and ERP [100]
Conduction velocity	Substrate changes secondary to ischaemia/HF lead to gap junction remodelling and reduced conduction velocity [97]	VNS modifies gap junction expression [101, 102]
Intracellular Ca^{2+} load	SNS increases Ca^{2+} load in SR, which increases premature contractions and delayed after depolarisations [6]	VNS reduces NA release, cAMP levels and SR Ca^{2+} load [99, 103]
Premature ventricular contractions (PVC)	Can induce/trigger re-entrant arrhythmias and reduce contractile function [104]	VNS reduces PVCs in animals with HF therefore reducing arrhythmia risk [16]

Table 1.1 Summary of physiological mechanisms that contribute to the development of ventricular arrhythmias and the effect of vagal nerve stimulation (VNS) on each parameter

1.6.1 Sympatho-vagal balance and accentuated antagonism

The two branches of the autonomic nervous system form a complex, interconnected, regulatory system as defined by Armour and Ardell [47]. The first description of this interaction by Samaan [105] described the decreased chronotropic response to sympathetic nerve stimulation (SNS) with concurrent VNS, leading to the term 'accentuated antagonism' being applied to this phenomenon by Levi and Zieske [99]. This effect is not restricted to heart rate responses alone, but similar observations have been seen with respect to contractility [99], $[Ca^{2+}]_i$ [99] and cardiac electrophysiology [103, 106]. This interaction on multiple facets of cardiac function occurs via pre- and post-synaptic mechanisms. Stimulation of the vagus results in release of acetylcholine (ACh) release which binds to muscarinic acetylcholine receptors (mACHRs) on cardiomyocytes (M_2) and pre-synaptic sympathetic nerve terminals (M_3) [103, 107-110]. Binding to these sites results in a reduction in cAMP in the cardiomyocyte and decreased NA release from sympathetic nerves. As discussed above, there is experimental evidence demonstrating loss of the anti-arrhythmic effect of VNS in the absence of sympathetic nerve activity, either by β-blockade [59] or crushing of the left stellate ganglia [58]. Furthermore, the central role of the muscarinic receptor has been shown by loss of VNS protection in the presence of atropine [59, 61, 66] and enhanced vagal effects in the presence of anti-cholinesterases [111, 112]. Sympathetic nerve activity also modulates vagal activity by opposing the effect of M_2 activation via NA coupling to a-adrenergic receptors and also co-transmission of other neuromodulators, which will be discussed in detail below.

1.6.2 Tissue heterogeneity

The ventricular myocardium undergoes fibrotic remodelling with ageing and in the context of disease leading to a pro-arrhythmic substrate due to increased source-sink mismatch, decreased CV, and increased PVCs. Direct VNS with the CardioFit system in a canine model of microembolisation-induced HF was able to reduce interstitial fibrosis [101]. Inflammatory pathways play a key role in cardiac fibrosis [113] and there is considerable interest in the modulation of these responses by the ANS, also known as the inflammatory reflex [114]. Potential clinical manifestations of this link are findings of reduced HRV in patients with high levels of inflammatory cytokines [115], and the higher incidence of ventricular arrhythmia in patients with acute myocarditis [116, 117]. High levels of inflammatory mediators also promote the formation of scar, fibrosis, and hypertrophy and impair oxygen delivery [118]. Transgenic murine models have provided further evidence in keeping with these observations. Overexpression of TNF-α results in a HF phenotype [119] and susceptibility to atrial and ventricular arrhythmias as well as altered Ca_i handling. Application of direct VNS in the above canine HF model resulted in normalisation of levels of IL-6 and TNF-α [120]. Chronic VNS has been shown to reduce plasma levels of angiotensin II [121], a potent pro-fibrotic mediator and potentially aid remodelling by exerting an anti-apoptotic influence on cardiomyocytes [122].

Heterogeneity of electrical activation in the ventricle is dependent upon gap junction distribution and function. Gap junctions provide a low resistance pathway for intercellular current flow and determine the magnitude and anisotropy of conduction [123]. Alteration in gap junction expression is seen in the context of ischaemia, HF and hypertrophic cardiomyopathy, all conditions with a higher risk of ventricular

arrhythmia. The underlying mechanism in these conditions include electrical heterogeneity, often due to increasing myocardial electrical impedance [124]. Data from Ando *et al.* [102] demonstrated that VNS resulted in maintenance of gap junction function as evidenced by preservation of phosphorylated connexin 43, the principle cardiac gap junction protein. The functional result of this was seen with an 87% reduction in post-myocardial infarction VT in a rat model. Similar observations have been reported by Sabbah [101], where chronic VNS resulted in normalisation of connexin 43 expression in a canine model of micro-embolization induced HF.

1.6.3 Heart rate reduction

Stimulating the cardiac vagus results in bradycardia and some studies have suggested that the anti-arrhythmic effect is attenuated if heart rate is controlled [55, 56, 60, 62]. Nitric oxide plays a key role in mediating this vagal bradycardia response and its mechanism is site specific.

The first observation of heart rate reduction by vagal stimulation was in the 1800s by Weber [125] and subsequently proven by Loewi in 1924 [126] leading to the award of the Nobel Prize. Stimulation of the vagus in an isolated frog heart resulted in bradycardia, and application of the perfusate resulted in bradycardia in an unstimulated heart, with the chemical substance ("vagusstoff") later identified as acetylcholine (ACh) by Dale in the 1930s [127].

Depolarization of nerve terminals resulted in calcium influx promoting the fusion of ACh containing vesicles to the neuronal membrane and release. ACh diffuses into the synaptic cleft and binds to sino-atrial node (SAN) cell M_2 receptors coupled to

inhibitory G proteins [128]. This results in coupling via Gβγ to an inward rectifying K^+ channel and hyperpolarization of SAN cells, increasing the time taken to reach depolarization threshold. The M_2 receptor are also coupled to Ge_{i2}, which reduces adenylate cyclase activity, and therefore cAMP. This reduces I_f and PKA dependent phosphorylation of I_{CaL}, thereby reducing diastolic depolarisation and heart rate.

The role of NO has been explored with respect to the contributions of both eNOS and nNOS and downstream signalling cascades. Inhibitors of NO have been shown to block the bradycardic response to ACh [129] and prevented the decrease in I_{CaL} in adrenergically stimulated SAN cells [130]. The mechanism attributed to this effect was cGMP-dependent stimulation of PDE2 and therefore a reduction in cAMP-PKA dependent increase in I_{CaL} [130]. The role of eNOS was further explored in eNOS knockout mice where ACh was unable to decrease adrenergically stimulated I_{CaL}. However, these observations could not be replicated by other authors in the same model using muscarinic agonists [131].

The role of nNOS in the cholinergic regulation of heart rate was alluded to by experiments in which NO donors [132] or cGMP analogues [133] augmented the bradycardic response to VNS in the absence of adrenergic stimulation [134], and effect that could be attenuated by nNOS and sGC inhibitors *in vivo* and *in vitro* [135]. The nNOS knockout mouse demonstrates a higher resting heart rate [136] and impaired vagal bradycardic response *in vitro* [137], mimicking the observations of pharmacological experiments.

The site of action of nNOS derived NO may be pre-synaptic or post-synaptic to modulate vagal neurotransmission. The pre-synaptic role was suggested by the observation that NO donors [132] and inhibitors of NO and sGC [135] do not affect the response to ACh *in vitro*. In addition, application of ACh to atria from nNOS knockout mice also remains intact despite impaired vagal responses [137] and there was a blunted chronotropic response to atropine *in vivo* [136]. These observations strongly support the pre-synaptic role of nNOS derived NO rather than a direct cotransmitter function. Release of radio-labelled ACh from field stimulated atria is increased by NO donors and abolished by soluble guanylyl cyclase (sGC) inhibitors [132], further supporting the role of NO potentiating vagal neurotransmission. Transmitter release is controlled by basal activity of the pre-synaptic cAMP-PKA system, which regulates N- and P-type calcium channels. NO may augment this system by cGMP-PDE3 mediated increase in cAMP with subsequent PKA-phosphorylation of N-type calcium channels leading to an increase in ACh release (figure 1.3). These elegant experiments provide mechanistic evidence supporting an autocrine role for nNOS derived NO rather than a direct paracrine effect.

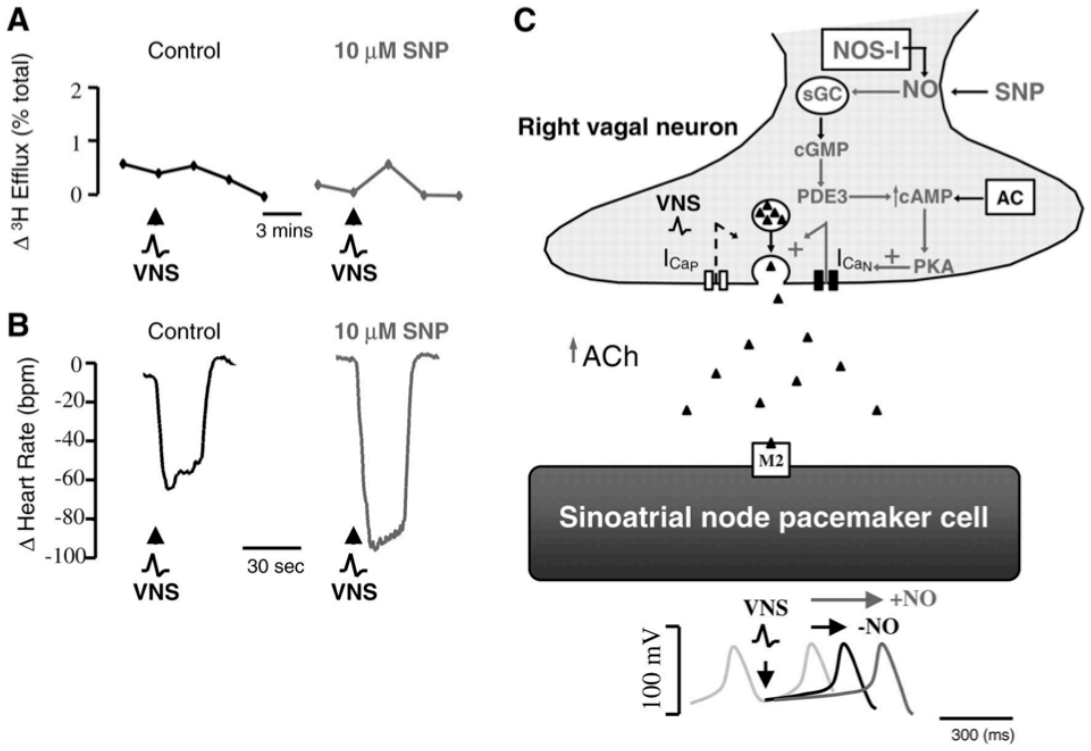


Figure 1.3 NO facilitates acetycholine release and vagal bradycardia

A. The NO donor, sodium nitroprusside (SNP) increases the release of radio-labelled ACh in response to field stimulation of atrial tissue and **B.** augments the bradycardic response to direct vagal nerve stimulation (VNS). **C.** Schematic of proposed mechanistic pathway underlying this response. Soluble guanylyl cyclase (sGC) stimulation results in increased intracellular cGMP, which may inhibit PDE3 to increase cAMP-PKA mediated phosphorylation of I_{CaN} which promotes calcium influx and exocytosis of ACh vesicles. The effect on heart rate is summarised by the lower panel showing SA node action potentials. Application of VNS in the presence of exogenous NO amplifies the rate reduction (dark grey trace) seen under baseline conditions (black trace)
Adapted from Herring et al. 2002

However Brack *et al.* [100] have recently shown that the anti-fibrillatory effect of direct VNS in the innervated, isolated rabbit heart is independent of heart rate but still dependent on NO. However, clinically the effect of heart rate reduction in improving prognosis is evidenced by the use of β-blockers and more recently I_f blockers improving outcomes in HF [138]. The mechanistic basis of the role of heart rate reduction remains unclear but is likely to involve a reduction in myocardial oxygen demand, rate dependent alterations in APD, and dispersion of refractoriness.

1.6.4 Direct effects of VNS on ventricular electrophysiology

The direct effects of VNS on ventricular electrophysiology have been studied by Ng and colleagues in a series of experiments utilising a Langendorff perfused rabbit heart with intact bilateral vagal innervation. Using a standard restitution pacing protocol (drive train with decrementing extra-stimuli), right or left VNS flattened the APD restitution curve, in keeping with the anti-arrhythmic mechanism suggested by the restitution hypothesis [139]. They further explored this anti-arrhythmic effect of VNS by determining ventricular refractoriness and VFT. Early studies in canine models undertook VFT testing [58, 59] in animals with intact circulations under anaesthesia, therefore introducing some confounding elements to the direct effect of VNS on the ventricle. The innervated model of Ng and colleagues allowed study of direct effect of VNS on the ventricle, however both efferent and retrograde afferent stimulation will take place despite transection of the cervical vagus. Vagal nerve stimulation prolongs ventricular APD and ERP [100, 139, 140], thereby flattening the APD restitution curve. This electrophysiological effect was reflected in the increased VFT seen with left or right VNS, despite differential heart rate reductions seen from either limb [94]. Furthermore, in contrast to early VNS studies, these observations were in the absence of background sympathetic stimulation (although not with co-perfusion of β-blocker) supporting a direct effect on the ventricle rather than the indirect 'accentuated' antagonism of adrenergic signalling. The pattern of ventricular repolarisation was also reversed with bilateral VNS [94], although the mechanistic or clinical relevance of this remains uncertain and requires further investigation.

Increases in ERP seen in this model and others is also likely to contribute to the anti-arrhythmic effect seen with VNS. The importance of refractoriness was first described

by Weidmann in 1952 [141]. The time course of repolarisation in purkinje fibres was studied and it was shown that membrane potential needed to return to at least -55mV following a triggered AP, before a subsequent activation could be generated. Therefore, any shortening of the refractory period would be arrhythmogenic, allowing shorter coupling and an increase in ERP without changes in conduction velocity would mechanistically protect from re-entrant arrhythmias. One caveat to be considered is that any prolongation in ERP must be homogenous, and VNS in canine models demonstrates this [142], but is not seen in the innervated rabbit heart [143]. The effect on ERP is likely to be prolongation of phase III of the action potential, and the anti-arrhythmic potential of this mechanism is supported by the efficacy of multiple anti-arrhythmic drugs effective against atrial and ventricular arrhythmias that exert the same effect including amiodarone and sotalol [144]. Lastly, uniform activation across the ventricle provides electro-mechanical synchrony, and heterogeneous APD dispersion contributes to wavebreak and re-entry around refractory regions [95]. While there is conflicting evidence of the effects of VNS on APD dispersion [142, 143], this may be considered in the context of the effects of SNS on APD dispersion, as arrhythmia is often triggered by sympathetic hyperactivity [145]. Direct SNS results in greater APD shortening at the base compared to apical regions [143], and this effect is supported by anatomical studies of sympathetic nerve distribution [146]. A proposed mechanism [104] may involve vagal inhibition of SNS mediated changes in APD dispersion, particularly in the context of HF where there is a chronic increase in sympathetic drive.

1.7 Vagal nerve stimulation and the role of NO

Historical and more recent data strongly supports the role of the cardiac vagus in exerting an anti-arrhythmic effect on the ventricle. The acute effects relate to

modulation of ventricular electrophysiology and antagonism of sympathetic signalling, whereas longer-term effects decrease inflammation and tissue heterogeneity.

The dogma of vagal or cholinergic signalling has been the release of ACh from cholinergic nerve terminals results in activation of M_2AChRs and downstream coupling to G_i, eNOS and G_k signalling cascades. G_i inhibits adenylyl cyclase and thereby reduces cAMP dependent stimulation of LTCC and PLB. M_2 dependent stimulation of eNOS activity has also been proposed as a mechanism for accentuated antagonism of beta-receptor stimulation when cAMP levels are already elevated [129, 130]. Generation of NO via this pathway may increase soluble guanylyl cyclase (sGC) generation of cGMP which may reduce cAMP levels via stimulation of phosphodiesterase 2 (PDE2) [147]. This role of this pathway is controversial [125] and many groups observe accentuated antagonism of both heart rate and contractility to be intact despite genetic deletion of eNOS [148]. M_2 receptor activation of G_k also increases I_{KAch} and other groups feel this is the main mechanism by which cholinergic accentuated antagonism is mediated [149].

The antiarrhythmic pathways by which the vagus acts has been challenged recently by Brack *et al.* [100] using the innervated, isolated, Langendorff perfused rabbit heart. Direct VNS of right or left vagus resulted in bradycardia, prolongation of APD and ERP, flattening of APD restitution and an increase in VFT independent of heart rate. The rise in VFT with VNS was surprisingly maintained in the presence of atropine and abolished with non-specific NOS inhibition. In addition, the changes in APD restitution were also abolished but interestingly, the increase in ERP remained

unaffected. The beneficial effects of VNS could be recovered by co-perfusion of L-arginine with NG-nitro-L-arginine (L-NA), due to its function as substrate for NOS competing for binding with L-NA. Brack *et al.* [100] also sought to confirm directly that VNS results in release of NO from the ventricle. Hearts were perfused with DAF-2 DA, a NO sensitive fluorescent dye and stimulation of left or right vagus resulted in an increase in fluorescence that was dependent on the intensity of stimulation. This increase in fluorescence was lost upon addition of L-NA to the perfusate in keeping with its non-specific NOS inhibition effect. However, the addition of TRIM, a putative inhibitor of nNOS, was able to abolish the increase in NO mediated fluorescence in response to VNS, while maintaining the baseline NO fluorescence that was lost in the presence of L-NA. These observations must take into account experimental limitations of both NO measurements via DAF-2DA and nNOS inhibition with TRIM. The use of DAF-2A is influenced by the presence of reactive oxygen species, divalent cations, and technical aspects of the recording spectrophotometer [150, 151]. Similarly, the specificity of TRIM is debated and its efficacy is affected by relative concentrations of L-arginine and in some studies has been shown to be less effective at nNOS inhibition than other non-specific NOS inhibitors [152-154].

In summary, these data were in agreement with the literature that VNS is anti-fibrillatory but differed in the potential mechanistic basis of this effect. The maintenance of the rise in VFT in the presence of atropine and loss with NOS inhibition implicated a wholly nitregic anti-arrhythmic effect. Moreover, the source of NO was thought to be nNOS derived given the loss of VNS induced NO in the presence of TRIM and hexamethonium. Brack *et al.* also excluded an endothelial-

based effect but demonstrating the preservation of VNS induced NO release following detergent induced endothelial denudation. Instead, they proposed the anti-fibrillatory action of the vagus was due to a paracrine, muscarinic receptor independent, action of NO via separate, nitrergic neurones within the ventricle. This 'tentative' conclusion in the author's own words [155] is supported by evidence that ACh and NO can act through parallel independent signalling pathways [136] and recent demonstration that the ventricle in many mammalian species has significant parasympathetic innervation.

Given the dual efferent and afferent vagal nerve stimulation in this preparation, I tested the hypothesis that a cholinesterase resistant analogue of acetylcholine, carbamylcholine, would also be antiarrhythmic and investigated if this action was dependent on neuronal nicotinic receptor stimulation or stimulation of myocyte muscarinic receptors.

The anatomical and mechanistic basis for the anti-arrhythmic effect of parasympathetic nerves and NO will be explored in the following section.

1.8 Vagal innervation of the ventricle

The potential for a paracrine, nitrergic, and anti-arrhythmic cardiac neural network may be supported by recent anatomical investigations that have moved away from the dogma that there is an absence of direct parasympathetic innervation of the ventricle. The parasympathetic innervation of the atria, SA node, AV node and his-purkinje conducting system is well defined [156, 157] with vagal activity resulting in bradycardia and slowing of conduction. However, there is considerable data demonstrating direct parasympathetic effects on the ventricle via excitation of clusters of ganglia on the

atrial and ventricular epicardium [158-160]. Furthermore, the ganglia exert local effects on adjacent cardiac muscle but can also influence other chambers [47].

Historical anatomical studies [161] have concluded that there was an absence of direct parasympathetic innervation of the ventricle. However, the development of newer techniques has led to the revision of these initial conclusions (figure 1.4). The immunohistochemical study of cardiac parasympathetic innervation had relied upon the thiocline method to identify AChE (acetylcholinesterase) and more recently CHAT (choline acetyltransferase) immunohistochemistry [162]. Cholinergic innervation by identification of AChE is suggestive of significant epicardial and endocardial innervation of atria and ventricles with similar staining seen in a variety of mammalian species such as mouse [163], rat [164], guinea-pig [165], dog [166], pig [167] and humans [168]. Identification of CHAT is a more reliable marker as it delineates only ACh synthesising fibres [162] and murine and rat studies have confirmed the presence of rich post-ganglionic parasympathetic innervation of the ventricular myocardium. The principle parasympathetic ganglia (sites of preganglionic nerve termination) have been shown to be variable across species [67, 158, 169], and this variation may underlie some of the variation in responses to VNS. These anatomical observations are supported by the identification of muscarinic receptors in both ventricles [170-172] and a high density of chemically identified AChE [164, 173].

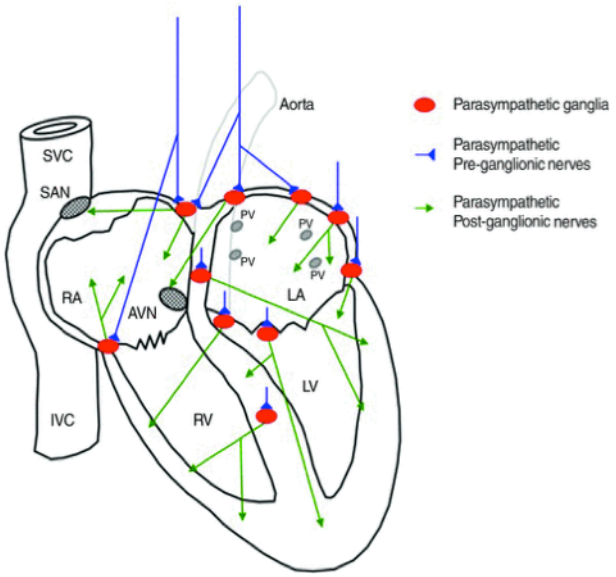


Figure 1.4 Schematic diagram of the anterior view of the heart with a summary of parasympathetic innervation

This diagram show the two vagal preganglionic nerves (blue) projecting to synapse in parasympathetic ganglia (red) that are distributed at several sites on the epicardium and within the atrial and ventricular septum. The parasympathetic postganglionic neurones send axons (green) to different regions of the heart including the conduction system and myocardium. There are also interneuron connections which are not shown on this diagram (see *Armour & Ardell, 2008).*
Adapted from Coote, 2013

1.9 Physiological effects of the vagus on the ventricle

The functional relevance of this dense network of parasympathetic innervation has been shown in a variety of physiological experiments. Microdialysis techniques have been used to demonstrate a vagal stimulation frequency dependent release of ACh from postganglionic sites in the left ventricle [174, 175], with ganglionic blockade with hexamethonium abolishing this effect [174, 175]. There are three principle mechanisms by which the terminal fibres of the vagus affect the ventricle. These include direct interaction with sympathetic nerves, direct action on the ventricular myocardium and interaction with neurones of the intrinsic cardiac plexi.

The negative inotropic effect of the vagal activity has been demonstrated in multiple species including rat [176], rabbit [177], and human [178] with the effect most marked in the

presence of sympathetic tone. The mechanism underlying this effect is thought to be a pre-junctional effect of ACh released by vagal post-ganglionic fibres on sympathetic nerves [156]. There may be contributory post-junctional mechanisms as muscarinic receptor activation increases I_{KAch} and inhibits both I_f and LTCC resulting in a lowering of heart rate and contractility [99, 179].

There are also data which indicates that the vagus is able to modulate ventricular physiology in the absence of sympathetic activity [180] with nNOS derived NO being a key effector [181] of changes including a reduction in heart rate and decreased AV conduction. The molecular basis of the pre-synaptic effect has been explored by a series of elegant experiments in guinea pig atria by Paterson's group. Depolarisation at parasympathetic nerve endings results in NO generation via nNOS which facilitates the release of ACh [132, 135, 182] and inhibits sympathetic neurotransmission [183, 184]. The release of NA is decreased via a cGMP and cAMP-dependent modulation of neuronal Ca^{2+} levels that in turn regulates exocytosis [185]. The effect of VNS on ventricular electrophysiology in the isolated, innervated rabbit heart has been described above [94, 139]. Less clear is the effect of VNS on inotropy with conflicting data in the literature in models without background sympathetic tone. Early studies were not able to demonstrate any change in contractility [186, 187] although studies in anaesthetised, *in-vivo* feline [159] and rabbit [188] heart models with β-blockade have shown a reduction in contractility. The variability is thought to be incomplete β-blockade or differential experimental stimulation of large and small vagal efferents [67], however the species variation in the distribution and density of vagal innervation may also be a contributory factor [67].

The parasympathetic and sympathetic innervation of the heart is increasingly not considered a simple relay system, but is more complex and intrinsic neurones form plexuses with connections throughout all cardiac chambers [47, 168]. Armour [47] discussed evidence that intrinsic nerves can enhance or depress parasympathetic action, but the mechanistic basis remains conjecture.

1.10 The anti-arrhythmic effects of NO

A unifying feature of cardiac-neurobiology is that NO is a critical effector with respect to autonomic modulation of ventricular mechanical and electrophysiological function. The earliest evidence of the anti-arrhythmic effect of NO was from clinical studies with nitrovasodilators. Early studies reported that nitroglycerin conferred protection against ventricular arrhythmias [189-192], although the mechanism was initially attributed to alleviation of ischaemia rather than a direct electrophysiological effect [192]. However, subsequent studies demonstrated that nitroglycerin's anti-arrhythmic effect was independent of ischaemic protection [193], and sodium nitroprusside was able to attenuate Ca^{2+} overload in isolated cardiomyocytes [194].

The mechanistic basis for the effect of NO on arrhythmogenesis was added to by studies in the 1990s following the development of specific NOS inhibitors. Studies continued to use the ischaemia or ischaemia-reperfusion paradigm to study the anti-arrhythmic effect of NO and demonstrated that non-specific NOS inhibition with L-NAME was able to attenuate the protective effects of ischaemic preconditioning [195] and increase the incidence of VF in isolated rate hearts post ischaemia-reperfusion (I/R) [196]. The majority of experimental studies have supported the anti-arrhythmic role of NO, and furthermore have implicated NO as a downstream mediator of the anti-arrhythmic action of other humoral agents such as oestrogen [197, 198] and

erythropoietin [199]. However, there are conflicting data from isolated heart experiments where NO donors or NOS inhibition had no influence on I/R induced arrhythmia [200, 201] with the lack of effect attributed to the absence of neuro-humoral activity in isolated heart models.

The observations from pharmacological studies have been further developed by the use of transgenic murine models. Knockout of eNOS ($eNOS^{-/-}$) has been shown to confer a pro-arrhythmic effect in isolated cardiomyocytes and *in vivo*. Cardiomyocytes from $eNOS^{-/-}$ and control animals were exposed to oubain and $eNOS^{-/-}$ cells demonstrated increased arrhythmic activity [202] and *in vivo* experiments demonstrated increased digoxin induced ventricular arrhythmia in $eNOS^{-/-}$ hearts [203]. In the converse experiment, cardiomyocytes with eNOS overexpression had reduced spontaneous arrhythmic activity [204], therefore supporting a role for eNOS in murine models of arrhythmia.

Brack *et al.* [100] implicated nNOS as the source of NO exerting the anti-arrhythmic effect in the isolated rabbit heart. This observation is supported by cardiomyocyte experiments from $nNOS^{-/-}$, $eNOS^{-/-}$ and double eNOS/nNOS knockout mice. These experiments indicated that NO prevents diastolic Ca^{2+} elevations and spontaneous arrhythmic activity [205], although spontaneous arrhythmic activity was a feature of $nNOS^{-/-}$ or double knockout, suggesting no role for eNOS derived NO in this model [205]. Burger *et al.* [206] generated a global $nNOS^{-/-}$ mouse and this too demonstrated increased ventricular arrhythmia in the setting of myocardial infarction or ischaemia-reperfusion (I/R) injury. However, given the global deletion, the site of nNOS derived action can not be ascertained given its critical role in modulation of neurotransmission

[125, 132, 135, 207] and in myocyte function [208, 209]. In a murine model of nNOS overexpression, Ca_i and adrenergic responses were diminished [210], indicating that nNOS derived NO confers anti-arrhythmic physiological changes, but the critical site of action remains unclear. Finally, there is no evidence that iNOS derived NO contributes to a reduction in arrhythmia. Mice overexpressing iNOS were found to have increased mortality and a high incidence of sudden cardiac death as a result of increased oxidative stress rather than NO [211-214]. I investigated whether any antiarrhythmic action of an acetylcholine analogue was linked to generation of NO from either eNOS or nNOS and also attempted to locate the source of NO as being neuronal or myocyte.

1.10.1 NO mediated anti-arrhythmic effects - mechanisms

Nitric oxide exerts pleiotropic effects within the cardiovascular system and its anti-arrhythmic effect is across multiple domains shown in figure 1.5 below. The key effects on cardiac electrophysiology will be discussed below.

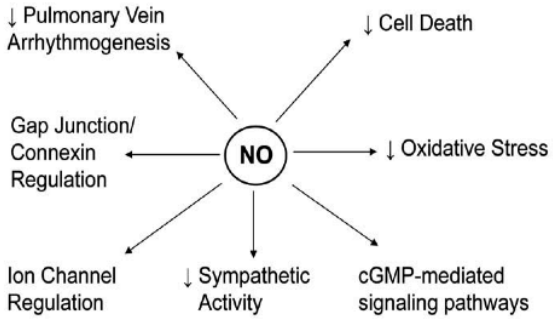


Figure 1.5 Putative mechanisms by which NO mediates protection against cardiac fibrillation

Adapted from Burger & Feng, 2013

1.10.2 Ion channel regulation and electrophysiological effects

In cardiomyocytes, NOS enzymes are expressed in distinct subcellular compartments and generate NO that then effects highly specific targets to exert varying and in some cases, opposite effects on cardiac function [215-217]. Endothelial NOS is localised in caveolae of the sarcolemma and T-tubuli, SR and might also be present in mitochondria [128, 215, 218]. Neuronal NOS is expressed more widely including cardiomyocytes, cardiac autonomic nerves and intracardiac ganglia. In cardiomyocytes, nNOS is localised in the SR, sarcolemma and might also be present in mitochondria [209].

The biological effect of NO is mediated via cGMP and cGMP-independent signalling pathways. Activation of cGMP results in modulation of the activity of cGMP-protein kinase (PKG) and cGMP-regulated phosphodiesterases (PDEs) [219]. The opposing downstream effects can be explained by variable effects of PDEs, including PDE2 enhanced cAMP breakdown and PDE3 stimulated increases in cAMP. These PDE effects are tissue and species specific and therefore may account for the variable actions of the NO-GC-cGMP pathway on cardiac ion channels [220]. NO also regulates cardiac ion channel function via s-nitrosylation (SNO), a ubiquitous post-translational modification system [221]. The figure below summaries the variable effects of NO on cardiac ion channels and the effects on critical Ca^{2+} and repolarising currents will be discussed in detail below.

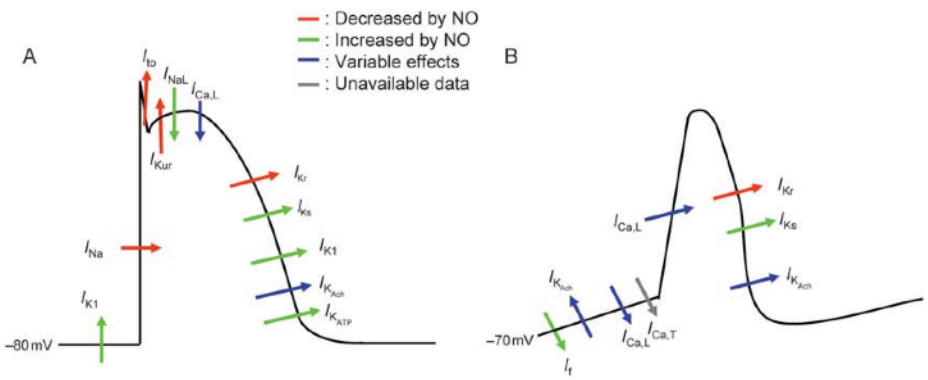


Figure 1.6 Electrophysiological effects of NO on (A) atrial and ventricular cells and (B) sino-atrial node currents which contribute to the action potential
Arrows indicate the ion movement direction, whereas colours indicate increase (green), decrease (red) or variable effects (blue) of NO

Adapted from Tamargo et al. *2010*

Following depolarisation, the AP plateau is generated by Ca^{2+} entry via the LTCC and subsequently by CICR via opening of the RyR_2 and maintained by Ca^{2+} removal by the electrogenic NCX. Studies to date have demonstrated variable NO mediated effects on LTCC in cardiomyocytes, including an increase in I_{Ca} via cGMP-inhibited PDE3 and cAMP increase [222-224] or via cAMP independent activation of PKG [222]. The LTCC and SR calcium channels are also subject to SNO, particularly following adrenergic stimulation [225] or I/R injury with resulting reductions in I_{Ca} [226] and SR Ca^{2+} loading. These modifications represent important cardio-protective mechanisms in the setting of cardiovascular disease. nNOS-derived NO is thought to mediate SNO of the LTCC [208, 210] and this is evidenced by $nNOS^{-/-}$ cardiomyocytes exhibiting higher LTCC activity [210]. Muscarinic activation of eNOS is thought to mediate the anti-adrenergic effect of NO on I_{Ca} via activation of cGMP-stimulated PDE2 [130, 227] and PKG via a pertussis toxin sensitive G_i protein that inhibits adenylate cyclase (AC) activity [228]. However, as discussed previously, this observation remains controversial [229] as not all studies replicated this effect.

Cardiac K^+ channels determine resting membrane potential and importantly APD, and therefore their modulation has an important role in the anti-arrhythmic effect of NO.

The rapidly activating delayed rectifier current (I_{Kr}) is largely responsible for repolarisation during phase 2 and 3 of the AP, therefore is critical in determining APD and refractoriness. NO donors inhibit I_{Kr} and this effect is thought to be due to interactions with ROS rather than a cGMP-PKG pathway [230]. The slowly activating delayed rectifier current (I_{Ks}) determines late repolarisation and is the main determinant of rate dependent APD shortening [220]. With increasing heart rate, these channels have less time to deactivate resulting in an accumulation of open channels, thereby increasing the rate of repolarisation [231]. NO donors enhance this effect via SNO [232, 233] and this mechanism may play a role in APD shortening in response to adrenergic stimulation or increases in Ca_i.

The inward rectifier current (I_{K1}) stabilises resting membrane potential and determines the shape of phase 3 of the AP. NO accelerates closing kinetics of this current [234] and this effect is also SNO mediated and results in marked shortening of the AP in mouse and human atrial cells and is important in the pathogenesis of chronic atrial fibrillation [235]. The acetylcholine activated current (I_{KAch}) also influences RMP, shortens APD [231] and NO produces M_2AChR-dependent activation of a cGMP-independent $G_{i/o}$ protein which opens these channels [236]. The ATP sensitive K^+ channels (I_{KATP}) in the sarcolemma and mitochondria couple cell metabolism to membrane potential and is enhanced by NO donors via a cGMP-PKG mediated pathway [237, 238]. The physiological relevance of this modulation is most evident in

cardiac ischaemic preconditioning which may have contributions from iNOS derived NO amongst other mechanisms [239].

Calcium release from the SR by the RyR_2 is a key process in excitation-contraction coupling. In rat ventricular myocytes, the SNO modification by NO on RyR_2 is dependent upon the level of t-adrenergic stimulation [240]. In the presence of high dose isoproterenol, NO decreases spontaneous Ca^{2+} sparks [240]. This is particularly relevant in HF where sympathetic activation is pronounced and RyR_2 are hyperphosphorylated and NO production is increased [215]. The NO mediated modification is nNOS dependent as the RyR_2 colocalise with nNOS in cardiomyocytes [217] and $nNOS^{-/-}$ results in hypo-SNO of the RyR_2.

Therefore, it is clear that NO modulates multiple ion channels via either a cGMP or SNO mediated mechanism to confer an anti-arrhythmic effect. The relative contributions of eNOS and nNOS remain under investigation, but current data would suggest that cardiomyocyte nNOS derived NO mediates key effects on K^+ and Ca^{2+} channels via SNO. However, no clear receptor based mechanism coupled to cardiomyocyte nNOS has been identified, and in particular nNOS activity in cholinergic neurons may modify upstream neurotransmission and influence M_2AChR-eNOS coupling and therefore downstream cGMP-PKG mediated effects. I sought to investigate therefore the source of NO generation by an acetylcholine analogue and the isoform by which this production was dependent. I also investigated if an NO donor could mimic the action of acetylcholine and whether this was also dependent on muscarinic receptor stimulation.

1.10.3 Cyclic GMP signalling pathways

Cyclic GMP is the common downstream effector pathway of NO and has been implicated in mediating its anti-arrhythmic effect. The site of effect may be at the level of the myocyte or pre-synaptically with its action on the vagal and sympathetic innervation of the heart and these are discussed above in this chapter.

1.10.4 Gap junction regulation

Connexin 43 (Cx43) is a major component of ventricular gap junctions and its loss is associated with significant increase in ventricular arrhythmia and sudden cardiac death [241-243]. Vagal nerve stimulation has been demonstrated to preserve Cx43 in HF models [101, 102] and therefore prevents heterogeneity in activation. Nitric oxide has also been shown to exert a protective effect in this respect. The NO donor, SNP has been shown to reduce I/R arrhythmia in a canine model with preservation of Cx43 phosphorylation and gap junction permeability. However, the effect on Cx43 may be isoform specific as iNOS derived NO decreased myocardial Cx43 expression [244].

1.10.5 Oxidative stress and cell injury

Physiological NO production has been shown to inhibit reactive oxygen species (ROS) production [245-247] whereas excess activation, for example by iNOS, is associated with increased arrhythmia and sudden cardiac death via a ROS mediated mechanism [248]. Furthermore, preconditioning mediated protection from arrhythmia in a canine model was linked to NO mediated reductions in superoxide production [249]. Nitric oxide at physiological levels also prevents apoptotic cell death [250] and therefore may prevent the development of tissue heterogeneity and scar, thereby preserving conduction and decreasing the risk of arrhythmia [251].

1.10.6 NO and autonomic ganglia

The augmentation of parasympathetic neurotransmission and accompanying reduction in NA release via NOS derived NO has been described above. Targeted nNOS overexpression in a guinea pig model of myocardial infarction was also shown to have favourable effects on autonomic neurotransmission and reduce post infarct mortality [252]. Gene transfer of an adenovirus vector containing nNOS into the vagal trunk or right atrial wall results in augmented vagally mediated bradycardia [253] and decreased responses to sympathetic stimulation [254]. In guinea-pigs with coronary ligation induced MI, ACh release from field stimulated atria 3 days post-MI is significantly impaired and mechanistically linked to reduced NOS activity and cGMP levels [252]. Adenoviral nNOS gene transfer in this model improved parasympathetic neurotransmission and is also associated with a significant reduction in mortality. The site of action of nNOS derived NO is uncertain and may be related to improved autonomic balance or augmented myocardial nNOS signalling. Nevertheless, these studies provide further evidence of the anti-arrhythmic effects of NO.

1.11 Sympatho-vagal crosstalk

The sections above have described the negative prognostic influence of sympatho-vagal imbalance that is seen in cardiovascular disease. In keeping with these observations, large outcome studies in patients have described excessive adrenergic activity as a negative prognostic indicator post myocardial infarction [15, 255] and during congestive cardiac failure [16, 256]. Furthermore, increased sympathetic activity is correlated with the development of hypertensive left ventricular hypertrophy [257], which is also an independent predictor of morbidity and mortality [258].

The cardiac vagus opposes the deleterious changes associated with sympathetic hyperactivity by reducing heart rate and preventing intracellular calcium overload [94, 145]. High vagal tone and direct vagal nerve stimulation have also been shown to raise the threshold for ventricular fibrillation [140, 145, 259]. Improvement in vagal tone through exercise [260] or via gene transfer of nNOS into sympathetic neurons [252] protects against mortality. In contrast, impaired sympathovagal balance is a feature of patients with HF [15] and hypertension [261]. Therefore the cardiac vagus would seem an attractive target for therapy but historically has been challenging to target pharmacologically. Emerging data supported the impact of direct vagal nerve stimulators in HF [48] but larger, randomised controlled trials that have reported to date have been less impressive with no benefits seen during early follow up [49, 50].

Therefore existing therapies have focused on targeting the sympatho-adrenal axis with considerable clinical trial evidence demonstrating the efficacy of beta-blockers and ACE inhibitors in cardiovascular disease [18, 21, 262, 263]. Despite their introduction over 50 years ago, beta-blockers remain the only anti-arrhythmic drug proven to reduce mortality after myocardial infarction and in congestive cardiac failure [21, 262]. Recently, the SHIFT trial [138] demonstrated that ivabradine, an I_f channel blocker decreased cardiovascular death and hospital admissions in patients with HF, but it has not been studied in the context of myocardial infarction. Despite the considerable benefit seen with beta-blockers and ACE inhibitors post myocardial infarction and in HF, a significant mortality remains in this patient group with over 70,000 sudden cardiac deaths annually in the UK alone [264].

Therefore the search for future therapies may lie away from ion channel based therapies directed at the end organ or complex device interventions on the cardiac vagus. Work from the Herring lab has highlighted the role of sympathetic cotransmitters and sympathovagal crosstalk and these mechanisms may potentially provide opportunities for antiarrhythmic targets that can be combined with the current regime of optimal medical and device treatment [265, 266].

The concept of cotransmission was first suggested by Burnstock in 1976 [267] with the idea that nerve cells may release more than one functional neurotransmitter with distinct targets. This contrasted with the prevailing hypothesis at the time, which was Dale's principle that nerves of the same class utilised one neurotransmitter [268]. These opposing views were redefined by Sir John Eccles [269] to state that 'at all the axonal branches of a neuron, there is liberation of the same transmitter substance or substances'. The release of cotransmitters requires high-level neuronal stimulation, where they act as slowly diffusing molecules. Therefore they have a longer biological half-life than the principle neurotransmitter, with the notable exception being ATP which is rapidly metabolised [270]. Cross talk within the central nervous system is a well-described modulator of neural activity [271-274] and recent evidence has alluded to the importance of this mechanism for autonomic control of cardiac function.

Cardiac sympathovagal crosstalk was first observed by Potter [275] who described a long lasting inhibition of cardiac vagal function *in vivo* following high level sympathetic stimulation in the presence of a β-blocker. This observation cannot be replicated *in vitro* by application of exogenous neurotransmitters but is seen following direct stimulation of the nerves involved [266]. This suggests that interneuronal

signalling is responsible rather than a mechanism convergent at the level of the myocyte. This feature may be responsible for a comment in the ATRAMI study that the reduction in vagal activity in patients with myocardial infarction is almost always accompanied by an increase in sympathetic activity [15].

1.12 Transmitter release during sympathetic nerve stimulation

1.12.1 NA and ATP

The sympathetic co-transmitters implicated in this interneuronal crosstalk include ATP, neuropeptide Y (NPY) and galanin [266, 276-278]. NA is not thought to directly influence the release of ACh, however a brief inhibitory effect has been reported in rat atrial tissue utilising α-adrenoceptors. In addition, ATP has not been shown to modulate ACh release in the human or guinea pig heart [279, 280].

1.12.2 Galanin and Neuropeptide Y

Galanin is a 29 amino acid peptide originally isolated from the porcine gut [281]. Immunohistochemical and *in situ* hybridisation techniques have demonstrated galanin and its receptor to be present and widely distributed in the central and peripheral nervous system of mammals [282]. This pattern points to its wide functional role in learning and memory, pain, neuroendocrine and cardiovascular control [266, 283]. Galanin has been shown to be involved in central regulation of the cardiovascular system at the level of the brainstem and can also act as a vasoactive substance [284]. These effects are mediated via 3 receptors, and knockout of the $GalR_1$ receptor prevents the attenuation of vagal induced bradycardia post sympathetic nerve stimulation in the mouse [280, 285]. Galanin has also been shown to be released from the liver and gut under conditions of high sympathetic stimulation [286, 287]. Exogenous galanin applied to an *in vitro* guinea pig atrial preparation with an intact vagus nerve

decreased the bradycardic effect of direct VNS, but not of the ACh analogue, carbamylcholine [266]. Furthermore, galanin also decreased the release of tritiated ACh in response to VNS, and these effects could be abolished by $GalR_1$ receptor and protein kinase C (PKC) inhibition [266].

Neuropeptide Y is a 36 amino acid peptide that was first isolated from the porcine brain [288] and is the most abundant cardiac neuropeptide having been first identified in intramural sympathetic nerves in close association with myocytes and coronary vessels [289]. In addition to its function as a neuromodulator, there is evidence implicating a role in the development and progression of hypertension [290, 291] and left ventricular hypertrophy [290]. There is also direct and indirect evidence demonstrating an important role for NPY in the context of coronary artery disease and myocardial infarction. NPY gene polymorphisms are associated with an increased risk of premature atherosclerosis [292], and NPY exerts an influence on angiogenesis and vascular remodelling via the Y_2 and Y_5 receptor. Animal studies of experimental myocardial infarction demonstrated release of NPY from cardiac sympathetic nerves [293] and historical clinical studies have shown that NPY levels are elevated following acute coronary syndromes and correlate positively with the severity of HF and one year mortality [294, 295]. These observations have been replicated in a more contemporary study in the setting of primary percutaneous coronary intervention for the treatment of myocardial infarction [296]. Plasma NPY levels were measured in patients presenting with ST elevation myocardial infarction (STEMI) and found to be significantly elevated from presentation and remained significantly higher at 48 hours in patients with no angiographic reflow [296]. Levels of NPY were also closely correlated to microvascular resistance, persistent ST elevation and size of MI assessed

by troponin elevation in keeping with the persisting nature of sympathetic hyperactivity in this context.

Levels of sympathetic stimulation that impair vagal function have been shown to release NPY into the perfusate of isolated atria *in vitro* [265] as well as coronary sinus samples *in vivo* [297]. Under similar experimental conditions, the release of galanin has been observed but at lower concentrations than NPY [266]. Antagonism of the Y_2 receptor (on presynaptic cholinergic neurons) can abolish this effect [265] as can genetic knockout of this receptor [298]. A potential confounder is that all these experiments are performed in the presence of β-blockade, and these drugs may inhibit the release of NE or NPY. However, given the strong evidence base for β-blocker use post-myocardial infarction and in HF, the study of crosstalk physiology with concomitant β-blockade is important.

The anatomical basis for this potential role in sympatho-vagal crosstalk is provided by demonstration of Y_2 receptor presence by immunohistochemistry on cholinergic vagal neurons and around the sino-atrial node [265] and, Y_1 receptor mRNA has been shown in myocyte from rats [299] and humans [300]. The application of exogenous NPY to an atrial preparation can reduce the response to direct vagal stimulation while having no effect on the response to the stable ACh analogue, carbamylcholine[265]. Furthermore, NPY also decreases the release of tritiated ACh following direct vagal nerve stimulation [265]. This response has also been demonstrated *in vivo* following intravenous administration of NPY and assessing vagal bradycardia [301, 302], although these observations may be influenced by changes in haemodynamic and circulating factors [302, 303]. The mechanism of this effect was explored using an atrial preparation

with intact vagal innervation [266]. Inhibitors of PKC were able to completely abolish the effect of exogenous NPY, while protein kinase A inhibitors had no effect. The mechanistic role of PKC was confirmed by application of a PKC activator which replicated these effects with reduced tritiated ACh release [266]. The exact mechanism linking the downstream messenger systems involving the response of these two neuropeptide co-transmitters have not yet been elucidated, but the observations to date further support a complex interaction of neurotransmitters at the pre-synaptic and end organ level in the modulation of cardiac physiology and electrophysiology.

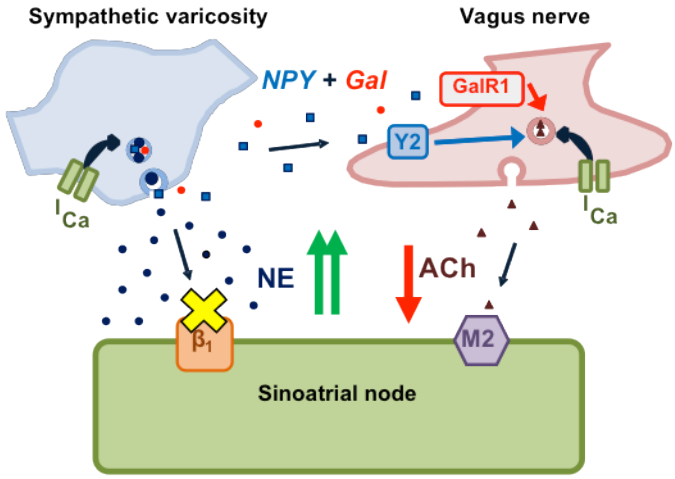


Figure 1.7 Cardiac sympatho-vagal crosstalk

Schematic of sympathetic co-transmission of NPY and galanin and the effects on cardiac vagal function. NPY and galanin are released following high level sympathetic stimulation. NPY acts via the Y_2receptor and Galanin via the GalR1 receptor to decrease the release of ACh from pre-synaptic, vagal neurones.
Adapted from Herring et al. 2008 and 2013

Interestingly NPY may also act directly to influence cardiac myocyte electrophysiology although these action appear complex, with contrasting observations in the literature, possibly due to differences in experimental protocols with and without concomitant application of β-blockers. Neuropeptide Y does not appear to affect the voltage-gated sodium (I_{Na}) current or the delayed rectifier

potassium current (I_K) [304] but can decrease the transient outward potassium current (I_{to}) via an inhibitory G-protein coupled pathway [305]. Its effect on the L-type calcium current (I_{CaL}) appears to be species specific, with inhibition and consequent negative inotropy seen in the guinea pig [306], while stimulation of this current is reported in the rat [307]. This effect on I_{CaL} is also reflected in data demonstrating increased cell shortening and the size of calcium transients in isolated rat myocytes via a Y_1 receptor dependent pathway coupled to activation of phospholipase C [308]. These observations suggest NPY could potentially play a role in arrhythmogenesis given that the higher levels of NPY are seen in the clinical context of high sympathetic drive and it can have direct effects on electrophysiology. I therefore sought to investigate whether endogenous NPY released during cardiac sympathetic nerve stimulation in the presence of a beta-blocker, or exogenous NPY lowers ventricular fibrillation threshold. I also sought to identify the NPY receptor(s) responsible for this effect as a potential novel anti-arrhythmic drug target.

1.13 Tetrahydrobiopterin: a molecular component of autonomic regulation?

Tetrahydrobiopterin (BH4) is a key cofactor for enzymes involved in multiple physiological systems including development, cardiovascular physiology (NOS), neurotransmitter synthesis (tyrosine hydroxylase) and inflammatory cascades. BH_4 is generated *de novo* from GTP by the step-wise action of 3 enzymes, with the rate-limiting step catalysed by GTP cyclohydrolase 1 (GTPCH) encoded by *GCH1* [309]. The biochemical cascade of BH_4 generation is shown below (figure 1.8).

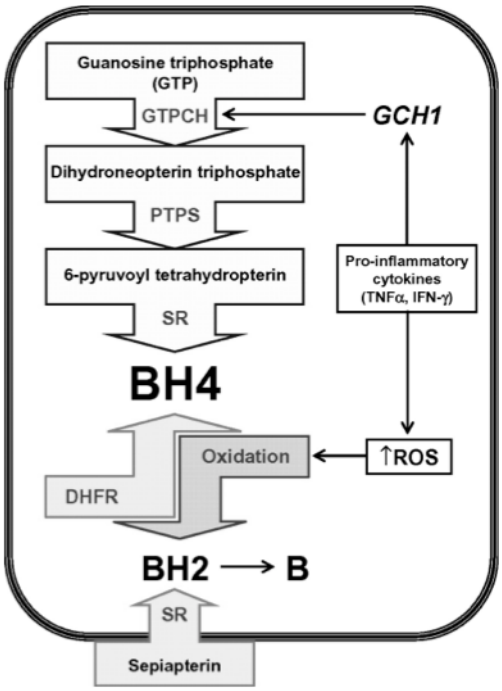


Figure 1.8 Tetrahydrobiopterin biosynthesis and metabolism

De novo BH4 synthesis occurs from the substrate GTP via a three-step enzymatic pathway. GTPCH, encoded by the GCH1 gene, is the rate- limiting enzyme under normal conditions. BH4 is susceptible to oxidation by reactive oxygen species, forming BH2 and ultimately B. Stimulation by inflammatory cytokines can upregulate GCH1 and increase BH4 synthesis; however, inflammation can also lead to oxidative loss of BH4 via increased production of reactive oxygen species. Synthesis of BH4 is also possible through the 'salvage pathway' from the exogenous synthetic pterin, sepiapterin, which is metabolised first to BH2 by SR and then to BH4 by DHFR. B, biopterin; BH2, dihydrobiopterin; BH4, tetrahydrobiopterin; DHFR, dihydrofolate reductase; GTPCH, GTP cyclohydrolase-1; IFNγ, interferon γ; PTPS, 6-pyruvoyl-tetrahydropterin synthase; ROS, reactive oxygen species; SR, sepiapterin reductase; TNFα, tumour necrosis factor α.
Adapted from Cunnington et al. 2010

BH4 plays a critical role in the function of nitric oxide synthase (NOS) enzymes by increasing the affinity for arginine based ligands [310, 311] and contributing to dimer stabilisation [312] and therefore BH4 is a key molecule in the maintenance of blood pressure and vascular function (figure 1.9). Common cardiovascular conditions such as hypertension, atherosclerosis and diabetes are characterised by endothelial dysfunction and impaired endothelial dependent vasodilatation [313] and mechanistic studies have provided evidence demonstrating that *GCH1* expression is a critical determinant of endothelial cell BH4 level and NOS function [314, 315]. In addition,

overexpression of *GCH1* improves endothelial function in murine models of vascular disease such as pulmonary hypertension [316], diabetes [317], and atherosclerosis [318].

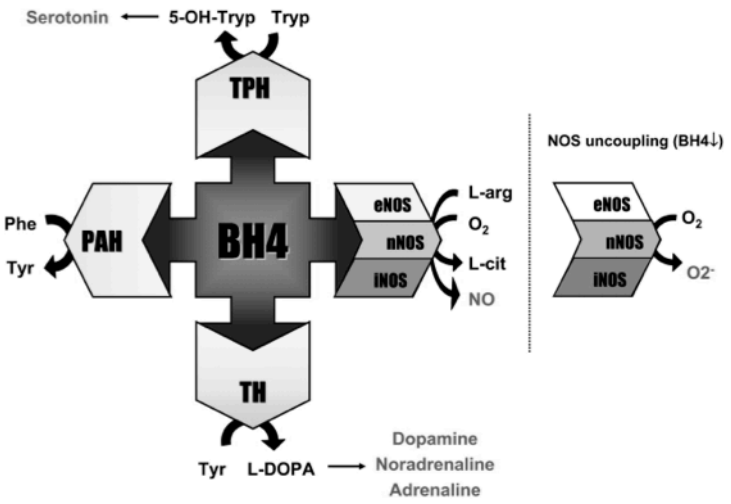


Figure 1.9 Enzyme cofactor activity of tetrahydrobiopterin

De novo BH4 synthesis occurs from the substrate GTP via a three-step enzymatic pathway. GTPCH, encoded by the GCH1 gene, is the rate- limiting enzyme under normal conditions. BH4 is susceptible to oxidation by reactive oxygen species, forming BH2 and ultimately B. Stimulation by inflammatory cytokines can upregulate GCH1 and increase BH4 synthesis; however, inflammation can also lead to oxidative loss of BH4 via increased production of reactive oxygen species. Synthesis of BH4 is also possible through the 'salvage pathway' from the exogenous synthetic pterin, sepiapterin, which is metabolised first to BH2 by SR and then to BH4 by DHFR. B, biopterin; BH2, dihydrobiopterin; BH4, tetrahydrobiopterin; DHFR, dihydrofolate reductase; GTPCH, GTP cyclohydrolase-1; IFNγ, interferon γ; PTPS, 6-pyruvoyl-tetrahydropterin synthase; ROS, reactive oxygen species; SR, sepiapterin reductase; TNFα, tumour necrosis factor α.
Adapted from Cunnington et al. 2010

1.13.1 BH4 and vascular function

The role of BH4 in the vascular system has been extensively studied and its therapeutic role continues to be the subject of study. Regulation of blood pressure and vascular tone is critical for the maintenance of organ perfusion and dysregulation contributes to adverse cardiovascular outcomes [319]. Endothelial dysfunction is the hallmark of multiple disease states such as diabetes, atherosclerosis, and hypertension. These conditions are characterised by impaired endothelial dependent vasodilatation [313]. Therefore, given the key role of BH4 in NOS function, a reduction in BH4

bioavailability is associated with reduced NO generation and altered endothelial function. This has been supported by experimental studies in a variety of models. The X haplotype in patients with coronary disease is defined by 3 SNPs in the *GCH1* gene and is associated with lower plasma BH4 with resulting increased superoxide and reduced endothelial dependent vasodilatation in venous segments [320]. In animal models, pharmacological inhibition leads to an increase in blood pressure which could be reversed with BH4 or its precursor sepiapterin [321]. Until recently, there were few genetic models to study these vascular effects and existing data in the hph-1 mouse (which has moderate reductions in total BH4) were conflicting in terms of the effects on blood pressure [322, 323]. In the converse experimental model, overexpression of *GCH1I* results in elevated BH4 levels and eNOS activity [324], and in the setting of vascular disease shows reduced ROS production [323]. However, recent data where *GCH1* was genomically deleted in endothelial cells confirmed the critical role of BH_4 in the maintenance of vascular tone and blood pressure [325].

1.13.2 BH4 as a therapeutic tool

In view of human and experimental data demonstrating the importance of BH4 in vascular function, its clinical utility as a therapy has been extensively studied. Treatment with BH4 results in reversal of the disease associated redox imbalance seen with BH4 deficiency [319] in animal models and human studies. Chronic BH4 treatment reduces angiotensin-II induced hypertension and endothelial dysfunction [326, 327] and decreases blood pressure in the spontaneously hypertensive rat [328]. In other models such as the $ApoE^{-/-}$ mouse that develops premature atherosclerosis, BH4 treatment did not reduce blood pressure, although endothelial function was improved [329].

The importance of BH4 to human vascular function has been demonstrated in human studies where BH4 supplementation improved vascular function in normal subjects and those with vascular disease such as smokers and patients with diabetes [330-337]. There is evidence that points to both acute and chronic treatment effects in patients with cardiovascular disease. Coronary infusions of BH4 in patients with coronary artery disease [338, 339], HF [340] and angina [338] improved the ability to vasodilate in response to ACh. Similarly, brachial artery infusions or oral supplementation had marked positive effects on endothelial dependent vasodilation [330, 331]. These effects may have some confounders including the supra-physiological levels of BH4 used that would have had anti-oxidant effects as well the effects on NOS function. Another limitation of these trials was the relatively short-lived effect of BH4 and therefore chronic administration has been tested in trials. Initial studies demonstrated favourable effects on blood pressure reduction [341] and endothelial dependent vasodilatation [342] but a more recent randomised controlled trial did not show any difference between BH4 treatment and control groups [343]. This study alluded the potential differences in the regulation of plasma and vascular BH4 and the importance of BH4:BH2 ratio rather than total BH4 levels alone.

1.13.3 Cardiac role of BH4

The cardiac role of BH4 has been studied in the context of recent studies that have identified endogenous nitric oxide (NO) generation by myocytes [129]. Endothelial NOS (eNOS) has been localised in coronary and endocardial endothelial cells and cardiomyocytes and neuronal NOS (nNOS) is found in the cardiomyocyte, autonomic nerves and ganglia [344, 345]. Activation of these enzymes leads to different responses as a consequence of distinct subcellular localisation [344-346] and the short diffusion

distance of NO within the cardiomyocyte as a consequence of myoglobin's affinity for NO and interaction with superoxide [183, 208, 347]. Recent evidence has shown that nNOS derived NO plays a critical role in maintaining basal NO production [348] and therefore some of the beneficial effects of BH4 may be myocyte rather than endothelial in origin.

The downstream effects of NO generation are dependent upon activation of soluble sGC and generation of cyclic guanosine monophosphate (cGMP). This results in intracellular cGMP accumulation and reduction in myofilament Ca^{2+} sensitivity and decreased contractility [349-351]. Recent data has suggested that the action of NO on ion channel activity and therefore its electrophysiological effect is independent of sGC and utilises s-nitrosylation (S-NO). Targets of S-NO include the RyR_2 [352, 353], SERCA [225] and the LTCC [226, 354] . There is data however, which also supports a cGMP/PKG mediated inhibition of LTCC activity [351].

1.13.4 BH4 and autonomic function

Ion channel and myofilament Ca^{2+} sensitivity are physiological processes that will affect heart rate and contractility and these parameters are also under autonomic control. Previous sections have discussed in detail the changes in autonomic function seen in cardiovascular conditions such as HF and following myocardial infarction. Large, prospective clinical studies have demonstrated that a shift towards sympathetic hyperactivity and the resulting impairment of heart rate variability and baroreceptor sensitivity independently predict mortality (UK-HEART, ATRAMI) [15, 16]. Mechanistically these changes are linked to NO which regulates sympathetic and

vagal control [355], with loss of NO mediated potentiation and inhibition of vagal and sympathetic outflow respectively [132, 182, 356, 357].

Given the critical role of BH4 in the synthesis of NO and catecholamines, it is likely that it would play a mechanistic role in modulating cardiac autonomic function. A recent study [358] investigated the impact of a common genetic variant in *GCH1* on autonomic function in humans. The C+243T SNP, discussed earlier in the context of its association with increased blood pressure and decreased levels of NO, was found in this study to be predictive of reduced urinary catecholamine excretion, reduced NO production and associated with decreased baroreflex sensitivity and heart rate variability. However, this study did not measure BH4 levels in the population studied. However, the X haplotype [320] with which this SNP is in tight linkage disequilibrium is associated with low BH4 levels, and therefore this may indicate that the observed effect was BH4 mediated.

Patients with mutations in *GCH1* can present with a rare movement disorder, DOPA-responsive dystonia (DRD) [359]. Mayahi *et al.* [360] assessed endothelial, sympathetic and cardiac function in 16 patients with DRD due to heterogeneous mutations in the *GCH1* gene. These patients demonstrated a high resting heart rate, low plasma catecholamines but otherwise unaffected flow mediated dilatation and intact autonomic and cardiac responses to sympathetic stimulation. The increase in heart rate was mechanistically attributed to a reduction in vagal drive rather than a specific sympatho-adrenal effect in this population given the reduction in plasma catecholamines seen.

1.13.5 Models of BH4 deficiency and autonomic dysfunction

Targeted disruption of the enzymes required for the generation of BH4 or catecholamines result in markedly adverse phenotypes precluding the long-term study of cardiac autonomic function. These models are summarised in the table below. The hph-1 mouse also demonstrates changes in the autonomic regulation of heart rate. In the setting of BH4 deficiency in this model, a resting tachycardia was demonstrated which persisted despite exercise training while blood pressure and heart rates were normal during exercise [361]. Mechanistically, this was linked to increased β-adrenergic receptor sensitivity to catecholamines while vagal function was unaffected. This observation reflected similar findings in patients with BH4 deficiency including those with a marked neurological presentation with dopa-responsive dystonia or individuals with no overt phenotype but carry the C+243T polymorphism [360], although via a different mechanism. Given the role for BH4 as a key co-factor for NA synthesis and NO production, I sought to investigate its role in sympathetic neurons by developing a novel mouse model where the gene encoding GTPCH, *Gch1* (murine gene) was deleted in sympathetic, TH expressing cells with the aim of undertaking cardiovascular phenotyping and determine if there was any influence on autonomic function.

Knockout model	Effect
GTPCH [362]	• Embryonically lethal • Survival rates: E9.5=100%, E12.5=25%, Term=0% • No major histological abnormalities • No rescue with BH4 (via sepiapterin) supplementation
Sepiapterin reductase [363]	• Viable and can survive for several weeks with marked growth retardation • Mechanism of viability thought to be alternative SPR pathways via aldoketoreductases and carbonyl reductases • Reduced TH protein in nerve terminals, brain>adrenals
6-pyruvoltetrahydrobiopterin synthase [364]	• Die shortly after birth • Reduced TH immunoreactivity seen in dopaminergic projections to caudate putamen and nucleus accumbens
HPH [361]	• Viable with normal growth • 80-90% reduction in BH4 levels • Phenotypic features include hypertension, pulmonary hypertension and tachycardia
Tyrosine hydroxylase [365]	• Essentially embryonically lethal (2.6% born) • Vascular congestion, dilated atria, myocyte heterogeneity • Bradycardia at E12.5 • 100% rescue with L-DOPA • Partial rescue with DOPS (cannot be converted to NA)
Neuronal NOS [137, 366]	• Paucity of nNOS in cardiac post-ganglionic sympathetic fibres and limited nNOS/TH colocalisation in WT animals • Attenuated response to applied NA indicates post-synaptic neuronal NO does not modulate SAN pacemaking in mice • Peripheral vagal control of HR is impaired despite intact downstream signaling

Table 1.2 Summary of knockout models targeting key enzymes in BH4, catecholamine and NO synthesis

1.14 Integrated cardiac-neural axis and the hearts "little brain"

This complex interaction of cardio-neural axis and potential molecular components has been elegantly explored and described by Armour and Ardell [47]. They describe cardiac control as a manifestation of 3 levels of neural hierarchy [12, 367]. Level 1 encompasses the spinal cord and medulla with higher centre modulation [67, 368, 369]. Level 2 incorporates extracardiac-intrathoracic neurons (including the stellate, middle cervical and mediastinal ganglia) [370-372] and level 3 includes all the intrinsic cardiac nervous system [47]. Levels 2 and 3 form cardiocentric control loops while level 1 sites modulate neural mechanisms for the regulation of the cardiac and peripheral vasculature [367, 373].

This integrated model and approach has moved away from the historical reciprocal thesis of cardiac control where the two major central outflow branches (parasympathetic and sympathetic) exerted an 'accelerator and brake' on cardiac function with intrathoracic and intracardiac neurones acting as relays [374]. Experimental studies in the 1980s and 1990s refuted this simplistic model with both anatomical and physiological evidence supporting a more complex local and central regulatory system.

Sensory neurones on the surface of the heart act to transduce the cardiovascular milieu. Neurones associated with these neurites display multiple chemical markers and have been identified in the nodose ganglia [375], dorsal root ganglia [376], multiple levels of the spinal cord [375] and connections to the extrathoracic and intrinsic cardiac ganglia [375, 377, 378].

Parasympathetic efferent preganglionic somata are primarily located in the ventral lateral region of the nucleus ambiguous [379] and project axons to the efferent postganglionic neurones located in the various atrial and ventricular plexuses [380]. Sympathetic preganglionic efferent neurons arise in the spinal cord (T1-T5) and synapse with postganglionic cardiac neurones [381] located in the cervical ganglia, stellate ganglia and major intrinsic cardiac ganglionated plexi [378, 382]. Postganglionic somata in each of these ganglia then project to widespread regions of the heart [379] therefore influencing widely divergent regions and local density not affecting the end organ effect. Evidence for local control has been demonstrated by the presence of axons connected to somata of intracardiac ganglia alone while others project to central neurones [383].

The effects of the two major branches have been well described [47] with sympathetic efferent neurones increasing cardiac chronotropism, dromotropism and inotropism [384] while the parasympathetic efferents do the opposite. In addition, neurones of the intrathoracic ganglia, including intracardiac ganglia are in constant communication [385] suggesting that reciprocal antagonism under normal conditions may be the exception rather than the rule [386] forming temporally dependent reflexes that control spatially overlapping regions. The physiologic relevance of local communication may include the concept of local neuronal memory and physiologic perturbations during a single arrhythmic beat may affect neuronal outputs for a few cardiac cycles [47]. In addition, a multi-synaptic system may serve to assure unperturbed control when the function of one part becomes compromised [47]. This mechanistic system is summarised in the diagram below (figure 1.10) and adapted to include the potential role of cotransmission and molecular control by cofactors such as BH4.

Emerging evidence also suggests that the intrinsic cardiac nervous system is directly affected by cardiac pathology [387]. Ischaemia can result in excessive activation of all levels of the cardiac neuraxis leading to complications such as arrhythmia [47]. Atrial fibrillation represents an alternative paradigm where increased vagal activity may be a contributor and some advocate ablation of cardiac ganglionated plexi as a treatment strategy [388, 389]. Results of this approach have been inconsistent and others have commented that since atrial and ventricular neurones are in communication with one another, ablation of one population may not prevent arrhythmia formation [390]. A further layer of complexity may arise from the concept of reinnervation, and transplant studies in canine models demonstrate partial reinnervation of transplanted hearts by extracardiac sympathetic neurones and pre-ganglionic neurones [391].

Therefore, a move towards therapies targeted at the autonomic nervous system requires a comprehensive understanding of the role of each level of the cardiac neuraxis, and experimental approaches that are integrated across multiple domains. In the next section, I outline the aims and objectives for each of the experimental chapters that are included in this thesis.

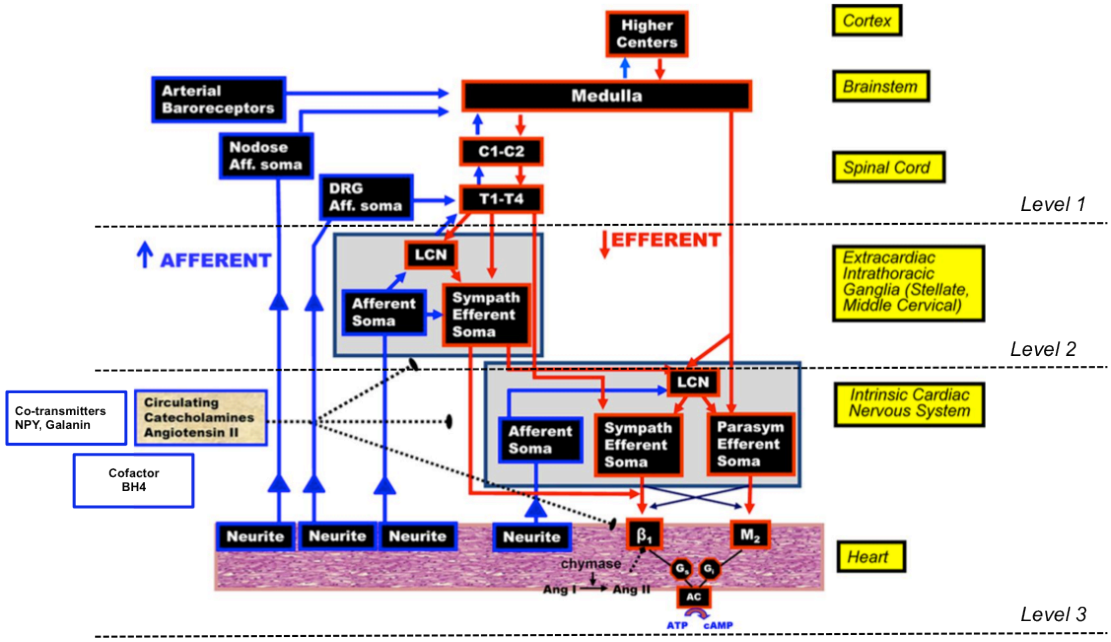


Figure 1.10 Schematic summary of proposed neural interactions encompassing central and peripheral autonomic control

Neurohumoral control and anatomic organization of cardiac innervation. AC indicates adenylate cyclase; Ang, angiotensin; Aff, afferent; C, cervical; DRG, dorsal root ganglion; LCN, local circuit neuron; Parasym, parasynpathetic; Sympath, sympathetic; and T, thoracic.
Adapted from Fukuda et al. 2015

1.15 Aims and objectives

I have attempted to study the mechanistic basis of sympatho-vagal modulation of ventricular arrhythmia with a multi-domain approach including cellular preparations, whole heart models and tissue specific gene knockout in mice. The aims and objectives of this thesis are summarised below.

I tested the hypothesis that a cholinesterase resistant analogue of acetylcholine, carbamylcholine, would be anti-arrhythmic and investigated if this action was dependent on neuronal nicotinic receptor stimulation or stimulation of myocyte muscarinic receptors.

I also investigated whether any antiarrhythmic action of an acetylcholine analogue was linked to generation of NO from either eNOS or nNOS and also attempted to locate the source of NO (neuronal or myocyte).

I also investigated if an NO donor could mimic the action of acetylcholine and whether this was also dependent on muscarinic receptor stimulation.

I investigated the sympathetic modulation of ventricular arrhythmia with respect to co-transmission. Specifically, whether endogenous NPY released during cardiac sympathetic nerve stimulation in the presence of a beta-blocker, or exogenous NPY lowers ventricular fibrillation threshold. I also sought to identify the NPY receptor(s) responsible for this effect as a potential novel anti-arrhythmic drug target.

Given the role for BH4 as a key co-factor for NA synthesis and NO production, I sought to investigate its role in sympathetic neurons by developing a novel mouse model where the gene encoding GTPCH, *GCH1* was deleted in sympathetic, TH expressing cells with the aim of undertaking cardiovascular phenotyping and determine if there was any influence on autonomic function.

Chapter 2 General Methods

All studies were performed in accordance with the UK Home Office Animals (Science Procedures) act 1986 (HMSO UK). Studies on transgenic mice were performed under the Project License (30/2630 and 30/3080).

2.1 Isolated Langendorff perfused heart

2.1.1 Historical context

Oscar Langendorff was a German physician and physiologist who revolutionised the study of the mammalian heart. His early work described vagal influences on the heart and was first to report that ventricular contraction following a pause may be stronger than normal systolic contraction. In his seminal paper in February 1895, “Untersuchungen am überlebenden Säugethierherzen” ("Investigation of the living mammalian heart") he demonstrated that retrograde perfusion of the aorta by artificial perfusate closed the aortic valve and therefore perfused the coronary arteries. This technique remains unchanged to this day and has contributed immeasurably to the study of cardiac physiology.

2.1.2 Advantages of the Langendorff system

The Langendorff perfused isolated heart from small mammals provides a highly reproducible preparation for the study of cardiac function in response to pharmacological and electrical stimulation. The measurements made which include haemodynamic, electrophysiological and biochemical indices are independent of the confounding factors such as other organs, systemic circulation and neurohumoral influences. An advantage of this approach is that it allows dissection of cardiac

responses from peripheral responses while recognising the limitation that the ventricles are unfilled and further removed from *in-vivo* physiology. Classically langendorff perfused preparation are denervated, but I will discuss modifications to the preparation which can allow stimulation of one or both branches of the autonomic nervous system. Isolated heart systems are also amenable to arrhythmia induction and detailed temporo-spatial study by techniques such as optical mapping.

2.1.3 Species selection

Species selection is a key step in experimental planning once the perfusion mode has been selected. The Langendorff principle has been applied to almost all mammalian hearts from mice to human, but the rat remains the best characterised. The size of the rat heart makes handling easier than with the mouse heart, allowing for cannulation, perfusion and intra-ventricular pressure recordings to be performed successfully. The rat also has a variety of disease models available (such as the spontaneously hypertensive rat) and the advent of transgenic rat technology will overcome one of the key limitations compared to the mouse where global and tissue specific transgene technology is widely available. Rabbit hearts have problems with anaesthesia [392, 393] and the guinea pig coronary circulation being densely collateralised makes studies of ischaemia and infarction difficult [394]. While the rat heart has been used extensively in the study of arrhythmia, the short action potential of this species is a limitation and will be discussed in more detail in the next chapters.

2.2 Isolated heart apparatus

The apparatus used in the course of my experiments is shown in the accompanying schematic diagram (Figure 2.1) and images (Figure 2.2). The apparatus was designed as a constant flow system to maintain perfusate and drug delivery to the heart,

although this does override the intrinsic autoregulatory mechanisms of the epicardial coronary arteries and microcirculation. An alternative method is constant pressure in which the perfusate chamber is raised above the heart and pressure measured to give a desired perfusion pressure under basal conditions. In these studies in which rapid pacing and ventricular fibrillation induction protocols were used, it was critical to maintain coronary perfusion at all times to maintain the viability of the preparation, hence a constant flow method was utilised. Additionally, the use of carbamylcholine and neuropeptide Y causes vasodilatation and vasoconstriction and therefore constant flow perfusion allows the assessment of electrophysiology and ventricular fibrillation threshold independent of these vascular effects.

The perfusion system used in these projects consisted of a series of water-jacketed chambers, each a different design aimed at achieving a specific function. Temperature in the water jackets was regulated to maintain perfusate temperature to within 0.5°C of 37°C at the tip of the aortic cannula. Perfusate was stored in the upper reservoirs and bubbled with a 95% O_2/5% CO_2 mixture to maintain temperature as above and pH (7.35-7.45). The reservoirs fed into a multi-port tap system allowing the heart to receive perfusate from any of the reservoirs, allowing pharmacological modulation of cardiac function. The multi-port system fed into the first peristaltic pump (Minipuls 3, Gilson UK) via silicon tubing. The next step before reaching the heart was filtration and optimal oxygenation. Perfusate was pumped through a cellulose pre-filter and filter (pore size 5μm, Millipore Corporation) in series to the perfusion circuit. Perfusate then passed through a heating block to maintain temperature before reaching the oxygenating chamber. This chamber permits distribution of a thin film of perfusate across its surface prior to reaching a small reservoir (50ml) at its base. The

chamber is filled with warm, humidified gas mixture (95% O_2/5% CO_2) and movement of fluid through the chamber and bubbling at the base ensures optimal oxygenation. A second peristaltic pump (Minipuls 3, Gilson UK) controlled perfusion to a heated junction block (AD technology, Oxford) immediately above the perfusion cannula. The tubing attached to this circuit was kept constant (peristaltic pump tubing, Gilson UK) to ensure uniform delivery at 10ml/minute across all experiments. Sampling of perfusate from the aortic cannula confirmed optimal oxygenation with typical values being pH 7.4, pO_2 >500mmHg and pCO_2 <30mmHg (ABL700, Radiometer Copenhagen).

The junction block design facilitates fine temperature control as a result of the tightly coiled spiral with the added advantage of a multiport header. This allows attachment of a pressure transducer for measuring aortic pressure and no touch delivery of drug boluses directly to the heart. A 20ml syringe was used as a crude windkessel to dampen any oscillations in perfusate delivery. The heart was attached to a custom made steel cannula.

2.3 Anaesthesia and surgical dissection

2.3.1 Isolated Langendorff heart preparation

Male Sprague Dawley (SD) rats weighing 300-350g were used throughout the studies presented in this thesis. Surgical anaesthesia was induced using isoflurane (100% w/w, Abbott), a volatile inhalational agent via a conventional closed circuit anaesthetic machine and custom-made perspex rodent chamber. Anaesthesia was induced with 5% isoflurane and 2 l/min 100% O_2. Surgical depth of anaesthesia was confirmed by loss of the pedal withdrawal reflex and following this the animal was

culled by cervical dislocation (Schedule 1 method in accordance with current ASPA guidance). The thorax was then opened and the heart excised (within 30 seconds of dislocation) and placed in ice cold, heparinised (100units/50ml) Tyrode's solution (composition in Results sections). Within 2 minutes, the aorta was cannulated, sutured and perfusion begun in constant flow mode as described above. Once perfusion was established and the coronaries had cleared, any lung tissue remaining was removed and the pulmonary artery incised to relieve pressure in the right ventricle. A thermal chamber was placed around the heart during the initial perfusion period to ensure temperature stability. The hearts were perfused for 30 minutes prior to commencing protocols to allow perfusion pressure, heart rate and contractile function to stabilise. A fully instrumented experimental preparation is shown in figure 2.3.

2.3.2 Isolated Langendorff heart with intact sympathetic innervation

The preparation described above was modified in order to facilitate dissection and stimulation of the right or left stellate ganglia. Surgical anaesthesia was once again induced with isoflurane (100% w/w inhalational vapour, Abbott). Cervical dislocation could not be used, as the neck tissue was needed intact for stellate dissection. Terminal anaesthesia was induced with intraperitoneal pentobarbital (0.3ml, 200mg/ml, JML). Following confirmation of terminal anaesthesia (loss of pedal reflex, agonal respiration), the thorax was quickly opened and reflected superiorly followed by incision through both lungs. The anterior section of the thymus was dissected to reveal the aorta. A 2-0 suture was passed underneath the aorta. The aorta was lifted gently and a small arteriotomy was made. The perfusion cannula was inserted and perfusion begun with ice cold, heparinised (100 units/100ml) Tyrode's solution (bubbled with 95% O_2/5% CO_2) at 5ml/minute. This maintained tissue

viability but kept heart rate low. The anterior ribs were cut and the preparation transected below the diaphragm to allow drainage of perfusate via the inferior vena cava. The thorax was then dissected free and transected above the first rib through the neck. The cardiac sympathetic nerves and ganglia lie anterior to the paravertebral muscle, posterior to the heart. The lungs were removed and the paravertebral muscles and superior mediastinal tissues were dissected en mass, taking care to maintain tissue integrity through the thoracic outlet. The preparation was then positioned so that the posterior surface was facing the operator and the trachea was pinned for stability. The muscle layer was removed with fine dissecting forceps. The nerve/ganglia complex then becomes evident and the surrounding connective tissue is carefully removed. The distal end of the stellate ganglia was then tied with 2-0 suture to allow it be identified and lifted onto the stimulation electrode. Once both stellate ganglia were secured, the dissected preparation was submerged in ice-cold buffer and then transferred to warm perfusion. The outflow and cannula were connected under water to minimise the risk of air embolus. Perfusion was maintained for 20 minutes after which the left ventricular balloon (LVB) was inserted and stellate stimulation started after 30 minutes. An example of a preparation with intact sympathetic innervation is shown in figure 2.4.

2.4 Measurements

Multiple parameters were measured in each preparation including aortic perfusion pressure, left ventricular developed pressure, the electrocardiogram (ECG) and heart rate (calculated from the R-R interval on the ECG). All signals were acquired and digitised by an amplifier (Biopac MP150, Linton Instruments, UK) and analysed with a physiology software package (Acknowledge 4.0, Biopac, Linton Instruments, UK).

Aortic pressure was measured by a pressure transducer attached in series to the perfusion circuit via the header on the junction block. The pressure transducer was calibrated to a range of pressures using a mercury manometer.

Left ventricular pressure was measured with a custom made balloon made from cling film. A 6x4cm piece of cling film was cut and folded over a blunted 21 gauge needle. A small (approx. 5mm) reservoir was left at the end of the tip and the remaining material secured around the needle with suture material (2-0 braided silk, Pearsalls, UK). The balloon was then filled with degassed distilled water and connected to a pressure transducer (calibrated as above). A small segment of the left atrial appendage was removed and the balloon inserted into the left ventricle. The balloon was filled slowly over 5 minutes to a target end-diastolic pressure (EDP) of 0-5mmHg until the maximal developed pressure was reached. Over inflation of the balloon resulted in arrhythmias hence the EDP was adjusted for each preparation.

The electrocardiogram was recorded using a custom made sprung electrodes. Epicardial contact was with 2mm silver chloride pellets (Harvard Apparatus, UK) housed in custom made plastic housing and sprung tubing to minimise pressure on the epicardial surface. Signal quality was improved by completing Einthoven's triangle by grounding the recording circuit on the metal perfusion cannula. Heart rate was calculated by real time software analysis of R-R intervals from the ECG. Experimental traces of these measurements are seen in figure 2.5.

2.5 Electrical pacing

The hearts were all paced from the epicardial surface of the right ventricular apex. A series of experiments were used to determine the optimal pacing electrode design for

pacing and arrhythmia induction in this model. Pacing protocols were custom drawn on Acknowledge 4.0 and delivered via the Biopac MP150 external stimulus module. Electrical impulses were generated by a constant current stimulator (Digitimer DS7, UK).

Pacing with a co-axial electrode (Linton Instruments, UK) was suitable for pacing at fixed cycle lengths, but upon very rapid burst pacing contact was lost. Therefore a custom made bipolar platinum electrode was designed. One cm platinum wire (Advent Research materials, UK) was cut and tapered in our workshop. The wires were then insulated and placed in custom made housing and connected to the DS7 stimulator.

2.6 Arrhythmia induction and ventricular fibrillation threshold testing

Induction of ventricular fibrillation is a commonly used end point in *ex vivo* studies of arrhythmia susceptibility. Induction methods can be either 'spontaneous' or 'induced' and the use of these methods is the subject of intense debate in the literature. Spontaneous ventricular arrhythmia is most often studied in the setting of coronary artery occlusion (CAO). Although this represents a physiologically relevant trigger, the measures of arrhythmia are often qualitative including premature ventricular complexes (PVCs), or VT/VF events during the occlusion with the outcomes stochastic. The Schwartz [65] canine model was an elegant advance on this and allowed quantification of arrhythmic events. The model required dogs to undergo ligation of the LAD to create an anterior MI and instrumentation to allow subsequent circumflex artery occlusion and invasive haemodynamic measurements. Animals were then recovered and surviving animals were subjected to ischaemic stress by exercise and circumflex occlusion to determine correlation between markers of vagal tone and VF

induction during exercise. However, this model would be technically demanding, time consuming and expensive for repetitive measures in a mechanistic investigation. Therefore, induction of VF using a pacing protocol allows the ventricular fibrillation threshold (VFT) to be defined reproducibly with examination of individual factors which influence arrhythmia susceptibility. This method is supported by studies that have utilised this approach in the study of arrhythmia susceptibility in a range of experimental conditions [60, 70, 395] including the studies of anti-arrhythmic drugs.

2.6.1 VFT pacing protocols

A pacing protocol was designed (Acknowledge 4.0) to test VFT independent of changes in heart rate. Hearts were paced for 20 beats at a fixed cycle length to regularise the refractory period (S1 drive cycle length (DCL), 150msec or 400 beats per minute) followed by a period of closely coupled impulses or 'burst' period. A number of protocols were tried in a control series to find the most effective, least aggressive strategy that could induce VF over a minimum of 3 stimulations separated by a 15 minute recovery period. The protocol chosen after these investigations was a DCL of 150msec followed by a 5 second 50Hz burst (2msec pulse width). In pilot experiments, this protocol was found to reproducibly induce VF, and this was subsequently confirmed in a series of control experiments (n=7, figure 2.6a). Following confirmation of this reproducibility, it was important to demonstrate that the protocol was able to detect a change in the VFT. This was achieved by perfusion of isoprenaline (10nM, n=7), a non-selective beta-adrenergic agonist. This has been previously shown to increase cAMP and decrease VFT [396] , and this finding was reproduced in our series (figure 2.6b).

2.6.2 Testing VFT

Retrograde perfusion of the heart was established as above and ECG electrodes and LVB inserted after 20 minutes of perfusion. The epicardial pacing electrode was positioned at the right ventricular apex and gentle pressure was applied on the contralateral left ventricular wall to secure it in position. Pacing threshold was determined by pacing at 150-200msec (depending upon baseline heart rate of the preparation) at the lowest available amplitude (0.2mA) and slowly increasing till pacing capture was seen. In all of the experiments, the baseline pacing threshold was 0.2-0.25mA, therefore the VFT protocol was begun at 0.5mA. The protocol was repeated with 0.5mA increments in applied current until VF was induced. Ventricular fibrillation was confirmed by demonstration of chaotic electrical activity on the ECG and absence of developed pressure from the LV and was sustained for a minimum of 5 seconds. Hearts were cardioverted with a bolus of 50mM potassium chloride (KCl) and allowed to stabilise for 15 minutes before the next induction. Experimental traces showing VF induction and successful cardioversion with KCl are shown in figure 2.7.

2.6.3 Ventricular arrhythmia scoring post ischaemia-reperfusion

Retrograde perfusion in constant flow mode (10ml/min) was established as above and experiments were designated as control or NPY groups (n=10/group). Following stabilisation (20 minutes), ECG electrodes were positioned but no LVB was used in these experiments. Complete ischaemia was induced by stopping perfusion for 7 minutes, during which clear ST elevation would be observed on the ECG, followed by reperfusion for 20 minutes. In the NPY group, NPY was perfused for 15 minutes prior to initiation of ischaemia and continued during reperfusion. During the reperfusion period, continuous ECG recording was conducted and a score generated for each

experiment from observed arrhythmias as follows; ventricular ectopics (1 point), non-sustained/sustained ventricular tachycardia (2 points) and ventricular fibrillation (3 points) and defined according to the Lambeth Conventions [397].

2.7 Whole heart electrophysiology

Testing ventricular fibrillation threshold is a useful technique to demonstrate changes in the propensity of the heart to develop VF in the presence of pharmacological or direct autonomic nerve stimulation. However the study of the electrophysiological properties of the heart in more detail provides mechanistic insights into parameters such as action potential duration (APD), conduction velocity (CV) and derived indices such as activation patterns and electrical restitution (discussed in Chapter 1). Initial attempts to study the electrophysiology were made using a contact electrode following which a shift to optical mapping technology was made. These methods will be discussed in detail below, including discussion of the reasons for switching approach.

2.8 Contact (suction) electrode action potential recordings

Local epicardial monophasic action potentials (MAP) were recorded with the use of a custom made, Franz design suction electrode [398]. Following established Langendorff perfusion, the suction electrode is positioned perpendicular to the epicardial surface. Suction was then applied using a 50ml luer lock syringe until a consistent MAP signal was seen via the Biopac/Acknowledge system. This system was effective at acquiring single point MAP signals but was limited by loss of signal quality and amplitude during prolonged recording, loss of suction during rapid pacing and epicardial necrosis due to suction resulting in loss of the MAP from the site.

2.9 Optical mapping

Surface contact mapping is limited by its spatial resolution which is dependent upon the number of contact electrodes, low depth of field and electrical interference as discussed above [399]. These limitations can be overcome by optical mapping using fluorescent probes which allow non-invasive study of the heart and cardiac cells.

Imaging with fluorescent voltage-sensitive dyes was first reported by Salzberg *et al.* in 1973 [400] to record changes in axonal impulse propagation. Cardiac imaging from multiple sites has been revolutionised by the development of image acquisition tools such as photodiode arrays and cameras with charge coupled device (CCD) or complementary metal oxide semiconductor (CMOS) technologies. Whole heart imaging to study atrial and ventricular arrhythmias using these technologies has shown its utility since the 1990s [401]. Recent developments in this field have been the ability to perform multi-parametric mapping to measure action potential and calcium dynamics simultaneously, allowing this key interplay to be examined in the setting of health and disease [402].

2.9.1 Photodetectors

A schematic of a typical optical mapping experiment in shown in figure 2.8 and raw experimental data acquired in figure 2.9. The photodetector is the critical component in the system. The electrical impulses that trigger each cardiac cycle are rapid and short lived. The change in fluorescence compared to background of current reporters (either voltage or intracellular calcium) in responses to this impulse is small, therefore high speed, low noise with high spatio-temporal resolution acquisition systems are needed. Three classes of detector fulfil these requirements including photodiode arrays (PDA), CCD cameras and CMOS cameras. Current literature has moved away

from PDAs with CCD/CMOS systems providing increased spatio-temporal resolution due to the increased pixel number and rapid data transfer. A recent innovation has been the development in CCD systems is on-chip electron multiplication (EMCCD), which utilise impact ionization to generate secondary electrons before conversion to a voltage signal [403]. This facilitates higher speed acquisition with reduced noise. Further details are beyond the scope of discussion in this chapter. In the studies presented, high-speed CCD cameras were used (Photometrics Evolve 128, Photometric, Tucson, Arizona). Further details of the system used will be provided below.

2.9.2 Illumination

High signal-to-noise ratio is dependent upon optimal illumination of the Langendorff perfused heart. Early optical mapping apparatus utilised xenon, mercury or halogen lamps for illumination and excitation of fluorescent probes [404]. These systems have several limitations including oscillations, thermal runaway and need for moving parts and shutters to control light duration. These systems have been superseded by light-emitting diode (LED) technology, which offer accurate wavelength delivery, high power, and rapid wavelength switching in real time [405]. This facilitates multi-parametric imaging (e.g. voltage and intracellular calcium) which is now allowing integration of electrophysiology and intracellular physiology at the organ level. The light source used in these studies comprised of two high power green LED (530nM) with a power controller to accurately control the light intensity (MacroLED, Cairn Research, UK).

2.9.3 Lenses and filters

Lens selection for optical mapping apparatus is dependent upon the field of view being studied and the image sensor area. The field of view for imaging rat hearts is 1x1cm^2 and the lens selection should be optimised to maximise the effective numerical aperture of the system, light collection and the signal/noise ratio of the optical recordings. To meet these criteria, a Nikon 50mm *f*0.95 lens was used.

Single parameter mapping of membrane voltage (V_m) was conducted with a single camera (Photometrics Evolve 128) with a band pass filter (>700nm, ThorLabs, UK). Band pass filters should allow 80% of light at peak wavelength, with a 99.99% block of infrared light [406].

2.9.4 Potentiometric dyes

These molecular probes were first described in the 1970s [407, 408] as compounds that embedded themselves into the plasma membrane of neurons or cardiac cells and interacted with the electrical status of the cell. The binding of the probes to the membrane led to a change in fluorescence or absorption reporting alternations in membrane potential. Potentiometric dyes deliver high spatial resolution in subcellular compartments [409], cells, monolayers [410] and in the whole heart [395]. Fluorescence changes in a linear fashion with membrane potentials in the physiological range with modern probes yielding>10% change in fluorescence.

Potentiometric dyes are classified into slow and fast response dyes dependent on their reactivity and mechanism of voltage sensitivity[411]. The stryl dyes developed by Loew *et al.* [412] are typically used, with the commonest being the ANEP

(aminonapthylethenylperidinium) dyes, di-4-ANEPPS and di-8-ANEPPS. These yield up to a 10% change in fluorescence per 100mV change in membrane potential and are commonly used for whole heart optical mapping. There are some minor differences in that di-4-ANEPPS is rapidly internalised therefore provides a short term optimal period of recording and d-8-ANEPPS is thought to be better retained in the outlet leaflet of the membrane leading to reduced phototoxicity [413]. They have some limitations including phototoxicity in cellular preparations and short wavelength excitation (blue/green), which can limit recording from deeper layers. New developments in dye technology have led to the synthesis of longer wavelength (red shifted) voltage sensitive dyes in the Salama laboratory [414] that can record action potentials from deeper layers in the heart and be easily combined with Ca^{2+} imaging dyes. The dyes (Pittsburgh I-VIII) exhibit to two absorption, two excitation and two voltage sensitive emission peaks with large Stokes shifts (>100nM). In the optical mapping experiments presented in the chapter 3, the voltage dye used was RH237. This choice was with a view to potential future experiments requiring multi-parametric, simultaneous voltage and calcium measurements with literature supporting the use of RH237 with Rhod-2AM [406].

2.9.5 Elimination of motion artefacts

Mechanical contraction significantly distorts optical signals recorded from an optical mapping system. In view of this, multiple strategies exist to individually or in combination remove these artefacts and therefore eliminate distortion of V_m signals.

2.9.6 Mechanical restraint

Salama *et al.* [406] have described using a custom-made heart restraint chamber where the heart is secured and squeezed onto a glass plate eliminating motion artefact

without affecting function. This system is effective in experienced hands, but limited by some residual motion and risk of coronary occlusion leading to ischaemia.

2.9.7 Electro-mechanical uncouplers

Electro-mechanical uncouplers are pharmacological agents that disrupt components of excitation-contraction coupling in myocytes, leading to normal electrical activation devoid of mechanical contraction.

Diacetyl monoxime (DAM) is a non-competitive inhibitor of myosin II that inhibits myosin ATPase activity but is reported to have significant effects on electrophysiology with alteration in APD and restitution, conduction velocity and Ca_i [415, 416]. Cytochalasin D is a fungal metabolite that inhibits actin polymerisation and therefore eliminates mechanical contraction [417]. Although there are no reports of effects on APD, it does induce significant changes in Na^+ [418] and K^+ channel activity [419] and changes mouse APD shape thereby making it unsuitable [415].

Blebbistatin is the most recently developed electro-mechanical uncoupler and is reported to non-competitively inhibit only certain types of myosin II with high specificity [420] and has minimal side effects on APD, APD shape and Ca_i [421]. This view has recently been challenged by Brack *et al.* [422] who have reported that blebbistatin affects APD and VFT in rabbit hearts. However, the seminal work of Fedorov [421] reported negligible effects in rat heart tissue when compared to gold standard microelectrode recordings, and given the rat heart model utilised in these experiments, I proceeded with blebbistatin as the uncoupler of choice. Furthermore, in the optical mapping experiments, VFT was not being tested and blebbistatin was

perfused at a fixed concentration throughout all protocols, the confounding effect of blebbistatin would be minimised.

2.9.8 Dye loading in Langendorff perfused rat hearts

Hearts were excised as described above and perfused for 20 minutes until heart rate stabilised. Perfusion was changed to recirculation mode and blebbistatin (Abcam, UK) added at a final concentration of 10μm. Motion was eliminated after 10-15 minutes and the perfusion flow rate was slowly reduced to 5ml/minute to facilitate dye loading. The left atrial appendage was cut and a 0.5mm ID silicon tube was inserted into the left ventricle to prevent build up of solution and tension within the left ventricle which would lead to ischaemia. RH237 (15μl, 1mg/ml in DMSO) was loaded over 2 minutes via the junction block using a Hamilton syringe. Drugs were prepared from stock solutions and mixed in Tyrode's solution with 10μM blebbistatin in another perfusion chamber.

2.9.9 Image acquisition

Voltage signals were acquired at 1kHz, 32x32 pixels, 4x4 binning and Ca^{2+} signals were acquired at 333Hz (slower signal profile), 128x128 pixels and 4x4 binning. Images were taken during sinus rhythm, fixed rate pacing (4-7Hz – dual mapping only) and S1-S2 pacing to determine electrical restitution (S1 cycle length 150msec, S2 140msec decrementing to 40msec in 10msec intervals). Fixed rate pacing stimuli were generated by a impulse generator (DG2A, Digitimer, UK) connected to a stimulator (DS7, Digitimer, UK) and delivered via a custom made platinum electrode as above. S1-S2 pacing was generated via a custom written timing script (Arduino microcontroller) connected to the Digitimer DS7. Camera and light timings were

controlled via the image acquisition software (Gview, custom written by Dr Gil Bub, Oxford, UK).

2.10 Dye free imaging of myocyte monolayers

2.10.1 Myocyte Isolation and Plating

Hearts from neonatal SD rat pups (PI-P3), killed by Schedule 1 (in accordance to UK Home Office Animals Scientific Procedures Act (1986)) were isolated. Ventricular myocytes were isolated and subjected to enzymatic digestions in trypsin (1mg/mL, Sigma Aldrich, UK) at 4°c for three hours followed by a series of digestions in collagenase (1mg/mL, Sigma Aldrich, UK), and then titrated to achieve a suspension of cardiac myocytes. Isolated cells were then pre-plated in an incubator (37°C, 5% CO_2) for an hour to allow fibroblasts to settle at the bottom of the dish. The ventricular myocytes in the supernatant were then carefully removed from the dish and a cell count performed using a haemocytometer and trypan blue, to identify viable cells. The myocytes were plated on 35 mm polylysine coated petri-dishes (Bio coat Poly-D-Lysine 35mm petri-plates, Corning, UK) at a density of 700,000 cells (per 35 mm petri-dish) in plating medium (85% DMEM, 17% M199, 10% Horse serum, 5% FBS and 1% penicillin/streptomycin, all from Sigma Aldrich). The dishes were maintained until imaging was performed, with media being refreshed every 48 hours.

2.10.2 Imaging

Imaging was performed from day seven onwards when the cultures displayed large connected wave patterns. The plates were placed in a stage-top incubation chamber (Okolab) which was kept at ~37°c, 5% C02 and at constant humidity. Cells were allowed to equilibrate for 15 - 20 minutes before imaging. An Olympus MVXI0 macroscope and Andor Neo sCMOS high speed camera was used to image and record

the activity of the cultures. Videos were recorded using an Andor Neo sCMOS camera. The imaging technique used was a variation of those previously described by Hwang *et al.* [423], where a macroscopic phase contrast system was used to visualise cell motion. This macroscopic high speed imaging system is based on off-axis illumination using two LED sources. Wave fronts are visualised using image processing filters that display absolute value of the change in pixel intensity over a 5 frame rolling window, allowing for experiments to be conducted in dye-free solutions. Videos were recorded at 50-100 frames per second with 0.01 second exposure time.

The camera was controlled using custom written Java based software and software for displaying the camera in real time. Saving and analysis of data was in a software combination of Java and Python (developed By Dr Bub). The analysis was done using custom written code in Gview software. Videos were recorded, and from these we were able to observe the propagation of cardiac waves across the plates by detecting the minute contractile motions of the myocytes. To assess drug effects on spontaneous activity of cultures, the FOV was divided into 16 equal ROI and the activity changes in each ROI was assessed following drug stimulation

2.11 Measurement of NO metabolites

Perfusate samples were collected from the stabilized preparation before and after administration of carbamylcholine (CCh 200nM) or CCh (200nM) and mecamylamine (10μM) every two minutes and immediately snap frozen in liquid nitrogen. After thawing, samples were injected into a vanadium chloride solution heated to 95°C to ensure complete conversion of NO metabolites to NO. Values were derived from a gas-phase chemiluminescence reaction between NO and ozone in which an intermediary radical dissociated to yield a single photon, and compared

across the two groups [424]. Blank Tyrode solution samples and a nitrite standard curve provided negative, and positive controls, respectively.

2.12 Measurement of neuropeptide Y by ELISA

Coronary effluent was collected at baseline (prior to sympathetic nerve stimulation) and following direct nerve stimulation and snap frozen in liquid nitrogen.

Neuropeptide Y levels were determined by ELISA using a commercially available kit (Merck Millipore, Cat no EZRMNPY-27K) according to the manufacturers instructions. Standards were prepared according to instructions with serial dilutions with the lowest detectable concentration of NPY being 0.01ng/ml. A 96 well plate was prepared with standards, internal controls and coronary perfusate samples and antibody solution was added to each well. The plate was covered and incubated at room temperature on a plate shaker for two hours. The solutions were decanted and washed x3 followed by addition of enzyme solution to each well and incaubated as above for 30 minutes. A further wash x6 was undertaken and substrate solution was added and placed on shaker for 20 minutes until blue colour was visible as an indication of NPY detection. Stop solution was added to terminate the reaction and this was evidenced by a blue to yellow colour change. The plate was then read on a plate reader at 450nm and 590nm within five minutes and differences in absorbances was calculated. Standard values were used to construct a calibration curve from which results of coronary perfusate samples was calculated.

2.13 Western blotting for NPY Y1 receptors on myocytes

Tissue was snap frozen in liquid nitrogen and following freeze-thaw, ice cold lysis buffer (75 mM Tris-HCl pH 6.8, 3.80% SDS, 4M Urea, 20% glycerol, 0.1% Triton X-100 with protease inhibitor cocktail) was added and the samples homogenised using a

Polytron homogeniser. Samples were then centrifuged at max speed (13000rpm) for 5 minutes followed by transfer of supernatant to new Eppendorf tubes. Protein concentration of the supernatant was determined by BCA assay (Roche). Samples for western blotting were then prepared in x4 NuPAGE® LDS sample buffer and x10 NuPAGE® reducing agent (Invitrogen, UK) and incubated at 70°C for 10 minutes before gel electrophoresis. Proteins were separated using SDS page (12%Tris-Glycine gels-Invitrogen) and transferred onto PVDF membranes. The membrane was blocked with 5% milk in Tris buffered saline (TBS) with 0.1% tween (TBST), before primary antibodies were left overnight (anti NPY1R ab183108, NPY1R blocking peptide ab193664, anti NPY2R ab31894, Abcam). Blocking peptides and negative tissue controls were used to ensure specificity of the signal. β-actin was used as a loading control. The blot was washed in TBST and developed using secondary HRP conjugated antibodies and the ECL kit (Amersham).

2.14 Immunohistochemistry for Y1 receptor on ventricular myocytes

Isolated rat ventricular myocytes were fixed with 4% paraformaldehyde and blocked (10% goat serum, 0.3%BSA, 0.1% triton X in PBS) before primary antibodies were added (Sacromeric alpha actinin A7811: 1:600 and Y1R AB73897: 1:200). This was followed by overnight incubation at 4°C. Secondary antibodies (1:1000) were added as appropriate (Alexa Fluor 488 and 647, Life Technologies, UK) and the cells were mounted using DAPI containing mounting media (Vectorlabs, UK). Samples were imaged using a Leica confocal microscope.

2.15 Genetic mouse models

Genetically modified mice were used to investigate the effect of a reduction in BH4 in the sympathetic arm of the autonomic nervous system. A novel mouse model was generated within the laboratory in which the gene *Gch1* (murine gene) which encodes

GTPCH (the rate limiting enzyme in BH4 synthesis) was deleted in cells expressing tyrosine hydroxylase (TH).

2.15.1 Cre-Lox technology

Cre-Lox recombination involves the target modification of a specific sequence of DNA using an enzyme called cre-recombinase. This method of genetic manipulation allows investigation of gene inactivation which if done systemically would result in embryonic lethality. The cre-recombinase enzyme is a site specific DNA recombinase and catalyses DNA modification at sites known as loxp sequences [425]. These sites contain specific binding sites for cre-recombinase and flank regions of DNA that will undergo recombination. Cre-recombinase proteins bind to the first and last 13 base pairs of the lox p sites leading to dimerisation which then binds to a dimer on another lox site resulting in a tetramer. The resulting double stranded DNA is cut at both loxp sites by the cre protein and rejoined with DNA ligase. The recombination event may result in inversion, deletion or translocation of genes depending upon the orientation of loxp sequences and can be directed to specific tissues using a specific promoter coupled to cre-recombinase [426].

2.15.2 The THcre GCH$^{f/f}$ mouse

In order for tissue specific models of BH4 deficiency to be studied, a 'floxed' Gch mouse was generated by the commercial provider, Genoway, in accordance with a targeting strategy and plasmid cloning by the Channon Group. A plasmid containing a FRT-PGK-promoter and a neomycin-FRT-LoxP positive selection cassette was inserted into the intron 3 sequence of *Gch1*. An additional LoxP site was inserted into intron 1 to flox exon 2-3. The *Gch1* floxed mouse was generated using homologous recombination in ES cells. Two chimeric male mice with 90-100% chimerism were

chosen for breeding and Flp-mediated excision was carried out by breeding with a Flp deletor female. These were bred on a C57BL/6 background to backcross 7 to generate pure lines of $GCH^{f/f}$ mice and an active colony maintained for breeding. The insertion of LoxP sites in the *Gch1* gene did no result in a hypomorphic allele evidenced by no differences in BH4 levels between $GCH^{+/+}$, $GCH^{f/+}$ and $GCH^{f/f}$ mice in heart, liver or lung tissue [362] indicating that the floxed gene does not change GTCPH expression. Furthermore, this observation supports the use of $GCH^{f/f}$ as control animals for the experiments undertaken in this thesis.

These mice were crossed with a mouse in which the activity of the cre-recombinase enzyme was under the control of TH as a promoter (THcre mouse (Jackson Laboratories, USA; a gift from Professor Ratcliffe's group, Oxford). This results in genomic deletion of *Gch1* in all cells expressing TH including the central nervous system, peripheral sympathetic ganglia and nerves, and chromaffin cells of the adrenal medulla [427].

A second breeding programme was also undertaken utilising an internal ribosome entry site (IRES) for expression of cre-recombinase under the control of TH as a promoter [428]. The transgenic approach (THcre) can be limited by difficulty in obtaining the normal expression from a promoter lacking some of its additional enhancer regions. This can lead variation between founder lines due to differences in integration site and copy number. The IRES approach links expression of cre-recombinase to that of the endogenous gene thereby resulting in restricted expression in the same pattern as the endogenous gene [428]. The breeding program was unchanged

other than the lines being crossed were $GCH^{f/f}$ as above and THires (a gift from Professor Ratcliffe's group, Oxford).

The breeding diagram (figure 2.10) summaries the generation of this model. The first generation litter was expected to generate THcre $GCH^{+/f}$ and $GCH^{+/f}$ in a 50:50 manner. The THcre $GCH^{+/f}$ mouse was again crossed with a $GCH^{f/f}$ mouse to generate an expected 25% yield of THcre $GCH^{f/f}$. The colony was then expanded by crossing this mouse with $GCH^{f/f}$ mice to generate knockout and control animals in a 50:50 distribution for study allowing for equal numbers of knock out and littermate controls for study. The breeding colony was maintained on a C57BL/6 background and new $GCH^{f/f}$ females were introduced to the colony intermittently to maintain the genetic diversity in the colony and avoid complications from accumulation of recessive genes. THcre$GCH^{f/f}$ and their $GCH^{f/f}$ littermates aged 12-20 weeks were used for all experiments. Male and female animals were used in molecular and biochemical studies and only males in non-invasive tail cuff blood pressure measurements. Animals from the THires breeding cycle were culled at day 21 (in accordance with license restrictions) for biochemical phenotyping.

2.16 Mouse welfare

Mice were housed in individually ventilated cages in a specific pathogen free environment. This animal facility was based on site within the Functional Genetics Facility in the Wellcome Trust Centre for Human Genetics in Oxford. The mice were kept under a 12 hour light/dark cycle, ambient temperature at 20-22°C and provided normal chow diet (2016 Teklad Global 16% protein rodent diet; Harlan, UK) and water *ad libitum*.

2.17 Tissue harvest protocol

Animals were sacrificed by overdose of isoflurane and cervical dislocation or exsanguination (stellate ganglia harvest only). Death was confirmed and the thorax and abdominal cavity were opened. The adrenal glands were dissected from the retroperitoneal space and immediately placed in Eppendorf tubes on dry ice (a microdissection modification to this procedure was made and is described below). Following this, the systemic and pulmonary circulations were flushed with phosphate buffered saline (PBS) via the heart. The brain, heart, lungs and liver were then harvested for analysis if required.

2.17.1 Adrenal micro-dissection

The adrenal medulla consists of predominantly chromaffin cells which express tyrosine hydroxylase and contain vesicles of catecholamines. In order to enrich samples for genetic and biochemical analysis, the adrenal glands (each measuring 1-2mm in diameter) were micro-dissected to remove the outer cortex from the central medulla. Following removal of the adrenal glands, they were placed on a Silgard (Dow Corning, USA) coated petri dish on ice. A small volume of ice cold PBS was dropped on each gland. Micro-dissection was carried out using small vannas scissors and a binocular microscope (Nikon SMZ1000, Nikon Europe BV, The Netherlands).

2.17.2 Stellate ganglia harvest

This protocol was developed in collaboration with Dr Neil Herring (Department of Physiology, Anatomy and Genetics, Oxford, UK). Animals were sacrificed with overdose of isoflurane and exsanguinated via the inferior vena cava (IVC). Blood was kept on ice and later centrifuged at 3000rpm for 15 minutes to separate plasma from the cellular components. Plasma was then removed and stored at -80°C for

catecholamine HPLC (high performance liquid chromatography). An identical dissection procedure to the one described above (rat heart-stellate ganglia preparation) was performed. The dissection was done using a binocular microscope (Nikon SMZ1000) and in this case, the stellate ganglia were dissected free from the paravertebral muscles, mediastinum and heart and stored on dry ice.

2.17.3 Midbrain dissection

Animals were sacrificed with overdose of isoflurane and exsanguinated via the inferior vena cava (IVC) as above and then the heart and circulation were perfused with PBS. The head was removed by cervical transection and the brain exposed via lifting the skull along the sagittal suture via the foramen magnum. The brain was gently lifted whole and then placed on a Silgaurd coated dish exposing the inferior surface. The cerebellum was gently removed and frontal and parietal lobes separated to reveal the midbrain which was removed using a small spatula and frozen in Eppendorf tubes on dry ice. This tissue was used for determination of biopterins due to the midbrain being the location of dopaminergic cell bodies.

2.18 Genotyping transgenic mice

Animals were marked for identification within each breeding cage by ear notch in a variety of positions. Tissue from the notch was used for DNA extraction and genotype analysis. Following experiments, confirmatory genotyping was carried out from cell pellets or alternative tissue if required.

2.18.1 DNA extraction

Salt extraction

Ear notch tissue, cell pellets or organ tissue was digested in 500µl of DNA lysis buffer (10mM Tris pH 8.5, 0.45% Non-idet P40, 0.45% Tween-20, 0.2mg/ml freshly added Proteinase K) and incubated for 4 hours at 55°C. Following digestion, 500µl of 6M sodium chloride solution was added and centrifuged at 14,000rpm (max speed) for 15 minutes. The supernatant (approximately 450µl) was transferred to a new Eppendorff tube and the extracted DNA was purified with a series of centrifugation steps with alcohol. Firstly, 250µl of isopropanol was added and centrifuged at max speed for 15 minutes. The supernatant was discarded and a small opaque DNA pellet could be seen at the base of the tube to which 250µl of ethanol was added. This was centrifuged at max speed for seven minutes following which the ethanol was discarded. The tubes were left open and allowed to air dry for 30 minutes. Once dry, 70-100µl of TE buffer (10mM Tris pH 8.0, 1mM EDTA) was added to resuspend the DNA pellet. Final DNA concentration was determined by spectroscopy (Nanodrop 2000, Thermo Scientific, UK) and 10ng of DNA was used for polymerase chain reaction (PCR) reaction.

Qiagen method (for quantified reverse-transcriptase PCR)

Tissue samples were lysed in 200µl ALT buffer with 20µl of proteinase K and heated at 56°C until the sample was dissolved. Following this 200µl of AL buffer and 100% ethanol was added and incubated at 56°C for 10 minutes. The total volume (600µl) was loaded onto a spin column and centrifuged at 8000rpm for 1 minute. The supernatant was then poured off and 500µl of AW1 buffer was added followed by centrifuge at 8000rpm for one minute. The supernatant was again poured off and

500µl of AW2 buffer was added followed by centrifuge at maximum speed for three minutes. The supernatant was poured off and 100µl of PCR grade water was added and the sample incubated at room temperature for one minute followed by centrifuge at 8000rpm for one minute. DNA concentration was determined by spectroscopy (Nanodrop) and samples prepared at a concentration of 10mcg/µl.

2.19 Polymerase Chain Reactions

Genotyping

The following PCR reactions were used for genotyping GCH and THcre transgenes. Reaction products were run on a 2% agarose gel for all reactions. Agarose was dissolved in x1 TAE buffer (2M tris-acetate and 100mM EDTA, pH 8.3) by heating. The mixture was allowed to cool to <60°C and 7µl/100ml agarose of ethidium bromide was added to the mixture. The gel was allowed to set for 30 minutes before loading samples and run in the gel at 120V in x1 TAE buffer. DNA bands were visualised using UV illumination with reference markers loaded into the gel (Hyperladder I, Bioline Inc, Taunton, MA, USA). Primers and reaction components are listed below:

GCH1 genotyping PCR

Primers:

- GX5128 Forward-GTCCTTGGTCTCAGTAAACTTGCCAGG
- GCH New Reverse-GCCCAGCCAAGGATAGATGCA
- Primer5 Forward-GCTCATCCCCCACACTTGTCT

Reaction mix (25µl)

3 primer reaction (ear snip/tissue genotyping)		2 primer reaction (genotyping post first breeding cross)		2 primer reaction (identifying KO band in THcre model)	
GX5128	0.025 µl	GX5128	0.025 µl	GX5128	0.025 µl
GCHnew	0.75 µl	GCHnew	0.75 µl	Primer 5	0.75 µl
Primer 5	0.5 µl	$MgCl_2$ 50mM	0.5mM	$MgCl_2$ 50mM	0.5mM
$MgCl_2$ 50mM	0.5mM	Biomix red	12.5 µl	Biomix red	12.5 µl
Biomix red	12.5 µl	DNA 10ng/ µl	2 µl	DNA 10ng/ µl	2 µl
DNA 10ng/ µl	2 µl	Water	Up to 25µl	Water	Up to 25µl
Water	Up to 25µl				

Thermocycle sequence

- Initial Denaturing 94°C 7 minutes
- Denaturation 94°C 30 seconds
- Annealing 63.5°C 30 seconds
- Extension 68°C 60 seconds
- Final Extension 58°C 5 minutes
- Cooling 10°C 1 minute

Cycle runs from step 2 to step 4 for 38 cycles

THcre genotyping PCR (a generic *cre* reaction was used for all *cre* models)

Primers:

- WT Forward Forward-CATCGCATAAACTGGGTGTG
- WT Reverse Reverse-TGAATCCCAAGCCATCTAGG
- TH Forward Forward-AGGTGCCTGTGACAGGGAT
- TH Reverse Reverse-AGGCAAATTTGGTGTACGG

Reaction mix (25µl)

2 primer reaction (cre identification)	
TH forward	0.25 µl
TH reverse	0.25 µl
WT Forward	0.25 µl
WT Reverse	0.25 µl
$MgCl_2$ 50mM	0.5mM
Biomix red	12.5 µl
DNA 10ng/µN	2 µl
Water	Up to 25µl

Thermocycle sequence

- Initial Denaturing 94°C 3 minutes
- Denaturation 95°C 30 seconds
- Annealing 55°C 30 seconds
- Extension 72°C 60 seconds
- Final Extension 72°C 10 minutes
- Cooling 10°C 1 minute

Cycle runs from step 2 to step 4 for 34 cycles

2.20 Cell culture

Cull culture techniques were used to generate samples for control experiments. Macrophages from Tie2cre $GCH^{f/f}$ mouse bone marrow have negligible levels of biopterins [429] and these were used as control samples in genotype reactions (see results section). The samples were kindly provided by Dr Eileen McNeil and a brief description of the isolation and culture technique is provided below. The immunohistochemical identification of GCH1 was developed initially in s.END-1 cells which express GCH1 avidly and have high biopterin levels [430]. These cells were kindly provided by Dr Mark Crabtree and their culture is also described briefly.

All culture experiments were performed in sterile conditions using laminar flow hoods and sterile materials. Culture media and supplements were purchased from PAA laboratories, Sigma-Aldrich and Lonza. Cell cultures were kept in CO_2 incubators at 37°C with a humidity saturated environment containing 5% CO_2.

2.20.1 Macrophage isolation from Tie2cre $GCH^{f/f}$ animals

Following induction of terminal anaesthesia with isoflurane, the hind legs were removed from control and knockout mice and flushed with 10ml of phosphate buffered saline (PBS) and collected. The sample was passed through a 70micron filter and centrifuged at 1200rpm for five minutes at room temperature. The supernatant was poured off and red cells with lysed with x1 red blood cell lysis solution (3 minutes/3ml per leg). RPMI (20ml) media was added and the sample of centrifuged at 1200rpm for 5 minutes. The supernatant was discarded and the sample pellet was washed with PBS. The supernatant was then poured off and the sample aliquoted into petri dishes. The cells were grown for five days in L-cell conditioned media (DMEM:F12) and then further media added at day five for feeding. At day 7, cells

were plated out at one million cells/well and stimulated with LPS and interferon-γ overnight before harvesting M1 macrophage cells and freezing in aliquots at -80°C for experimental use.

2.20.2 sEND-1 cell culture

The sEND-1 mouse endothelioma cell line was originally reported by Williams *et al.* in 1989 [430] and avidly express GCH1 and therefore have high levels of biopterins.

sEND-1 cells were grown in Complete Medium (DMEM high glucose containing 10% FCS, 100U/ml penicillin, 0.1mg/ml streptomycin and 2mM L-glutamin). Confluent cells were detached using 0.05% trypsin EDTA and passaged 1 in 10 or plated out in the desired density.

2.21 RNA techniques

Quantified reverse transcriptase PCR (qRT-PCR) was used to determine the gene expression of GCH1 in whole and microdissected adrenal tissue to assess the efficacy of genomic excision of GCH1 by cre-recombinase under the control of the TH promoter.

2.21.1 RNA extraction

Total RNA was extracted from adrenal tissue by adding 1ml of Trizol (Sigma Aldrich, UK) to tissue in Eppendorff tubes and frozen on dry ice. Samples were then thawed and 200µl of chloroform was added and centrifuged at max speed, 4 of Trizol (Sigma Aldrich, UK) to tissue in Eppendorff tubes and frozen on dry ice. Samples were then thawed and 200 excision of GCH1 by cre-recombinase under the control of the TH promoter. 2ptvxft, UK). The solution was transferred to RNeasy spin columns and

centrifuged as directed. RNA binds to the membrane in the column and contaminants including DNA are washed through. RNA was finally eluted in the included elution buffer (50µl) and final concentration quantified by spectroscopy (Nanodrop, Thermo Scientific, UK).

2.21.2 Complementary DNA synthesis

Complementary DNA (cDNA) was synthesised using SuperScript™ II Reverse Transcriptase (Invitrogen, UK). Extracted RNA was prepared at a concentration 2.5µg/20µul and 2µl of random hexamers (500µg/ml) was added. This mixture was incubated at 65°C in a PCR machine for five minutes and then chilled on ice. 18µl of mastermix (8µl x4 First-Strand buffer, 2.5µl 8mM dnTP mix, 4µul 0.1mM DTT, 3µil H_2O and 0.5µl SuperScript™ II) was added and incubated at 42° for one hour in a PCR machine. The reaction was inactivated by heating to 70°C for five minutes before storing synthesised cDNA at -20°C. Negative controls were generated by exclusion of SuperScript™ II from the mastermix and substituting H_2O.

2.21.3 Real time RT-PCR using Taqman® probes

The initial step in this process is reverse transcription of RNA into cDNA and cDNA amplification as described above. 25. 25e.cDNA was used per reaction and each sample was run in duplicate.

RT-PCR using Taqman® gene expression assays were performed using an iCycler IQ real-time detection system (BioRad Laboratories, USA) in 96 well optical plates (Applied Biosystems, USA). Each reaction volume was 25re generated by e(25ng), 12.5µl Taqman® Universal Master Mix and 1.25erformed ® gene expression assays) and the reaction sequence was as follows: 50°C for 2 minutes, 95°C for 10 minutes,

37 cycles of 95°C for 15seconds/60°C for 1 minute. All probes were designed and optimised by Applied Biosystems USA. Primers and probes spanned 2 introns to avoid amplification of genomic DNA.

Taqman® probes are oligonucleotides labelled with a reporter fluorophore and quencher fluorophore at the 5' and 3' termini respectively. They bind to DNA regions amplified by a specific set of primers. During the PCR reaction, TAq polymerase extends the primer eventually cleaving the probe and releasing the reporter fluorophore. Therefore with each cycle, fluorescence intensity increases each cycle until the reaction becomes limiting and fluorescence reaches a plateau. The threshold cycle (CT) value represents an arbitrary threshold crossed by the detected fluorescence and is inversely proportional to the initial PCR template. The threshold level is set above the baseline and within the exponential growth region of the amplification curve to detect changes in gene expression between samples. Inter sample variability is controlled for by house keeping genes which are run for each sample on the same plate as the target gene. In these experiments, GAPDH was used as the housekeeper target and inter-sample variability was adjusted for by calculating the ΔCT value for each duplicate (target gene CT – housekeeper gene CT).

2.22 Determination of protein concentration using the BCA™ Protein Assay Kit

The protein concentration of each sample was determined by using the reducing agent compatible BCA (Bicinchoninic acid) protein assay (Pierce, USA). This is a highly sensitive colorimetric assay and its assay solution is contains Cu^{2+} ions which are reduced to Cu^{+} by peptide bonds in the protein sample and is proportional to the amount of protein in the sample. The reduced Cu^{+} ions are chelated by BCA and this results in a purple product that absorbs slight at 562nm. Incubation of the sample with

iodoacetamide (10mg/ml) inactivates the reducing agents and allows accurate determination of protein concentration.

Experimental samples were divided into samples for analysis and 12µl aliquoted for protein concentration determination. Iodoacetamide (12µl, 20mg/ml in 0.4% NaOH) was added and incubated at 37°C for 15 minutes. BCA reagent (480µl) was then added and further incubated at 37°C for 30 minutes. This mixture was then loaded in 200µl duplicates in a 96 well plate. Protein standards prepared from bovine serum albumin diluted in the same buffer as in the sample (4mg/ml to 0.125mg/ml) were loaded on the sample plate in duplicate. The final plate was read in a microplate reader at 562 nm.

2.23 Western immnoblotting for GTPCH and TH

Western immunoblotting was used for the quantification of GTPCH, TH and GAPDH (loading control). Tissue (whole adrenal gland, micro-dissected cortex/medulla) was homogenised in CellLytic™ buffer (Sigma Aldrich, UK) with 1 tablet/10ml of protease inhibitor (Complete Mini, EDTA free, Roche, UK). Tissue was disrupted in an Eppendorff tube using an Eppendorff pestle and then put through 2 freeze-thaw cycles on dry ice to maximise release of protein. The samples were then centrifuged at max speed, 4°C for 5 minutes. The supernatant containing the extracted protein was transferred to a new tube and the cell pellet stored at -80°C for DNA extraction if needed. Protein concentration was determined by the BCA assay as described above. Samples for western blotting were prepared in x4 NuPAGE® LDS sample buffer and x10 NuPAGE® reducing agent (Invitrogen, UK) and incubated at 70°C for 10 minutes before gel electrophoresis. Protein lysates (5-20µg) were resolved by SDS-PAGE using NuPAGE® 4-12% Bis-Tris gel in NuPAGE® MOPS SDS running buffer

(Invitrogen, UK). Resolved protein was then transferred to a polybinylidene difluoride (PVDF) membrane and blocked for 2 hours in 5% non-fat milk in PBS with 0.1% Tween-20 (PBST) at room temperature. Primary antibodies were made up in 5% non-fat milk in PBST and incubated overnight at 4°C. The anti- primary antibodies included anti-GTPCH (1:50,000, a generous gift to the laboratory from Professor Steve Gross, Cornell University, New York, USA), anti-TH (1:20,000, Sigma, UK) and anti-GAPDH (1:20,000, Sigma, UK). Appropriate HRP-conjugated secondary antibodies (Promega, USA) were used at concentrations of 1:5000 (in PBST) and incubated at room temperature for 1 hour. Protein bands were visualised by chemiluminescence (Supersignal, Pierce, USA) and band intensity was quantified using ImageJ (National Institutes of Health, USA).

Membranes were stripped for 30 minutes at 50°C in stripping buffer (6.25mM Tris (pH 6.8), 2% SDS, 100mM β-mercaptoethanol) and blocked in 5% milk in PBST to allow re-probing with an different primary antibody.

2.24 Measurement of biopterins: BH4, BH2 and biopterin

Tetrahydrobiopterin and oxidised biopterins were measured separated in samples by high-performance liquid chromatography followed by electrochemical detection of BH4 and fluorescent detection of BH2 and biopterin [431, 432].

Snap frozen tissue samples were homogenized in ice-cold resuspension buffer (50mM phosphate buffered saline, 1mM dithioerythriol (DTE), 100mM EDTA, pH 7.4) as above and put through 2 freeze-thaw cycles on dry ice to promote cell lysis. Samples were then spun at max speed, 4°C for five minutes and the supernatant was removed to a new tube. Samples were prepared at the desired dilution (1 in 10 for all

adrenal tissues) with ice-cold resuspension buffer and protein removed by addition of precipitation buffer (1M orthophosphoric acid, 2M trichloracetic acid, 1mM DTE) and centrifuging for five minutes at max speed at 4°C. Optimisation of the method for detection of biopterins from adrenal tissue was required in order to identify the eluted BH4 peak (figure 2.11). Initial samples demonstrated a large peak eluted between 5 and 6 minutes consistent with the elution time of BH4 and corresponded to applied standards. However, the peak was broad based and the true peak could not be seen and appeared to more in keeping with a contaminant or other eluted product. Reducing the concentration of sample run of did not change these appearances. Therefore, the columns were washed systematically with methanol (overnight) followed by water (24h) and mobile phase (12h) prior to running samples. For additional quality control, control adrenal tissue (wild type) were prepared and run in pairs (adrenal, adrenal+ 2µl biopterin standard) to confirm that BH4 could be identified.

External standards were prepared from stock solutions of BH4, BH2 and biopterin (Shirks, Switzerland) over a range of concentrations. These were prepared in resuspension buffer and injected before adding experimental samples.

Samples were injected onto an isocratic HPLC system and quantified using sequential electrochemical detection (Coulochem III, ESA Inc., UK) and fluorescent detection (FP2020, Jasco, UK). Samples were separated using a 250mm ACE C-18 coloumn (Hichrom, UK) and mobile phase at 1.3ml/min (50mM sodium acetate, 5mM citric acid, 48µM EDTA, 160µM DTE, pH 5.2; all chemicals and water HPLC grade). Currents across electrochemical cells E1 and E2 were adjusted to +500 to +600nA

and -50 to -60nA respectively. The cells were adjusted at the start of sample injection and not readjusted mid experiment. Samples were quantified by comparison to external standard and normalised to protein concentration (protein assay as above or Nanodrop).

2.25 Measurement of plasma catecholamines

Whole blood was collected from the inferior vena cava (IVC) of THcreGCH$^{f/f}$ and control GCH$^{f/f}$ animals after schedule 1 sacrifice as described above into heparinised syringes. Whole blood samples were centrifuged at 4°C, 3000rpm for 15 minutes to separate plasma from red cells. Plasma was transferred to a new Eppendorff tube and frozen at -80°C.

For catecholamine determination [433], samples were prepared in a 50:50 dilution with perchloric acid centrifuged through a 0.22µm filter (VWR) at max speed, 4°C for three minutes. Samples (50µl) were injected onto an isocratic HPLC system and quantified using electrochemical detection (LC-4B) and carbon working electrode held at +0.7V vs a Ag/AgCl electrode (Decade SDC, Antec). HPLC separation was performed using a 250-mm Microsorb C18 reverse-phase column (Agilent) and mobile phase comprising methanol (13% v/v), NaH_2PO_4 (120mM), EDTA (0.8mM), and sodium octane sulfonate (3.2mM), pH 3.27 at a flow rate of 1ml/min. Catecholamine quantification was done relative to freshly prepared standards (figure 2.12).

2.26 Non-invasive blood pressure recordings

Systolic blood pressure was measured in THcreGCH$^{f/f}$ mice (male) and GCH$^{f/f}$ littermate controls using the Visitech® computerised tail-cuff system (Visitech, USA). This system employs plethysmography to identify pulsatile blood blow in the

mouse-tail. Individual mice are placed on a warmed plate in small cage restrainers and the tail is pulled through a small inflatable blood pressure cuff (the system accommodates six mice simultaneously). The tail is taped to the stage to limit movement artefact. The pulse is identified and the cuff inflated automatically until the pulse signal is lost and this is the systolic blood pressure. Mice were habituated for five consecutive days with recordings done in the morning to capture the 'awake' circadian cycle of mice with subsequent daily recordings over five days. Twenty recordings were taken per mouse of which the first 10 were discarded. A mean of the remaining appropriate traces was used to calculate the systolic blood pressure. Heart rate was determined and analysed in a similar manner.

2.27 Motion tracking

The effect of GCH deletion in the THires mediated knockout model on mobility was established by undertaking automated motion tracking based on an established protocol from the Nuffield Department of Clinical Neurosciences at the University of Oxford [434]. Mice were housed individually in standard ventilated cages (IVCs) with and illuminated by an overhead cool white LED light source. A conventional webcam (Logitech) was used to acquire one minute videos of THires $GCH^{f/f}$ and littermate controls. All videos were recorded at three frames/second and stored in the AVI format. Video files were then analysed in a blinded fashion using ANY-maze 4.5 (Stoelting, Wood Dale, Illinois) to determine the total distance travelled during the acquisition. Raw data was then un-blinded for analysis.

2.28 Statistics and data analysis

Data were analysed using Microsoft Excel (Microsoft, USA), Graphpad Prism (Graphpad Software, USA) and Statplus (AnalystSoft Inc, USA). All data is presented

as mean ± standard error of mean. Normally distributed data (determined by Shapiro-Wilk) was analysed by ANOVA (with post hoc test as appropriate), paired t-test, unpaired t-test or Mann-Whitney U test as appropriate. A p value of less than 0.05 was considered significant.

2.29 Chapter 2 Figures

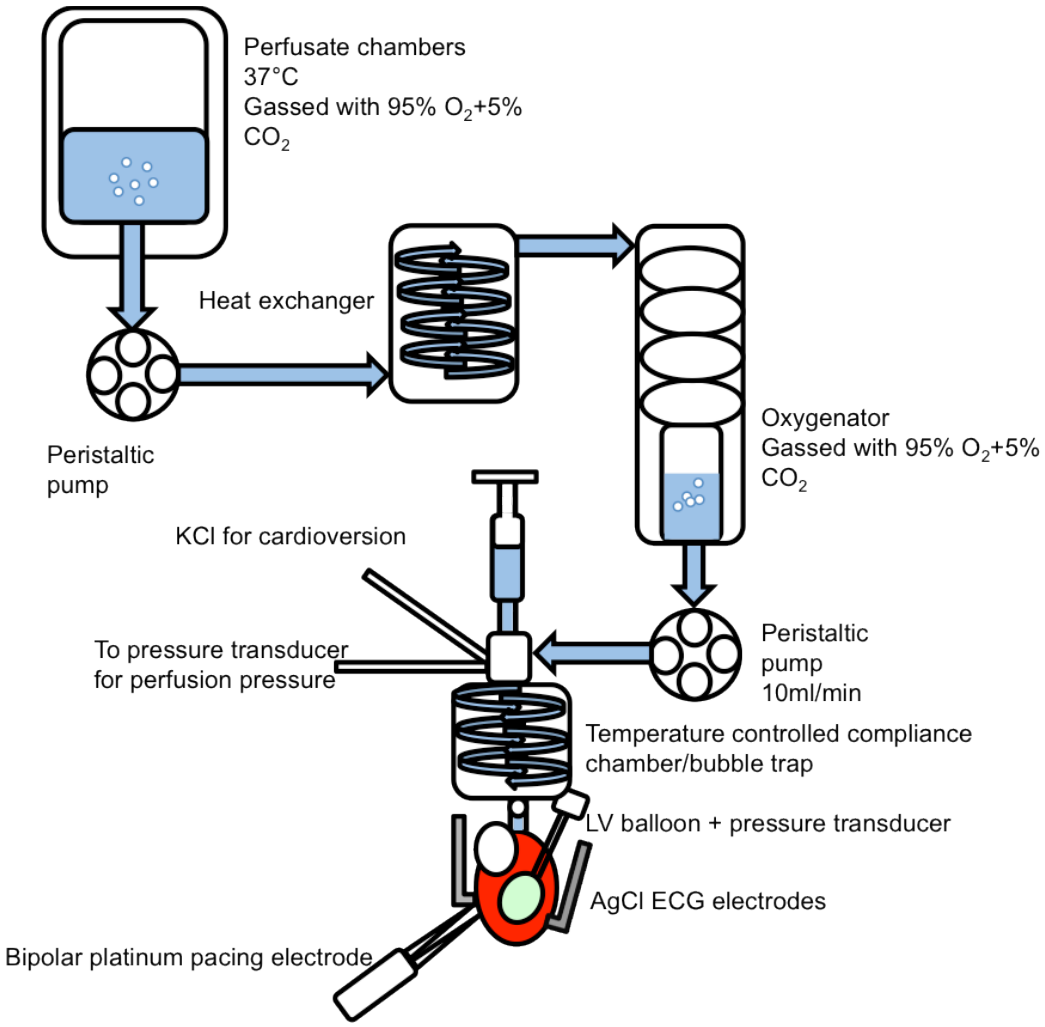


Figure 2.1 Schematic of Langendorff apparatus for whole heart experiments

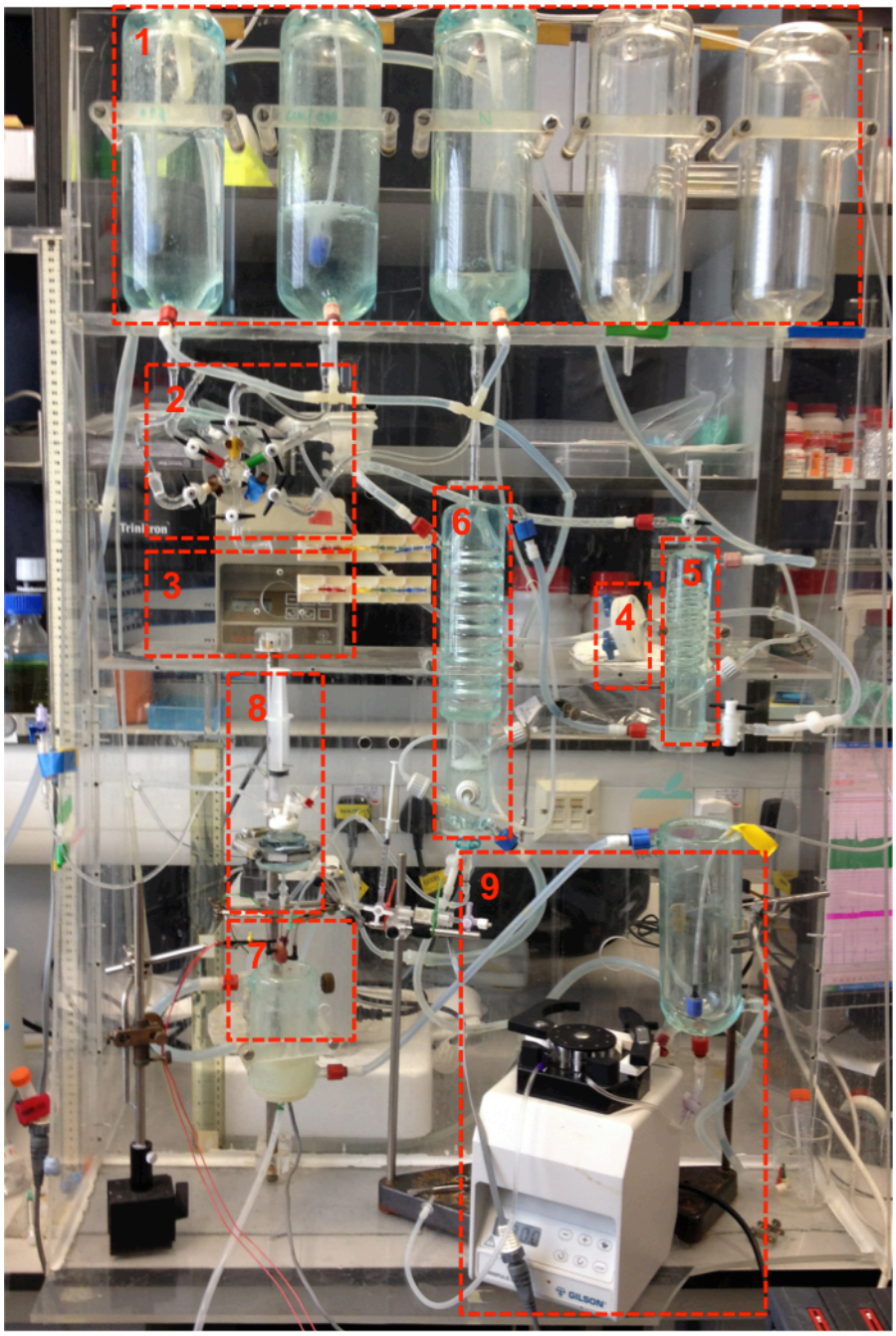


Figure 2.2 Photograph of Langendorff apparatus used for whole heart experiments

All glassware was water-jacketed and the water bath kept at 38°C. Perfusate was kept in the (1) perfusate chambers and gassed with carbogen (95% O_2+5% CO_2) and delivery controlled via (2) a multiport tap system. This fed into (3) pump no.1, which pushed the perfusate through (4) a 5micron filter to the (5) heat exchanger which prevented a significant drop in perfusate temperature during transit. Perfusate then passed to (6) the oxygenation chamber which was also gassed with carbogen and optimised oxygenation. (7) Pump no.2 was calibrated to deliver 10ml/min to the mounted heart via (8) the junction block with maintained temperature and allowed measurement of perfusion pressure and delivery of drugs. A 20ml syringe was used a windkessel to minimise oscillations in perfusate flow. (9) An additional chamber and pump was added to the system for additional drug perfusion as required where a smaller volume was needed.

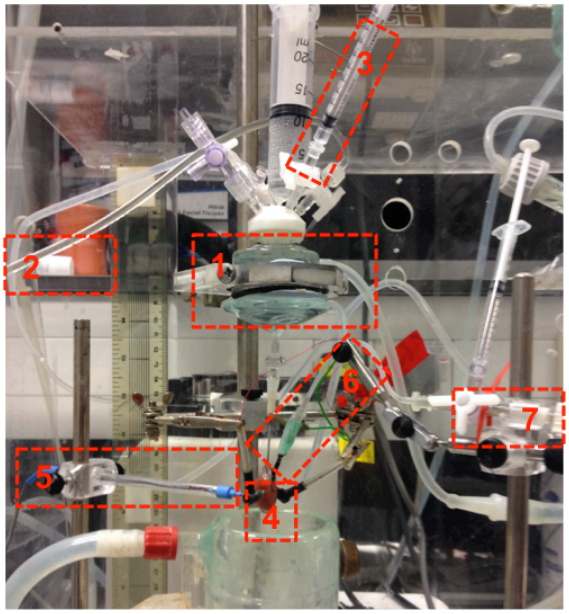


Figure 2.3 Photograph of typical experimental preparation

Perfusate was pumped at 10ml/min into the (1) junction block with a header unit (white) which allowed connection to (2) pressure transducer for perfusion pressure (not in image) and (3) drug delivery for cardioversion. ECG was recorded by (4) silver chloride electrodes and the heart was stimulated by a (5) custom made platinum bipolar pacing electrode. Left ventricular developed pressure was measured by a (6) custom made, water filled balloon inserted via the left atrium connected to a (7) pressure transducer.

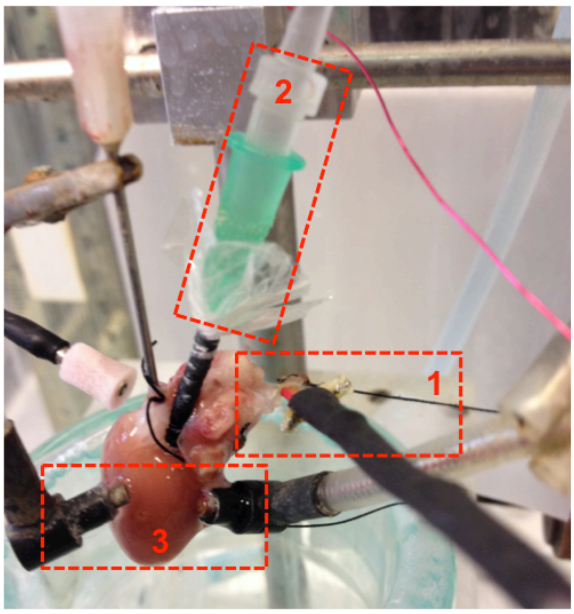


Figure 2.4 Photograph of an experiment of an isolated rat heart with intact sympathetic innervation

A (1) custom made, platinum electrode was used to hook the stellate ganglia and stimulate with a custom made stimulator (not in image). Developed pressure was measured as above with a (2) custom made balloon and ECG acquired with (3) silver chloride electrodes. A bipolar pacing electrode (not shown) was used for pacing.

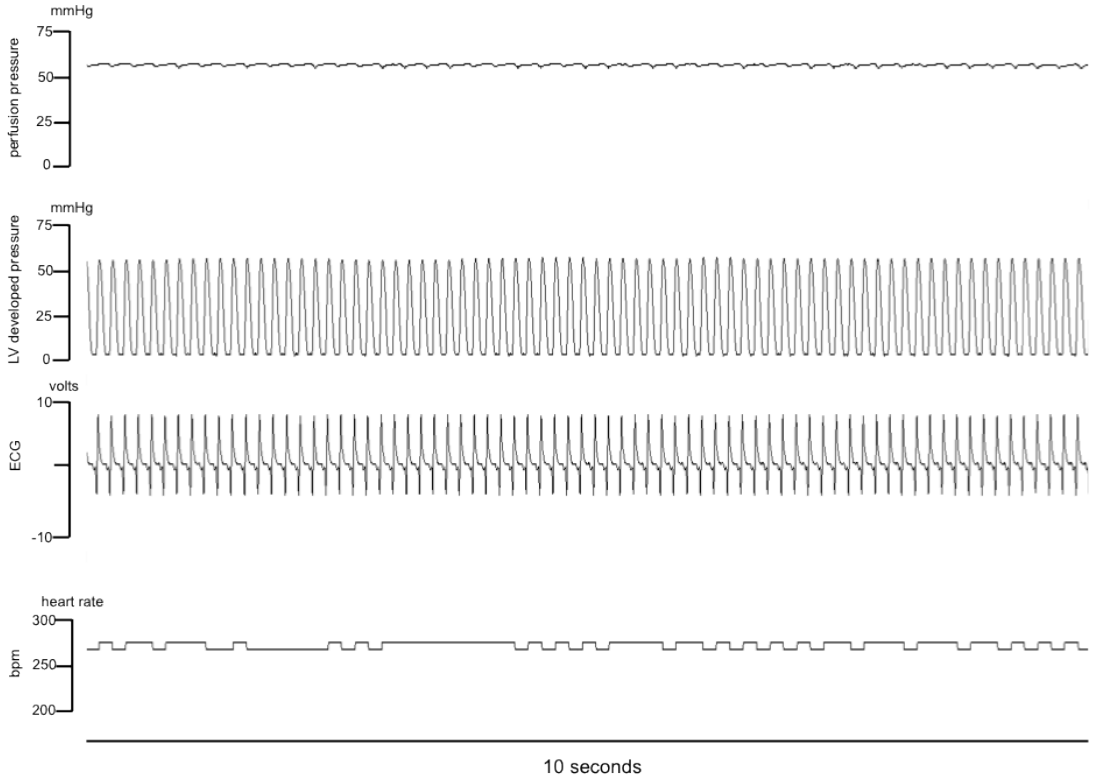


Figure 2.5 Raw data trace of measured physiologic parameters

Experimental traces from an isolated rat heart preparation following stabilisation. Perfusion pressure was measured via a pressure transducer connected in parallel to the junction block. Left ventricular developed pressure was measured by a custom made, water filled balloon inserted via the left atrium into the left ventricle connected in series to a pressure transducer. Custom-made silver chloride electrodes acquired a single channel ECG and heart rate was derived from the R-R interval on the ECG channel.

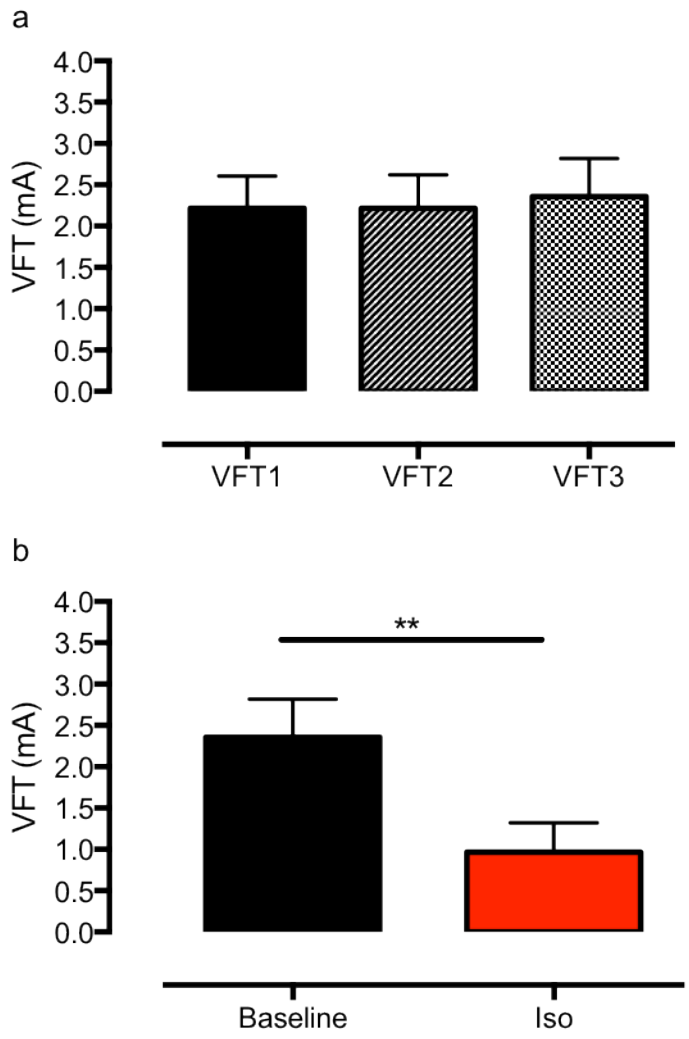


Figure 2.6 Ventricular fibrillation threshold: control data

(a) Ventricular fibrillation threshold (VFT, mA) remained consistent over 3 inductions separated by 15 minutes (n=7, p=ns, ANOVA). (b) The protocol was able to detect a change in VFT with pharmacological modulation with isoprenaline (Iso 10nM, n=7, $p<0.01$, paired t-test)

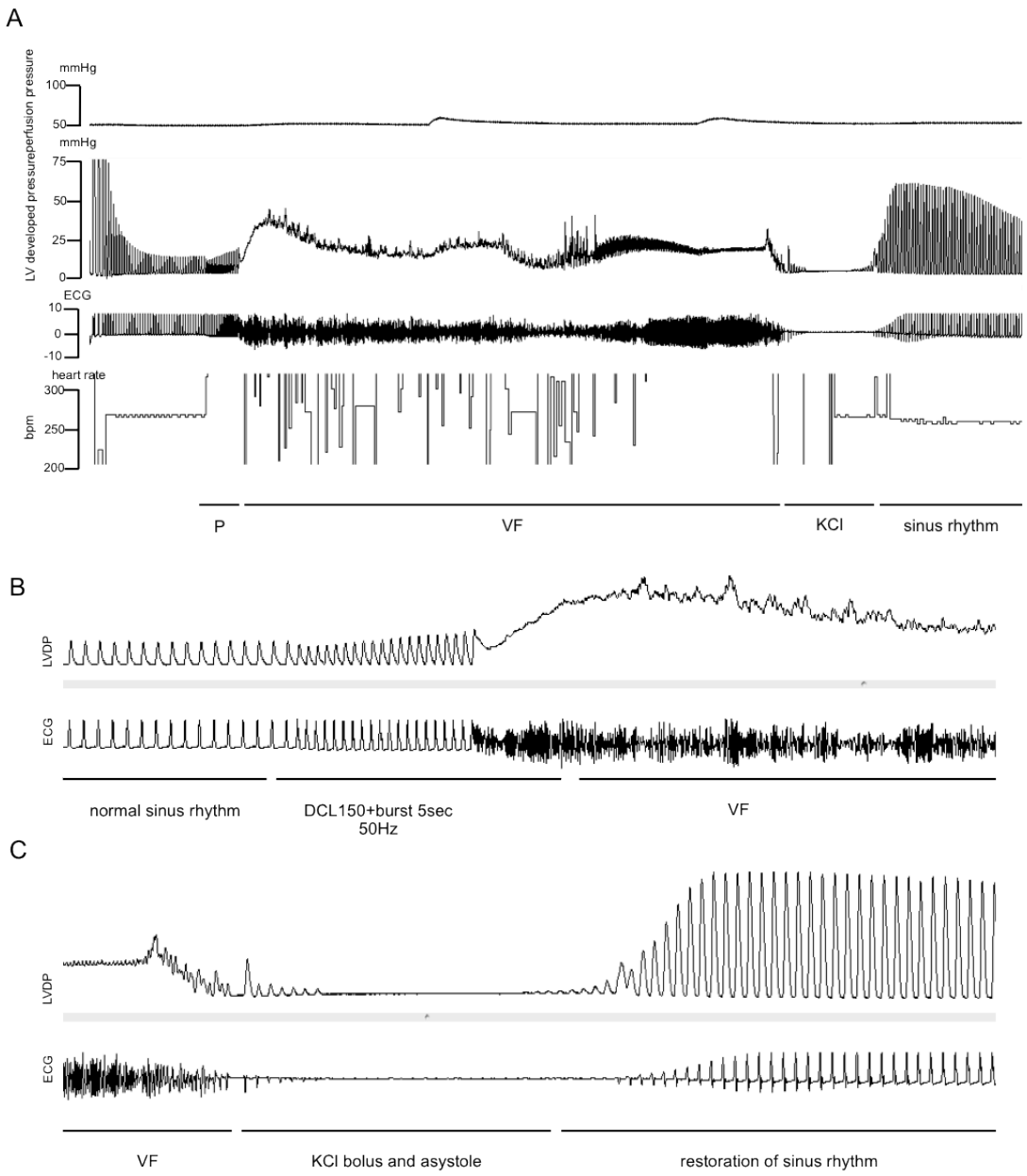


Figure 2.7 Ventricular fibrillation threshold testing

Panel A: Experimental data demonstrating induction of VF. The heart was paced at a cycle length of 150msec for 20 beats followed by a 5 second 50Hz burst (P). VF in then induced and LV developed pressure becomes unrecordable. The current at which VF was induced was recorded as the VFT (mA). VF is cardioverted with a 1ml bolus of KCl (50mM) with initial asystole and restoration of normal rhythm and contractile function as the KCl is washed out with normal perfusate.
Panel B: Focused data trace demonstrating induction of VF
Panel C: Focused data trace demonstrating cardioversion of VF with a 1ml bolus of KCl (50mM). Following KCl administration, there may be some evidence of organised electrical activity on the ECG (asystole phase) but no functional contraction takes place until the KCl is washed out and sinus rhythm is restored.

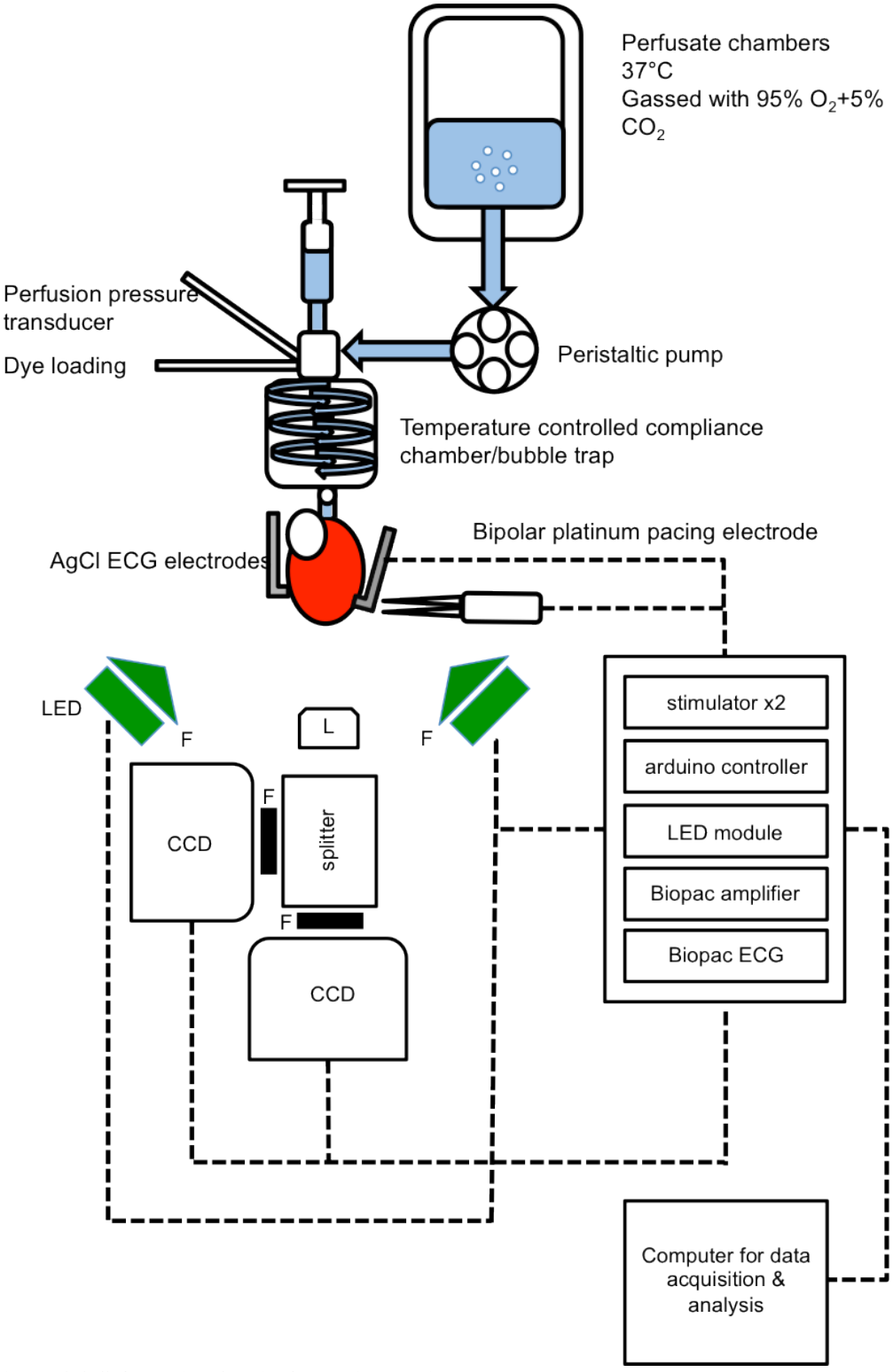


Figure 2.8 Schematic of optical mapping equipment

A modified Langendorff apparatus was used to retrograde perfusion. Fluorescent dyes were loaded directly above the perfusion cannula via the multiport header to the junction block. Blebbistatin loading was via the perfusate chambers The preparation was illuminated by 2 green LED lights with filters (wavelength). Emitted light was captured with CCD cameras housed on an optical splitter to allow multi-parametric imaging. Pacing and imaging acquisition was controlled via a computer connected to an arduino module for timing, Biopac amplifier and x2 stimulators (Digitimer DS7 and DS2). The system was mounted on a pressurised air table to prevent motion artefact.
(AgCl: silver chloride, LED: light emitting diode, F: filter, CCD: charge coupled device, L: lens)

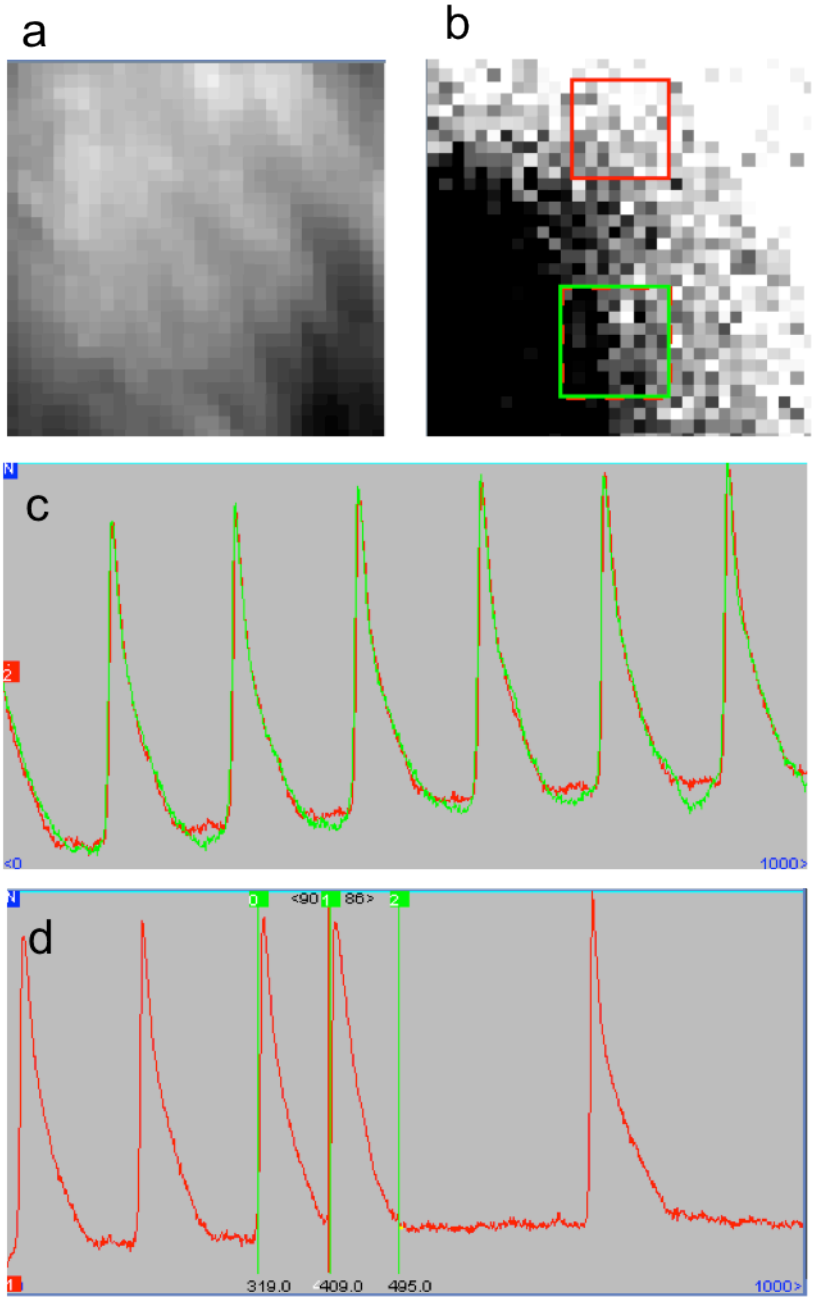


Figure 2.9 Optical mapping of whole hearts

Raw data panel of optical mapping of membrane voltage with RH237. (a) shows a raw image of the anterior LV wall following dye loading which is then (b) normalised to allow the fractional change in fluorescence during depolarisation to be seen. An advancing wave is shown with 2 regions of interest marked (red/green) at base and apex. (c) Action potentials (APD) from both regions during 6Hz pacing are shown demonstrating consistency of AP duration over a 1000msec acquisition. (d) Raw data trace of S1-S2 (150msec-70msec) pacing to generate a restitution curve with a custom made script used to measure APD (green lines, APD (msec) shown in between timing cursors).

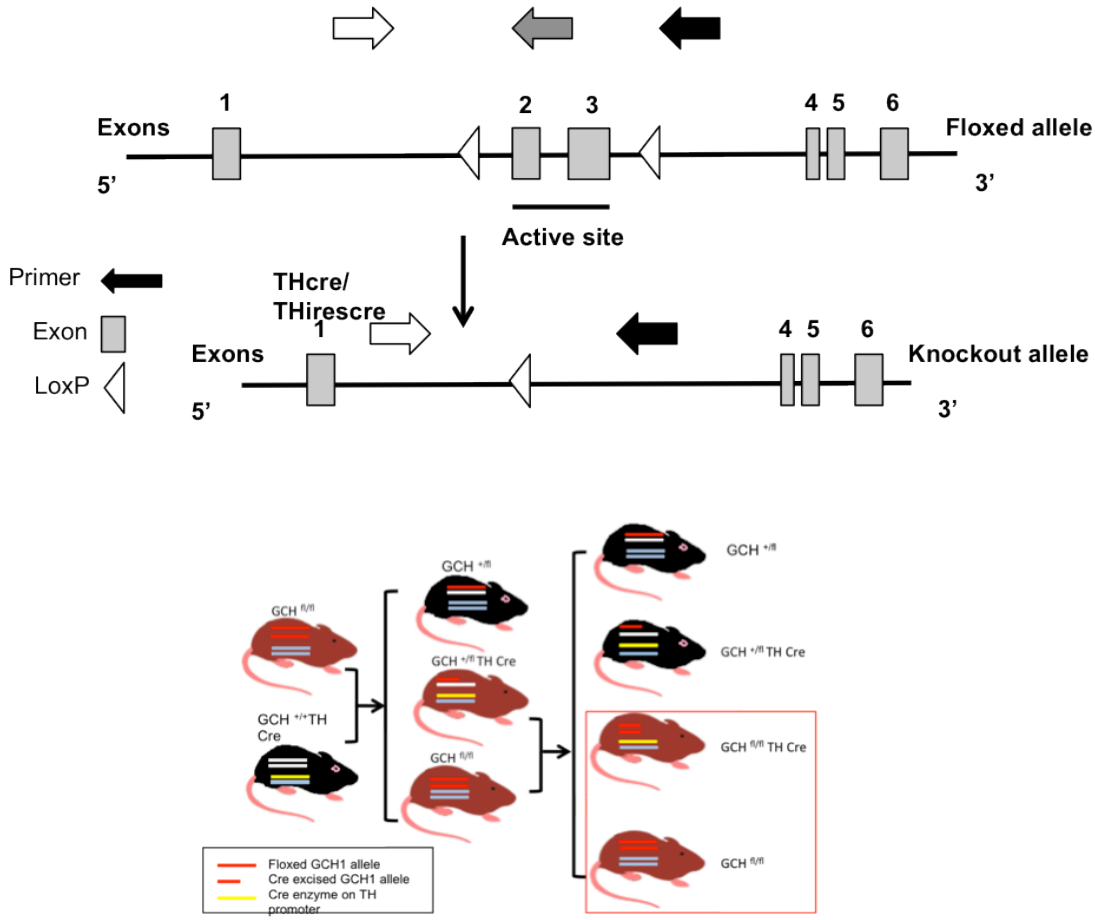


Figure 2.10 Breeding protocol for generation of tissue specific GCH1 knockout mouse model

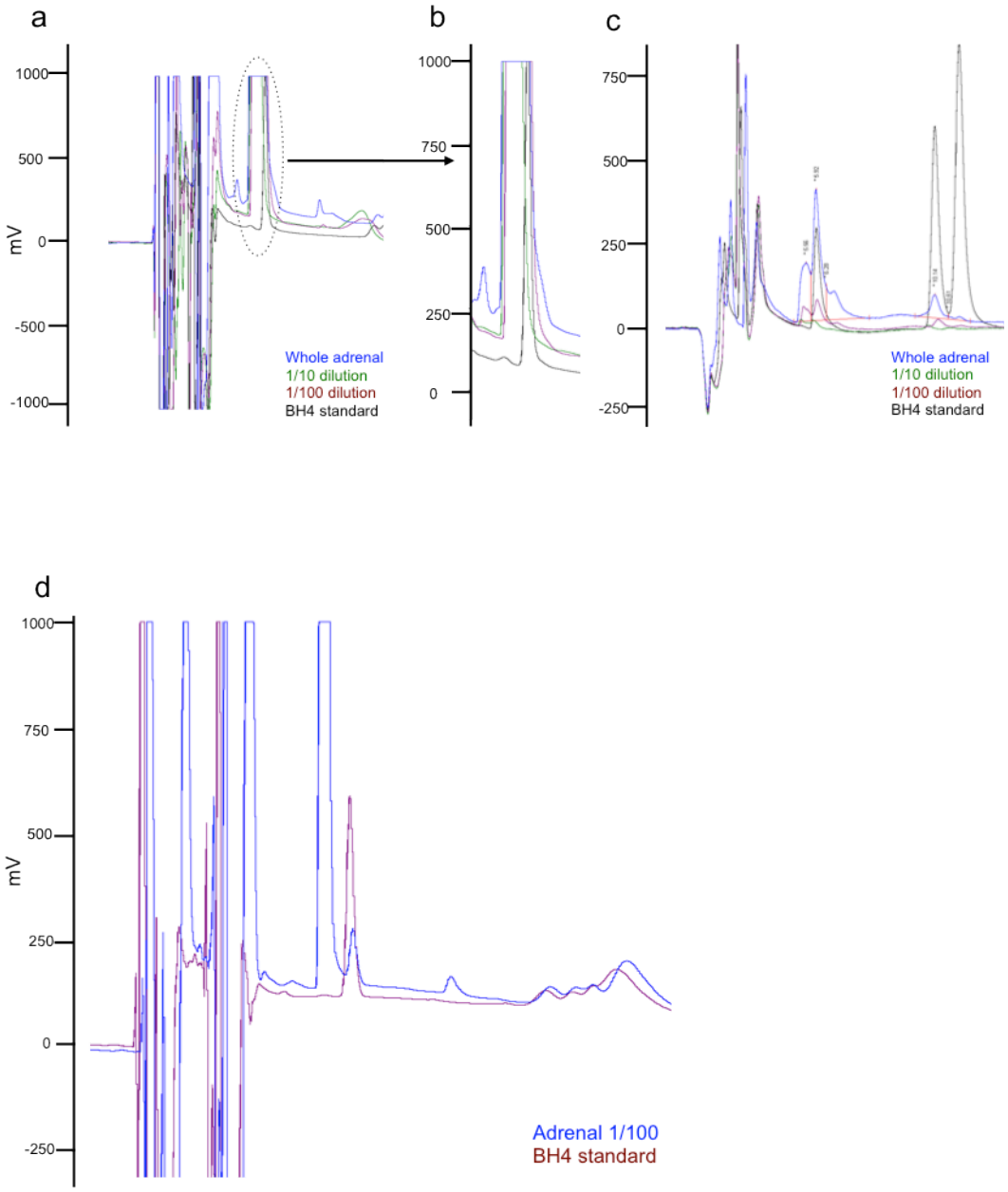


Figure 2.11 Optimisation of BH4 determination by HPLC in adrenal tissue

(a). Initial experiments with whole adrenal tissue identified a wide based elution product with electrochemical detection corresponding to the BH4 standard. This signal could not be interpreted despite serial dilutions. b. Magnified panel of eluted product shown in (a). (c). BH4 could be identified using fluorescent detection but a multiple peak product was again identified as seen previously in analysis of human plasma samples (Cunnington *et al.* 2010). (d). Following meticulous preparation of the apparatus, electrochemical detection is able to detect a split product with the second, smaller peak corresponding to BH4.

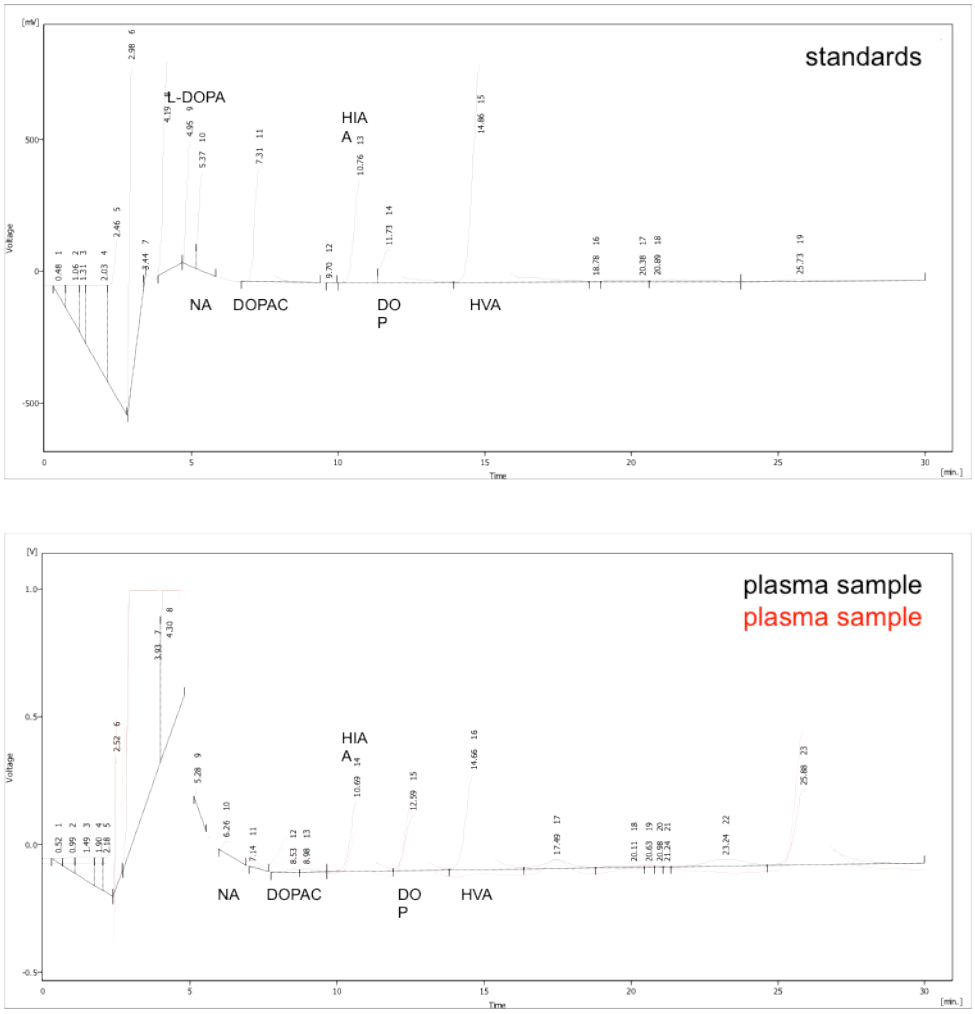


Figure 2.12 Catecholamine determination by HPLC in mouse plasma

Electrochemical detection was used to determine plasma catecholamine levels in mouse plasma. Freshly prepared standards (a) were used to determine catecholamine and metabolites and used to (b) identify eluted products in plasma samples. Not all products could be identified due to the solvent front in plasma samples being wider and therefore masking L-DOPA and noradrenaline chromatograms.

Chapter 3 The cholinergic modulation of ventricular fibrillation threshold

3.1 Introduction

The anti-arrhythmic action of the vagus on the ventricle is well established [53, 58, 60, 145, 259]. Early studies demonstrated that vagal nerve stimulation reduces the occurrence of ventricular arrhythmia post coronary artery occlusion (CAO) in canine models, and raised ventricular fibrillation (VF) threshold (VFT) independent of heart rate (HR) changes [60]. Conversely, bilateral vagotomy in the setting of CAO increased mortality [61]. There are a range of mechanisms by which stimulation of the cardiac vagus may prevent the initiation of ventricular ectopics, re-entry and subsequent wavebreak, that leads to VF. These include reducing myocyte calcium load [99, 103], prolonging action potential duration (APD) and reducing dynamic APD shortening (electrical restitution) [139], prolonging refractory period [142, 435, 436], increasing conduction velocity [101, 102], and reducing the spatial dispersion of these variables [98, 99]. In the long term, chronic vagal stimulation also improves conduction velocity by modifying gap junction expression [102].

Despite these observations, the pathways that link cardiac vagal nerve stimulation to these mechanisms remain controversial. Early studies demonstrated that the anti-fibrillatory effect of the vagus on the ventricle was abolished by the muscarinic receptor antagonist atropine [59, 61, 66]. Muscarinic agonists such as oxotremorine and methacholine can also reduce ventricular arrhythmias following myocardial infarction [111, 112]. More recently, in an isolated Langendorff perfused rabbit heart, the anti-fibrillatory action of vagal stimulation appears to be preserved in the presence of atropine [100], but rather dependent on the generation of nitric oxide by neuronal nitric

oxide synthase (nNOS) acting in a paracrine fashion [94, 140, 437]. This seemed surprising given previous observations with atropine and muscarinic agonists *in-vivo,* and the fact that NO generated by nNOS can facilitate acetylcholine release [132]. I therefore sought to determine whether a stable acetylcholine analogue, carbamylcholine (CCh) directly raises VFT in an isolated Langendorff perfused heart. Moreover I also investigated whether the VFT was dependent on muscarinic and/or nicotinic receptor stimulation and the generation of NO.

3.2 Methods

3.2.1 Animals

Male Sprague-Dawley rats (300-350g, n=92), were sourced from Harlan (Bicester, UK) and kept under standard laboratory conditions in accordance with the Animals (Scientific Procedures) Act 1986 (UK) and the Guide for the Care and Use of Laboratory Animals published by the US National Institutes of Health (NIH Publication No. 85-23, revised 1996). Experiments were performed under British Home Office Project License PPL 30/2630.

3.2.2 Langendorff perfused rat heart

Following thoracotomy the heart was removed and placed in ice-cold heparinised Tyrode's solution (50 units/mL) before mounting on to a cannula in order to establish retrograde perfusion via the ascending aorta with constant flow (10 ml/minute). An in line pressure transducer was used to record perfusion pressure (PP). The heart was left to stabilize for 15 minutes before the left atrial appendage was removed and a custom-made fluid-filled, balloon introduced into the left ventricle to measure left ventricular developed pressure (LVDP). The balloon was inflated to obtain an end diastolic pressure of 0-5mmHg. An electrocardiogram (ECG) was recorded via custom-made

silver chloride contact electrodes. Heart rate (HR) was calculated from ECG and the signals displayed in real time. All signals were amplified by a data acquisition system (Biopac System MP150) and were recorded using Acknowledge 4.0 software (Biopac systems, USA). Experimental protocols commenced after a 30-minute equilibration period by which time measurements had stabilized (±5 bpm/mmHg respectively). Only one experimental protocol was run on an individual heart and these were a maximum duration of 120 minutes during which time physiological parameters remained stable.

3.2.3 Ventricular fibrillation threshold testing

Electrical pacing protocols were designed on Acknowledge 4.0. A custom-made bipolar platinum electrode, approximately 2mm apart, was inserted into the apex of the right ventricle. This was connected to a constant current stimulator (Digitimer DS7A). VFT was obtained with pacing using a fixed 20 beat drive train at a cycle length of 150msec followed by a 5 sec 50Hz burst scanning the refractory period. The current delivered was increased by 0.5mA, from 0.5mA, until VF was induced. VF was defined as chaotic, fractionated electrical activity [21] persisting for >5 seconds and was cardioverted to sinus rhythm with a bolus injection of 1ml potassium chloride (50mmol/L) within 10 seconds. Hearts were given 15 minutes to re-stabilise following VF induction, until HR and LVDP were back to pre-stimulation levels (±5bpm/mmHg respectively).

3.2.4 Optical mapping of voltage

Following a stabilization period of 20 minutes, hearts were perfused with the excitation-contraction (EC) uncoupler blebbistatin (10μM, Invitrogen) and loaded with voltage-sensitive dye RH237 (15μL of 5mg/mL over two minutes) [399, 438, 439].

The anterior surface of the heart was illuminated by two 530nm green lights using the left anterior descending artery as a landmark. A Photometrics Evolve optical imaging camera was used to acquire 32x32 pixel frames for voltage mapping. Acquisition and data analysis was performed using custom-written software (courtesy of Dr Gil Bub and Jakub Tomek). Action potential duration restitution curves were generated by applying an exponential function to the data (OriginPro 9, Northampton, MA, USA) and their maximum gradients determined using a tangent function.

3.2.5 NOx chemiluminescence assay

Perfusate samples were collected from the stabilized preparation before and after administration of CCh (200nM) or CCh (200nM) and mecamylamine (10μM) every two minutes and immediately snap frozen in liquid nitrogen. After thawing, samples were injected into a vanadium chloride solution heated to 95°C to ensure complete conversion of NO metabolites to NO. Values were derived from a gas-phase chemiluminescence reaction between NO and ozone in which an intermediary radical dissociated to yield a single photon, and compared across the two groups[424]. Blank Tyrode solution samples and a nitrite standard curve provided negative, and positive controls, respectively.

3.2.6 Solutions and drugs

The Tyrode's solution contained (mM) NaCl 120, KCl 4, $MgSO_4*7H_2O$ 1.3, $NaH_2PO_4*2H_2O$ 1.2, $CaCl_2$ 1.2, $NaHCO_3$ 25.2, Glucose 11, and was constantly aerated with carbogen (95% O_2, 5% CO_2), to maintain pH 7.35-7.45. All solutions were filtered before passing through two oxygenators and a bubble trap as part of the Langendorff apparatus. All glassware was water-jacketed to maintain a coronary perfusate temperature of 37±0.5°C. Drugs were prepared in Tyrode's solution at the

desired concentration. The concentration of CCh (200nM, Sigma) was chosen to produce a stable physiological change in HR (~20%), whilst the muscarinic receptor antagonist atropine (0.1μM, Sigma) was used at a concentration that completely blocked the CCh mediated bradycardia. Mecamylamine (10μM, Sigma) was used at a concentration that had no effect on the CCh mediated bradycardia but that has previously been shown to block the nicotinic receptor [440]. The SNP concentration used (10μM, Sigma) had previously been shown to produce a maximal tachycardia in cardiac tissue [441]. Concentrations of the non-specific NOS inhibitor L-Nitro Arginine (L-NA, 100μM, Sigma) [135], the nNOS inhibitor N-(4S)-4-amino-5-[aminoethyl]aminopentyl-N'-nitroguanidine (AAAN, 10μM, Tocris) [442], the soluble guanylyl cyclase inhibitor 1H-[1,2,4]oxadiazolo[4,3-a]quinoxalin-1-one (ODQ, 10μM, Tocris) [132] and the NOS substrate L-Arginine (L-Arg, 5mM, Sigma) [135] are above the reported K_{50} for the isolated enzymes and similar to concentrations used in previous studies of cardiac tissue.

3.2.7 Statistical analysis

Data are presented as mean ± standard error of the mean. All significance tests are two-tailed and all data passed a normality test (Shapiro-Wilk). One-way ANOVA was applied to all grouped data, with post-hoc analysis to determine significance (Neuman-Keuls, $p<0.05$). A paired or unpaired t-test assuming unequal variance was used to determine significance between groups where appropriate.

3.3 Results

3.3.1 Inclusion criteria

Hearts were excised as described above and retrograde perfusion via the ascending aorta was established in under 60 seconds. The hearts were then allowed to perfuse and equilibrate for 30 minutes. After the equilibration period the physiological parameters of heart rate (>240bpm), LVDP (>45mmHg) and perfusion pressure (>50mmHg) had stabilized and remained constant throughout each protocol unless otherwise stated.

3.3.2 Protocol for testing VFT

A number of pacing protocols were tested (see Chapter 2) in order to determine the most reproducible protocol for induction of VF. A series of control experiments with a 20 beats drive train (150msec) followed by a 5 second 50Hz burst demonstrated that VFT remained constant over successive inductions (VFT1 2.21±0.39 vs. VFT2 2.21±0.40 vs. VFT3 2.35±0.45mA, n=7) with no deterioration in Langendorff physiology or epicardial trauma (n=7).

3.3.3 The effect of CCh on haemodynamics and VFT

An experimental trace of CCh perfusion is shown in figure 3.1. Figure 3.2 describes the haemodynamics effect of CCh (200nM) perfusion (n=9). There was a significant reduction in heart rate (baseline 292±8 vs. CCh 224±6 vs. wash out 285±9bpm) without alteration in perfusion pressure (baseline 65±9 vs. CCh 71±10 vs. wash out 69±8mmHg) or left ventricular developed pressure (baseline 69±2 vs. CCh 61±3 vs. wash out 64±4mmHg). Ventricular fibrillation threshold was increased significantly by CCh (baseline 1.5±0.25 vs. CCh 2.4±0.4, vs. wash out 1.14±0.18mA, n=9) and this

effect was lost upon wash out of the drug (figure 3.3). This effect was independent of heart rate as the VFT protocol included a 20 beat drive train at 150msec (400bpm) prior to the application of the 5 second 50Hz burst.

3.3.4 The effect of CCh on ventricular electrophysiology

In view of the increase in VFT seen with CCh, the aim of this series of investigations was to determine the changes in ventricular electrophysiology seen with CCh perfusion. The hypothesis was that there would be favourable changes in action potential duration (APD) and electrical restitution in the presence of CCh. Initial attempts were made to acquire this data by a suction electrode [398] applied to the epicardial surface of the left ventricle during CCh perfusion. This technique was limited by its spatial resolution as it interrogated only one small region of the ventricle and technical challenges in maintaining stable suction during rapid pacing.

Therefore this question was investigated by optical mapping as described above and in Chapter 2. This provided the ideal platform for spatial and temporal assessment of electrophysiology in the isolated heart. Conduction velocity was assessed by fixed rate pacing and is represented by the isochronal map and summary data in figure 3.4a and 3.4c. There was a trend towards an increase in conduction velocity at all pacing rates (5-9Hz, n=6), most marked at 5Hz, but this did not reach statistical significance. However, APD is prolonged at fixed rate pacing as shown in figure 3.4b which represents a map of median APD_{80} during 5Hz pacing. This effect on APD was explored with the application of an extra-stimulus following a 20 beat drive train at 150msec (S2 140-40msec). This demonstrated less marked shortening of the APD in response to the extra-stimulus compared to control (figure 3.4d). This relationship

when plotted against the diastolic interval between the last beat of the drive train and extra-stimulus beat generated the electrical restitution curve (figure 3.4e), which was flatter in the presence of CCh. This was in keeping with its anti-fibrillatory effect. This effect was consistent and statistically significant, with a greater than 50% reduction (baseline 0.35±0.1 vs. CCh 0.15±0.05) in maximal slope of the restitution curve in the presence of CCh (figure 3.4f).

3.3.5 Role of muscarinic receptor

Once the anti-fibrillatory effect of CCh was established by demonstrating the increase in VFT and change in global electrophysiological properties during CCh perfusion, the following experiments aimed to define the receptor dependence of this effect.

Ventricular fibrillation threshold was determined in the presence of atropine to investigate the role of the muscarinic receptor in this pathway. Atropine was applied at a concentration of 10μM (n=6) and repeated at 0.1μM (n=6) in view of reports of higher doses of atropine potentially causing non-specific ion channel effects (Professor Derek Terrar, personal communication). The bradycardia in response to CCh was completely abolished by the muscarinic antagonist atropine at both concentrations (atropine 0.1μmol/L: atropine 276±7 vs. atropine+CCh 286±8bpm, n=6, p=ns, paired t-test) while perfusion pressure and LVDP were unaffected (figure 3.5a-c). Both concentrations of atropine were able to abolish the increase in VFT seen with CCh (figure 3.5d, atropine 0.1μM: atropine 2.4±0.35 vs. atropine+CCh 2.5±0.22 vs. atropine 2.58±0.3mA, n=6).

3.3.6 Role of nitric oxide

Nitric oxide has been recently implicated as the key mediator of the anti-fibrillatory effect of vagal and therefore cholinergic stimulation. This effect was first studied by perfusing the NO donor, sodium nitroprusside (SNP 10μM, n=8) and determining its effect on VFT. The haemodynamic effects of SNP perfusion are shown in figures 3.6a-d. There was a non-significant reduction in perfusion pressure due to the vasodilating effect in the coronary circulation (baseline 52±7 vs. SNP 38±1 vs, wash out 34±5mmHg) and this effect was not lost upon wash out of the drug. There was no change in LVDP whilst there was a trend towards tachycardia previously reported [441] (baseline 270±10 vs, SNP 298±12 vs wash out 284±8bpm, p=0.06). Increasing NO by SNP perfusion also increased the VFT independent of heart rate (figure 3.7, baseline 1.38±0.13 vs. SNP 2.9±0.83 vs. wash out 1.19±0.23, n=8).

3.3.7 The role of NO in mediating the anti-fibrillatory effect of CCh

To investigate if the increase in VFT with CCh was dependent on NO generation, CCh was perfused during NOS inhibition with the competitive non-specific NOS inhibitor L-NA (100μM, n=6). The haemodynamic parameters are summarized in the table below and figure 3.8a-c. Perfusion of L-NA resulted in a significant vasoconstrictive effect with consequent rise in perfusion pressure with no accompanying change in LVDP or heart rate. The bradycardic effect of CCh was not impeded in the presence of L-NA and the heart rate remained reduced with the addition of L-arginine (L-Arg). Addition of L-NA did not affect the baseline VFT (figure 3.8d). Moreover, the ability of CCh to increase VFT was abolished in the presence of L-NA. Restoration of the substrate for NO generation by NOS, L-Arg

(5mM) was able to restore the anti-fibrillatory effect of CCh, and as previously shown, this effect was lost upon wash out of all the study drugs.

	Baseline	L-NA	L-NA+CCh	L-NA+CCh+ L-Arg	Washout
Perfusion pressure (mmHg)	60.5±7.3	106.7±9.3	141.5±5	142.3±1.5	114.3±5.8
Developed pressure (mmHg)	58±3.3	65±4.7	56.3±4.6	60.6±3.1	60.8±3.4
Heart rate (bpm)	330±9.2	305±8.7	227.8±9	214.7±10.2	307.2±7.1

Table 3.1 Summary of haemodynamic parameters observed during co-perfusion of L-NA with CCh

These data supported a cholinergic, muscarinic receptor dependent anti-arrhythmic mechanism but did not localize the source and isoform of NOS enzyme responsible. The muscarinic receptor dependency was suggestive of either a myocyte eNOS dependent pathway [443] or a pre-synaptic nNOS dependent pathway.

3.3.8 Which NOS isoform is involved in this signalling cascade?

The first experimental series employed S-methyl-L-thiocitrulline (SMTC 10μM) as an nNOS inhibitor. The protocol described above was repeated with SMTC in place of L-NA (n=11). Perfusion pressure is similarly increased with SMTC perfusion with no change in LVDP (figures 3.9a-b). The effect on perfusion pressure is partially reversed upon addition of L-Arg (5mM) but remains greater than baseline and does

not return to pre-drug levels despite wash out of all drugs. Heart rate reduction by CCh was also limited in the presence of SMTC with only a modest, non-significant reduction seen (figure 3.9c). Finally, the anti-fibrillatory effect of CCh was also lost in the presence of SMTC and could not be reversed by addition of L-Arg (figure 3.9d).

These data implied that nNOS might be the NOS isoform contributing to the increase in VFT seen with CCh. However the absence of a significant bradycardia implied potential non-specific effects interfering with muscarinic receptor activation. In addition, the vasoconstriction seen implied incomplete isoform selectivity with eNOS inhibition the likely mechanism contributing to this observation.

Therefore this pathway was re-explored with a more specific nNOS inhibitor, N-[(4S)-4-amino-5-[(2-aminoethyl)amino]pentyl]-N'-nitroguanidine tris(trifluoroacetate) (AAAN, 10μM). This inhibitor is known be cell permeable (SMTC is known to require prolonged incubation for tissue permeability, personal communication, Dr Ricardo Carnicer, University of Oxford) and is more specific for nNOS than SMTC and other inhibitors. Perfusion of AAAN with and without CCh has no effect on perfusion pressure or LVDP (figure 3.10a and 3.10b) in contrast to the effect seen with L-NA and SMTC. The heart rate reduction with CCh was also preserved in the presence of AAAN (figure 3.10c). Perfusion of AAAN led to a significant reduction in VFT which was not reversed or increased above baseline by the addition of CCh (n=6) with no return to baseline following a wash out period (3.10d). The reduction in VFT was not seen with L-NA or SMTC and therefore, to exclude a non-specific effect this protocol was repeated with CCh perfusion before AAAN. In this series, heart rate was significantly reduced by CCh and maintained in the presence of AAAN without

affecting perfusion pressure or LVDP (figure 3.10e-g, n=6). The anti-fibrillatory action of CCh was confirmed with an increase in VFT seen compared to baseline, but this effect was lost upon addition of AAAN (figure 3.10h), confirming that nNOS derived NO is involved in this signalling cascade.

Previous data has shown that the intracellular action of NO is linked to the generation of cGMP via soluble guanylyl cyclase (sGC) and downstream increase in cAMP by PDE3 to increase vagal neurotransmission [132]. In order to confirm the mechanistic relevance of CCh generated NO, the sGC inhibitor inhibitor 1H-[1,2,4]oxadiazolo[4,3-a]quinoxalin-1-one (ODQ, 10μM) was perfused with CCh (figures 3.11a-d, n=6). A significant rise in perfusion pressure was seen (baseline 102±7.6 vs. ODQ 136±6 mmHg) with no effect on LVDP or the bradycardia induced by CCh. Ventricular fibrillation threshold was decreased compared to baseline by ODQ alone (baseline 2.4±0.33 vs. ODQ 1.29±0.18mA, n=6) with no increase upon addition of CCh. This effect was not reversed upon wash out of the drug.

3.3.9 Localisation of nNOS activity

The experiments above provided evidence that cholinergic signalling with CCh is anti-fibrillatory utilising a mechanism dependent upon muscarinic receptor activation and the generation of NO by nNOS. The site of nNOS activity could have been either in the pre-synaptic parasympathetic neurons or at the level of cardiomyocyte. Previous work has localized nNOS to the sarcoplasmic reticulum [444] but to date no evidence has been published linking muscarinic receptor activation and nNOS activity [148]. Therefore, the likely domain of nNOS activity is the pre-synaptic parasympathetic neuron. In order to investigate this, nicotine (1μM) was perfused to demonstrate heart

rate reduction providing evidence of intact parasympathetic ganglia function despite the absence of direct vagal innervation of the preparation (baseline 282±9 vs. nicotine 191±22bpm, n=3). Therefore, CCh would have activated nicotinic and muscarinic receptors during perfusion. In order to dissect this pathway, the nicotinic receptor antagonist mecamylamine (10μM) was perfused throughout the protocol and CCh added (n=6). The results are shown in figure 3.12a-d, with mecamylamine having no effect on perfusion pressure or LVDP while allowing the bradycardia caused by muscarinic activation to be preserved. Despite adequate muscarinic receptor activation, the CCh effect on VFT was not evident in the presence of mecamylamine, indicating that both nicotinic and muscarinic receptor is prerequisite for the anti-fibrillatory action to be seen.

3.3.10 Release of NO upon CCh perfusion

The evidence for the generation of NO in response to CCh perfusion was inferred by NOS inhibitor studies rather than direct evidence of NO generation. To directly measure NO production we collected coronary perfusate samples before and after the application of CCh, and measured the concentration of NO metabolites (NOx) using an ozone chemiluminescence assay. Samples collected from the stabilized preparation displayed no significant temporal variation in their NOx content, whereas CCh perfusion evoked a significant increase (n=8) in perfusate NOx content which became manifest at peak bradycardia (after 10 minutes perfusion; see figure 3.13). The increase in NOx production was abolished by the nicotinic receptor antagonist mecamylamine (10μM, n=8) despite a similar bradycardia from muscarinic receptor stimulation, suggesting that the source of NO production was neuronal.

3.3.11 Autocrine versus paracrine effects of NO

The site and mechanism of the effect of NO generated by cholinergic signaling via pharmacological or direct nerve stimulation remains controversial. The work by Brack *et al.* [100] suggests a paracrine effect independent of muscarinic receptor blockade which is contradicted by these data. In order to determine if NO is able to act in a paracrine manner to exert an anti-fibrillatory effect, the ability of SNP to increase VFT (as shown above) was tested in the presence of atropine (0.1μM). Perfusion of SNP (10μM) resulted in the same haemodynamic profile seen in earlier data in the absence of atropine, with a modest tachycardia, reduction in perfusion pressure with no effect on LVDP (figure 3.14a-c). However, the effect of SNP on VFT could be blocked in the presence of atropine (atropine 0.1μM, 2.5±0.2 vs. SNP+atropine 2.9±0.3mA, n=10, figure 3.14d).

3.4 Discussion

The main findings of our study are

1. In the isolated rat heart, the acetylcholine analogue, carbamylcholine raises ventricular fibrillation threshold and flattens the electrical restitution curve.
2. The anti-fibrillatory action of carbamylcholine was dependent upon stimulation of nicotinic receptors, and the generation of NO from neuronal NOS. This was mimicked by the NO donor sodium nitroprusside.
3. The anti-fibrillatory action of both carbamylcholine and sodium nitroprusside was ultimately dependent on muscarinic receptor stimulation since all effects were blocked by atropine.

These data add to the growing evidence base supporting the role of cholinergic signalling in exerting an anti-fibrillatory effect on the ventricle. Whilst this observation was described over 100 years ago by Einbrodt [53], and later supported through the seminal experiments of Kolman [58], Kent [60] and De Ferrari [259], the mechanistic basis of this effect has recently been questioned by Brack *et al.* [100]. In contrast to the previous evidence that described an obligatory role for muscarinic receptor activation in the mechanism of vagal protection, their innervated rabbit heart model demonstrated preservation of the anti-fibrillatory effect of vagus stimulation in the presence of atropine. The mechanism proposed was a paracrine effect by nNOS derived NO from parasympathetic ganglia acting directly on the ventricular myocardium. This observation was supported by evidence of NO release by DAF2 fluorescence and blocking the VNS associated rise in VFT with hexamethonium, a nicotinic AChR antagonist [140]. Although, stimulation of the cervical vagus activates efferent preganglionic parasympathetic neurons to lower HR and reduce inotropy via stimulation of muscarinic receptors on myocytes, up to 70% of the fibres are sensory afferents [445] that can be retrogradely stimulated. The NO generated during these conditions may therefore originate from nNOS in sensory fibres, postganglionic parasympathetic neurons or indeed myocytes [446]. By using an acetylcholine analogue that is resistant to cholinesterase and produces reliable and persistent responses at both muscarinic receptors on ventricular myocytes and nicotinic receptors on postganglionic parasympathetic ganglia, we therefore tried to localize the source of NO in terms of its anti-fibrillatory action.

Role and source of NO as a cholinergic antiarrhythmic modulator

Using an ozone chemiluminescence method to quantify the absolute concentration of NO metabolites, perfusion of CCh in our model resulted in release of NO as evidenced by a rise in NOx in the coronary perfusate. The source of NO as a result of CCh perfusion could have been via endothelial NOS (eNOS) through its coupling to the M_2 receptor [443] or via nNOS activation from nicotinic receptors on cholinergic ganglia. Therefore we used mecamylamine, a nicotinic receptor antagonist without the cross reactivity for cardiac muscarinic receptors that has been reported for hexamethonium [447], to dissect this pathway. Our results support Brack *et al.*'s [100] findings that the source of NO during vagus nerve stimulation signalling is neuronal since mecamylamine prevented the increase in NOx seen during CCh perfusion, whilst the muscarinic receptor activated bradycardia remained intact.

However, these data support a direct neuronal NO mechanism rather than an indirect paracrine effect of NO as a co-transmitter on the ventricular myocardium [100]. If NO was acting in a paracrine manner, the addition of atropine would have had no influence on this effect. However, we clearly show that atropine was able to block the anti-fibrillatory action of CCh. Moreover, the anti-fibrillatory effect of SNP was also not seen in the presence of atropine indicating that NO is acting upstream of the muscarinic receptor. We propose that the most likely unifying mechanistic explanation of these observations is that neuronal NO generated by nNOS facilitates acetylcholine release from release sites of the ganglionic projections via a cyclic guanosine monophosphate–phosphodiesterase-3 dependent pathway increasing protein kinase A dependent phosphorylation of N-type calcium channels as we have demonstrated previously [132].

Recent evidence from anatomical and immunohistochemical studies have moved us away from the dogma that there is an absence of parasympathetic innervation of the ventricles. A variety of techniques have demonstrated significant epicardial and endocardial innervation of atria and ventricles in multiple mammalian species, albeit with some variation in numbers of parasympathetic ganglia [67]. In addition, stimulation of the vagus nerve can reduce ventricular contractility in humans [178]. These studies have supported the anti-fibrillatory role of the vagus on the ventricle.

The antiarrhythmic action of muscarinic receptor stimulation

Our data establishes the critical pathway in the anti-fibrillatory action of cholinergic signalling played by the muscarinic receptor, an effect that can be enhanced by nNOS driven parasympathetic transmission [182, 252]. De Ferrari *et al.* (1991b) demonstrated the mechanistic importance of muscarinic stimulation in their elegant canine model of coronary artery ligation and assessment of vagal tone. They found that muscarinic blockade with atropine was associated with an increase in ventricular arrhythmia compared with control. Ando *et al.* (2005) reported a similar observation in a rat model of vagus nerve stimulation during coronary artery occlusion where the pre-conditioning protective effect of vagus stimulation was lost in the presence of atropine. More recently, vagus nerve stimulation has been shown to be anti-arrhythmic in the clinically relevant setting of ischaemia-perfusion via effects on mitochondrial function with atropine abolishing this effect [448].

Ventricular arrhythmias are a major source of morbidity and mortality in patients with myocardial infarction and heart failure. The mechanisms underlying this increased propensity include changes in action potential duration due to alterations in ion

currents including I_{CaL} [449, 450] and I_K [451, 452], shortening of refractory period, steepening of the electrical restitution curve, changes in SR Ca^{2+} release [453] and slowing of conduction velocity. These changes lead to early and delayed after depolarisations (EADs/DADs) which act as major initiators of ventricular tachyarrhythmia [454]. In addition, structural changes post myocardial infarction and in heart failure leads to fibrosis, reductions in connexin 43 [455, 456] and I_{Na} availability resulting in areas of slower conduction. This contributes to regional heterogeneity in conduction velocity, which promotes local conduction block and re-entry [457, 458].

Cholinergic stimulation via the muscarinic receptor counters pathophysiological changes by inhibiting adrenergic and cyclic adenosine monophosphate (cAMP)-protein kinase A dependent increases in I_{CaL} activity, initially termed 'accentuated antagonism' by Levy in 1971 [459]. Mechanistically, direct and indirect pathways have been proposed for this effect. Direct inhibition of β adrenergic stimulation occurs via direct interaction of adenylate cyclase with the α subunit of PTX-sensitive G_i/G_o proteins of the M_2 receptor [460, 461]. Indirect effects may also be dependent upon the generation of NO by eNOS, leading to cGMP production and increased phosphodiesterase-2 activity leading to breakdown of cAMP and subsequent reduction in I_{CaL} [147, 443, 462], although this is controversial [131, 229]. nNOS is also present in ventricular myocytes associated with the sarcoplasmic reticulum [209], although there is no direct link between muscarinic receptor stimulation and generation of NO by nNOS [148]. The importance of nNOS derived NO in regulating basal myocyte function and Ca^{2+} handling at the level SR has been demonstrated by Sears *et al.* [208] and $nNOS^{-/-}$ animals have an increased incidence of ventricular arrhythmia [206]. These observations may be possible explanations for the reduction in VFT seen upon

perfusion of AAAN alone in our data. The possibility of AAAN working at the level of intracardiac ganglia or a non-specific effect may also be considered, but the physiologic importance of nNOS derived NO in myocyte function has been demonstrated clearly by the above studies. These cellular mechanisms contribute to global changes in ventricular physiology as evidenced by APD prolongation and flattening of the electrical restitution curve by our data and direct vagus stimulation in the isolated rabbit heart [139]. Furthermore, recent evidence has also shown an increase in connexin-43 expression in response to chronic vagus nerve stimulation promoting homogeneity in conduction velocity [101, 102].

Limitations

There is evidence that parasympathetic innervation of the ventricle varies regionally and therefore perfusion of CCh is unlikely to mimic the localised release of acetylcholine from efferent post-ganglionic fibres. In addition, vagal nerve stimulation has the potential to elicit a complex profile of mediators and modulators from efferent and afferent fibres. It also engages multiple levels of the cardiac neuraxis to alter peripheral neural processing and central-peripheral neural interactions, including central drive [463]. However, the direct physiological effects of CCh perfusion in terms of heart rate and developed pressure closely matched the physiological parameters seen in studies of direct vagus nerve stimulation across species. *In-vitro* preparations are also removed from the haemodynamic and neuro-humoral perturbations that contribute to arrhythmogenesis, and therefore the *in-vitro* preparation may not give a full quantitative mechanistic account of the pathways involved.

Whilst several studies highlight prolongation of refectory period as being an additional anti-arrhythmic mechanism of vagus stimulation that results from action potential prolongation, we were unable to effectively measure this in the rat heart as our S1-S2 coupling interval only went down to 40msec where we still had ventricular capture. Nevertheless the antiarrhythmic properties of cholinergic stimulation appear consistent across a range of species with differing ion channel expression and electrophysiology. Optical mapping is a powerful tool in imaging global electrophysiology although there is conflicting evidence regarding the influence of electro-mechanical uncoupling with blebbistatin on electrophysiology [421, 422]. Conversely, the use of electrode mapping limited spatial resolution and variation in signal magnitude over time. In our data, blebbistatin was applied at a fixed concentration during control and CCh perfusion, which should therefore obviate any confounding effect.

Testing VFT may not reflect the mechanism of VT and VF initiation *in-vivo* but it does allow for reproducible testing of arrhythmogenicity removed from the stochastic nature of arrhythmia induction seen with ischaemia-reperfusion or infarct models. Baseline VFT will also vary depending on the size of the heart and position and contact of the pacing electrode, as we observe between our different protocols. However, all comparisons in the experimental protocols are within experiments, paired analysis (not unpaired comparisons). Many similar papers report VFT in terms of percentage change but we have chosen to present the raw data for clarity. The ability of CCh to raise VFT does not appear to be dependent on the baseline VFT however. For example, CCh was unable to raise VFT in the presence of 0.1μM

atropine when baseline VFT was 2.4±0.35mA or in the presence of 10μM atropine when baseline VFT was. 1.91±0.19mA.

The real time measurement of NO and its metabolites is challenging and we employed ozone chemiluminescence on the collected perfusate. There is temporal variation in the onset of bradycardia and peak of NOx seen and this observation is likely to be related to both the cellular mechanisms by which CCh brings about both effects and the method of perfusate collection. The action of CCh on the sinoatrial node will occur shortly after application of the drug with rapid changes in ion channel activity on stimulation of muscarinic receptors. Stimulation of nNOS activity and diffusion of NO from dispersed groups of cholinergic ganglia throughout the heart is likely to lead to a slow NOx accumulation in the perfusate, especially when this is only being sampled every 2 minutes. A more acute temporal relationship may have been achieved by utilizing a localized microdialysis approach.

Clinical significance

Cardiac sympathetic over activity increases the risk of lethal ventricular arrhythmias [464]. Conversely large-scale human studies have established markers of parasympathetic activity, including increased baroreflex sensitivity and HR variability as positive prognostic indicators in patients post-myocardial infarction (ATRAMI [15]), and with chronic heart failure (UK HEART [16]).

Whilst β adrenergic receptor blockade is the mainstay of therapy in these conditions, surgically implanted vagal nerve stimulators have emerged as a promising adjunctive treatment strategy [465]. Whilst these devices may improve ejection fraction and quality

of life in chronic heart failure [48], a long-term reduction in ventricular arrhythmias or sudden cardiac death in patients has yet to be demonstrated. Moreover, this approach stimulates both cholinergic efferent and afferent fibres and surgical implantation of such devices is not without risk.

Our study demonstrates that muscarinic receptor activation and neuronal generation of NO are critical steps for the anti-fibrillatory effect of cholinergic signalling. A nicotinic receptor based NO mediated mechanism that converges on the muscarinic receptor is conceivably amenable to a more targeted gene therapy or pharmacologic treatment strategy. For example, percutaneous cardiac gene transfer of nNOS increases vagal neurotransmission and bradycardia [182] and reduces mortality three days post myocardial infarction in the guinea pig [252]. Whether gene transfer of nNOS into cardiac cholinergic ganglia provides a direct anti-fibrillatory action on the ventricle that could be exploited therapeutically remains to be established.

3.5 Chapter 3 Figures

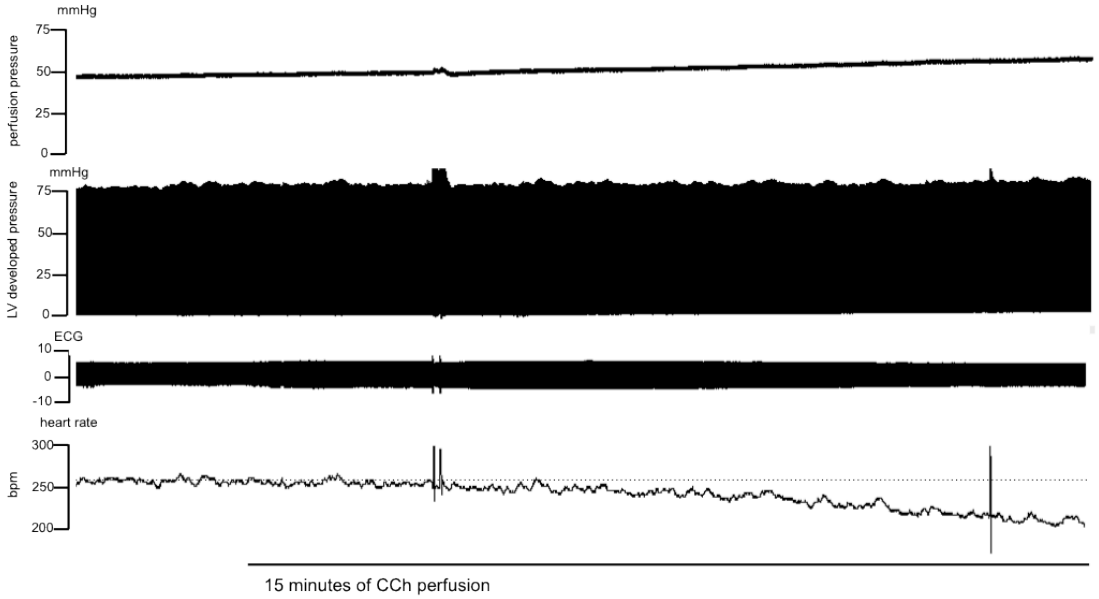


Figure 3.1 Experimental raw data trace of CCh perfusion

Panel showing raw data trace of CCh (200nM) perfusion following stabilisation of an isolated heart preparation. Perfusion pressure and LV developed pressure were not significantly altered during perfusion of CCh and marked reduction in heart rate was seen (dotted line demarcates baseline, stable heart rate). The effect on heart rate was reversed upon wash out of the drug.

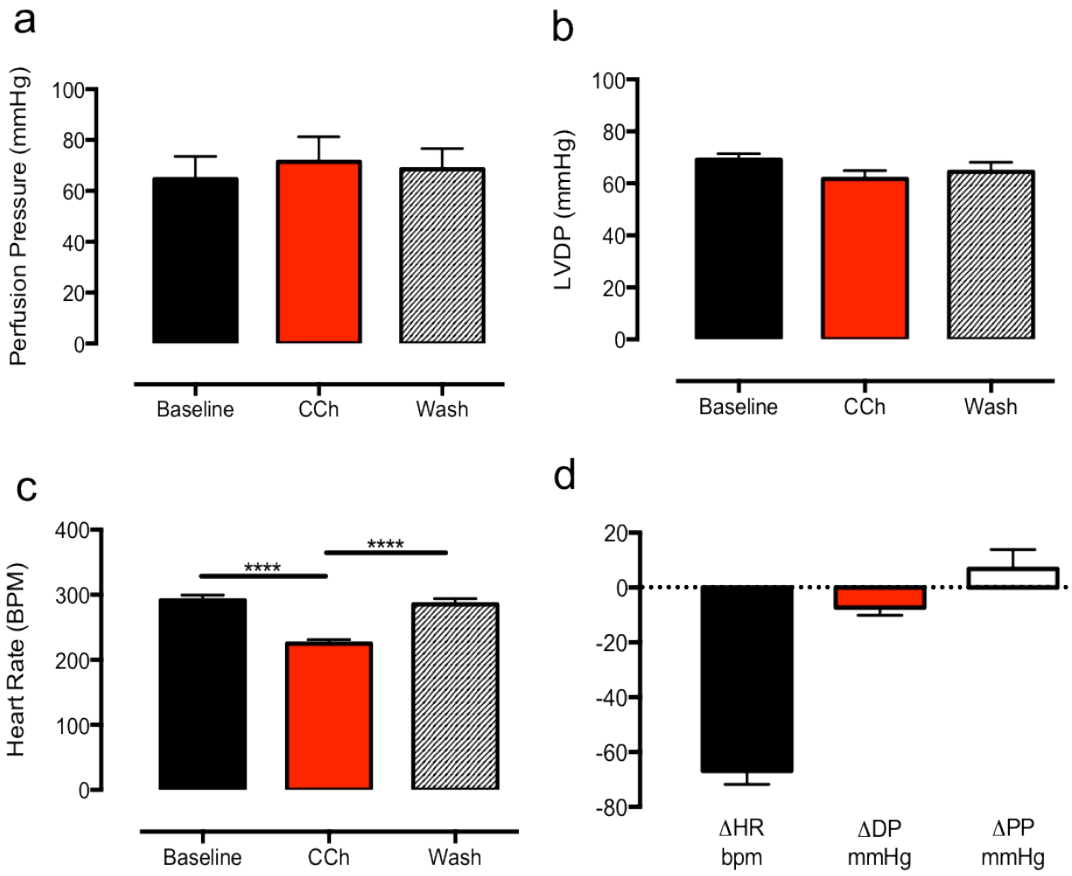


Figure 3.2 Haemodynamic changes during perfusion of Carbamylcholine 200nM

Perfusion of carbamylcholine 200nM (CCh, n=9) results in (a) no significant change in perfusion pressure and (b) left ventricular developed pressure. (c) A significant reduction in heart rate is seen ($p<0.001$, ANOVA) and this effect is lost upon wash out of the drug. (d) Summary delta heart rate, developed pressure and perfusion pressure data

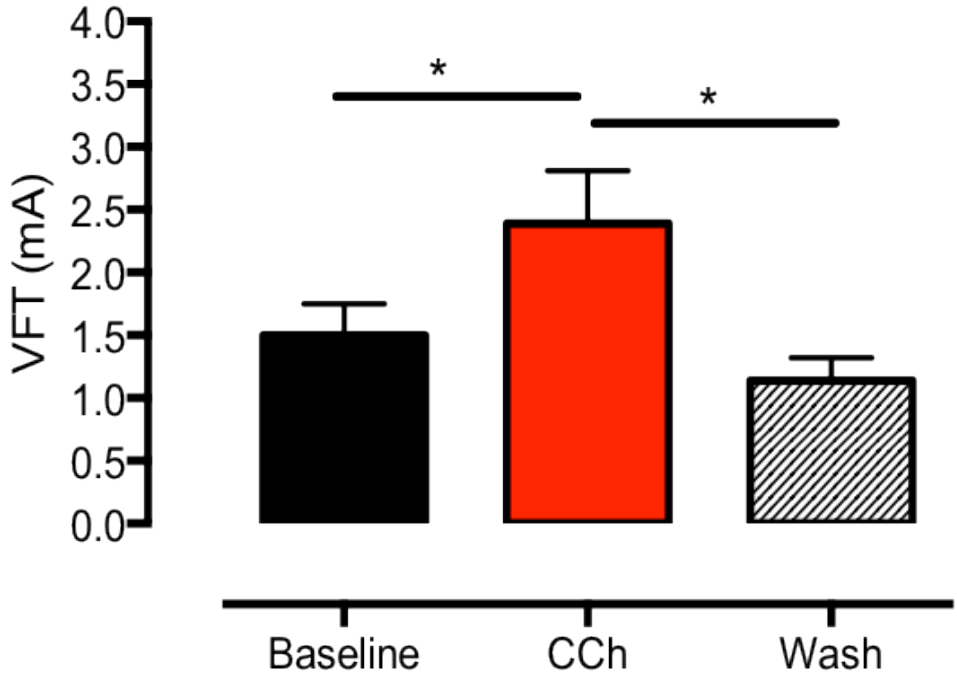


Figure 3.3 Ventricular fibrillation threshold (VFT) is increased by Carbamylcholine 200nM

Perfusion with CCh results in an increase in VFT independent of heart rate. This effect is lost upon wash out of the drug. ($p<0.05$, ANOVA, n=9)

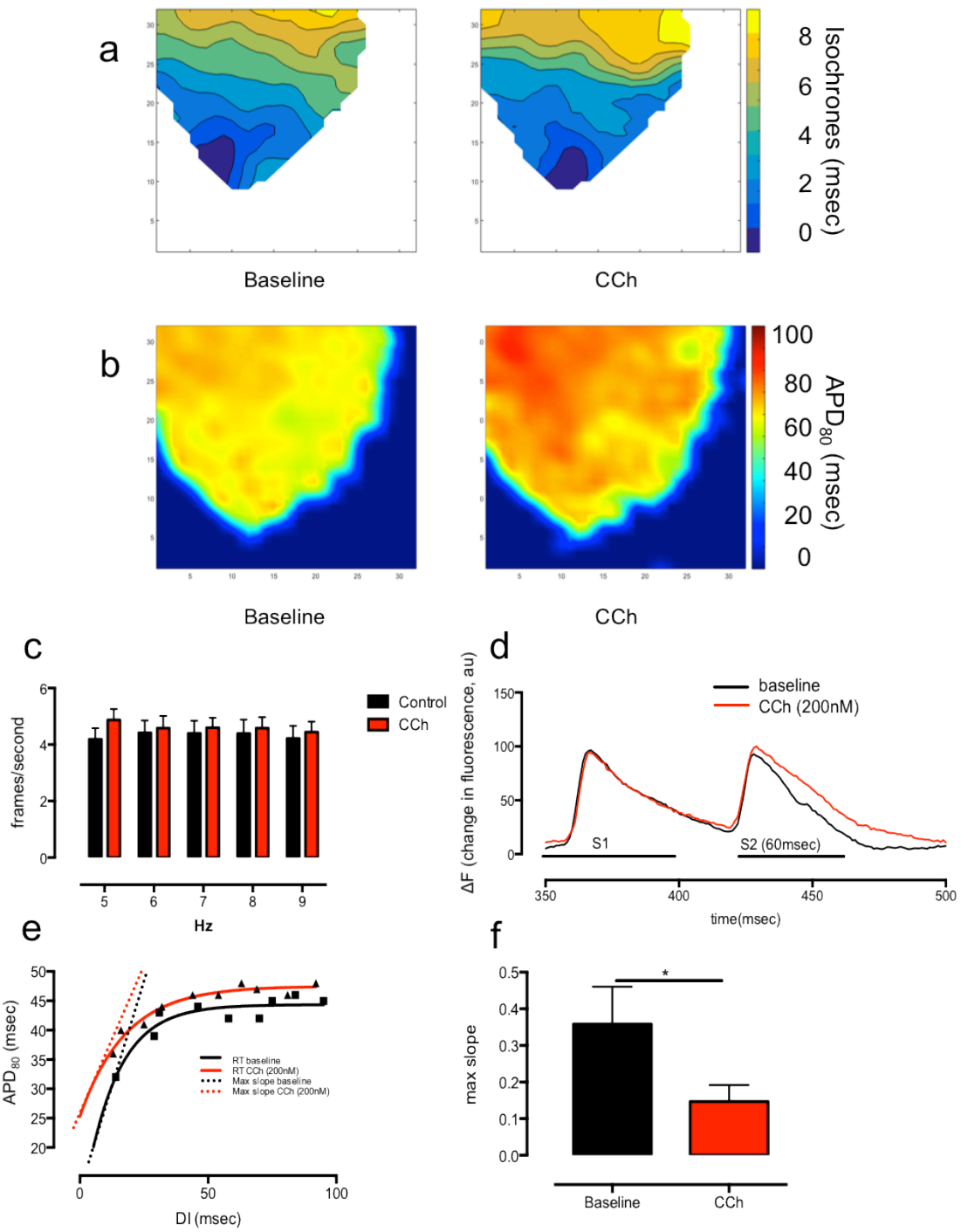


Figure 3.4 Optical mapping of ventricular repolarisation and electrical restitution during CCh perfusion

(a) Isochronal maps during 5Hz pacing from the RV apex with and without CCh perfusion demonstrating no significant change in conduction velocity. (b) Median APD_{80} maps of the anterior LV demonstrating global prolongation of APD in the presence of CCh during 5Hz pacing. (c) Summary data of conduction velocity during fixed rate pacing. (d) CCh perfusion results in reduced shortening of the ventricular APD in response to a short coupled S2 stimulus following a 20 beat drive train and (e) flattening of the maximum slope of electrical restitution curve (RT). (f) Summary data demonstrating that CCh decreases the maximum slope of restitution (*$p<0.05$, paired t-test, n=6).

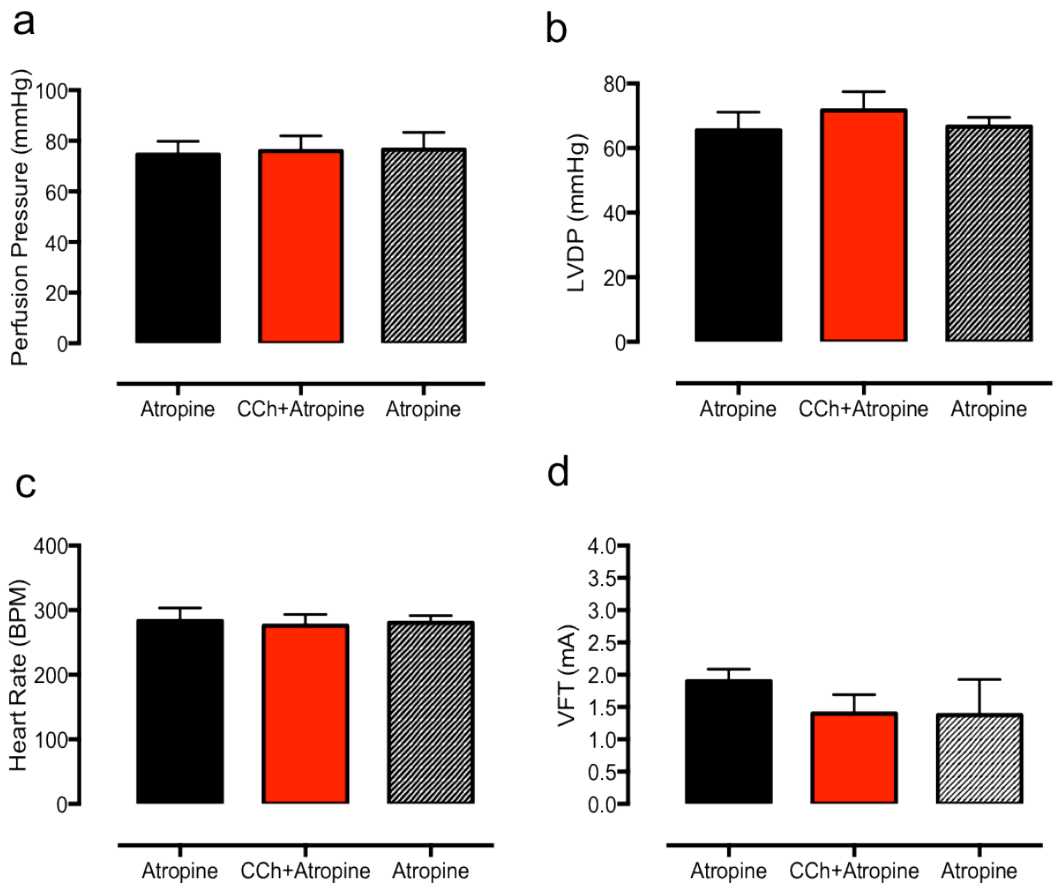


Figure 3.5 Haemodynamic and VFT changes during investigation of the effect of muscarinic receptor blockade with atropine during CCh perfusion

(a-c) Perfusion pressure, LVDP and heart rate remained constant through this protocol with no change upon addition of CCh 200nM. (d) The anti-fibrillatory effect of CCh was lost upon muscarinic receptor blockade with Atropine 10μM (n=6) and similar results were seen with Atropine 0.1μM (n=6).

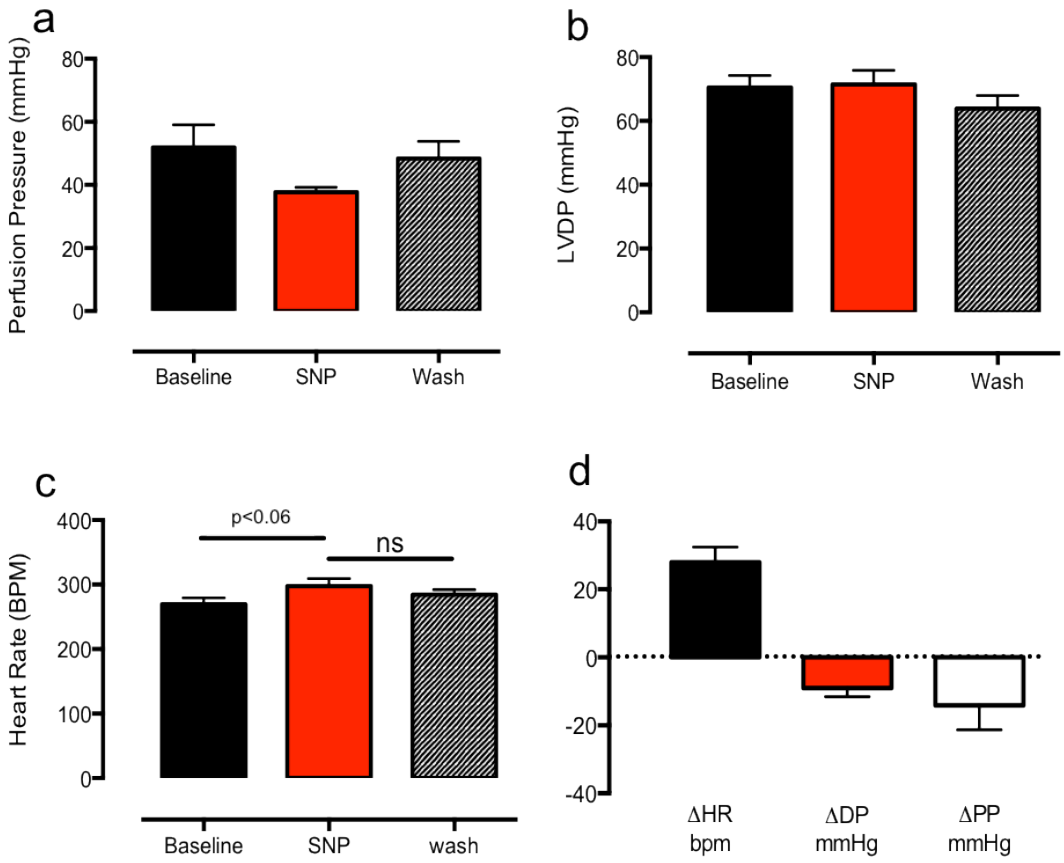


Figure 3.6 Haemodynamic changes during perfusion of sodium nitroprusside 10μM

Perfusion of sodium nitroprusside (SNP, n=8) results in (a) a reduction in perfusion pressure but this effect was not statistically significant (baseline vs. SNP p=0.09, SNP vs. wash p=0.1) and (b) left ventricular developed pressure was unchanged during perfusion. (c) A trend to increase heart rate is seen ($p<0.06$, ANOVA) during SNP perfusion. (d) Summary delta heart rate, developed pressure and perfusion pressure data

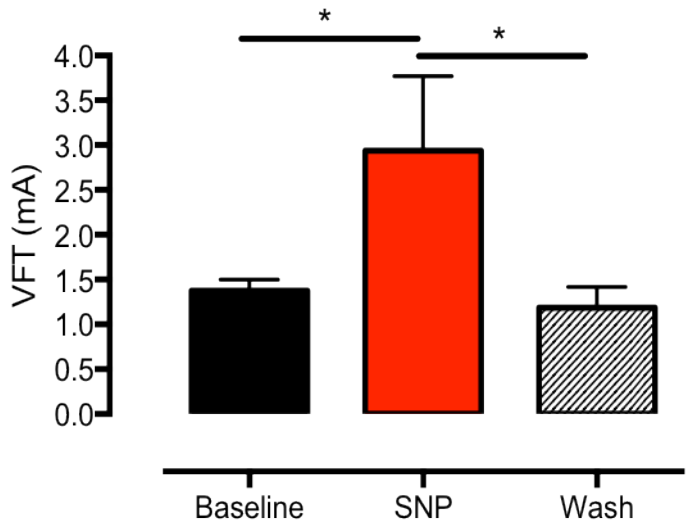


Figure 3.7 Ventricular fibrillation threshold (VFT) is increased by sodium nitroprusside 10fu

Perfusion with SNP results in an increase in VFT independent of heart rate. This effect is lost upon wash out of the drug. ($p<0.05$, ANOVA, n=8)

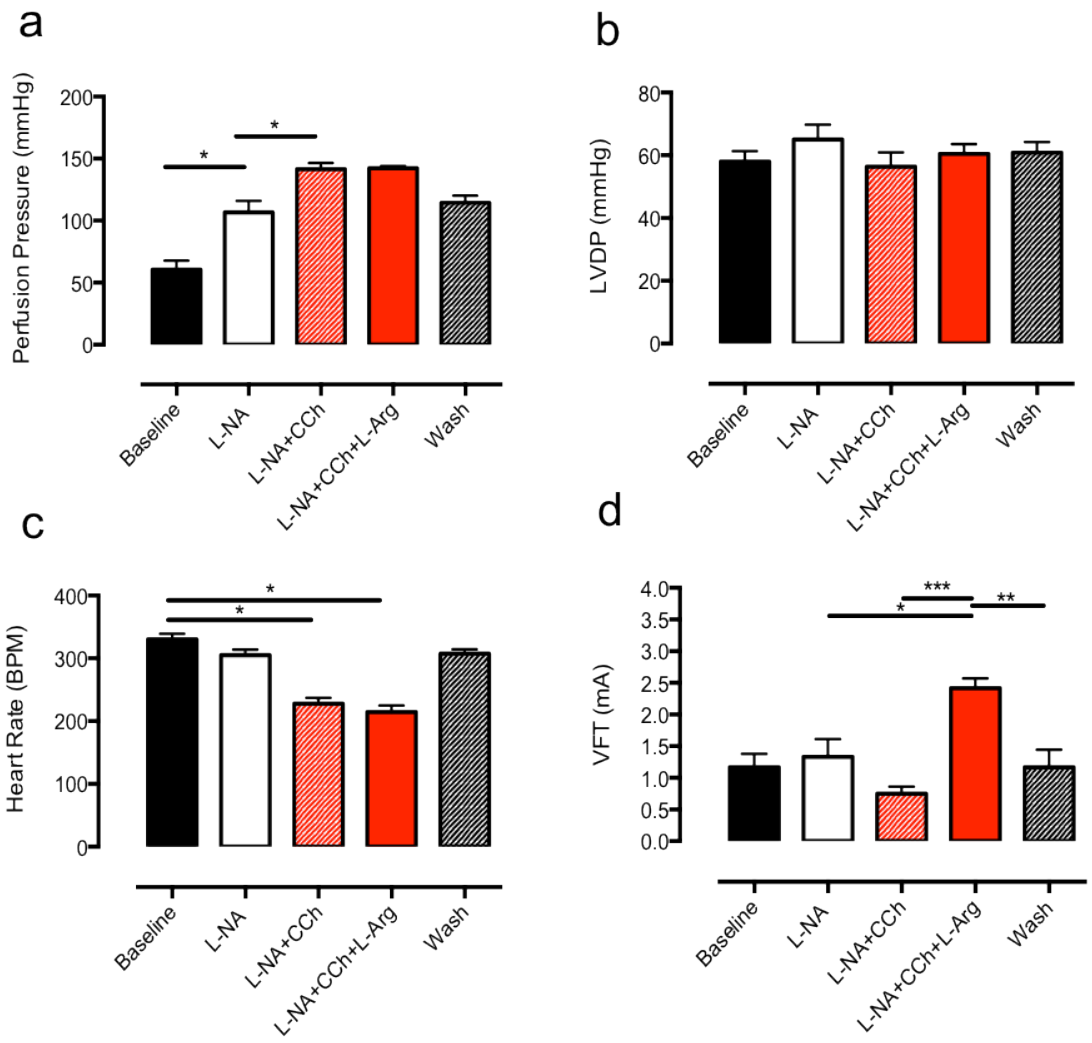


Figure 3.8 Haemodynamic and VFT changes during investigation of the effect of NOS blockade and substrate restoration during perfusion with carbamylcholine

(a) A significant increase in perfusion pressure is seen upon perfusion of L-NA (10μM) for 15 minutes and a further significant increase with prolonged perfusion in the presence CCh 200nM. Addition of L-Arg (5mM) does not reverse the vasoconstriction and there is a partial reversal upon washout of all drugs. (b) LVDP remains unchanged during this experiment despite marked changes in PP. (c) The bradycardic effect of CCh is unaffected by the presence of L-NA/L-NA+L-Arg. (d)VFT is unchanged from baseline during L-NA perfusion and there is trend towards a reduction with L-NA+CCh. The anti-fibrillatory effect of CCh is restored by addition of L-Arg (5mM) and this effect is returned to baseline upon washout of all the drugs. (n=6, *$p<0.05$, **$p<0.01$, ***$p<0.001$, ANOVA)

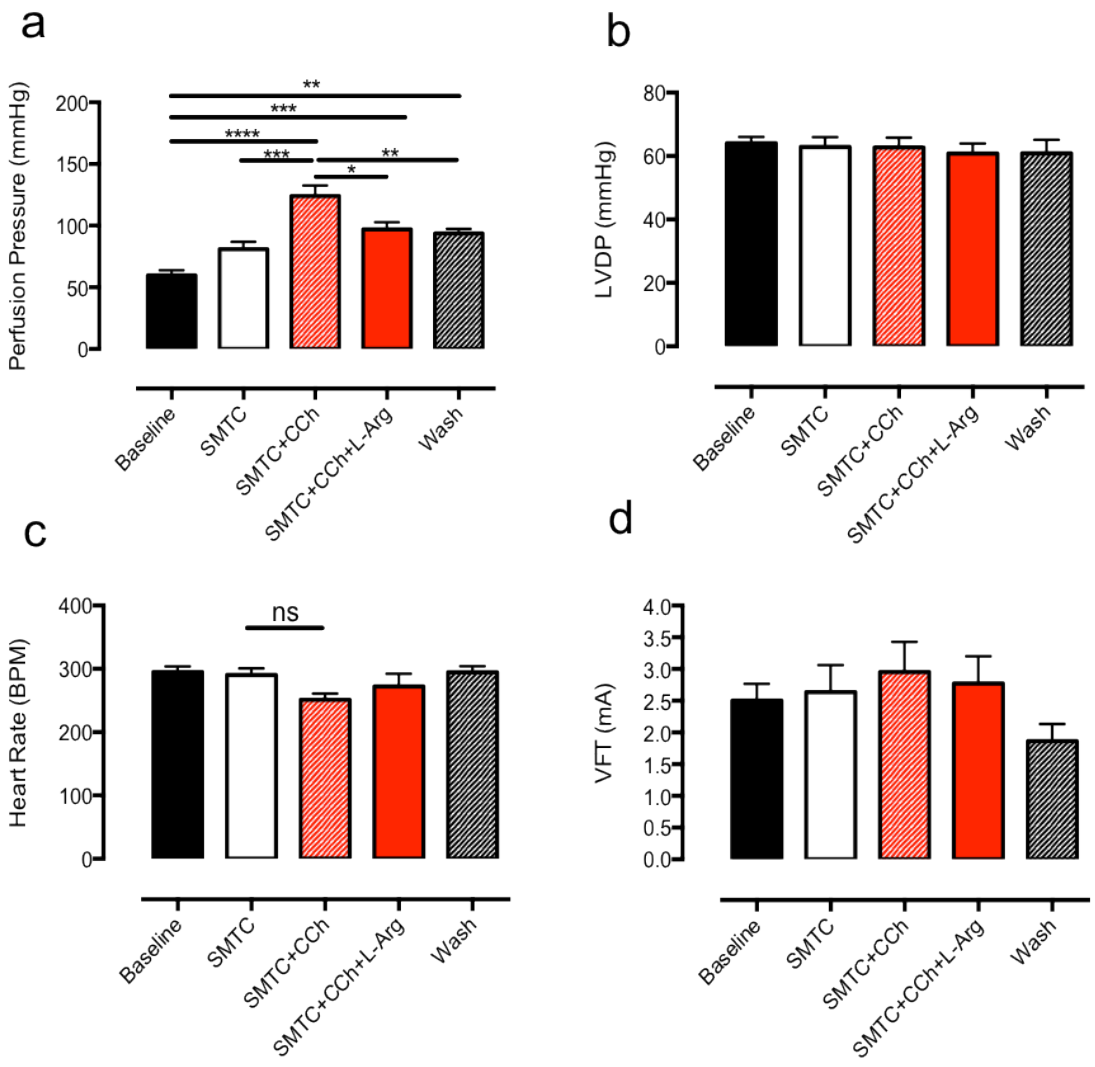


Figure 3.9 Haemodynamic and VFT changes during investigation of the effect of nNOS blockade with SMTC and substrate restoration during perfusion with carbamylcholine

(a) A significant increase in perfusion pressure is seen upon perfusion of SMTC (10μM) + CCH (200nM) (30 minutes total SMTC perfusion) and this reversed upon addition of L-Arg (5mM). There is some washout effect but perfusion pressure does not return to baseline. There is no change in (b) LVDP and although (c) addition of CCh to SMTC did result in a reduction in heart rate, the overall effect was non-significant. (d). The anti-fibrillatory effect of CCh was lost upon co-perfusion of SMTC and no rescue of the effect with addition of L-Arg. (n=11, *p<0.05, **p<0.01, ***p<0.001, ****p<0.0001, ANOVA)

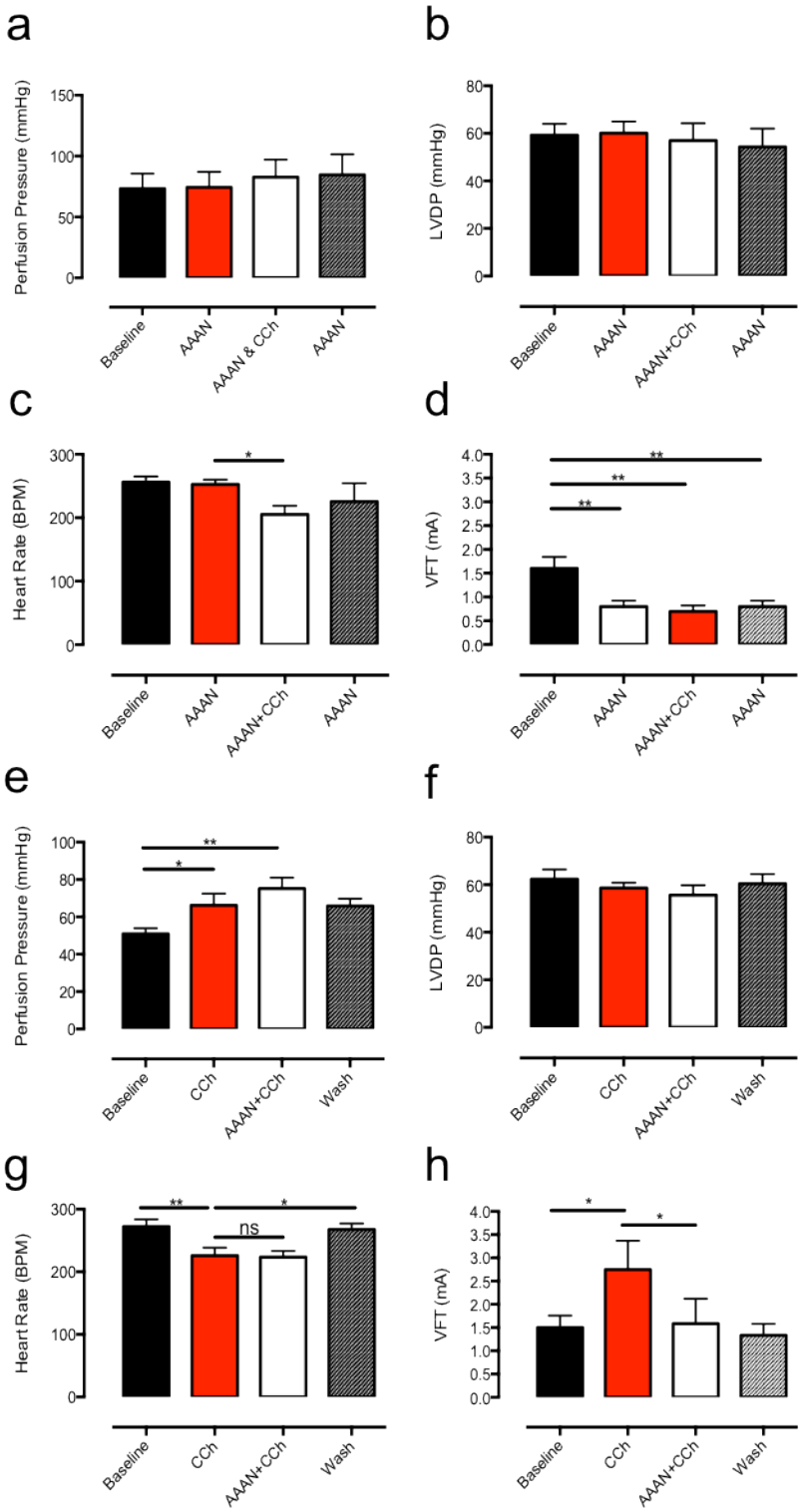


Figure 3.10 Haemodynamic and VFT changes during investigation of the effect of nNOS blockade with AAAN during CCh perfusion

(a-c) AAAN perfusion ± CCh resulted in no significant changes in perfusion pressure, LVDP and a modest reduction in heart rate *p<0.05, ANOVA). (d) AAAN perfusion resulted in a decrease in VFT which could not be increased by the addition of CCh (n=5). This was then repeated to determine if the anti-fibrillatory effect of CCh could be maintained with the addition of AAAN. (e) A stepwise increase in perfusion pressure was seen, (f) no change in LVDP, (g) with preservation of the bradycardic effect of CCh which could be washed out. (h) CCh was shown to increase VFT, an effect lost with the addition of AAAN (n=6, *p<0.05, **p<0.01, ANOVA)

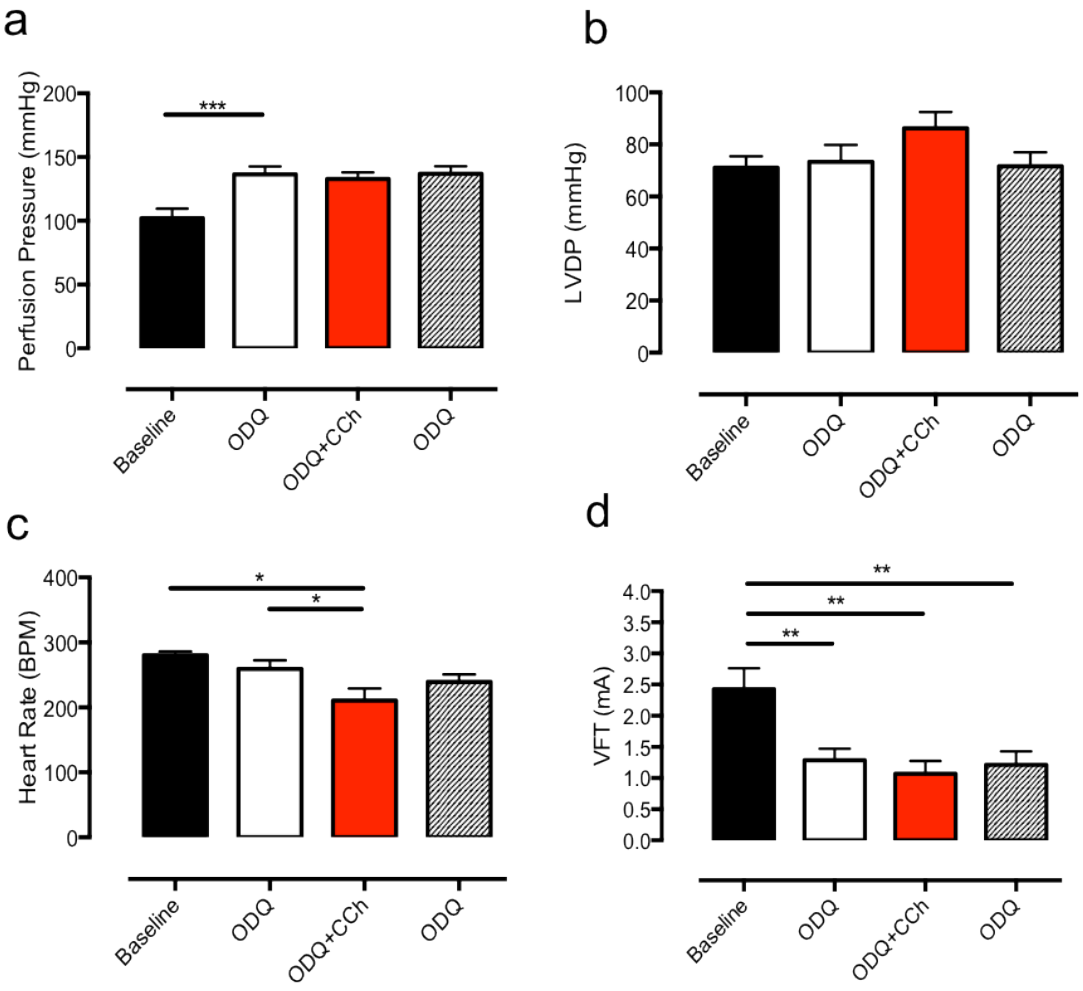


Figure 3.11 Haemodynamic and VFT changes during investigation of the effect of sGC blockade with ODQ during CCh perfusion

(a) Perfusion pressure was significantly elevated with ODQ (10μM) and remained elevated though the protocol with (b) no change in developed pressure. (c) Heart rate reduction with CCh 200nM was unaffected but (d) ODQ was independently pro-arrhythmic and VFT was not increased with the addition of CCh. (n=6, *p<0.05, **p<0.01, ***p<0.001, ANOVA)

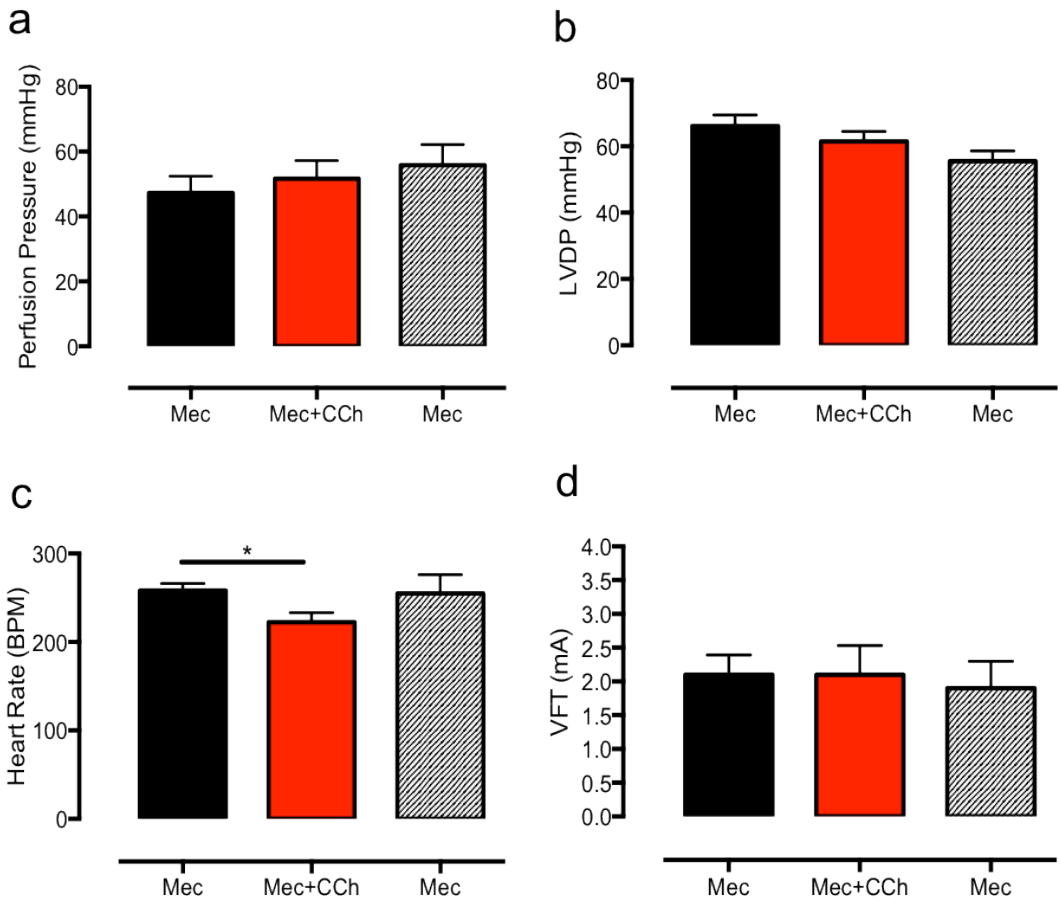


Figure 3.12 Haemodynamic and VFT changes during investigation of the effect of nicotinic receptor blockade with mecamylamine during CCh perfusion

(a-c) Perfusion pressure, LVDP and heart rate remained constant through this protocol with no change upon addition of CCh 200nM. (d) The anti-fibrillatory effect of CCh was lost upon nicotinic receptor blockade with mecamylamine 10μM (n=6) despite a significant bradycardia being induced indicating muscarinic receptor activation.

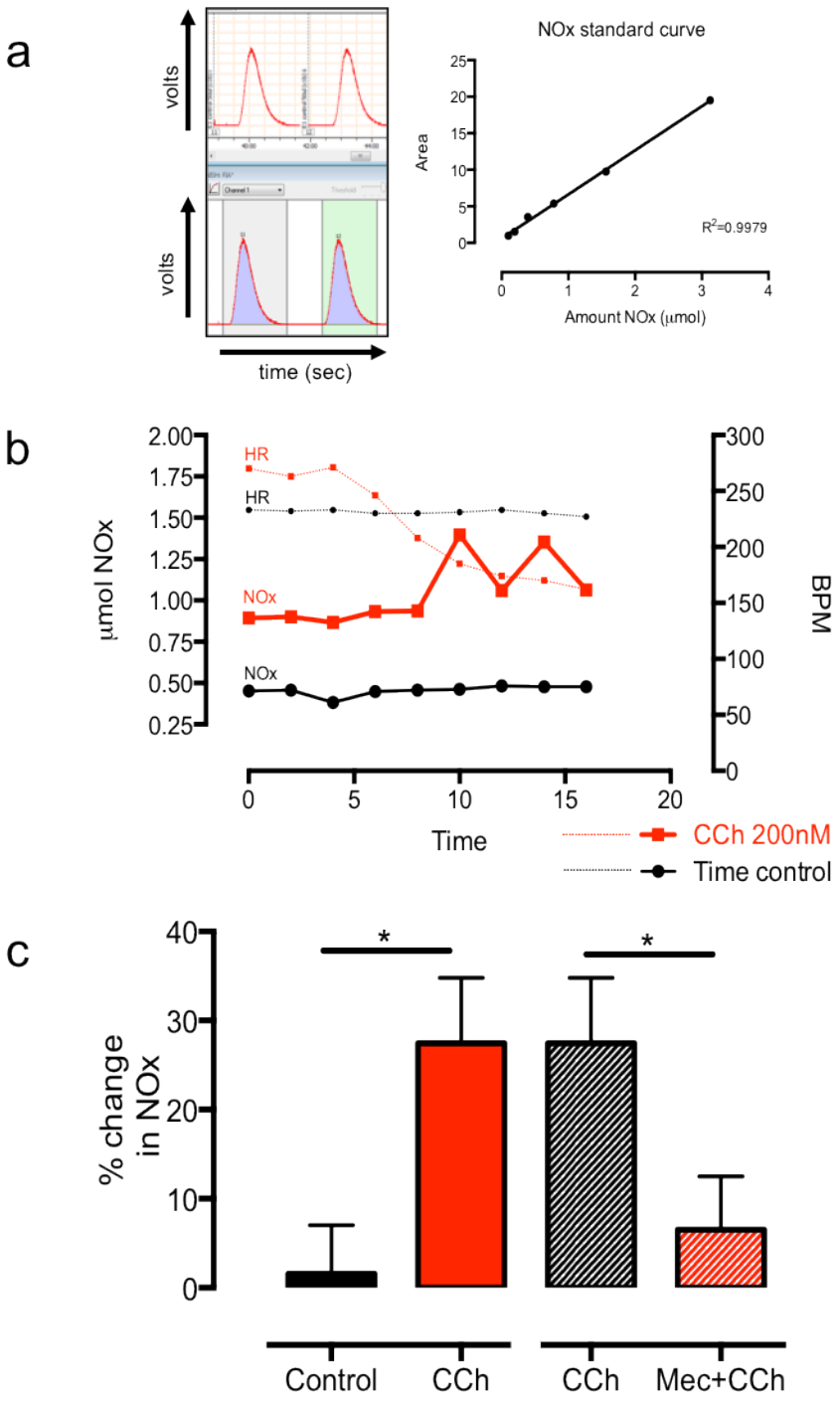


Figure 3.13 Detection of NO release during CCh stimulation and the effect of nicotinic receptor blockade

(a) An ozone chemiluminescent assay was used to detect NO metabolites (NOx: nitrate/nitrite) in snap frozen coronary effluent (experimental sample trace shown/quantification by area under the curve) and analysed against a standard curve. (b) NOx detection in time control experiment and during CCh 200nM perfusion. NOx levels increase during CCh perfusion and peak following establishment of peak bradycardia after 10 minutes. (c) Summary data demonstrating % change in NOx with CCh (*$p<0.05$, paired t-test, n=8) and a reduction in the increase seen during nicotinic receptor blockade with mecamylamine (Mec 10µM, *$p<0.05$, unpaired t-test, n= 8/group)

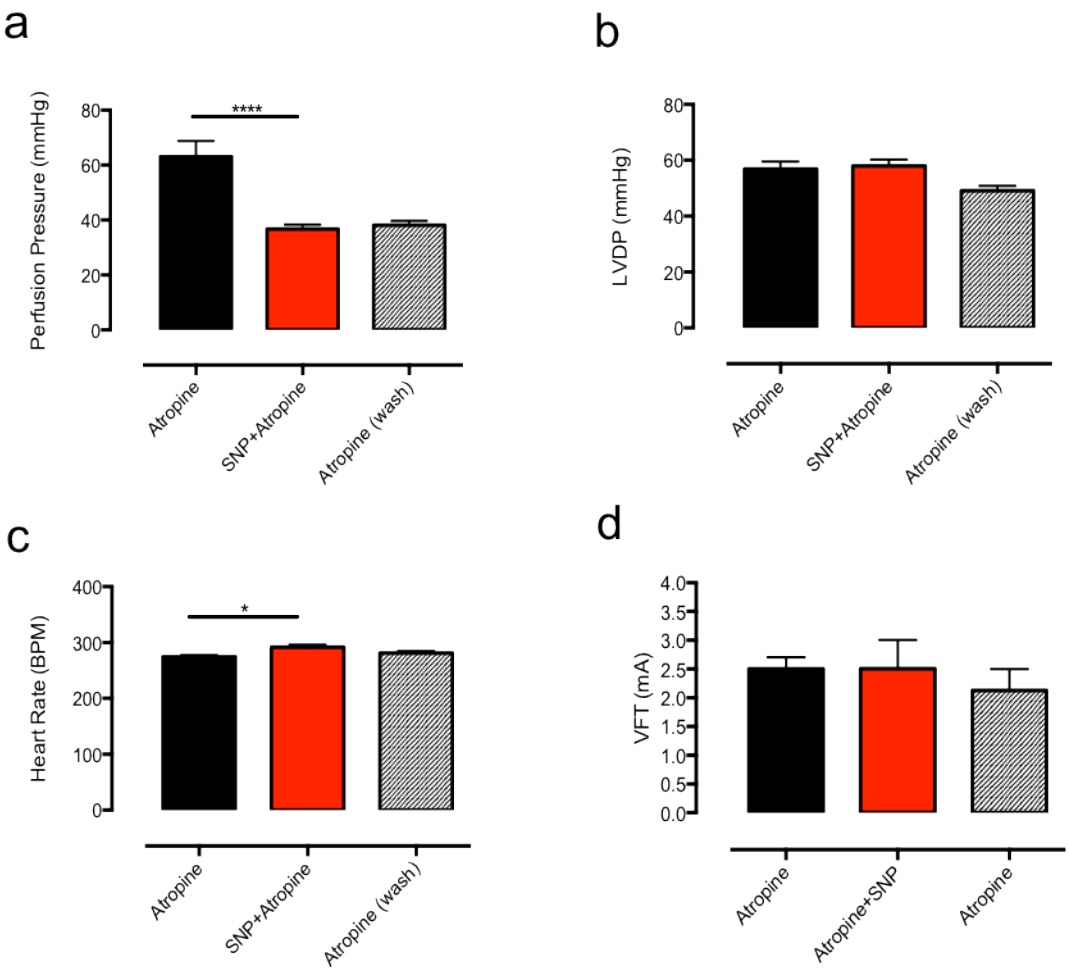


Figure 3.14 Haemodynamic and VFT changes during perfusion of sodium nitroprusside 10μM and atropine 0.1em

(a) SNP perfusion results in a significant reduction in perfusion pressure due to vasodilatation and this effect persists through the washout period with (b) no effect on developed pressure. (c) SNP causes a modest but significant tachycardia in the presence of atropine but the (d) anti-fibrillatory effect of SNP is lost upon co-perfusion of atropine (n=10, *$p<0.05$, ****$p<0.0001$, ANOVA)

Chapter 4 Neuropeptide Y and sympathetic modulation of ventricular fibrillation threshold

4.1 Introduction

A high level of sympathetic activity promotes myocyte calcium influx, increases inotropy and myocardial oxygen demands [6, 396, 466, 467]. In the setting of coronary ischaemia or structural heart disease, the increase in sympathetic activity can exacerbate the physiological impact of the underlying condition and increase the risk of ventricular arrhythmia [144, 466, 467]. These changes in physiological function are reflected in large outcome studies that have described excessive adrenergic activity as a negative prognostic indicator post myocardial infarction (MI) [15, 144, 255] and during congestive cardiac failure [16, 256]. Sympathetic hyperactivity is also a hallmark of hypertension [261] and correlates with the development of left ventricular hypertrophy [257], which is also an independent predictor of morbidity and mortality [145]. Pharmacological targeting of the sympatho-adrenal axis with β-blockers and ACE-inhibitors is supported by considerable clinical trial evidence with improvements in morbidity and mortality seen [18, 21, 262, 263]. However, despite the first use of β-blockers over 50 years ago, they remain the only class of anti-arrhythmic drug proven to reduce mortality after myocardial infarction and in heart failure [21, 262]. Despite the clear benefit of these medications post-MI and in heart failure, a significant mortality remains in this patient group with over 70,000 sudden cardiac deaths annually in the UK alone [264].

The search for future therapies may need to move away from conventional targets and molecules co-released with norepinephrine from cardiac sympathetic neurons may be potential targets. Neuropeptide Y (NPY) is a 36 amino acid peptide released

following high level sympathetic stimulation [297] and its levels remain elevated despite the rapid uptake of norepinephrine. Levels of NPY in plasma are also elevated following acute coronary syndromes and correlate positively with the severity of heart failure and one year mortality [294, 295]. Similar results have been reported in the setting of primary percutaneous coronary intervention for the treatment of MI [296] with elevated plasma NPY levels at presentation and persistently high levels at 48 hours, in keeping with the sympathetic hyperactivity associated with MI. Neuropeptide Y also influences cellular electrophysiology and therefore may have an influence on arrhythmogenicity. In rat ventricular myocytes, I_{CaL} and inotropy are increased [307] and reflected in isolated myocytes where calcium transients and cell shortening both increase via a Y_1 receptor dependent pathway [308]. An increase in cellular calcium transients is a key change that promote ventricular arrhythmia [6, 467] and therefore NPY may represent an independent pro-arrhythmic trigger and exert this effect despite β-blockade.

Therefore, I hypothesised that high level sympathetic stimulation retains a pro-arrhythmic effect despite β-blockade. I also sought to explore if NPY perfusion decreases ventricular fibrillation threshold and if this mechanism is receptor dependent.

4.2 Methods

4.2.1 Animals

Male Sprague-Dawley rats (300-350g, n=90) were sourced from Harlan (Bicester, UK) and kept under standard laboratory conditions in accordance with the Animals (Scientific Procedures) Act 1986 (UK) and the Guide for the Care and Use of

Laboratory Animals published by the US National Institutes of Health (NIH Publication No. 85-23, revised 1996). Experiments were performed under British Home Office Project License PPL 30/2630.

4.2.2 Langendorff perfused heart

Following thoracotomy the heart was removed and placed in ice-cold heparinised Tyrode's solution (50 units/mL) before mounting on to a cannula in order to establish retrograde perfusion via the ascending aorta with constant flow (10 ml/minute). An in line pressure transducer was used to record perfusion pressure (PP). The heart was left to stabilize for 15 minutes before the left atrial appendage was removed and a custom-made fluid-filled, balloon introduced into the left ventricle to measure left ventricular developed pressure (LVDP). The balloon was inflated to obtain an end diastolic pressure of 0-5mmHg. An electrocardiogram (ECG) was recorded via custom-made silver chloride contact electrodes. Heart rate (HR) was calculated from ECG and the signals displayed in real time. All signals were amplified by a data acquisition system (Biopac System MP150) and were recorded using Acknowledge 4.0 software (Biopac systems, USA). Experimental protocols commenced after a 30-minute equilibration period by which time measurements had stabilized (±5 bpm/mmHg respectively). Only one experimental protocol was run on an individual heart and these were a maximum duration of 120 minutes during which time physiological parameters remained stable.

4.2.3 Langendorff perfused heart with intact sympathetic innervation

The conventional, retrograde perfused Langendorff isolated heart model was modified to allow direct sympathetic nerve stimulation. The technique is described in detail in Chapter 2 and summarised here. Following induction of surgical anaesthesia and

intraperitoneal pentobarbitone and heparin, retrograde perfusion was started with cold, oxygenated Tyrode's solution by placing the perfusion cannula via an arteriotomy in in the ascending aorta. The lungs were excised and sympathetic nerves isolated from the paravertebral muscles. The heart-nerve preparation was then transferred to the warm perfusion apparatus and perfusion continued as above.

The preparation was allowed to stabilise for 30 minutes during which time the ECG electrodes, LV balloon (as above) and nerve stimulation electrodes were positioned. Once stabilised, nerve stimulation was tested at 5Hz with incremental increase in output voltage until nerve capture (evidenced by increase in heart rate/developed pressure) was achieved, confirming that the dissected nerve was functional. Maximal sympathetic response was determined at 10Hz (20V, 1msec pulse duration) for 30 seconds. Stimulation was performed at 20V to ensure reliable and reproducible capture of the sympathetic nerve/stellate ganglia complex across all experiments. Metoprolol (10erimentscomplex0V to ensure reliable and reproducible capture of the or 30 seconds.alloon (as above) and nerve stimulation electrodes were positioned. Once stabilised, nerve stimure excluded from the experimental protocol if there was no response to stimulation from either nerve or incomplete β-blockade seen.

4.2.4 Ventricular fibrillation threshold testing

Electrical pacing protocols were designed on Acknowledge 4.0. A custom-made bipolar platinum electrode, approximately 2mm apart, was inserted into the apex of the right ventricle. This was connected to a constant current stimulator (Digitimer DS7A). VFT was obtained with pacing using a fixed 20 beat drive train at a cycle length of 150msec followed by a 5 sec 50Hz burst scanning the refractory period. The

current delivered was increased by 0.5mA, from 0.5mA, until VF was induced. VF was defined as chaotic, fractionated electrical activity persisting for >5 seconds and was cardioverted to sinus rhythm with a bolus injection of 1ml potassium chloride (50mmol/L) within 10 seconds. Hearts were given 15 minutes to re-stabilise following VF induction, until HR and LVDP were back to pre-stimulation levels (±5bpm/mmHg respectively).

For protocols with pharmacological testing with exogenous NPY or NE, drugs were perfused for 15 minutes prior to VFT testing. Preparations were allowed to recover to baseline parameters over 15 minutes prior to the next drug perfusion and induction.

In experiments with the sympathetic nerve innervated, Langendorff perfused heart, baseline VFT was determined after 15 minutes perfusion with metoprolol. Following cardioversion, the preparation was allowed to stabilise with on going metoprolol perfusion. Sympathetic nerve stimulation (10Hz) was then delivered for 2 minutes and VFT was determined immediately after this period. This duration and frequency of stimulation has previously been shown to cause NPY release in isolated cardiac tissue [266].

4.2.5 Dye free mapping of myocyte monolayers

Hearts from neonatal SD rat pups (PI-P3), killed by Schedule 1 (in accordance to UK Home Office Animals Scientific Procedures Act (1986)) were isolated. Ventricular myocytes were isolated and subjected to enzymatic digestions in trypsin (1mg/mL, Sigma Aldrich, UK) at 4°c for 3 hours followed by a series of digestions in collagenase (1mg/mL, Sigma Aldrich, UK), and then titrated to achieve a suspension

of cardiac myocytes. Isolated cells were then pre-plated in an incubator (37°C, 5% CO_2) for an hour to allow fibroblasts to settle at the bottom of the dish. The ventricular myocytes in the supernatant were then carefully removed from the dish and a cell count performed using a haemocytometer and trypan blue, to identify viable cells. The myocytes were plated on 35 mm polylysine coated petri-dishes (Bio coat Poly-D-Lysine 35mm petri-plates, Corning, UK) at a density of 700,000 cells (per 35 mm petri-dish) in plating medium (85% DMEM, 17% M199, 10% Horse serum, 5% FBS and 1% penicillin/streptomycin, all from Sigma Aldrich). The dishes were maintained until imaging was performed, with media being refreshed every 48 hours.

Imaging was performed from day seven onwards when the cultures displayed large connected wave patterns. The plates were placed in a stage-top incubation chamber (Okolab) which was kept at ~37°c, 5% C02 and at constant humidity. Cells were allowed to equilibrate for 15 - 20 minutes before imaging. An Olympus MVXI0 macroscope and Andor Neo sCMOS high speed camera was used to image and record the activity of the cultures (as shown in Figure 5). The imaging technique used in this study is a variation of those previously described in Hwang *et al.* [423], where a macroscopic phase contrast system was used to visualise cell motion. This macroscopic high speed imaging system is based on off-axis illumination using two LED sources. Wave fronts are visualised using image processing filters that display absolute value of the change in pixel intensity over a five frame rolling window, allowing for experiments to be conducted in dye-free solutions. Videos were recorded at 50-100 frames per second with 0.01 second exposure time.

The camera was controlled using custom written Java based software. Software for displaying the camera in real time, saving and analysing data was written in a combination of Java and Python (developed By Dr Gil Bub). Analysis was done using custom written code in Gview software. Videos were recorded, and from these we were able to observe the propagation of cardiac waves across the plates by detecting the minute contractile motions of the myocytes. To assess drug effects on spontaneous activity of cultures, the field of view was divided into 16 equal regions of interest (ROI) and the activity changes in each ROI was assessed following drug stimulation with NPY±BIBO3304.

4.2.6 Determination of coronary perfusate NPY levels by ELISA

Coronary effluent was collected at baseline (prior to sympathetic nerve stimulation) and following direct nerve stimulation and snap frozen in liquid nitrogen.

Neuropeptide Y levels were determined by ELISA using a commercially available kit (Merck Millipore, Cat no EZRMNPY-27K) according to the manufacturers instructions. Standards were prepared according to instructions with serial dilutions with the lowest detectable concentration of NPY being 0.01ng/ml. A 96 well plate was prepared with standards, internal controls and coronary perfusate samples and antibody solution was added to each well. The plate was covered and incubated at room temperature on a plate shaker for two hours. The solutions were decanted and washed x3 followed by addition of enzyme solution to each well and incubated as above for 30 minutes. A further wash x6 was undertaken and substrate solution was added and placed on a shaker for 20 minutes until blue colour was visible, an indication of NPY detection. Stop solution was added to terminate the reaction and

this was evidenced by a blue to yellow colour change. The plate was then read on a plate reader at 450nm and 590nm within five minutes and differences in absorbance were calculated. Standard values were used to construct a calibration curve from which results of coronary perfusate samples was calculated.

4.2.7 Western blotting of ventricular lysates

Tissue was snap frozen in liquid nitrogen and following freeze-thaw, ice cold lysis buffer (75 mM Tris-HCl pH 6.8, 3.80% SDS, 4M Urea, 20% glycerol, 0.1% Triton X-100 with protease inhibitor cocktail) was added and the samples homogenised using a Polytron homogeniser. Samples were then heated at 95 degrees for five minutes on a heating block before the samples were centrifuged at 13000 rpm for five minutes. Supernatants were transferred to new Eppendorf tubes before protein concentrations were assayed using a BCA assay (Roche). Proteins were separated using SDS page (12%Tris-Glycine gels, Invitrogen) and transferred onto PVDF membranes. The membrane was blocked with 5% milk in Tris buffered saline (TBS) with 0.1% tween (TBST), before primary antibodies were left overnight (anti NPY1R ab183108, NPY1R blocking peptide ab193664, anti NPY2R ab31894, Abcam). Blocking peptides and negative tissue controls were used to ensure specificity of the signal and, beta actin was used as a loading control. The blot was washed in TBST and developed using secondary HRP conjugated antibodies and the ECL (Amersham) kit.

4.2.8 Isolated ventricular myocyte immunohistochemistry

Isolated rat ventricular myocytes were fixed with 4% Paraformaldehyde and blocked (10% goat serum, 0.3%BSA, 0.1% triton X in PBS) before primary antibodies were added (Sacromeric alpha actinin A7811: 1:600 and Y1R AB73897: 1:200). This was followed by overnight incubation at 4°C. Secondary antibodies (1:1000) were added

as appropriate (Alexa Fluor 488 and 647, Life Technologies, UK) and the cells were mounted using DAPI containing mounting media (Vectorlabs, UK). Samples were images using a Leica confocal microscope.

4.2.9 Determining the effect of NPY on ventricular arrhythmias post ischaemia-reperfusion

Retrograde perfusion in constant flow mode (10ml/min) was established as above and experiments were designated as control or NPY groups (n=10/group). Following stabilisation (20 minutes), ECG electrodes were positioned but no LVB was used in these experiments. Complete ischaemia was induced by stopping perfusion for seven minutes followed by reperfusion for 20 minutes. In the NPY group, NPY was perfused for 15 minutes prior to initiation of ischaemia and continued during reperfusion. During the reperfusion period, continuous ECG recording was conducted and a score generated for each experiment from observed arrhythmias as follows; ventricular ectopics (1 point), sustained ventricular tachycardia (2 points) and ventricular fibrillation (3 points), according to the Lambeth Conventions [397].

4.2.10 Solutions and drugs

The Tyrode's solution contained (mM) NaCl 120, KCl 4, $MgSO_4*7H_2O$ 1.3, $NaH_2PO_4*2H_2O$ 1.2, $CaCl_2$ 1.2, $NaHCO_3$ 25.2, Glucose 11, and was constantly aerated with carbogen (95% O_2, 5% CO_2), to maintain pH 7.35-7.45. All solutions were filtered before passing through two oxygenators and a bubble trap as part of the Langendorff apparatus. All glassware was water-jacketed to maintain a coronary perfusate temperature of 37±0.5°C. Drugs were prepared in Tyrode's solution at the desired concentration. The concentration of NPY (250nM, Anachem) was chosen as it provided maximal inhibition of vagal responses *in-vitro* [265], whilst the Y_1 (BIBO3304

1μM, Tocris) and Y_2 (BIIE 0246 1μM, Tocris) inhibitors were used at concentrations that blocked the effect of NPY *in-vitro* [265]. Metoprolol was perfused at 10μM (Sigma) as it blocked the haemodynamic changes associated with maximal sympathetic nerve stimulation or NA (10μM, Sigma).

4.2.11 Statistical analysis

Data are presented as mean ± standard error of the mean. All significance tests are two-tailed and normality checked using a Shapiro-Wilk test. One-way ANOVA was applied to all grouped data, with post-hoc analysis to determine significance (Neuman-Keuls, $p<0.05$). An unpaired t-test assuming unequal variance was used to determine significance between independent groups where appropriate. Discrete data was compared using Fisher's exact test in contingency tables. Non-normally distributed data were compared using a Mann-Whitney U test.

4.3 Results

4.3.1 Inclusion criteria

Hearts were excised as described above and retrograde perfusion via the ascending aorta was established in under 60 seconds. The innervated preparation underwent cold perfusion for no longer than 15 minutes prior to initiation of warm perfusion. The hearts were then allowed to equilibrate for 30 minutes. After the equilibration period, the baseline physiological parameters of heart rate (>240bpm), LVDP (>45mmHg) and perfusion pressure (>50mmHg) had stabilized and remained constant throughout each protocol unless otherwise stated.

4.3.2 Protocol for testing VFT

A number of pacing protocols were tested (see Chapter 2) in order to determine the most reproducible protocol for induction of VF. A series of control experiments with a 20 beat drive train (150msec) followed by a 5 second 50Hz burst demonstrated that VFT remained constant over successive inductions (VFT1 2.21±0.39 vs. VFT2 2.21±0.40 vs. VFT3 2.35±0.45mA, n=7) with no deterioration in Langendorff physiology or epicardial trauma (n=7). An unpaired t-test confirmed that perfusion of metoprolol (10 that VFT remained baseline VFT significantly.

4.3.3 Effect of NPY perfusion on haemodynamics and VFT

A raw data trace during NPY perfusion is shown in figure 4.1. Figure 4.2 (a-d) describes the haemodynamic effects of NPY (250nM) perfusion (n=6). There is a significant increase in perfusion pressure during NPY perfusion (baseline 78.5±4.8 vs. NPY 112±0.53 vs. wash out 97.8±7.16 mmHg). However, the vasoconstrictive effect persists despite a 15-minute wash out period. Calculated coronary vascular resistance (perfusion pressure/flow rate (ml/min)) demonstrates the same effect. Left ventricular developed pressure increases significantly upon NPY perfusion, consistent with previous studies demonstrating positive inotropy in the rat heart and in contrast to its effect on the vasculature and perfusion pressure, the effect is reversed upon wash out of the drug (baseline 58±1.2 vs. NPY 77±3 vs. wash out 61±5.1 mmHg). There was no significant change in heart rate as a result of NPY perfusion. A summary of the haemodynamic changes is shown in Figure 4.2d.

Perfusion of NPY significantly decreased VFT compared to baseline and this effect was not reversed upon wash out of the drug (baseline 2.42±0.15 vs. NPY 1.16±0.31

vs. 1.08±0.27mA) as shown in figure 4.3. The greater than 50% reduction in VFT seen with NPY was similar to the reduction in VFT seen with perfusion of isoprenaline (n=4).

4.3.4 Receptor dependency of the effect of NPY

The experiments above demonstrated that NPY was able to independently decrease VFT in the isolated rat heart alongside haemodynamic effects which included an irreversible increase in perfusion pressure and reversible increase in LVDP. The following experiments aimed to determine if this effect was dependent upon the Y_1 or Y_2 receptor.

This was achieved by co-perfusion of the receptor specific antagonists BIBO3304 (Y_1 antagonist, 1μM, Tocris, n=6) and BIIE2046 (Y_2 antagonist, 1μM, Tocris, n=6). These results are shown in Figure 4.4a-f. Perfusion of BIBO3304 had no significant effect on perfusion pressure or LVDP and prevented NPY increasing these parameters, whereas in the presence of BIIE2046, NPY was able to increase perfusion pressure but no change in LVDP was seen. The haemodynamic parameters are summarised in the tables below.

	Baseline	BIBO3304	BIBO3304+NPY	Washout
PP (mmHg)	70±8	73±11	74±12	82.2±6
LVDP (mmHg)	51±3	51±3	50±5	50±6

	Baseline	BIIE2046	BIIE2046+NPY	Washout
PP (mmHg)	64±5	68±4	95±9	84±8
LVDP (mmHg)	57±2	60±2	59±2	57±3

Table 4.1 Summary of haemodynamic changes during NPY perfusion in the presence of Y_1 (BIBO3304) and Y_2 blockade (BIIE2046)

Ventricular fibrillation threshold was tested at baseline, in the presence of the receptor antagonists alone and antogonist co-perfused with NPY followed by washout. The antagosists themselves had no effect on VFT compare to baseline but the decrease in VFT seen with NPY could be abolished by Y_1 receptor blockade with BIBO3304 but not Y_2 blockade with BIIE2046. The VFT data is summarised are Figure 4.5.

4.3.5 Monolayer mapping

A myocyte monolayer platform was utilised in order to confirm the pro-arrhythmic properties of NPY seen in the isolated rat heart. Figure 4.6a demonstrates the effect of the addition of NPY (250nM) to a quiescent myocyte monolayer. The control plate demonstrates no activity. The effect of the addition of NPY is captured over the following 3 panels, each separated by 40msec. The arrows highlight the increase in activity and wave generation over the plate. Each plate was divided into 16 equal sized regions of interest (ROI) and wave activity quantified using custom written

software (Gview, courtesy of Dr Gil Bub) in the presence of NPY and with the Y_1 receptor antagonist, BIBO3304 (1μM). Figure 4.6b demonstrates that NPY leads to a significant increase in active regions at three and five minutes compared to minimal change in the presence of NPY and BIBO3304.

4.3.6 Confirmation of Y_1 receptor presence on ventricular myocytes

The data above provide pharmacological evidence that NPY can independently act as a proarrhythmic molecule with the mechanism being dependent upon the Y_1 receptor. Therefore, in order to generate evidence for the presence of the Y_1 receptor on rat ventricular myocytes, immunohistochemistry was performed on isolated ventricular myocytes and western blotting for the receptor protein in ventricular lysates.

Figure 4.7a provides the first evidence for the membrane localisation of Y_1 receptor protein in the ventricle. The specificity of the bands identified in the atria, ventricle and stellate ganglia tissue was confirmed by demonstration of loss of antibody binding in the presence of a blocking peptide (antibody ab183108, peptide ab193664). Figure 4.7b adds to this observation by immunohistochemical demonstration of the Y_1 receptor on cultured ventricular myocytes. These data provide anatomical evidence to support the mechanistic data from the pharmacological studies shown above.

4.3.7 The sympathetic nerve innervated isolated rat heart model – effects of direct nerve stimulation

The experiments above provide significant support for NPY being an independent pro-arrhythmic trigger. In order to test this hypothesis in an integrated physiological model, an innervated preparation was developed in which both thoracic sympathetic chains and stellate ganglia were dissected and connections to the heart maintained.

Figure 4.8 details results from direct stimulation of right and left stellate ganglia (RSG/LSG) individually.

Figure 4.8a shows experimental data from direct RSG stimulation. Nerve stimulation resulted in an increase in heart rate and contractility that was frequency dependent. The responses could be abolished by stimulation following perfusion with metoprolol (10μM), indicating the specificity of the nerve stimulation. Figure 4.8b shows grouped data (n=6/group) for RSG and LSG stimulation with respect to heart rate and LVDP. Both RSG and LSG stimulation led to significant increases in HR which could be abolished by β-blockade (BB). However, the magnitude of the LVDP response was greater with LSG stimulation compared to RSG stimulation, although not statistically significant by unpaired t-test. The mean haemodynamic data for RSG and LSG stimulations at 10Hz is summarised in the table below and figure 4.8b.

RSG	Baseline	+SG 10Hz	+BB	+BB+SG 10Hz
HR (bpm)	263±5	305±9	261±6	269±6
LVDP (mmHg)	56±3	72±9	51±3	56±4

LSG	Baseline	+SG 10Hz	+BB	+BB+SG 10Hz
HR (bpm)	260±14	308±10	252±11	257±11
LVDP (mmHg)	67±8	102±16	65±7	71±8

4.3.8 Direct SG stimulation and VFT

The next experimental series aimed to determine if direct SG stimulation remained pro-arrhythmic in the setting of β-blockade. The protocol is described in the methods section above and results are shown in Figure 4.9.

Direct right (n=6) and left stellate ganglia (n=7) stimulation at 10Hz for 2 minutes in the presence of metoprolol remained pro-arrhythmic as evidenced by a decrease in VFT in both groups (Figure 4.9a-b).

In keeping with the hypothesis discussed above and data that NPY is independently pro-arrhythmic via an Y_1 receptor dependent mechanism, the protocol above was repeated with perfusion of metoprolol (10μM) and BIBO3304 (1μM) during RSG stimulation (n=7, Figure 4.9c). In this setting, no decrease in VFT was seen suggesting that the pro-arrhythmic effect seen following SG stimulation in the presence of β-blockade alone was due to NPY (VFT: BB 1.93±0.28 vs. BB+BIBO+RSG 10Hz 1.93±0.28mA).

4.3.9 Validation of baseline data and β-blockade efficacy

In order to exclude a confounding effect of metoprolol perfusion on baseline VFT, an unpaired t-test was carried out comparing control VFT data and VFT from all VF inductions under conditions of β-blockade. Figure 4.10a demonstrates that perfusion of metoprolol (n=13) did not alter baseline VFT compared to control inductions (n=14) with normal Tyrode's perfusion (control 2.2±0.27 vs. metoprolol 1.92±0.28mA).

Metoprolol (10μM) was able to abolish the increase in heart rate and contractility during direct sympathetic nerve stimulation indicating the specificity of the stimulation site and also efficacy of β adrenergic receptor blockade. In order to further verify the efficacy of this dose, VFT was determined during perfusion of norepinephrine (1μM) with and without metoprolol (Figure 4.10b). Noradrenaline (NA) decreased VFT significantly and this effect was blocked by co-perfusion of metoprolol (n=4). There was no significant difference between VFT under baseline conditions compared with NA and metoprolol (baseline 2.13and this effect was blocked by co-perfusion of metoprolol (n=4). There was no significant difference between VFT under baseline conditions compa

4.3.10 Neuropeptide release during direct stellate ganglia stimulation

The experiments above have demonstrated that exogenous NPY is an independent pro-arrhythmic agent and direct sympathetic nerve stimulation remains pro-arrhythmic despite effective β-blockade. Antagonism of both the β_1 adrenergic receptor and the Y_1 receptor prior to direct SG stimulation was able to attenuate the pro-arrhythmic effect of high level sympathetic stimulation. In order to confirm that NPY release was responsible for the residual pro-arrhythmic effect during SG stimulation, coronary effluent was sampled and snap frozen in liquid nitrogen before and after 2-minute RSG/LSG (n=6/group) stimulation and NPY levels determined by ELISA.

Direct SG stimulation resulted in a significant increase in NPY levels in the perfusate compared to pre-stimulation levels, with the magnitude of increase more marked

following LSG stimulation (Figure 4.11b), which may reflect the greater inotropic effect seen with LSG stimulation (Figure 4.8b).

4.3.11 NPY increases ventricular arrhythmias in the context of ischaemia-reperfusion

The trigger for ventricular arrhythmia can be ischaemia and subsequent reperfusion as seen during myocardial infarction. Therefore, the incidence and severity of ventricular arrhythmia in this context was determined in the setting of global ischaemia for 7 minutes followed by reperfusion for 20 minutes. Neuropeptide Y was perfused for 15 minutes prior to ischaemia. Global ischaemia resulted in ST elevation on the ECG and fully resolved during successful reperfusion.

Using the arrhythmia-scoring algorithm detailed above, perfusion of NPY increased the total arrhythmia score (control 0.3±0.2 vs. NPY 2.0±0.4, $p<0.05$, Mann-Whitney U test) with 80% of control experiments demonstrating no arrhythmia compared to 60% of NPY experiments resulting in VT or VF (Figure 4.12).

4.4 Discussion

The main findings of this study are:

1. High level sympathetic nerve stimulation remained pro-arrhythmic and decreased ventricular fibrillation threshold despite effective β-blockade in the isolated rat heart with intact sympathetic innervation
2. The Y_1 receptor is expressed on ventricular myocytes and neuropeptide Y exerts a Y_1 receptor dependent, pro-arrhythmic effect in the isolated rat heart and ventricular myocyte monolayers

3. High level sympathetic stimulation results in increased NPY levels in the coronary effluent of the isolated rat heart
4. NPY increases the incidence of significant ventricular arrhythmias in the setting of ischaemia-reperfusion
5. A combination of β-blockade and Y_1 receptor blockade can abolish the pro-arrhythmic effect of high level sympathetic stimulation

NPY is a novel, independent, pro-arrhythmic trigger

These data demonstrate that exogenous NPY decreases VFT via a Y_1 receptor dependent mechanism in the isolated rat heart. This mechanism was confirmed in an alternate spatial domain with demonstration of an increase in spontaneous activity and wave generation in quiescent monolayers of ventricular myocytes, an effect that could be prevented with pre treatment of the monolayer with an Y_1 receptor antagonist. These pharmacological and functional observations were supported by anatomical evidence of the presence of the Y_1 receptor on myocytes by immunohistochemistry and the first demonstration to our knowledge of the presence of Y_1 receptor protein in ventricular lysates.

In order to explore these observations in a more physiologically relevant model, a Langendorff perfused rat heart with intact sympathetic innervation was developed. Direct unilateral sympathetic nerve stimulation resulted in tachycardia and positive inotropy and this was prevented by metoprolol. Our data demonstrate that a maximal concentration of noradrenaline lowers VFT, and the same dose of metoprolol completely blocks this effect, indicating its efficacy as an anti-arrhythmic and confirming that this dose was appropriate to use in the innervated model to antagonise

the release of noradrenaline from direct nerve stimulation. Interestingly, metoprolol was unable to prevent the fall in VFT following prolonged high-frequency stimulation of either the right or left stellate ganglion, despite the chronotropic and inotropic responses being blocked. Therefore, this suggests that an additional neurotransmitter released during nerve stimulation may be generating a pro-arrhythmic environment. The pharmacological studies in the isolated heart and myocyte monolayers clearly demonstrated that NPY can act an independent trigger, and consistent with these observations, a combination of metoprolol and Y_1 receptor blockade during high frequency stellate ganglia stimulation abolishes the fall the VFT. Furthermore, we were able to demonstrate that levels of NPY in the coronary effluent were increased significantly by prolonged stimulation of either stellate ganglia during perfusion with metoprolol.

Mechanism of pro-arrhythmic action

The exact mechanism behind this pro-arrhythmic action beyond the activation of the Y_1 receptor remains to be elucidated. Existing data on the ion channel effects of NPY are variable and complex. No alteration in I_{Na} or I_K current activity has been demonstrated [304] but I_{to} was reduced [305], but these changes are unlikely to significantly influence the APD in the rat heart. Interestingly, the effect of NPY on I_{CaL} has been shown to be species dependent with inhibition in guinea pig myocytes [306] and stimulation in rat myocytes [307]. Furthermore, calcium sparks and transients in isolated myocytes have been shown to increase in response to NPY [308]. Therefore, one could speculate that the pro-arrhythmic action seen was more dependent upon changes in calcium dynamics as evidenced by the changes in contractility and spontaneous wave generation in monolayers rather than an effect predominantly on repolarising currents.

Calcium overloading [449, 450, 454] can lead to delayed afterdepolarisations and is also the trigger for ischaemia-reperfusion injury as a rise in I_{Na} from increased NHE (sodium-hydrogen exchanger) activity leads to intracellular calcium loading via NCX (sodium-calcium exchanger) [453]. Optical mapping of voltage and calcium together would allow further exploration of this hypothesis.

Clinical implications

Studies over the last two decades have demonstrated that plasma NPY levels are elevated following acute coronary syndromes and during left ventricular failure and levels correlate with severity of heart failure and one year mortality [294, 295]. Contemporary management of acute myocardial infarction is primary percutaneous coronary intervention, and recent data has once again demonstrated that plasma NPY levels were significantly elevated, and despite revascularisation, remained elevated even after 48 hours of treatment [296]. In view of the persistent sympathetic hyperactivity associated with chronic heart failure and post myocardial infarction and the long plasma half-life of NPY, the neuromodulatory action of NPY at the level of the myocyte may well contribute to the pathophysiology of these conditions. This potential clinical implication was tested in the setting of an ischaemia-reperfusion model. These data demonstrated that NPY perfusion prior to the onset of ischaemia significantly increased the incidence of VT or VF in the reperfusion phase. Further mechanistic exploration of this effect is warranted to study the influence of β-blockade and Y_1 receptor antagonism in this model system.

Sympathetic hyperactivity also plays a role in the initiation and maintenance of ventricular arrhythmias [468, 469] in patients with structural heart diseases or abnormal

electrical substrate such as long QT syndrome (LQTS) and catecholaminergic polymorphic ventricular tachycardia (CPVT). Patients with these conditions are at high risk of recurrent ventricular arrhythmia and sudden cardiac death necessitating implantable cardiovertor defibrillator therapy [3-5]. Despite optimal medical therapy, which universally includes ical substrate suchs may present with recurrent ventricular arrhythmia and multiple shocks from the ICD [5, 470, 471]. The current standard of care in this scenario of arrhythmia storm is anti-arrhythmic medication and catheter ablation [472] but arrhythmia recurrence can remain high in this group [473] with the physical and psychological impact of recurrent ICD shocks substantial.

Neuromodulation by targeting the sympathetic nervous system has demonstrated efficacy in animal studies and clinically, thoracic epidural anaesthesia and cardiac sympathetic denervation (CSD) are the commonest used strategies in arrhythmia management [64, 474-476]. In the largest case series of CSD to date, Vaseghi *et al.* [477] presented data on 41 patients who underwent left or bilateral stellectomy for refractory ventricular arrhythmia requiring ICD therapies and previous failed catheter ablation. The majority of patients were on multiple antiarrhythmic medications and 73% were taking β-blockers. The remaining 27% of patients were unable to tolerate β-blockade due to hypotension, a feature often seen in patients with significant left ventricular impairment. In this study, CSD resulted in almost 50% of patients being free of ICD shocks at 1 year with the remaining patients experiencing a significant reduction in the burden of arrhythmia and ICD therapies. A similar approach has also been explored in channelopathies such as LQTS [478, 479] and CPVT [480]. Patients with mutations in ion channel function leading to these conditions can present with syncope, ventricular arrhythmia or sudden cardiac death precipitated by physical or

emotional stress. In this recent series [481], 17 patients with either LQTS or CPVT underwent left CSD for recurrent arrhythmia despite all patients being on β-blockers. During follow up (median 34 months), 87% of patients had significant reduction in cardiac events following LCSD. Other neuromodulatory strategies, which have also demonstrated efficacy in patients presenting with arrhythmia storm, include thoracic epidural anaesthesia [476] and renal sympathetic denervation [482], which act to modify cardiac sympathetic outflow rather than remove the source of neurotransmitters.

These small but interesting studies demonstrate that some patients continue to experience life threatening ventricular arrhythmia despite optimal medical and device therapy. Surgical resection of the lower stellate ganglia may therefore not only reduce the release of NA but potentially also NPY, thereby conferring the additional reduction in cardiac events compared to β-blockade alone. This hypothesis warrants exploration through the study of plasma or coronary sinus NPY levels post CSD and assessment of change in electrophysiological parameters in appropriate animal models and patients.

Limitations

These data reflect studies in a multi domain approach utilising myocyte monolayers, Langendorff perfused isolated heart and an innervated heart preparation. *In-vitro* preparations are however removed from the haemodynamic and neuro-humoral perturbations that contribute to arrhythmogenesis, and therefore may not give a full quantitative mechanistic account of the pathways involved. In addition, healthy hearts were used to delineate the changes in VFT accurately, and further study in appropriate infarction or heart failure models is warranted. Despite the significant pro-arrhythmic

effects seen with NPY perfusion and SG stimulation, the cellular mechanisms responsible beyond the Y_1 receptor remain to be determined. There are differences in ion channel expression in the rat heart and those of other rodents in comparison to the human heart. It would be of interest to assess electrophysiological changes in large animal models such as the pig and dog where the action potential is similar to that seen in the human heart. Optical mapping is also powerful tool in imaging global electrophysiology and calcium handling although there is conflicting evidence regarding the influence of electro-mechanical uncoupling with blebbistatin on electrophysiology [421, 422]. Conversely, the use of electrode mapping gives limited spatial resolution and variation in signal magnitude over time. Testing VFT may not reflect the mechanism of VT and VF initiation *in-vivo* but it does allow for reproducible testing of arrhythmogenicity removed from the stochastic nature of arrhythmia induction seen with ischaemia-reperfusion or infarct models.

Conclusions

These data provide mechanistic evidence to support the emerging neuro-modulatory therapies targeting the cardiac sympathetic nervous system in the context of ventricular arrhythmias. Targeting NPY receptors pharmacologically may offer a therapeutic strategy, with potentiation of parasympathetic tone via Y_2 blockade and Y_1 receptor inhibition on the myocyte exerting an anti-fibrillatory effect. This strategy would be expected to add synergistically with existing therapies including β-blockers, ACE inhibitors and cardiac devices including implantable cardiovertor defibrillators.

Chapter 4 Figures

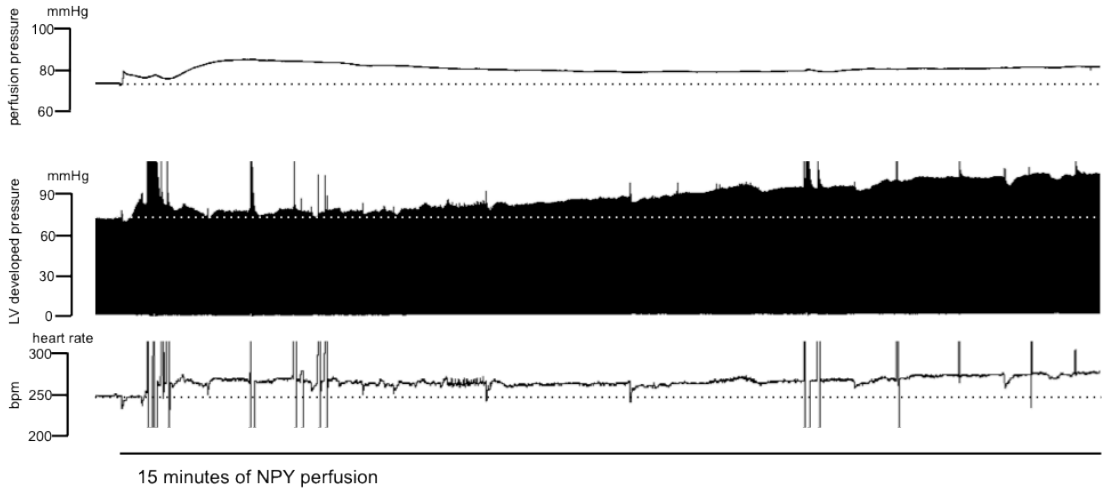


Figure 4.1 Experimental trace of neuropeptide Y (NPY) perfusion

Raw data trace demonstrating haemodynamic changes during NPY (250nM) perfusion to an isolated heart following stabilisation. There is an acute rise in perfusion pressure upon initiation of NPY perfusion followed by a sustained increase compared to baseline values (dotted line). Initiation of NPY perfusion also results in ectopy throughout perfusion and a gradual increase in contractility and while the changes in heart rate were variable across the preparations (see Figure 4.2 summary data).

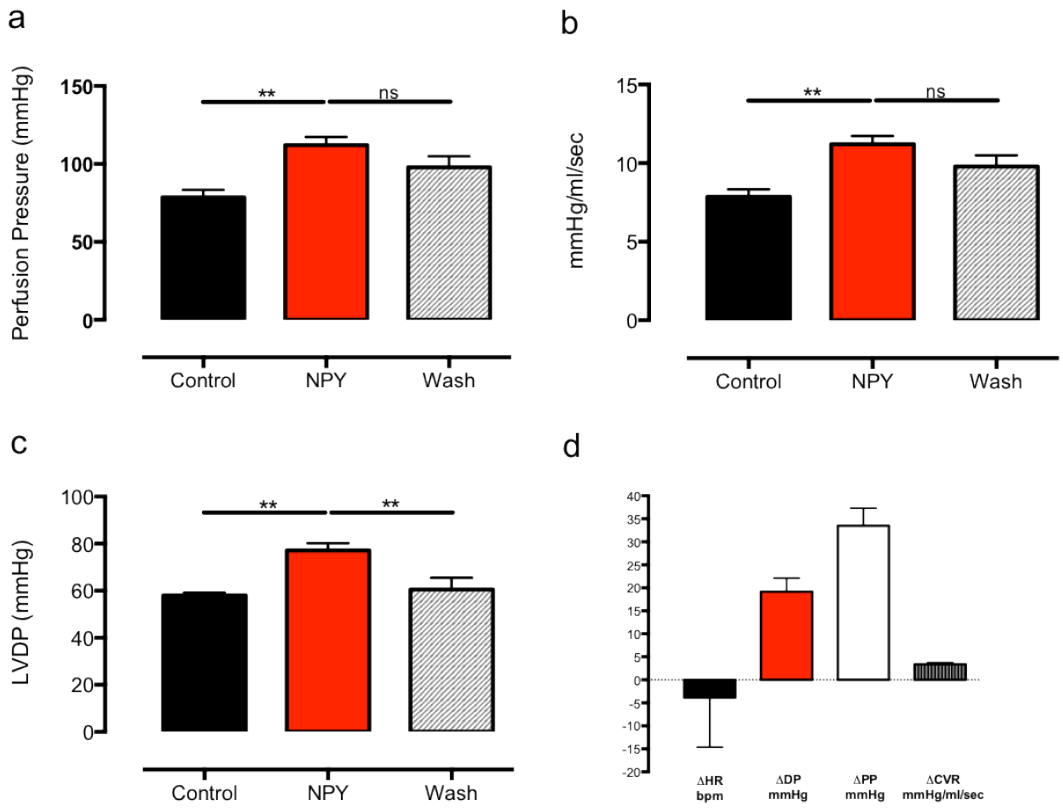


Figure 4.2 Haemodynamic effects of neuropeptide Y (NPY) perfusion

(a) Perfusion pressure is increased during NPY (250nM) perfusion with the effect sustained despite washout and this is (b) reflected in the coronary vascular resistance. (c) LVDP is increased during NPY perfusion and this effect is lost upon wash out. (d) Summary data of absolute changes in HR/DP/PP/CVR during NPY perfusion (n=6, **p<0.01, ANOVA)

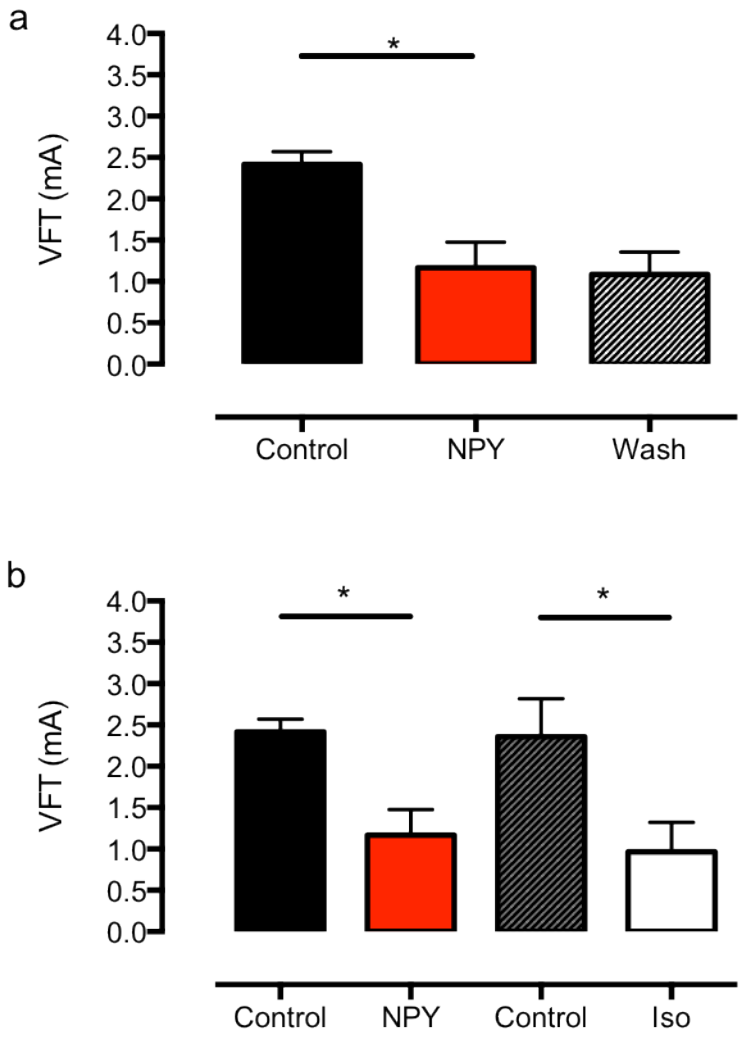


Figure 4.3 NPY lowers VFT independent of HR

(a) NPY (250nM, n=6, *p<0.05, ANOVA)) lowers VFT independent of HR and the pro-arrhythmic effect is sustained despite wash out of the drug and this effect (b) is comparable to the pro-arrhythmic effect of isoprenaline (10nM, n=4, *p<0.05, paired t-test)

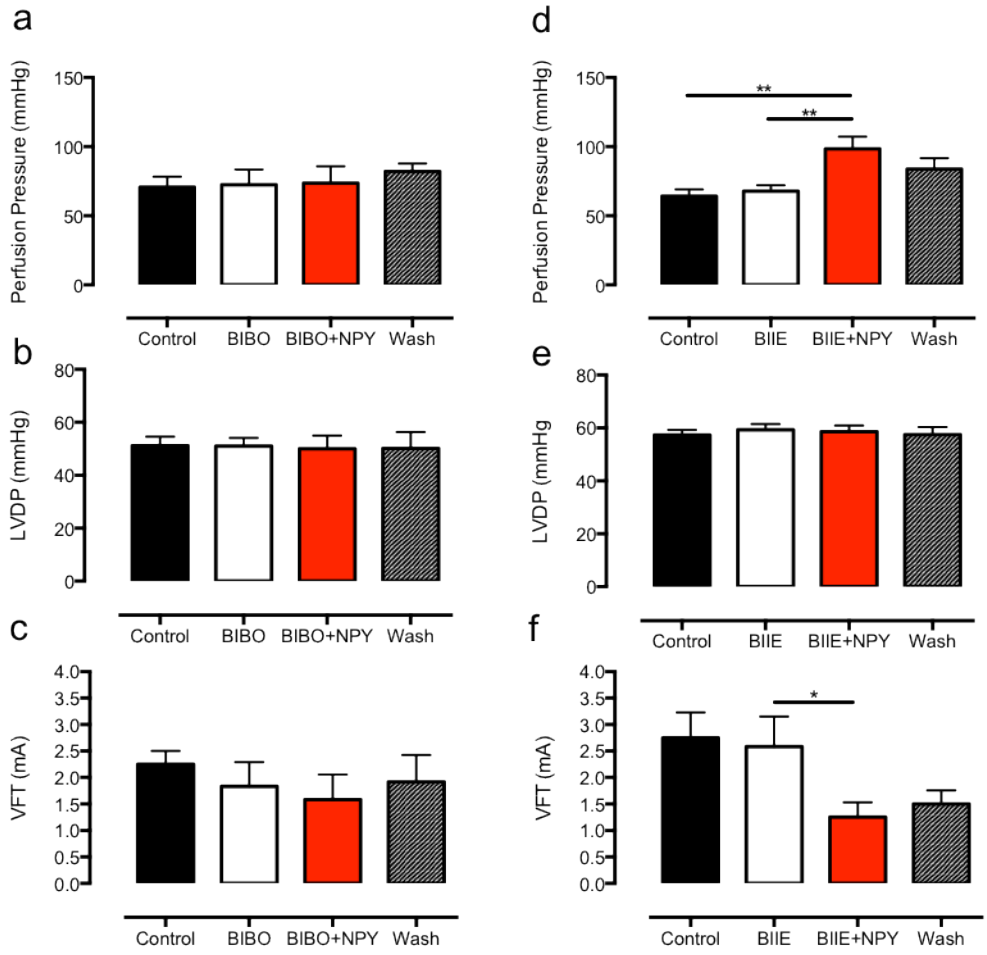


Figure 4.4 NPY lowers VFT independent of heart rate via a Y_1 receptor dependent mechanism

Co perfusion of the Y_1 receptor antagonist, BIBO3304 (1μM, n=6) prevents the rise in (a) perfusion pressure, (b) LVDP and (c) VFT seen with NPY perfusion alone. In comparison, co perfusion of the Y_2 receptor antagonist, BIIE0246 (1μM, n=6) demonstrates preservation of the increase in (d) PP (**p<0.01, ANOVA), (e) no change in LVDP while the (f) reduction in VFT remains unaffected

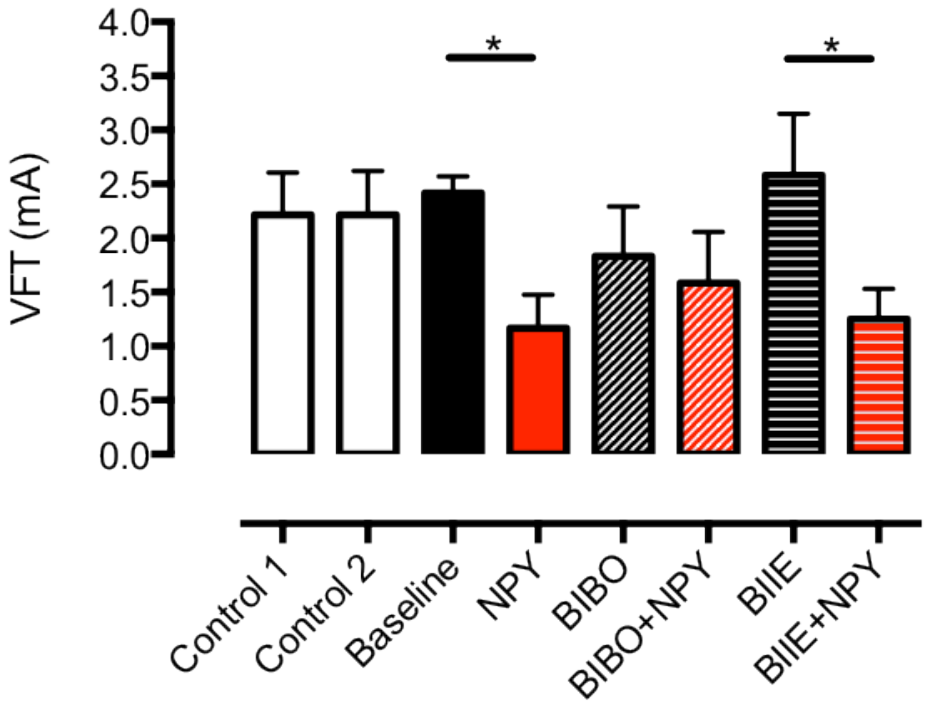


Figure 4.5 NPY lowers VFT independent of heart rate via a Y_1 receptor dependent mechanism

Summary data comparing changes in VFT during control stimulation, NPY perfusion in the presence of Y_1 receptor (BIBO3304) and Y_2 receptor (BIIE0246) antagonists (*$p<0.05$, paired t-test, n=6/group)

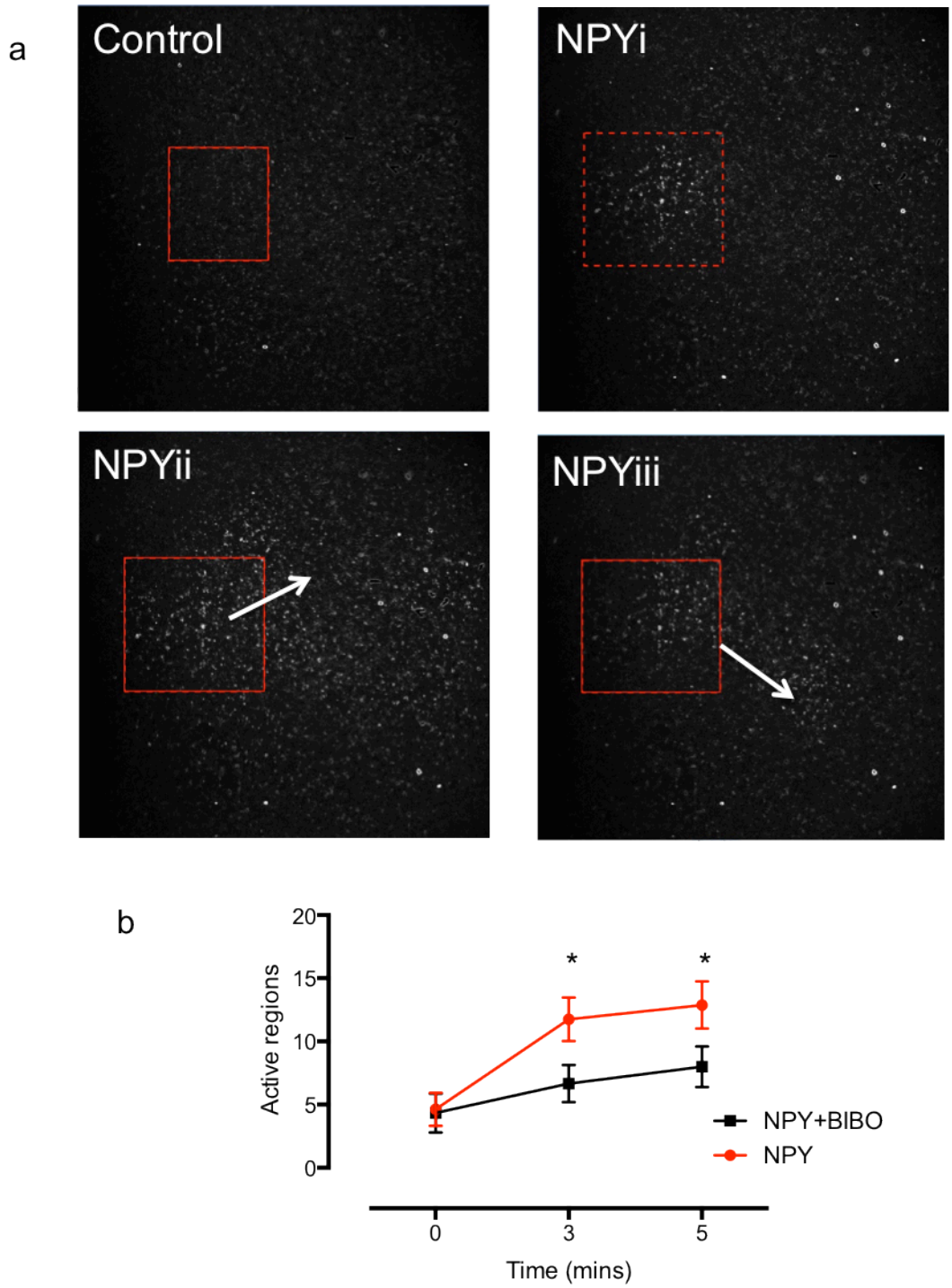


Figure 4.6 NPY results in spontaneous wave activity in quiescent myocyte monolayers

(a). Addition of NPY results in an increase in spontaneous activity with wave propagation (white arrow, each images 40msec apart). (b) NPY results in a significant increase in active regions (16 regions per monolayer) at 3 minutes and 5 minutes post addition of NPY 250nM (n=8, *p<0.05 v's t=0mins, paired t-test). This effect is blocked by Y_1 receptor blockade (BIBO3304 1μM, n=6)

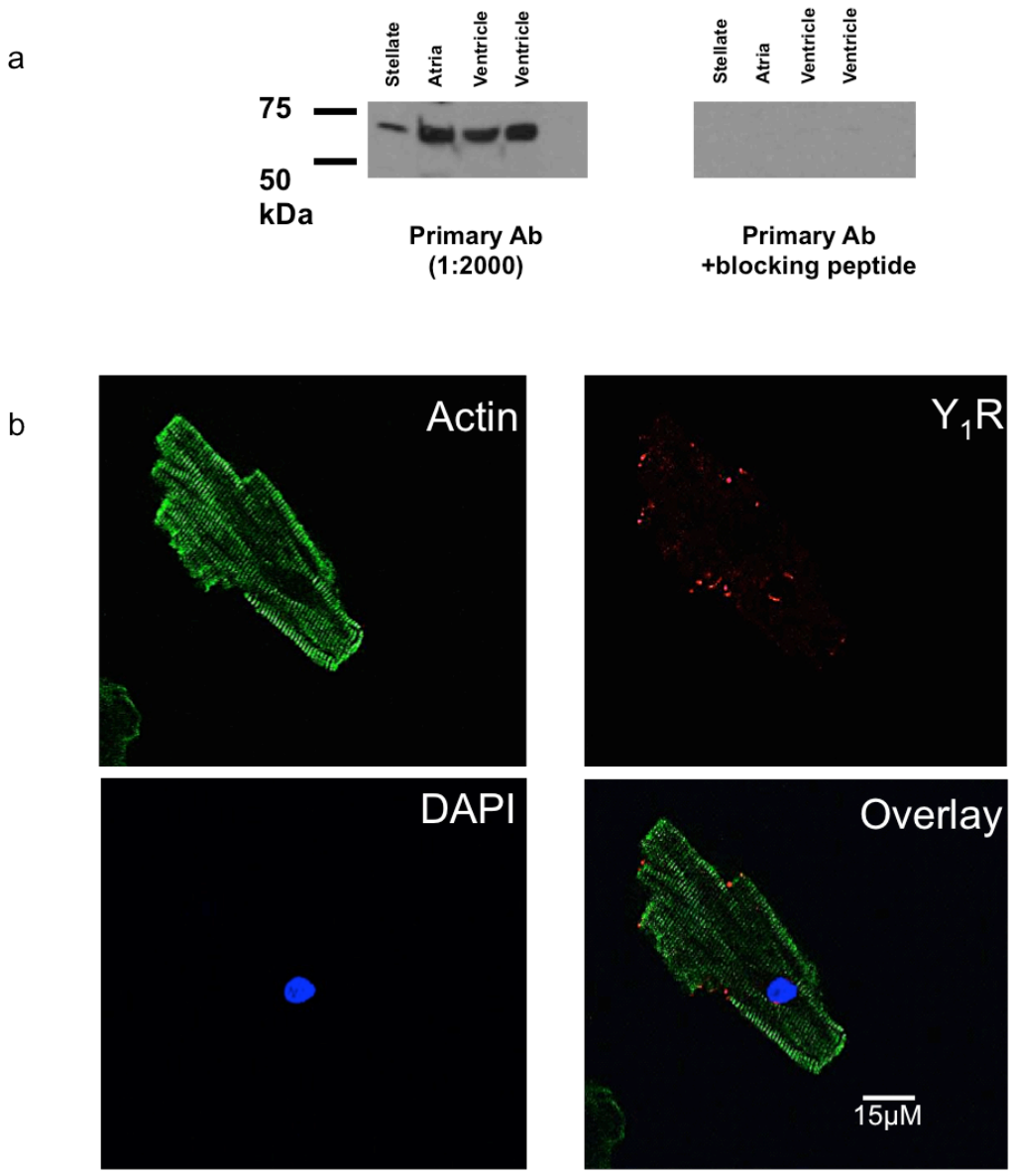


Figure 4.7 NPY Y_1 receptor is present on cardiomyocytes

(a) Western blotting demonstrating the presence of the Y_1 receptor protein in stellate ganglia, atria and ventricular homogenates with loss of band with addition of a blocking peptide. (b) Immunohistochemical evidence of the presence of Y_1 receptor on isolated ventricular cardiomyocytes.

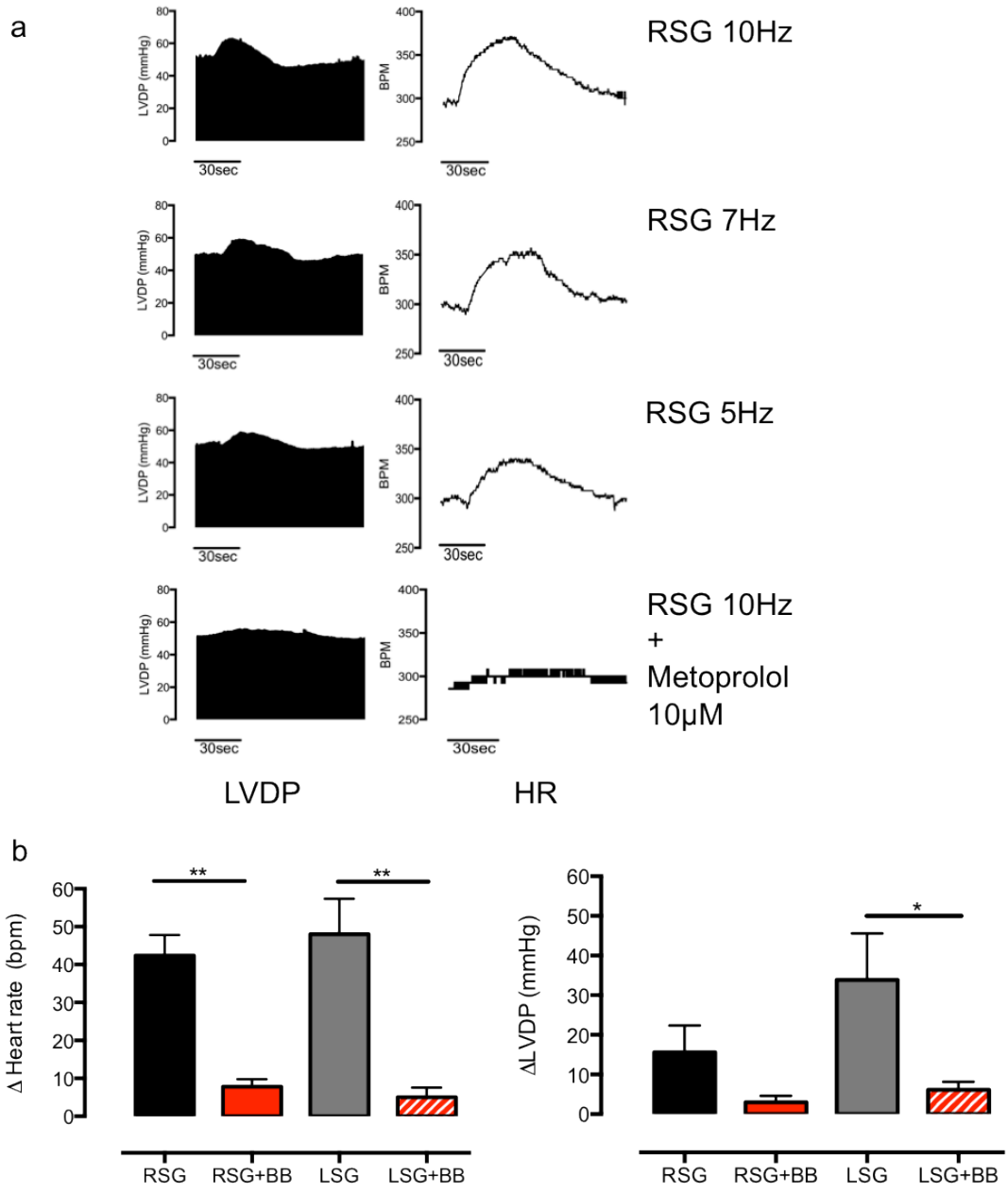


Figure 4.8 Direct stellate ganglia stimulation and haemodynamics

(a) Frequency dependent changes in LVDP and heart rate during direct RSG stimulation and loss of the inotropic and tachycardia response in the presence of metoprolol (10µM) (b) Summary data of the absolute change in HR and LVDP during RSG/LSG stimulation and repeated in the presence of beta-blockade (*p<0.05, **p<0.01, paired t-test, n=6/group)

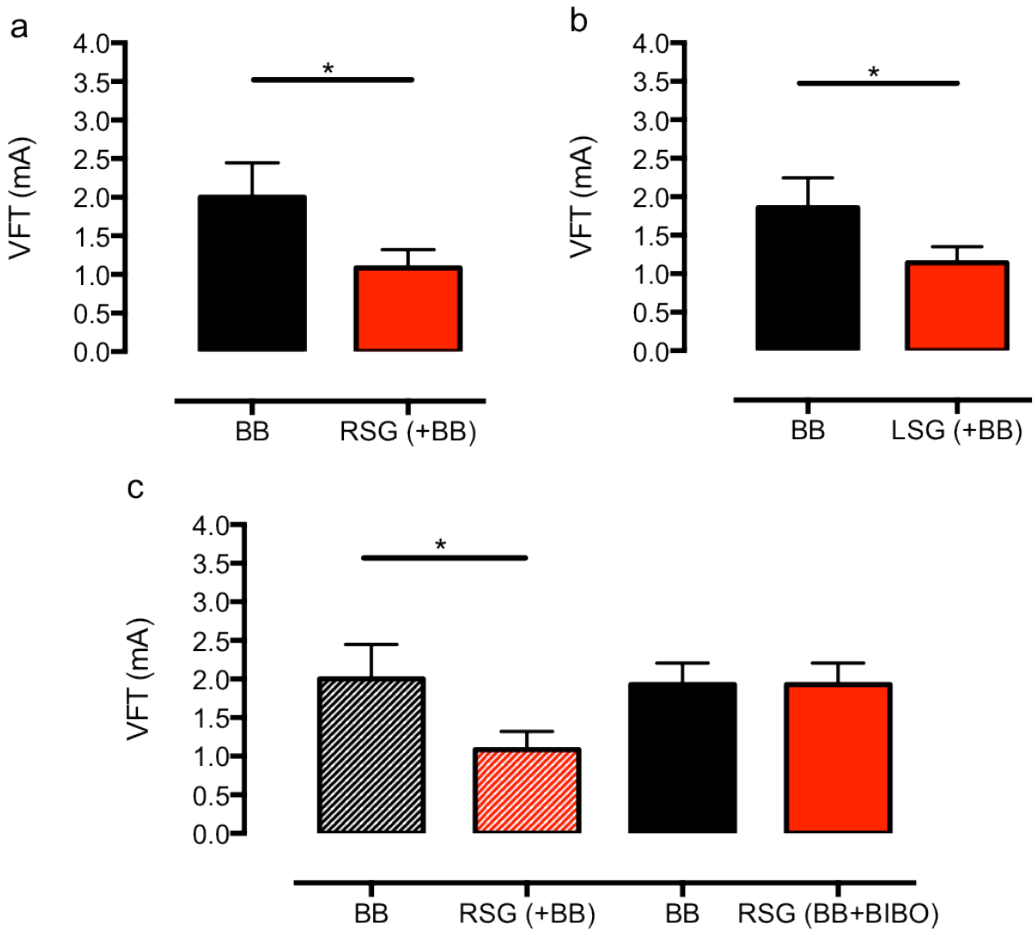


Figure 4.9 Direct stellate ganglia stimulation and VFT

(a) RSG stimulation lowers VFT in the presence of a beta-blocker (metoprolol 10μM, *p<0.05, n=6). (b) LSG stimulation lowers VFT in the presence of a beta-blocker (metoprolol 10μM, *p<0.05, paired t-test, n=6. (c) Co-perfusion of the Y_1 receptor antagonist abolishes the residual pro-arrhythmic effect of RSG stimulation (BIBO3304 1he res<0.05, paired t-test, n=6)

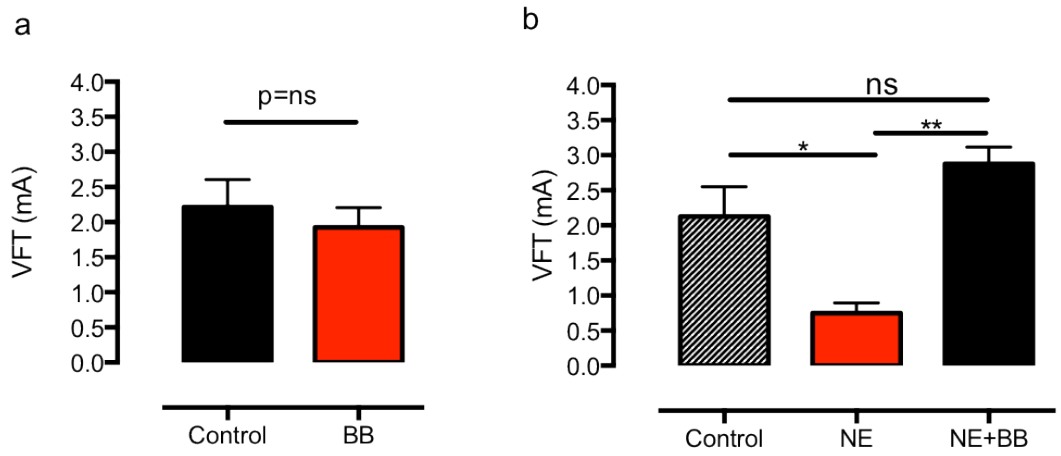


Figure 4.10 The pro-arrhythmic effect of norepinephrine is abolished by beta-blockade

(a) Perfusion of metoprolol 10μM (BB) does not change baseline VFT (n=6/group, unpaired t-test). (b). Norepinephrine (NE, 10μM) significantly lowers VFT and this effect is blocked by co-perfusion of metoprolol 10μM (*p<0.05, **p<0.01, ANOVA, n=4).

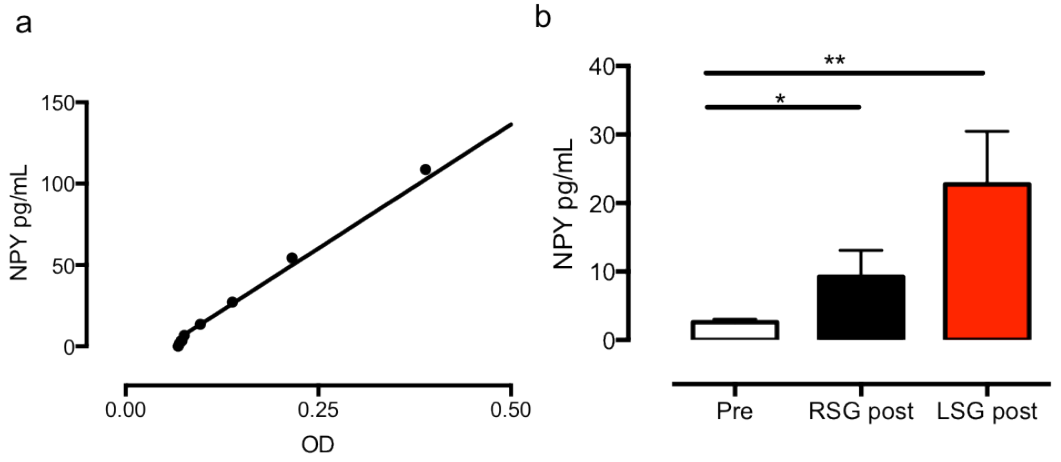


Figure 4.11 Direct stellate ganglia stimulation results in increased NPY levels in coronary perfusate

(a) Standard curve of NPY standards by ELISA (b) Direct RSG and LSG stimulation leads to a significant increase in NPY levels detectable by ELISA in snap frozen coronary perfusate (n=6-12/group, *p<0.05, **p<0.01, unpaired t-test)

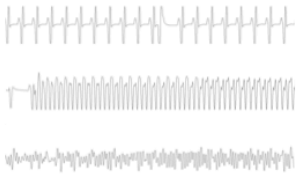
ECG example	Arrhythmia (score)	Arrhythmia frequency	
		Control (n=10)	NPY (n=10)
	None (=0)	8	1
	VEs (=1)	1	3
	VT (=2)	1	1
	VF (=3)	0	5
	Mean Score	**0.3±0.2**	**2.0±0.4****

Figure 4.12 NPY increases the incidence of ventricular arrhythmias following ischaemia reperfusion

Incidence of ventricular arrhythmias during ischaemia (7mins) - reperfusion (20mins) is significantly higher following 15mins NPY perfusion (250nM, n=10) compared to control (n=10) (90% vs. 20%, $p<0.01$, Fishers exact) with a significantly higher arrhythmia score per experiment (** $p<0.01$, Mann-Whitney U-test)

Chapter 5 Tetrahydrobiopterin and autonomic control of cardiovascular function

5.1 Introduction

Tetrahydrobiopterin (BH4) is a key cofactor for enzymes involved in multiple physiological systems including development, cardiovascular physiology, neurotransmitter synthesis and inflammatory cascades. BH4 is generated de novo from GTP (discussed in detail in Chapter 1) by the step-wise action of 3 enzymes, with the rate-limiting step catalysed by GTP cyclohydrolase 1 (GTPCH) encoded by *GCH1* [309].

BH4 plays a critical role in the function of nitric oxide synthase (NOS) enzymes by increasing the affinity for arginine based ligands [310, 311] and contributing to dimer stabilisation [312]. Therefore BH4 is a key molecule in the maintenance of blood pressure and vascular function. Common cardiovascular conditions such as hypertension, atherosclerosis and diabetes are characterised by endothelial dysfunction and impaired endothelial dependent vasodilatation [313]. Mechanistic studies have provided evidence demonstrating that *GCH1* expression is a critical determinant of endothelial cells BH4 level and endothelial NOS function [314, 315]. In addition, overexpression of *GCH1* improves endothelial function in murine models of vascular disease such as pulmonary hypertension [316], diabetes [317], and atherosclerosis [318].

The role of BH4 in the vascular system is clear (discussed in detail in Chapter 1) and its therapeutic potential continues to be the subject of study. The importance of BH4

to vascular function has been demonstrated in human studies where BH4 supplementation improved vascular function in normal subjects and those with vascular disease such as smokers and patients with diabetes [330-337].

The cardiac role of BH4 has been studied in the context of recent studies that have identified endogenous nitric oxide (NO) generation by myocytes [129]. Endothelial NOS (eNOS) has been localised in coronary and endocardial endothelial cells and, cardiomyocytes. Neuronal NOS (nNOS) is found in the cardiomyocyte, autonomic nerves and ganglia [344, 345]. Activation of these enzymes leads to different responses as a consequence of distinct subcellular localisation [344-346] and the short diffusion distance of NO within the cardiomyocyte as a consequence of myoglobin's affinity for NO and interactions with superoxide [183, 208, 347].

The downstream effects of NO generation are dependent upon activation of soluble guanylyl cyclase (sGC) and generation of cyclic guanosine monophosphate (cGMP). This results in intracellular cGMP accumulation and reduction in myofilament Ca^{2+} sensitivity and decreased contractility [349-351]. Recent data has suggested that the action of NO on ion channel activity and therefore its electrophysiological effect is independent of sGC and utilises s-nitrosylation (S-NO). Targets of S-NO include the ryanodine receptor Ca^{2+} release channel (RyR_2) [352, 353], SR Ca^{2+} ATPase (SERCA) [225] and the L-type Ca^{2+} channel [226, 354]. Other data, however, support cGMP/PKG mediated inhibition of L-type Ca^{2+} channel activity [351].

Ion channel and myofilament Ca^{2+} sensitivity are physiological processes that affect heart rate and contractility and these parameters are also under autonomic control.

Previous chapters have discussed in detail the changes in autonomic function seen in cardiovascular conditions such as heart failure and following myocardial infarction. Large, prospective clinical studies have demonstrated that a shift towards sympathetic hyperactivity and the resulting impairment of heart rate variability and baroreceptor sensitivity independently predict mortality (UK-HEART, ATRAMI) [15, 16]. Mechanistically these changes are linked to NO which regulates sympathetic and vagal control [355], with loss of NO mediated potentiation and inhibition of vagal and sympathetic outflow respectively [132, 182, 356, 357].

Given the critical role of BH4 in the synthesis of NO and catecholamines, it is plausible that it would play a mechanistic role in modulating cardiac autonomic function. A recent study [358] investigated the impact of a common genetic variant in *GCH1* on autonomic function in humans. The C243T SNP, discussed earlier in the context of its association with increased blood pressure and decreased levels of NO, was found in this study to be associated with reduced urinary catecholamine excretion, reduced NO production and decreased baroreflex sensitivity and heart rate variability. The X haplotype [320] with which this SNP is in tight linkage disequilibrium is associated with low BH4 levels, and therefore this may indicate that the observed effect was BH4 mediated. However, this study did not measure BH4 levels in any samples from the population studied, so the observations remain associations between genotype and some physiological phenotypes, but without rigorous mechanistic links. Patients with mutations in *GCH1* can present with a rare movement disorder, DOPA-responsive dystonia (DRD) [359]. Mayahi *et al.* [360] assessed endothelial, sympathetic and cardiac function in 16 patients with DRD due to heterogeneous mutations in the *GCH1* gene. These patients demonstrated a high resting heart rate, low plasma

catecholamines but otherwise unaffected flow mediated dilatation and intact autonomic and cardiac responses to sympathetic stimulation.

The hph-1 mouse also demonstrates changes in the autonomic regulation of heart rate. In the setting of BH4 deficiency in this model, a resting tachycardia was demonstrated which persisted despite exercise training while blood pressure and heart rates were normal during exercise [361]. Mechanistically, this was linked to increased β-adrenergic receptor sensitivity to catecholamines while vagal function was unaffected. This observation reflected similar findings in patients with BH4 deficiency including those with a marked neurological presentation with dopa-responsive dystonia or individuals with no overt phenotype but carrying the C+243T polymorphism [360].

A variety of approaches were considered in order to investigate the interesting observations linking a critical cofactor for NOS and TH activity to the regulation of heart rate. Previous studies demonstrating the importance of BH4 synthesis have utilised systemic pharmacologic inhibitors of GTPCH [321, 483] or the hph-1 mouse [361]. Both these approaches achieve only moderate and variable reductions in BH4 and therefore the enzyme systems in question will continue to function. Genomic deletion of *Gch1* (murine GCH1 gene) would therefore be a more specific strategy. However, total genomic deletion of *Gch1* [362] results in embryonic lethality by E13.5 (E: embryonic day) in the absence of structural abnormalities. Global *Gch1* deletion could not be rescued to viability by maternal supplementation of BH4 and L-DOPA, thereby preventing physiological study. A tissue specific approach has recently been developed and has demonstrated the importance of *Gch1* in endothelial cells in the regulation of vascular tone and blood pressure [325]. Hence, we investigated whether a

tissue specific knockout mouse model of BH4 deficiency in TH expressing sympathetic neuronal cells would provide mechanistic evidence to support a cell autonomous role for BH4 in this context.

As discussed earlier, β-blockers remain the only anti-arrhythmic medications that reduced mortality post myocardial infarction and in congestive cardiac failure [21]. Targeted disruption of catecholaminergic signalling at the level of the sympathetic neuron by tissue specific knockout of BH4 may provide a novel mechanism of reducing local sympathetic drive. Furthermore, disruption of local noradrenaline release may also provide a further target to decrease co-transmission of substances such as neuropeptide Y. The murine model is an ideal system in which to explore this as previous data has shown a relative paucity of nNOS in cardiac parasympathetic and sympathetic ganglia, thereby allowing study of this interaction without the deleterious effects of uncoupled nNOS which may be seen in other species [208].

5.2 Methods

5.2.1 Generation of the THcre GCH$^{f/f}$ and THiresGCH$^{f/f}$ mouse models

In order for tissue specific models of BH4 deficiency to be studied, a 'floxed' Gch mouse was generated by the commercial provider, Genoway, in accordance with a targeting strategy and plasmid cloning by the Channon Group. A plasmid containing a FRT-PGK-promoter and a neomycin-FRT-LoxP positive selection cassette was inserted into the intron 3 sequence of *Gch1*. An additional LoxP site was inserted into intron 1 to flox exon 2-3. The *Gch1* floxed mouse was generated using homologous recombination in ES cells. Two chimeric male mice with 90-100% chimerism were chosen for breeding and Flp-mediated excision was carried out by breeding with a Flp

deletor female. These were bred on a C57BL/6 background to backcross 7 to generate pure lines of $GCH^{f/f}$ mice and an active colony maintained for breeding. The insertion of LoxP sites in the *Gch1* gene did not result in a hypomorphic allele evidenced by no differences in BH4 levels between $GCH^{+/+}$, $GCH^{f/+}$ and $GCH^{f/f}$ mice in heart, liver or lung tissue [362] indicating that the floxed gene does not change GTCPH expression. Furthermore, this observation supports the use of $GCH^{f/f}$ as control animals for the experiments described below.

These $GCH^{f/f}$ mice were crossed with a mouse in which the activity of the cre-recombinase enzyme was under the control of TH as a promoter (THcre mouse; Jackson Laboratories, USA; a gift from Professor Ratcliffe's group, Oxford). This results in genomic deletion of *Gch1* in all cells expressing TH including the central nervous system, peripheral sympathetic ganglia and nerves, and chromaffin cells of the adrenal medulla [427].

A second breeding program was also undertaken utilising an internal ribosome entry site (IRES) for expression of cre-recombinase under the control of TH as a promoter [428]. The transgenic approach (THcre) can be limited by difficulty in obtaining the normal expression from a promoter lacking some of its additional enhancer regions. This can lead to variation between founder lines due to differences in integration site and copy number. The IRES approach links expression of cre-recombinase to that of the endogenous gene thereby resulting in restricted expression in the same pattern as the endogenous gene [428]. The breeding program was unchanged other than the lines being crossed were $GCH^{f/f}$ as above and THires (a gift from Professor Ratcliffe's group, Oxford).

The breeding diagram (Figure 5.1) summaries the generation of this model and further details of colony maintenance are described in Chapter 2. THcreGCH$^{f/f}$ and their GCH$^{f/f}$ littermates aged 12-20 weeks were used for all experiments. Male and female animals were used in molecular and biochemical studies and only males in non-invasive tail cuff blood pressure measurements.

THiresGCH$^{f/f}$ animals and their littermate controls were culled at day 21 due to severity restriction on the project license and used for biochemical and molecular phenotyping. Motion analysis was also conducted up to this time point (Anymaze experiments).

5.2.2 Genotyping GCH$^{f/f}$; cre loci

Mice were genotyped by polymerase chain reactions prepared from ear biopsies or target tissues such as adrenal glands. Details of DNA extraction and primer sequences used for identification of *Gch1* and cre loci are described in detail in Chapter 2.

5.2.3 Determination of tissue BH4 and biopterin levels

BH4 and oxidised biopterins (BH2 and biopterin) were determined by high performance liquid chromatography (HPLC) with electrochemical and fluorescent detection respectively, following a well-established protocol (see Chapter 2). Snap frozen tissues underwent 2 freeze-thaw cycles and homogenisation in ice-cold resuspension buffer (50mM phosphate-buffered saline, 1mM dithioerythriol, 1mM EDTA, pH 7.4). The samples were then centrifuged at 13,200rpm for 10 minutes at 4°C. The supernatant was removed and ice cold acid precipitation buffer (1M phosphoric acid, 2M trichloroacetic acid, 1mM dithioerythriol) was added (sample preparation detailed in Chapter 2) and re-centrifuged at 13,200rpm for 10 minutes at

4°C. The supernatant was removed and injected into the HPLC system. Quantification of peaks obtained for BH4 and oxidised biopterins was obtained by comparison with external standard and normalised to protein concentration determined by BCA protein assay.

5.2.4 Determination of catecholamine levels

Whole blood was collected into heparinised syringes from the IVC of THcreGCH$^{f/f}$/THiresGCH$^{f/f}$ and control GCH$^{f/f}$ animals after overdose of anaesthetic. Whole blood samples were centrifuged at 4°C, 3000rpm for 15 minutes to separate plasma from red cells. Plasma was transferred to a new Eppendorff tube and frozen at -80°C.

For catecholamine determination [433], samples were prepared in a 50:50 dilution with perchloric acid centrifuged through a 0.22μm filter (VWR) at max speed, 4°C for 3 minutes. Samples (50μl) were injected onto an isocratic HPLC system and quantified using electrochemical detection and carbon working electrode held at +0.7V vs a Ag/AgCl electrode (Decade SDC, Antec). HPLC separation was performed using a 250-mm Microsorb C18 reverse-phase column (Agilent) and mobile phase comprising methanol (13% v/v), NaH_2PO_4 (120mM), EDTA (0.8mM), and sodium octane sulfonate (3.2mM), pH 3.27 at a flow rate of 1ml/min. Catecholamine quantification was done relative to freshly prepared standards.

5.2.5 Real time quantified RT-PCR

Total RNA was obtained from homogenised adult tissue by Trizol extraction. RNA was checked for purity and quantity by Nanodrop (ThermoScientific, USA). Reverse transcription was carried out using the QuantiTect reverse transcription kit (Qiagen,

UK) on 1μg total RNA. Quantitative real-time RT-PCR was performed with an iCycler IQ real time detection system (BioRad laboratories, USA) using primers and probes from the TaqMan Gene Expression Assay system (Applied Biosystems, UK) with analysis using the delta-CT method with GAPDH as control.

5.2.5 Measurement of heart rate and arterial blood pressure

Blood pressure and heart rate was measured by non-invasive, tail cuff plethysmography using the Visitech® system following 5 days training and recordings on 5 consecutive days.

5.2.6 Western immunoblotting

Western immunoblotting was used for the quantification of GTPCH, TH and GAPDH (loading control). Tissue (whole adrenal gland, micro-dissected cortex/medulla) was homogenised in CellLytic™ buffer (Sigma Aldrich, UK) with 1 tablet/10ml of protease inhibitor (Complete Mini, EDTA free, Roche, UK). Tissue was disrupted in an Eppendorff tube using an Eppendorff pestle and then put through 2 freeze-thaw cycles on dry ice to maximise release of protein. The samples were then centrifuged at max speed, 4°C for 5 minutes. The supernatant containing the extracted protein was transferred to a new tube and the cell pellet stored at -80°C for DNA extraction if needed. Protein concentration was determined by the BCA assay as described above. Samples for western blotting were prepared in x4 NuPAGE® LDS sample buffer and x10 NuPAGE® reducing agent (Invitrogen, UK) and incubated at 70°C for 10 minutes before gel electrophoresis. Protein lysates (5-20μg) were resolved by SDS-PAGE using NuPAGE® 4-12% Bis-Tris gel in NuPAGE® MOPS SDS running buffer (Invitrogen, UK). Resolved protein was then transferred to a polybinylidene difluoride (PVDF) membrane and blocked for 2 hours in 5% non-fat milk in PBS with

0.1% Tween-20 (PBST) at room temperature. Primary antibodies were made up in 5% non-fat milk in PBST and incubated overnight at 4°C. The anti- primary antibodies included anti-GTPCH (1:50,000, a generous gift to the laboratory from Professor Steve Gross (Cornell University, New York, USA)), anti-TH (1:20,000, Sigma, UK) and anti-GAPDH (1:20,000, Sigma, UK). Appropriate HRP-conjugated secondary antibodies (Promega, USA) were used at concentrations of 1:5000 (in PBST) and incubated at room temperature for 1 hour. Protein bands were visualised by chemiluminescence (Supersignal, Pierce, USA) and band intensity was quantified using ImageJ (National Institutes of Health, USA).

Membranes were stripped for 30 minutes at 50°C in stripping buffer (6.25mM Tris (pH 6.8), 2% SDS, 100mM β-mercaptoethanol) and blocked in 5% milk in PBST to allow re-probing with an different primary antibody.

5.2.7 Motion analysis in the THiresGCH$^{f/f}$ model

The effect of GCH deletion in the THires mediated knockout model on mobility was established by undertaking automated motion tracking based on an established protocol from the Nuffield Department of Clinical Neurosciences at the University of Oxford [434]. Mice were housed individually in standard ventilated cages (IVCs) and illuminated by an overhead cool white LED light source. A conventional webcam (Logitech) was used to acquire 5 minute videos of THires GCH$^{f/f}$ and littermate controls. All videos were recorded at 3 frames/second and stored in the AVI format. Video files were then analysed in a blinded fashion using ANY-maze 4.5 (Stoelting, Wood Dale, Illinois) to determine the total distance travelled during the acquisition. Raw data was then un-blinded for analysis.

5.2.8 Statistical analysis

Data were analysed using Microsoft Excel (Microsoft, USA), Graphpad Prism (Graphpad Software, USA) and Statplus (AnalystSoft Inc, USA). All data is presented as mean ± standard error of mean. Normally distributed data was analysed by paired t-test, unpaired t-test or Mann-Whitney U test as appropriate for non-normally distributed data. Normality was determined by Shapiro-Wilk normality test. A p value of less than 0.05 was considered significant.

5.3 Results

5.3.1 Generation of the THcre GCH$^{f/f}$ mouse

Figure 5.1 details the breeding strategy used to generate the THcreGCH$^{f/f}$ mouse line. Animals homogeneous for the floxed *Gch1* gene and expressing THcre were viable and demonstrated normal growth (figure 5.1c) from weaning at day 18 to the end of the measurement period (day 45) after which animals were considered suitable for study.

5.3.2 Genotyping animals from generation of THcreGCH$^{f/f}$ animals

Genotyping of animals was performed from tissue from ear snips (Figure 5.2a). This PCR protocol was able to identify expression of cre (upper panel) and all three genotypes generating by the first stage of the breeding protocol or after introduction of wild type animals to prevent accumulation of recessive genes.

In order to confirm excision of the *Gch1* allele, PCR was undertaken in whole adrenal glands as an easily accessible TH-expressing target tissue from knockout animals and littermate controls (Figure 5.2b). A combination PCR reaction with three primers

(GX5128, GCHnew, Primer 5) which was able to identify the floxed and knockout allele in other mouse models such as the Tie2creGCH$^{f/f}$ [325] was only able to identify the floxed DNA (upper panel). A systematic study was undertaken to modify the constituents of the PCR reaction, but was not able to identify the excised fragment. A 2 primer reaction (GCHnew, Primer 5) was able to identify the excised allele and correlated with the presence of Cre identification in the adrenal tissue (middle panel). The presence of THcre was confirmed by a separate PCR reaction.

5.3.3 Comparison of tissue biopterin levels in THcreGCH$^{f/f}$ animals and littermate controls

Determination of biopterin levels in adrenal and stellate ganglia tissue is detailed in figure 5.3. The HPLC detection system required significant optimisation (see Chapter 2) in order to demonstrate the presence of BH4 by electrochemical detection and an example chromatogram of a standard and sample is shown in figure 3a. Confirmation of the BH4 signal from adrenal tissue is detailed in chapter 2.

There was no significant difference in BH4 or total biopterin in whole adrenal (figure 5.3b) from THcreGCH$^{f/f}$ and littermate controls (114±9.28 vs. 122.7±10.75pmol biopterin/mg protein, n=12-14/group; $p>0.05$, unpaired t-test).

In view of genomic confirmation of *Gch1* gene knockout, adrenal microdissection separating medulla from cortex was utilised in order to improve the detection of BH4 in TH positive cells by removing the contribution of BH4 in non-TH cells. These were analysed as pairs of medulla/cortex pooled into one sample. Samples of medullary tissue were enriched for biopterin with near doubling of BH4 and total

biopterins in knockout and control tissue (figure 5.3c). Furthermore, there was a trend towards a reduction in BH4 levels in THcre$^{f/f}$ animals (THcre GCH$^{f/f}$ 176.7±20.6 vs. GCH$^{f/f}$ 229.9±18.7pmol biopterin/mg protein, n=10/group, p=0.0696 unpaired t-test). There was no significant difference in BH4 and biopterin levels from cortical tissue and levels were in similar in range to whole adrenal tissue (figure 5.3d). In order to explore the trend towards a decrease in BH4 levels in tissue with a greater concentration of TH expressing cells, stellate ganglia dissection was undertaken as this tissue is composed almost entirely of cells expressing TH for the generation of catecholamines. Analysis from this tissue is shown in figure 5.3e-f and demonstrates no significant difference in BH4 or total biopterin levels (n=3-8/group) when adjusted per stellate or normalised to protein concentration.

5.3.4 Comparison of plasma catecholamines levels in THcreGCH$^{f/f}$ animals and littermate controls

There was a trend towards a reduction in BH4 levels seen in the adrenal medulla in THcreGCH$^{f/f}$ animals and therefore determination of plasma catecholamines (and metabolites) by HPLC was undertaken to see if this observation was mirrored. No significant differences were seen in plasma noradrenaline and the catecholamine metabolites DOPAC, HIAA and HVA and the results from this analysis are shown in figure 5.4.

5.3.5 Comparison of blood pressure and heart rate in THcreGCH$^{f/f}$ animals and littermate controls

The physiological effect of genomic deletion of *Gch1* in TH expressing cells was determined by measurement of blood pressure and heart rate by non-invasive tail cuff

plethysmography (Figure 5.5). No significant differences were demonstrated between the THcreGCH$^{f/f}$ and control male mice and the data is shown below (n=12/group).

	GCH$^{f/f}$	THcreGCH$^{f/f}$	p value
Blood pressure	110±2 mmHg	113±3 mmHg	0.33
Heart rate	736±6 bpm	743±6 bpm	0.39

5.3.6 Inefficient gene excision by cre-recombinase in THcreGCH$^{f/f}$ animals

Despite apparent genomic deletion of *Gch1*, no significant differences were seen in biochemical or physiological indices. Therefore, in order to dissect this lack of effect, the efficiency of genomic deletion of the floxed *Gch1* allele was assessed by qRT-PCR, in comparison with *Gch1* deletion in a population of cells with known excision of the floxed allele (Figure 5.6). The rationale for these experiments was to determine whether the lack of effect was due to failure of cre mediated deletion of *GCH1,* or due to a lack of cell specific requirement for BH4 in the target tissue.

Interestingly, assessment by qRT-PCR demonstrated a significant reduction in *Gch1* and TH gene expression in THcreGCH$^{f/f}$ (n=6/group). The Tie2creGCH$^{f/f}$ model has been designed to target tissue specific deletion of *Gch1* in endothelial cells [325] but was also found to result in knockout of *Gch1* in bone marrow cells [429]. Therefore M1 macrophages were derived from bone marrow samples in Tie2cre GCH$^{f/f}$ animals and littermate controls and prepared in fixed dilutions as demonstrated in figure 6b. The 2 primer (GCH new+Primer 5) PCR reaction described above was undertaken in this

tissue and in whole adrenal glands from THcreGCH$^{f/f}$ animals and controls. Lung tissue from Tie2creGCH$^{f/f}$ animals was used as a positive control. This experiment provided a qualitative assessment of gene excision efficiency by band intensity and indicated that *Gch1* excision by THcre in this model is in the range of 1-10%.

5.3.7 GTPCH protein expression was not decreased in THcreGCH$^{f/f}$ animals

GTPCH protein levels were determined in whole adrenal gland tissue from knockout and control mice, using a custom made antibody (a generous gift from Dr S Gross, Cornell University, New York)) and the results are shown in figure 5.7. In accordance with the estimation of *Gch1* excision efficiency, qualitative (figure 5.7a) and quantitative (figure 5.7b) analysis demonstrated no significant difference in the levels of GTPCH protein between the two sample cohorts.

5.3.8 Generation of the THiresGCH$^{f/f}$ model

In view of the lack of biochemical and physiological phenotype seen in the above THcreGCH$^{f/f}$ model, due to incomplete excision of the floxed *Gch1* allele, an alternative breeding strategy was undertaken, utilising a THires-cre (THires) driver line, with the aim of improving excision efficiency of the GCH$^{f/f}$ allele. The breeding strategy was the same as the model above.

Strikingly, animals born from the THires x THiresGCH$^{f/f}$ matings were found to be significantly smaller, and failed to thrive (figure 5.8a) requiring elective culling at day 21 in accordance with the severity limit for the experiment. This was despite no gross morphological differences seen at E12.5. Figure 5.8b demonstrates a significant reduction in body weight at day 21 between the two groups (GCH$^{f/f}$ 9.36±0.24g (n=18) vs. THiresGCH$^{f/f}$ 4.77±0.17g (n=11), $p<0.0001$, unpaired t-test). The growth

curves (figure 5.8c) of control and knockout animals show that there was a significant difference in body weight at all time points from day 9 although both groups gained weight up to weaning at day 16-18. After day 16 (post-weaning), THiresGCH$^{f/f}$ animals failed to thrive and lost weight to day 21 at which point they were culled electively. Qualitative assessment of behaviour demonstrated smaller animals with reduced mobility and reduced feeding drive.

5.3.9 TH ires-cre results in effective deletion from central and peripheral TH expressing cells

DNA extraction and genotyping of ear snips and target tissue (adrenal) was performed as detailed above for animals from the THcreGCH$^{f/f}$ cohort. Figure 5.9 demonstrates results from the 3 genotyping primer reaction in tissues from TH expression tissue including adrenal and midbrain samples compared to control tissue in knockout and littermate control animals. This panel demonstrates that the GCH$^{f/f}$ bands (1030bp) are identified in both groups of animals in liver, heart, lung, and whole brain. In contrast, in adrenal and midbrain tissue, a lower intensity GCH$^{f/f}$ band is seen as well as the excised allele in knockout animals.

5.3.10 GTPCH protein expression was decreased in THiresGCH$^{f/f}$ animals

Western immunoblotting was undertaken as above to determine if *Gch1* deletion in this cohort had an effect on the levels of GTPCH protein (figure 5.10). This demonstrated a significant reduction ($p<0.05$, unpaired t-test) in GTPCH protein levels in whole adrenal tissue from knockout animals compared to GCH$^{f/f}$ controls.

5.3.11 Comparison of tissue biopterin levels in THiresGCH$^{f/f}$ animals and littermate controls

Tissue biopterins were determined by HPLC as detailed above in TH expressing tissue (whole adrenal and midbrain) and control tissue (heart, lung and liver) in knockout animals and littermate controls. Total biopterin and BH4 levels were significantly reduced in whole adrenal and midbrain tissue samples from THiresGCH$^{f/f}$ animals compared to littermate controls (figure 5.11) whereas no differences were seen in non cre expressing tissue such as heart, liver, lung in keeping with the tissue specificity of the excision.

5.3.12 Comparison of plasma catecholamine levels in THiresGCH$^{f/f}$ animals and littermate controls

Plasma dopamine was measured by HPLC as described above for detection of plasma catecholamines (figure 5.11f). Plasma dopamine levels were significantly reduced in THiresGCH$^{f/f}$ animals compared to controls ($p<0.01$, Mann-Whitney U-test).

5.3.12 Movement was significantly decreased in THiresGCH$^{f/f}$ animals compared to littermate controls

THiresGCH$^{f/f}$ animals demonstrated a clear qualitative difference with respect to size and movement around day 18. Therefore, systematic assessment of motion in this cohort was undertaken by analysis of individual animals using the Anymaze platform (Stoelting Co, USA). Animals were recorded for 1 minute and video tracking used to determine the distance travelled. Video analysis confirmed the marked decrease in motor function and distance travelled in 1 minute and this is demonstrated in Figure 5.12a-b which displays the path taken by animals during the recording period and a

significant reduction in distance travelled (Figure 5.12c, controls 1.49±0.33m vs. THiresGCH$^{f/f}$ 0.47±0.08m, n=6-8/group, $p<0.001$, unpaired t-test) was seen.

5.4 Discussion

The main findings of this investigation were:

- Knockout of *Gch1* by THcre is modest and results in no significant biochemical or physiological phenotype
- Excision of *Gch1* by THires results in normal embryonic development and viable animals at birth
- THiresGCH$^{f/f}$ animals demonstrate significant reduction in BH4 and biopterins in tissue with TH expressing cells including the midbrain and adrenal gland
- Loss of *Gch1* in TH expressing cells in the central and peripheral nervous system results in failure to thrive and subsequent reduced growth and mobility post D12.5

These data demonstrate the generation of a novel mouse model of sympathetic, TH expressing cell specific *Gch1* deletion to test the cell specific requirements for BH4. While the intention of this study was to generate this model in order to investigate the role of BH4 in cardiac autonomic function at the level of the sympatho-adrenal system, the model generated presents with a marked neurological phenotype which may provide an exciting platform for further investigation. The clinical relevance of this model may be more in keeping with dopa responsive dystonia or *GCH1* mutation related Parkinson's disease or phenylketonuria where a reduction in biopterins and catecholamines is seen.

Effective deletion of *Gch1* in TH expressing cells was attempted in these experiments with 2 different approaches with the aim of cre-recombinase mediated deletion of *Gch1* in TH expressing cells. The first series of experiments utilised cre-recombinase under the control of TH as a promoter against a *Gch1* flanked by LoxP sites. The breeding strategy generated viable animals with evidence of genomic deletion of *Gch1* in adrenal tissue which was chosen as an easily accessible source for analysis of TH expressing cells. However, there was no biochemical evidence of a reduction in BH4 or total biopterins in whole adrenal, adrenal medulla or stellate ganglia and this was reflected in no haemodynamic differences in terms of blood pressure and heart rate. In addition, no differences were seen in GTPCH protein expression in whole adrenal tissue or plasma catecholamines. The lack of biochemical and physiological phenotype in this particular model was investigated further and these data demonstrate the efficacy of *Gch1* by TH cre-recombinase was less than 10%, thereby providing a mechanistic basis for the initial unexpected observations. The THcre model used in this initial breeding program has been applied extensively in the study of cre mediated excision in the central nervous system targeting genes such as Bcl-x [484] and α-synuclein [485], both important in substantia nigra development and function, rather than peripheral TH expressing targets.

Therefore, in order to improve on the efficiency of *Gch1* knockout in TH expressing cells, a further breeding program was undertaken with an alternative cre-recombinase system under the control of TH with an internal ribosome entry site which links expression of cre-recombinase to that of the endogenous gene thereby resulting in restricted expression in the same pattern as the endogenous gene and improves tissue specific targeting [428]. Other potential strategies could have included a tamoxifen

inducible system or the use of more specific promoters directed at cardiac sympathetic nerves.

This strategy led to the generation of a viable model which despite no differences in embryonic development demonstrates a reduction in body weight at birth in THiresGCH$^{f/f}$ animals and they remain significantly smaller during early development and lose weight following weaning. By day 21, the animals with TH-specific *Gch1* deletion have a 50% reduction in body weight, have reduced mobility and were also observed to have lower feeding drive. In accordance with our license, I culled these animals at day 21 due to their failure to thrive and tissue analysis confirmed genomic *Gch1* deletion, decreased GTPCH protein expression in whole adrenal with corresponding significant reductions in BH4 and total biopterins in TH expressing tissue compared to controls. In keeping with the observed effect on BH4 and biopterins, plasma dopamine was also significantly reduced in knockout animals compared to controls. Levels of plasma BH4 were not tested due to the limited yield of plasma from the smaller THiresGCH$^{f/f}$, although this effect will be investigated in future studies. No cardiovascular phenotype assessments were possible due to the model not being able to age to 12 weeks.

Therefore, tissue specific deletion of *Gch1* in TH expressing cells in the central nervous system (midbrain) and peripheral sympatho-adrenal tissue (sympathetic nerves and adrenal gland) leads to a significant reduction in tissue specific biopterin levels and plasma dopamine with a marked neurological phenotype characterised by low body weight and severely restricted mobility. The most appropriate other models for comparison of effects include early studies of global knockout of genes involved

in either catecholamine synthesis (TH knockout) or dopaminergic enzymes (dopamine β-hydroxylase knockout).

Inactivation of both TH alleles was undertaken by Zhou *et al.* [486] to generate a complete TH knockout ($TH^{-/-}$) mouse model. No $TH^{-/-}$ mutants were viable implying the requirement of TH function in utero. Embryonic analysis demonstrated only 25% of embryos viable at E11.5 were $TH^{-/-}$, reducing to 5% by E15.5, and of all animals born, 2.6% were $TH^{-/-}$. Histological examination of $TH^{-/-}$ embryos demonstrated dilated atria, hepatic and vascular congestion and bradycardia, indicating the critical role of catecholamines in embryonic cardiac development and function. This severe phenotype was rescued with continuous maternal supplementation of L-DOPA from E8.5 of pregnancy with all $TH^{-/-}$ viable at birth. The naturally born and rescued $TH^{-/-}$ animals were severely runted, had defective motor function and died within 5 weeks. The dopamine β-hydroxylase (DBH) enzyme is critical in the generation of norepinephrine and epinephrine and therefore Thomas *et al.* [487] generated a DBH knockout ($DBH^{-/-}$) model to determine the role of these neurotransmitters independent of dopamine in embryonic development. Once again, genotypes of animals born suggested most $DBH^{-/-}$ embryos died in utero and only 12% survived to term, compared with 2.6% with the $TH^{-/-}$ line. Interestingly, viable animals at birth were not grossly different from controls, but 40% died within 48h of birth and a further 20% died between the third and fifth post-natal weeks. The weaning period and growth phase in surviving animals was also delayed and knockout animals reached approximately 80% of the body weight of controls. This model could be rescued in a dose dependent manner by dihydroxyphenylserine (DOPS), which can be converted to noradrenaline but not dopamine.

Therefore deletion of *Gch1* in TH expressing cells results in a phenotype with similarities to both these models, likely reflecting the reduction in dopamine and catecholamines during development and the post-natal phase. Gross embryonic development appears normal with TH expressing cell specific *Gch1* knockout and genotypes of animals born fit normal mendellian inheritance patterns. However, THiresGCH$^{f/f}$ animals at birth have decreased body weight, impaired weight gain and display weight loss after weaning. These observations indicate effects on feeding drive, which is regulated by the production of dopamine [488]. Furthermore, THiresGCH$^{f/f}$ animals demonstrated significant reduction in motor activity as observed albeit with a more marked phenotype than in the TH$^{-/-}$ cohort. The lack of weight gain, failure to thrive and depressed motor function in our model of cell specific *Gch1* deletion necessitated elective culling of animals by day 21 (in keeping with experimental license restrictions), an observation similar to that seen in the DBH$^{-/-}$ cohort where 60% of animals had died by the 5th post-natal week.

Role of BH4 in neurological disease

The aim of the experimental study was to study the cardiovascular and cardiac autonomic effects of TH expressing cell specific *Gch1* deletion. However, given the severity of neurological phenotype observed, these hypotheses could not be tested. Further work with this model may focus on mechanisms of biochemical rescue with a view of the study of cardiovascular parameters, and also the potential study of the role of BH4 in the regulation of central dopaminergic function, particularly in the clinical context of dopa-responsive dystonia (DRD) or Parkinson's disease. Phenotypic rescue may include maternal supplementation of BH4 or dopamine, followed by

supplementation of THiresGCH$^{f/f}$ animals post weaning. Patients with DRD can respond well to regular L-DOPA treatment and this may indicate a potential therapeutic strategy in this experimental model. In addition, biochemical rescue to adult age would allow study of THiresGCH$^{f/f}$ stellate ganglia to determine peripheral *Gch1* excision, biopterin levels and effects on cardiovascular parameters.

Recent work from Mencacci *et al.* [489] used exome re-sequencing to demonstrate loss of function variants in the *GCH1* gene are a major cause of DOPA-responsive dystonia but are enriched in patients' relatives with adult-onset parkinsonism. In addition, this study identified *GCH1* variants in patients with Parkinson's disease (PD) compared with control subjects. The variants discovered in this study increased the risk of PD by 7.5 fold and the authors put forward a number of mechanisms for the significant role of these loss of function variants in the aetiology of PD. These include increased nigral degeneration due to loss of anti-apoptotic signalling via dopamine receptors and low striatal dopamine levels leading to lower threshold for nigral cell loss to result in clinical parkinsonism. A number of patients with PD also develop multi-system atrophy (MSA) and this is associated with autonomic failure including postural hypotension, dry mouth, urinary incontinence, constipation and vocal cord dysfunction [490]. The pleiotropic role of BH4 in cellular function includes its cofactor role for NOS, amino acid hydroxylases, tyrosine hydroxylase and as an anti-oxidant and its role in catecholamine synthesis may link the motor and non-motor aspects of PD. The observations from this study are supported by other data including identification of a SNP at the *GCH1* locus that is associated with PD [491] and Parkinson's associated protein α-synuclein modulates *GCH1* activity and cellular BH4 levels [432].

Therefore these recent data suggest a link between BH4 bioavailability, regulation of amino acid hydroxylases, neuroinflammation and oxidative stress in PD. The THiresGCH$^{f/f}$ model may allow further exploration of these mechanistic pathways as it points towards a cell specific role for BH4 and its loss leads to a marked neuro-developmental phenotype. Clinically, BH4 supplementation had no immediate therapeutic benefits in small studies of PD [492, 493] but this model may allow exploration of disease modifying genes and novel therapeutic targets. Furthermore, this model may be amenable to neurological biochemical rescue and ageing with either sepiapterin or dopamine supplementation, and therefore would allow exploration of the cardiovascular effects of *Gch1* knockout at the level of the sympathetic nervous system. A rescue model may also allow determination of specific effects on mobility using alternative tests such as balance and grip which could not be demonstrated in the current knockout model.

In summary, these data are the first demonstration of selective reduction of TH expressing cell BH4 synthesis by targeted *Gch1* deletion, results in a significant neuro-motor phenotype supported by the observed reduction in plasma dopamine. This model has similarities to global TH and DBH knockout models and may be amenable to biochemical rescue, allowing study of cardiac autonomic function in this context. Interestingly, this model provides further mechanistic evidence supporting the role of *GCH1* variants that have been shown to be associated with PD.

Chapter 5 Figures

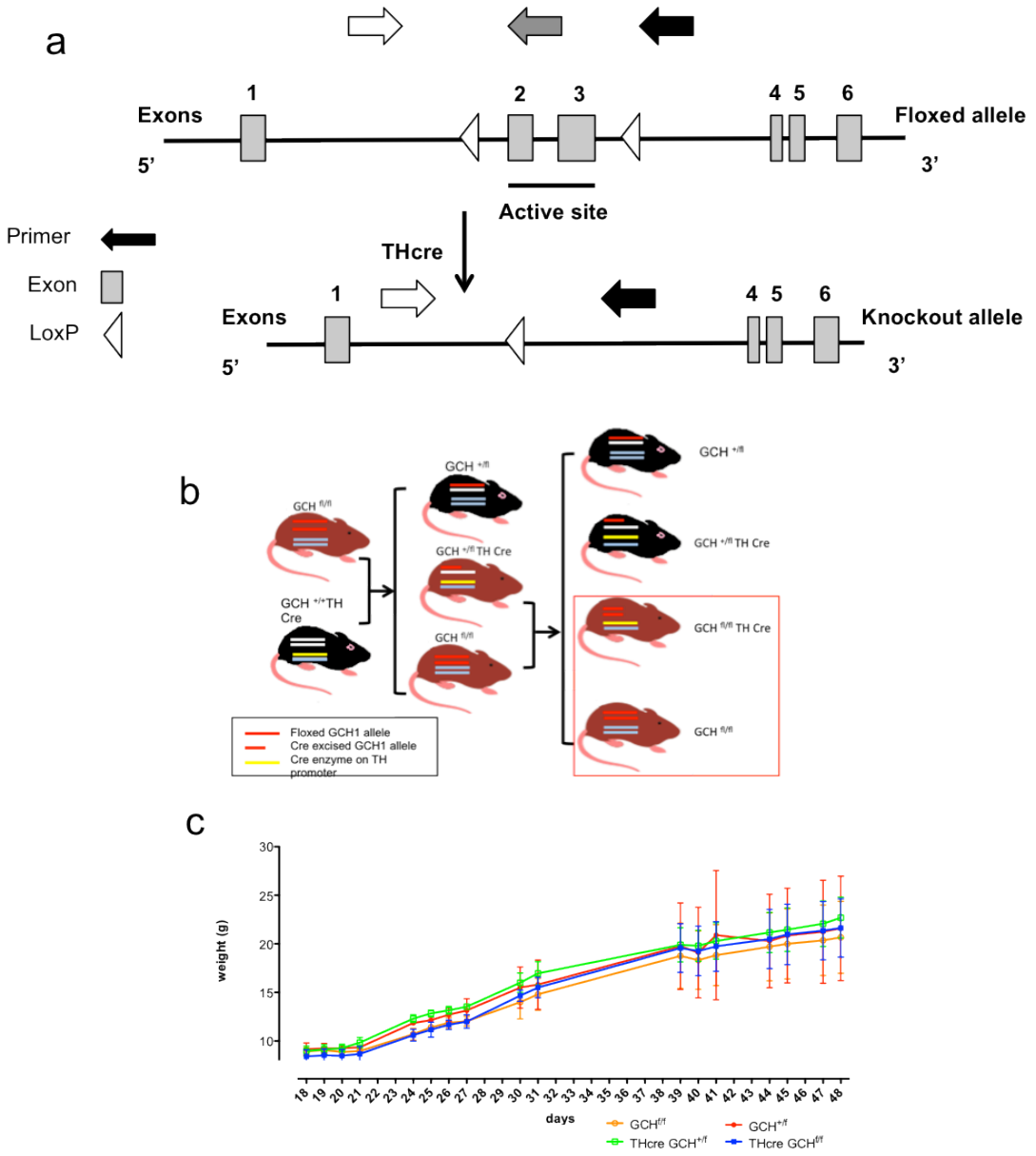


Figure 5.1 Generation and breeding of the THcreGCH$^{f/f}$ mouse

(a) Schematic showing the targeting of the mouse *GCH1* locus with loxP sites flanking the exons (2 and 3) encoding the active site of the GTP cyclohydrolase I (GTPCH) protein. Arrows show polymerase chain reaction primers for the *GCH1* floxed and THcre-excised allele, *GCH1* floxed allele (white and grey arrows), and deleted allele (white and black arrows). (b) Schematic of breeding strategy and crosses undertaken to generate knockout animals (THcre GCH$^{f/f}$) and littermate controls (GCH$^{f/f}$). (c) Growth curve of all 4 genotypes generated (n=4/group) demonstrating no variation in growth from weaning at day 18 to day 48.

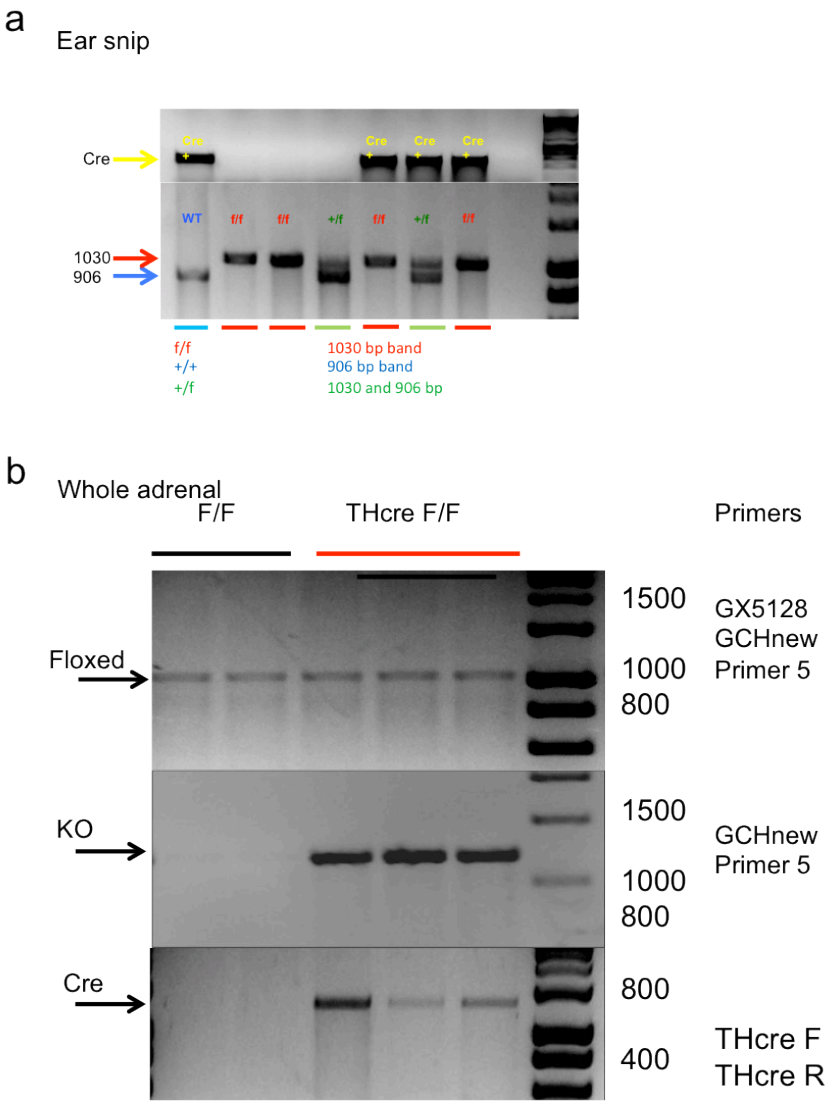


Figure 5.2 Confirmation of genotype in ear snip and target tissue

(a) PCR of ear snip tissue identifying all three genotypes generated by the breeding strategy. (b) Multiple PCR reactions undertaken in order to confirm genomic deletion of the GCH gene in whole adrenal gland in which TH expressing cells in the medulla are the target. The multiplex reaction (3 primer) is unable to identify the knockout allele although this is clearly identified by the 2 primer reaction. The lower panel identifies cre expression with corresponding generation of the knockout allele (middle panel).

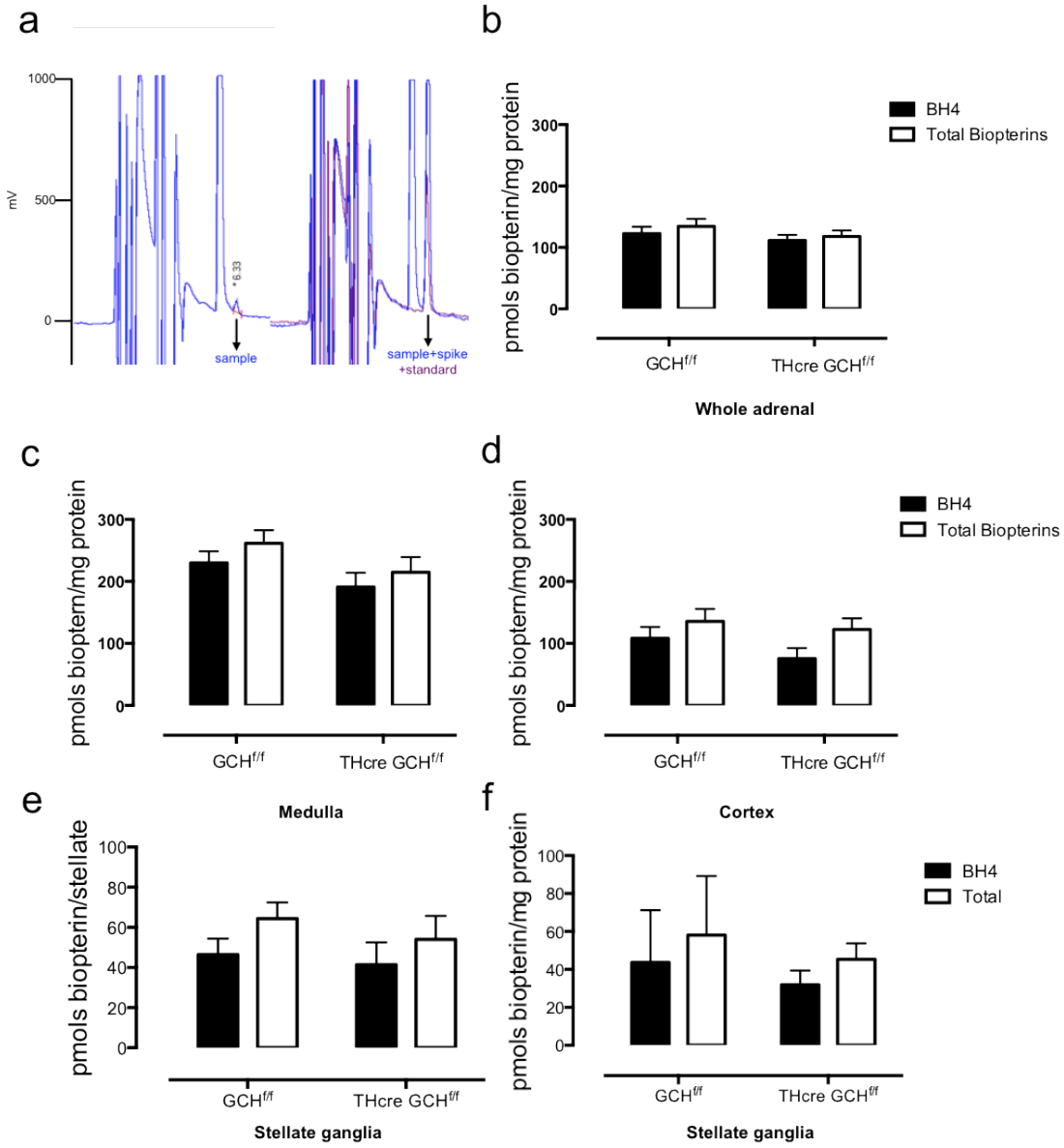


Figure 5.3 Comparison of tissue biopterin levels in THcreGCH$^{f/f}$ animals and littermate controls

(a) Actual experimental chromatogram of sample run through electrochemical detection. BH4 elution in sample (blue) followed a large unknown peak, and was confirmed by running same sample with added biopterin standard which corresponded to elution of standard (purple) alone (b) HPLC of knockout tissue and littermate controls demonstrating no significant reduction in BH4 and total biopterins in whole adrenal glands. (c) Enrichment of sample with adrenal microdissection resulted in increased BH4 and biopterins in the medullary sample compared to (d) cortical samples, although no significant reduction was seen. (e/f) No difference in BH4 or biopterins was seen in stellate ganglia tissue either by pairs of stellate ganglia or normalised to protein concentration

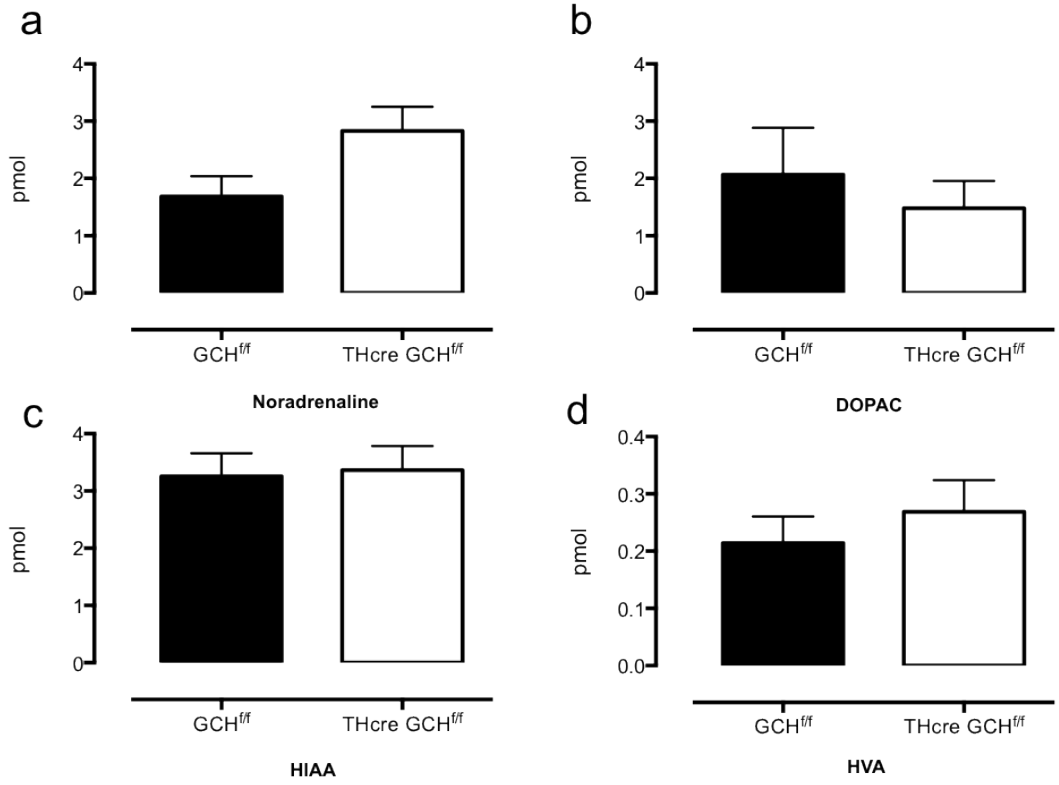


Figure 5.4 Comparison of plasma catecholamines levels in THcreGCH$^{f/f}$ animals and littermate controls

No significant reduction in catecholamines or metabolites were seen in plasma from knockout animals compared to littermate controls

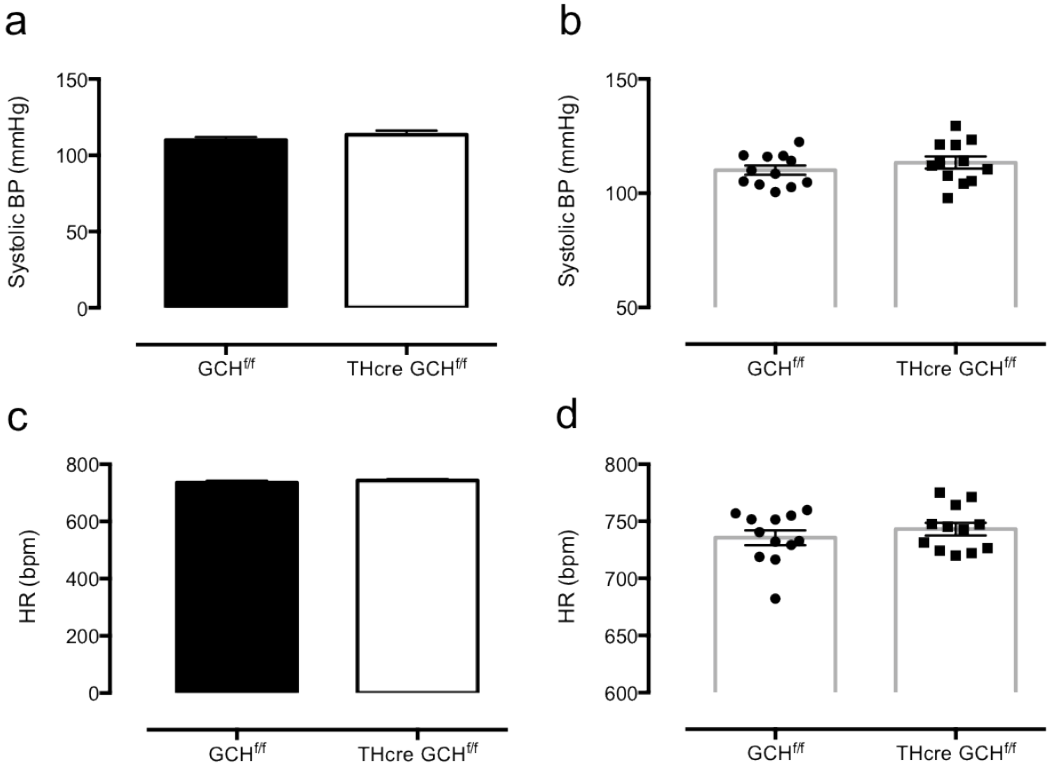


Figure 5.5 Non-invasive tail cuff plethysmography blood pressure and heart rate assessment in THcreGCH$^{f/f}$ animals and littermate controls

Blood pressure assessment in age matched male cohorts of knockout and littermate controls demonstrated no significant difference in (a/b) systolic blood pressure or (c/d) heart rate (grouped mean data and individual data points shown)

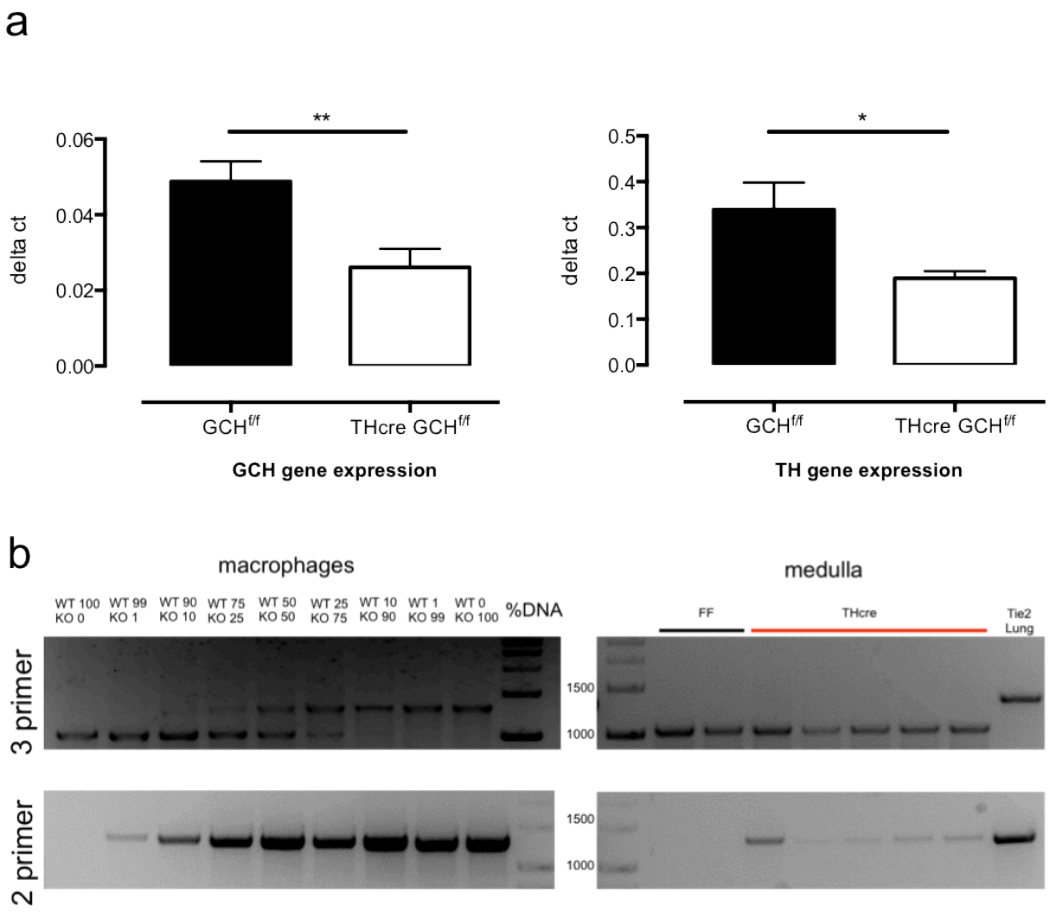


Figure 5.6 Assessment of efficiency of gene excision by qRT-PCR and PCR in THcreGCH$^{f/f}$ animals

(a) qRT-PCR demonstrated a significant reduction in GCH1 and TH gene expression however (*p<0..05, **p<0.01, unpaired t-test) (b) comparison of knockout allele band intensity with proportional samples of wild type/knockout macrophages indicated that excision efficiency was in the region of 1-10% whereas Tie2cre lung demonstrated significant excision by band intensity.

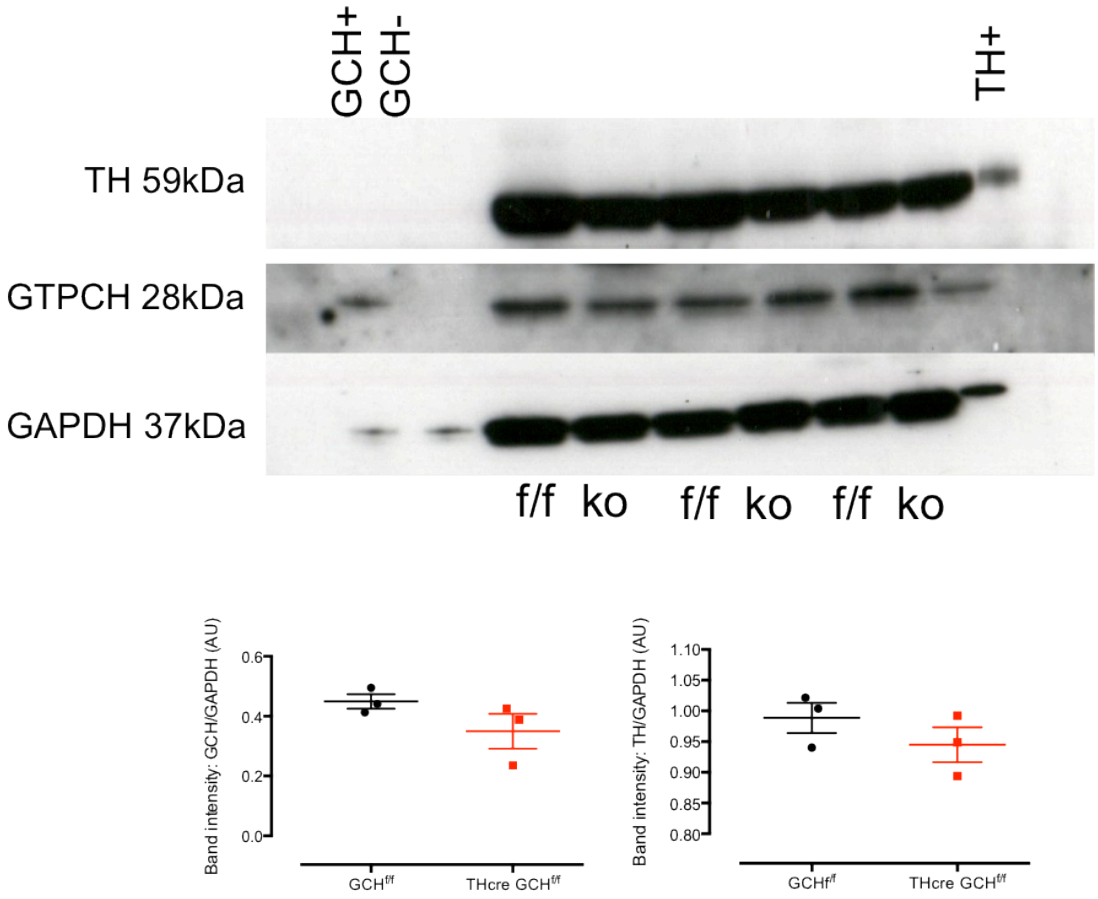


Figure 5.7 GTPCH protein was not decreased in whole adrenal from THcreGCH$^{f/f}$ animals compared to littermate controls

No difference was seen in GTPCH expression in whole adrenal for THcre GCH$^{f/f}$ animals and littermate controls. Control samples for GTPCH (lung tissue from GCH$^{f/f}$ (positive control) and Tie2creGCH$^{f/f}$ (negative control) and TH (Human BE(2)-M17 neuroblastoma cell line) are shown in lanes 1,2 and 9.

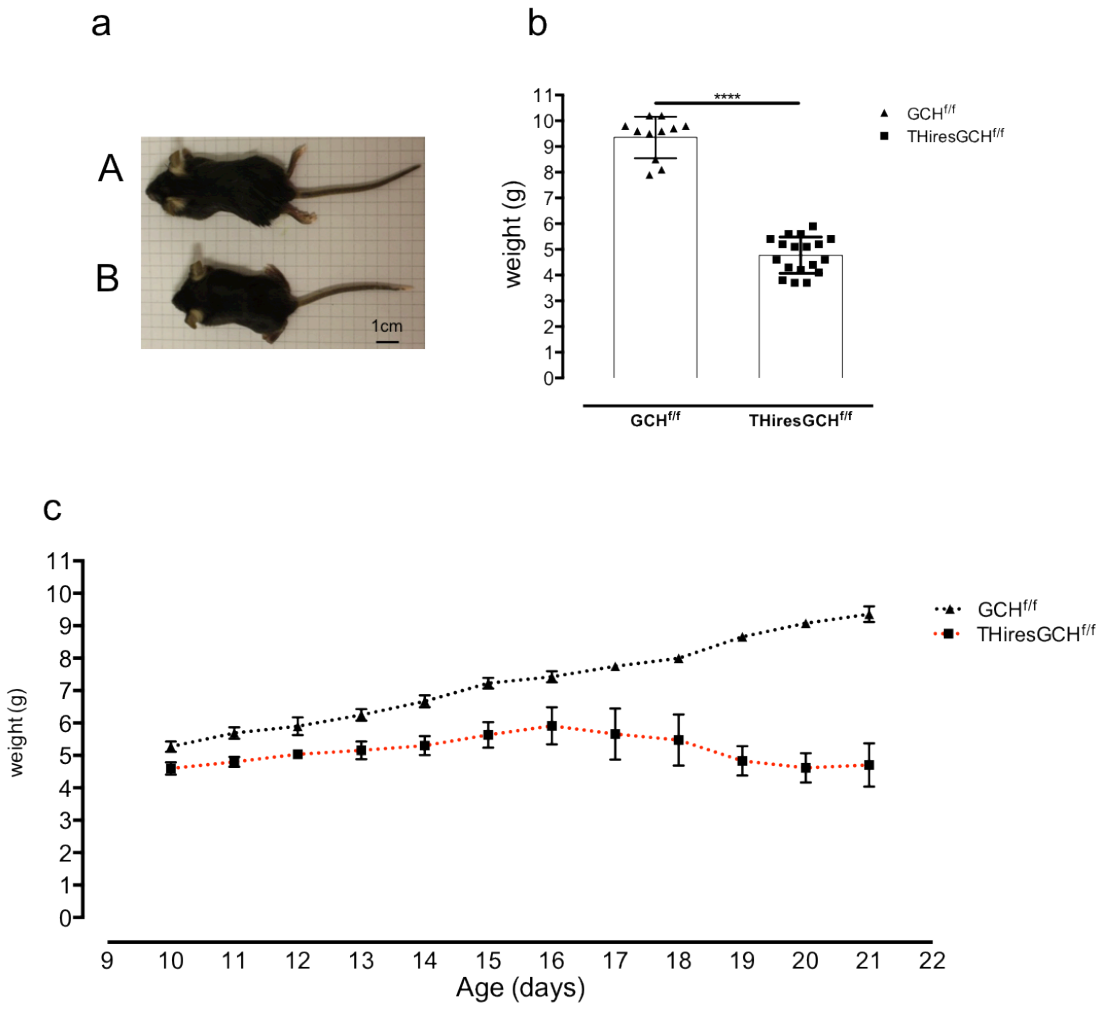


Figure 5.8 Generation of the THiresGCH$^{f/f}$ mouse

(a) An identical breeding program lead to the generation of THiresGCH$^{f/f}$ and littermate controls (GCH$^{f/f}$) with knockout animals visually smaller than their WT littermates at Day 21 but no gross morphological differences were noted at embryonic day 12.5. (b) A significant reduction in body weight was seen at Day 21 (****p<0.0001, unpaired t-test, n=11-18/group) and (c) body weight was lower at all time points between days 9-21, although both groups gained weight pre weaning (to day 16) after which THiresGCH$^{f/f}$ began to lose weight until culled at day 21.

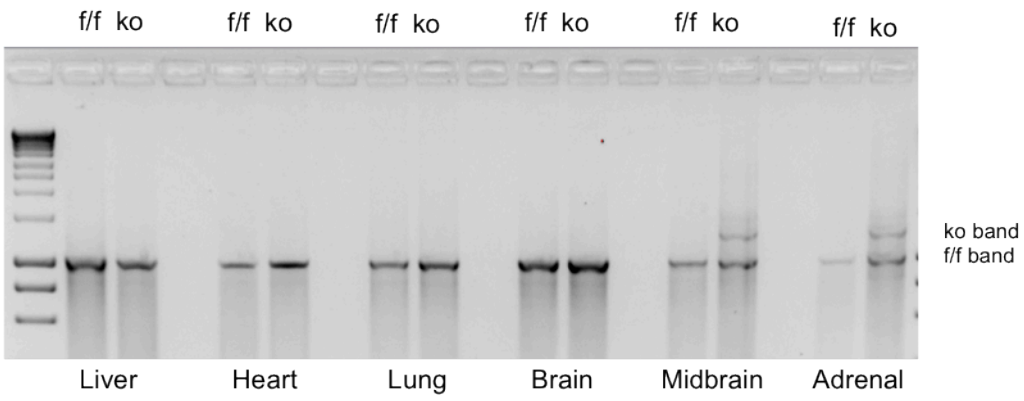


Figure 5.9 Genomic deletion of GCH1 in target tissues from THiresGCH$^{f/f}$ animals

3 primer reaction in target tissue (midbrain, adrenal) and non-TH expressing organs (liver, heart, lung, whole brain) confirming genomic deletion of GCH1 by THires.

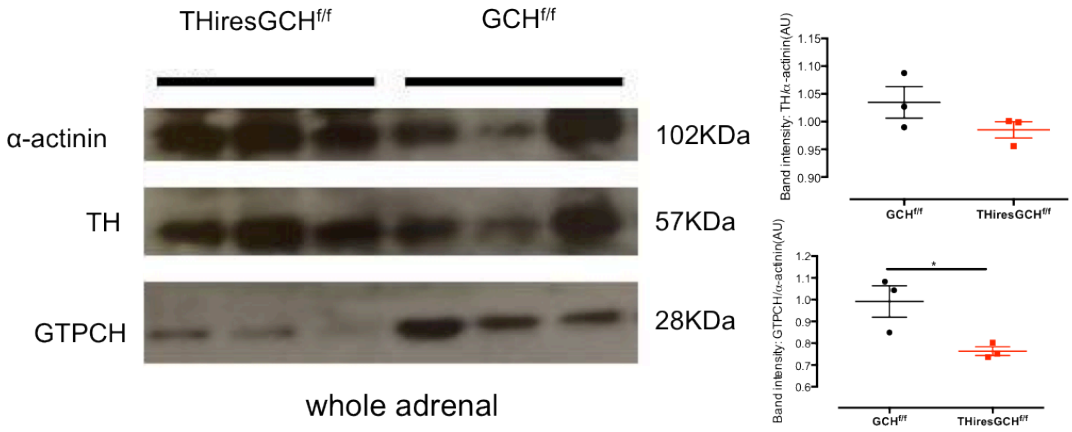


Figure 5.10 Decreased GTPCH protein expression in THiresGCH$^{f/f}$ animals

Expression of THires in whole adrenal glands results in a significant decrease in GTPCH protein expression in whole adrenal glands (*p<0.05, unpaired t-test)

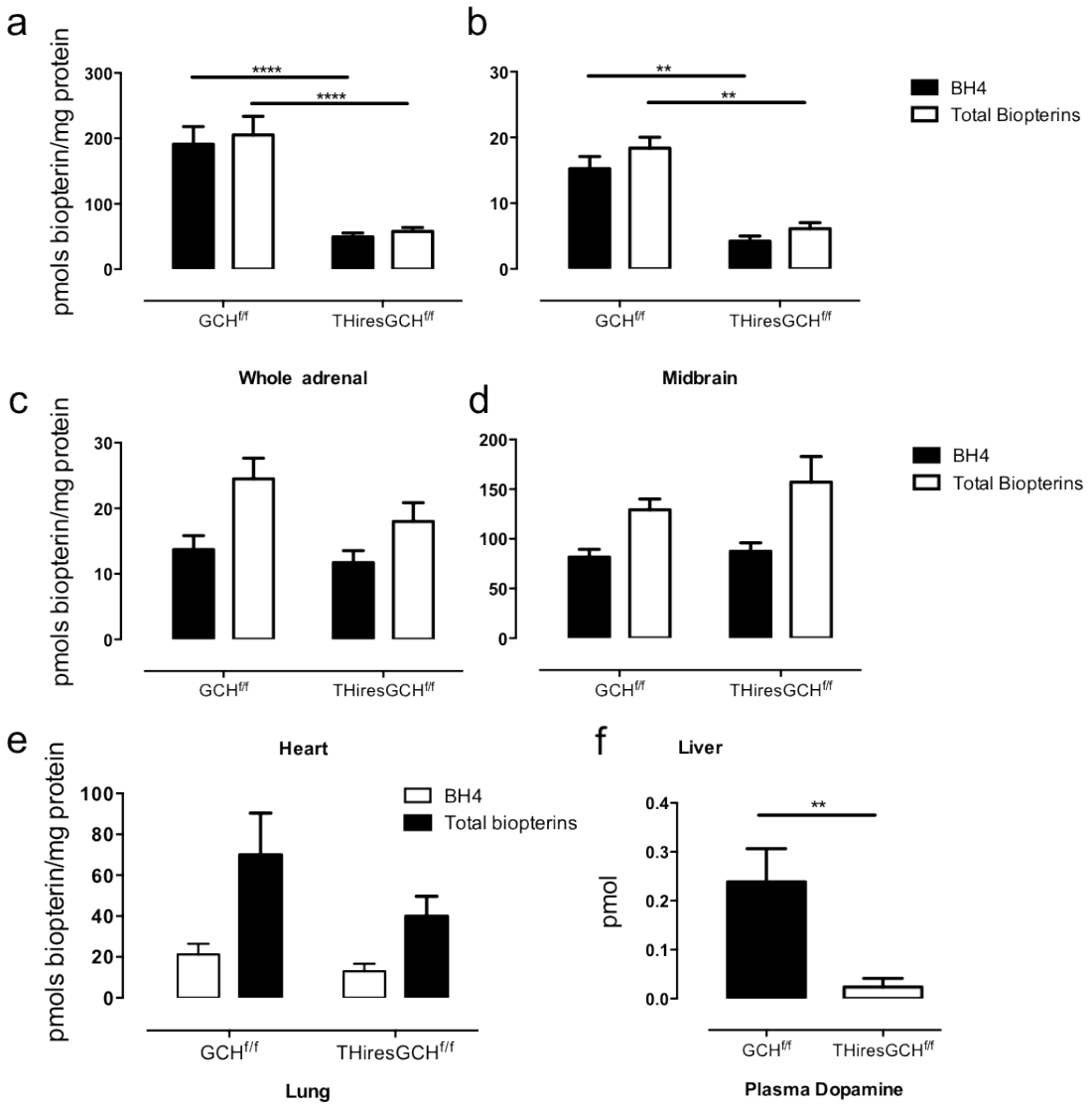


Figure 5.11 Comparison of tissue biopterin and plasma dopamine levels in THiresGCH$^{f/f}$ animals and littermate controls

HPLC of TH expressing tissue demonstrating a significant reduction in BH4 and total biopterins in (a) whole adrenal (n=10-11/group, ****p<0.0001, Mann-Whitney U test) and (b) midbrain (n=5-6/group, p<0.001, Mann-Whitney U-test) with no significant reduction was seen in non TH expressing tissue such as (c) heart, (d) liver and (e) lung. (f) HPLC of plasma demonstrated a significant reduction in dopamine levels (n=6-7/group, p<0.01, Mann-Whitney U-test)

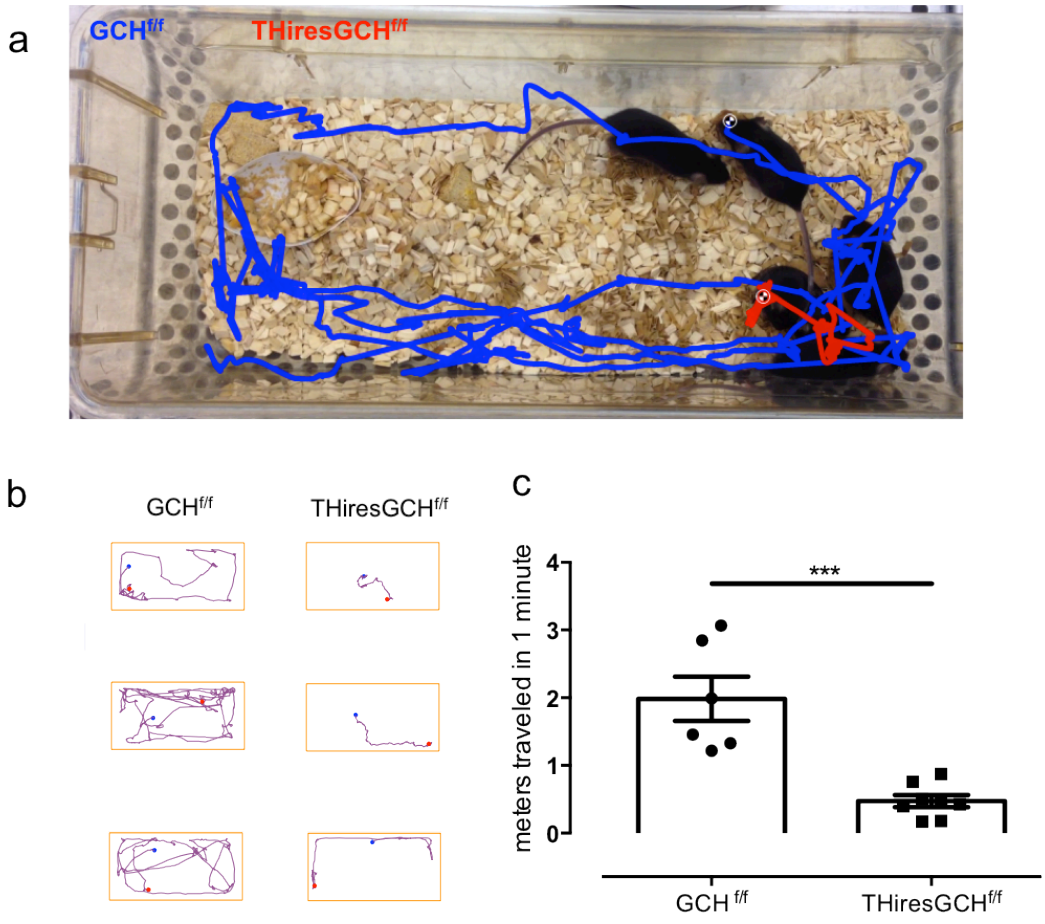


Figure 5.12 Comparison of movement by motion tracking of THiresGCH$^{f/f}$ animals and littermate controls

(a) Raw data of qualitative experimental analysis of a 30sec video sequence of one THiresGCH$^{f/f}$ animal (red) and one littermate control (blue) demonstrating a clear reduction in the distance travelled within the cage. (b) Experimental traces from quantitative analysis (Anymaze platform) of individual THiresGCH$^{f/f}$ mice and littermate controls demonstrating a reduction in the distance travelled in 1 minute. (c) Grouped data demonstrating a significant reduction in distance travelled by THiresGCH$^{f/f}$ animals (***$p<0.001$, unpaired t-test, n=6-8/group)

Chapter 6 Concluding discussion

The work in this thesis focused on investigating the mechanisms involved in the autonomic influence on arrhythmogenesis. The relevance of these studies is highlighted by existing evidence that cardiac autonomic dysregulation is a central theme in the development and progression of most cardiovascular disorders. These include hypertension, heart failure and myocardial infarction [12]. Sympatho-vagal imbalance is a negative prognostic indicator for morbidity and mortality [15, 16] due to arrhythmia and sudden death. This has lead to the development of interventional neuro-axial modulation techniques and further focus on the scientific basis of these observations [469, 494]. A detailed mechanistic understanding may act to improve outcomes from current strategies such as vagal nerve stimulation and renal sympathetic denervation, which to date have both reported no significant improvement in clinical trials [49, 50]. Furthermore, scientific enquiry may allow lower cost, innovative therapies to be developed to improve patient outcomes on a wider scale [12].

The autonomic nervous system consists of an elegant system of interacting feedback loops that can be envisaged as a multi-level system [47, 463]. This maintains physiological stability with respect to rhythm and contractile function.

This thesis focused on the neuron-myocyte interface in order to add to the mechanistic understanding and contribute to evidence that underpins the paradigm shift seen with neur-axial therapies. Furthermore, this interface is more therapeutically accessible pharmacologically and interventionally than higher levels of the system.

The studies in this thesis investigated the mechanistic basis of the anti-fibrillatory action of cholinergic signalling, dissected the pro-arrhythmic action of sympathetic co-transmission and finally, attempted to determine the role of tetrahydrobiopterin in autonomic cardiovascular control. The experimental approach encompassed multiple spatial domains including myocyte monolayers, Langendorff perfused whole hearts with and without autonomic innervation, and the generation of tissue-specific gene knockout mouse models. A wide range of molecular, physiological and imaging techniques were utilised to target the aims and objectives listed in Chapter 1 and this concluding discussion summarises the main findings of this thesis, places them in a physiological and clinical context and discusses avenues for further research.

6.1 Key findings from this thesis

Chapter 3

1. In the isolated rat heart, the acetylcholine analogue carbamylcholine raises ventricular fibrillation threshold and flattens the electrical restitution curve.
2. The anti-fibrillatory action of carbamylcholine was dependent upon stimulation of nicotinic receptors and the generation of NO from neuronal NOS. This was mimicked by the NO donor sodium nitroprusside.
3. The anti-fibrillatory action of both carbamylcholine and sodium nitroprusside was ultimately dependent on muscarinic receptor stimulation, since all effects were blocked by atropine.

Chapter 4

4. High level sympathetic nerve stimulation remains pro-arrhythmic and decreases ventricular fibrillation threshold despite effective β-blockade in the isolated rat heart with intact sympathetic innervation.

5. The Y_1 receptor is expressed on ventricular myocytes and neuropeptide Y exerts a Y_1 receptor dependent, pro-arrhythmic effect in the isolated rat heart and ventricular myocyte monolayers.
6. High level sympathetic stimulation results in increased NPY levels in the coronary effluent of the isolated rat heart.
7. NPY increases the incidence of significant ventricular arrhythmias in the setting of ischaemia-reperfusion.
8. A combination of β-blockade and Y_1 receptor blockade can abolish the pro-arrhythmic effect of high level sympathetic stimulation.

Chapter 5

9. Knockout of *Gch1* by THcre is modest and results in no significant biochemical or physiological phenotype.
10. Excision of *Gch1* by THires results in normal embryonic development and viable animals at birth.
11. These animals demonstrate significant reductions in BH4 and biopterins in tissue with TH expressing cells, including the midbrain and adrenal gland.
12. Loss of *Gch1* in TH expressing cells in the central and peripheral nervous system results in failure to thrive and subsequent reduced growth and mobility post D12.5.

6.2 The cholinergic autonomic modulation of ventricular arrhythmia

The data from chapter 3 provided further confirmatory evidence with respect to the anti-fibrillatory effect of cholinergic signaling on the ventricle. A series of seminal, historic experimental studies [58-60, 65] demonstrated the efficacy of direct vagal nerve stimulation in preventing VF in the presence or absence of structural heart disease.

While some models required the presence of background adrenergic tone for this effect to be seen, the attenuation of the anti-fibrillatory effect of VNS by atropine (muscarinic receptor antagonist) was universal [59, 61, 66]. This observation was supported by more recent data in the setting of central optogenetic central vagal control [495] and ischaemia-reperfusion [448] where once again, atropine was able to abolish the physiological effects of VNS. Furthermore, in the post-MI setting, patients treated with muscarinic agonists or acetylcholine esterase inhibitors demonstrated reduced ventricular arrhythmia [111].

This established physiological cascade was recently challenged by the work of Ng and colleagues utilising a Langendorff-perfused rabbit heart model with intact vagus nerve bilaterally. They were able to demonstrate a direct effect on ventricular electrophysiology independent of heart rate with an increase in ventricular ERP and flattening of the restitution curve [94, 139]. The key finding which challenged the current evidence base was that the anti-fibrillatory effect of VNS was maintained in the presence of atropine. This was due to the paracrine effect of nNOS-derived NO [100], attributed to a potential nitrergic, parasympathetic innervation of the ventricular myocardium.

I aimed to reassess this mechanistic cascade in an isolated, Langendorff perfused, rat heart model. Pharmacological rather than direct cholinergic stimulation was used to generate an equivalent bradycardia to direct VNS. Pharmacological inhibitors of second messenger systems were also used to probe the signaling pathways involved. I was able to demonstrate that carbamylcholine (CCh) increased ventricular fibrillation threshold (VFT) independently of heart rate and released nNOS-derived NO. The

anti-fibrillatory effect was also dependent upon nicotinic and muscarinic receptor and soluble guanylyl cyclase stimulation. Whist this supports the observations of Brack [100] that the generation of NO by cholinergic stimulation is a critical component of the anti-fibrillatory effect, the site of action differs in my data suggesting an autocrine effect with potentiation of cholinergic neurotransmission. The observation that the rise in VFT with the NO donor sodium nitroprusside was prevented by atropine also supports this cascade.

It is important to discuss potential experimental confounders in both models that may have influenced these divergent observations. There are variations in parasympathetic innervation amongst mammalian species [67], which may influence the temporo-spatial influence of VNS. However, muscarinic dependency of vagal physiology has been shown in a variety of species [67]. While CCh perfusion will not mimic the local release of ACh from efferent post-ganglionic fibres, direct VNS effects may also be confounded by NO release from sensory afferents which may constitute up to 70% of fibres in the cardiac vagus [445]. Coote [67] refers to targeting the rostral part of the vagus nearer the nodose ganglion to target the cardiac vagus. This anatomical approach will isolate VNS from collateral stimulation of sympathetic nerves, without obviating the responses from sensory afferents. Nevertheless, the role of sensory afferent in the clinical application of VNS as a potential source of nNOS derived NO [446] may need to be considered for study in a more integrated model. This is in keeping with the Armour and Ardell view of integrated rather than isolated neuro-cardiology [47, 463]. The integrated heart-brainstem-vagus nerve model of Paton [496] may provide a suitable model for study in this context. The critical role of pre-synaptic nNOS was determined by ganglionic blockade in both experiments, however hexamethonium has

been shown to cross react with the muscarinic receptor [447], a property not shared by mecamylamine.

Experiments from both studies add to the evidence base that nNOS-derived NO is a key molecular player in the anti-fibrillatory effect of vagal signaling and provides a foundation for the discussion of avenues for further study. While these data demonstrated the temporal relationship between CCh perfusion and NO release by the measurement of NO metabolites (NOx), it would be interesting to ascertain the mechanism of NO action. While the anti-fibrillatory effect of CCh could be abolished by inhibition of sGC by ODQ, there is considerable data supporting s-nitrosylation of ion channels being a critical mechanism of NO-dependent modulation [208, 210, 221, 225]. Mass spectrometry based techniques in CCh stimulated versus control ventricular tissue may be able to dissect the relative contributions of these mechanisms at the level of the myocyte.

The initiation of ventricular arrhythmia *in vivo* is closely coupled to changes in calcium dynamics [449, 450, 453] leading to early/delayed afterdepolarisations. The next step in imaging in my experimental series would be to undertake multi-parametric voltage and calcium imaging with CCh perfusion during pacing at fixed cycle lengths to identify voltage/calcium alternans and during S1-S2 pacing for restitution analysis. In the long term, application of these imaging technologies in disease models would allow investigation of the electrophysiological effects of cholinergic signaling in this context.

A further avenue for research using the techniques in these experiments would be to investigate the role of the nNOS adaptor protein, NOS1AP (also known as CAPON) in influencing cardiac electrophysiology. Genome wide association studies in several populations have identified single nucleotide polymorphisms that are associated with changes in the QT interval and sudden cardiac death [497, 498]. NOS1AP was first identified in rat brain neurons [499] and has also been shown to be present in cardiac myocytes [500] and a variety or peripheral neural tissue [501, 502]. The electrophysiological role of NOS1AP was explored by Chang *et al.* [500] by overexpression of NOS1AP in guinea pig ventricular myocytes. This resulted in inhibition of I_{CaL} and an increase in I_{Kr} resulting in shortening of the action potential. NOS1AP has also been shown to reside in sympathetic neurons [503], co-localise with cardiomyocyte L-type Ca^{2+} channels and K^+ channels [504] and localise to gap junctions [505]. These data, along with the observation than NOS1AP may have a role in stabilizing nNOS and activating nNOS-derived NO signaling cascades [500], suggests that a potential role for NOS1AP in arrhythmogenesis is plausible. I undertook preliminary experiments using an adenovirus with a CMV promotor to increase NOS1AP expression in ventricular myocytes as previously described with nNOS gene transfer [207, 252, 356]. Percutaneous ventricular injections were carried out and subsequent determination of VFT did not demonstrate any differences between control and virus treated groups, including with background adrenergic stimulation. This lack of effect was due to a lack of virus expression and NOS1AP upregulation as confirmed on western blotting. Therefore, this study warrants further optimisation with modification of the virus with either an adenovirus associated virus or lentiviral platform with myocyte or neuronal specific promotors to target NOS1AP or nNOS upregulation. This would allow utilisation of

the techniques in this thesis for electrophysiological phenotyping and assessment if a direct anti-fibrillatory effect is conferred.

The clinical relevance of these data relates to the absence of alternatives to β adrenergic receptor blockade for the pharmacological reduction of ventricular arrhythmia and sudden death risk. Vagal nerve stimulators have moved quickly from bench to bedside [48, 506] but the randomised controlled trials to date [49, 50] have not yielded positive heart failure end-points. The long term effects on arrhythmia risk still remain to be seen. However, these devices require surgical implantation and are not without risk. Therefore a pharmacological strategy of augmenting cholinergic stimulation in the setting of arrhythmia storm may warrant investigation. Furthermore, gene transfer technological has reached the clinical domain [507], but whether this approach could be applied to nNOS transfer to cardiac cholinergic ganglia to provide a direct anti-fibrillatory action on the ventricle remains to be established.

6.3 Sympathetic co-transmission and the pro-arrhythmic effect of sympathetic stimulation

The data from Chapter 4 identified neuropeptide Y (NPY) as a novel, direct, pro-arrhythmic molecule using a multi-domain experimental approach. The aim of this series of experiments was to determine the potential mechanisms underlying the residual arrhythmia risk in patients treated with β-blockers, and if the sympathetic co-transmitter NPY was able to modulate VFT.

Sympathetic hyperactivity is a hallmark of cardiovascular disease and in the setting of myocardial ischaemia or heart failure can increase the risk of ventricular arrhythmia

[396, 464, 467]. Historic and more contemporary studies in acute coronary syndromes have demonstrated that NPY levels are elevated post-MI and correlate with infarct size, severity of heart failure and 1-year mortality [294-296, 508]. *In vitro* studies of NPY application to isolated rat myocytes increased calcium transients and contractility via a Y_1 receptor based pathway [308]. The combination of sympathetic co-transmission and effects on calcium handling, both associated with ventricular arrhythmia, led me to consider NPY a viable candidate molecule for further investigation.

These data demonstrate that NPY is an independent, direct pro-arrhythmic trigger in a variety of experimental models including ventricular myocyte monolayers, isolated rat heart and innervated rat heart models. The pro-arrhythmic action of NPY in all experimental domains could be abolished by the Y_1 receptor antagonist BIBO3304.

In order to study the effect of NPY in a clinically relevant model, we developed an isolated rat heart preparation with intact right and left stellate ganglia and sympathetic nerves. Direct sympathetic stimulation resulted in increased heart rate and contractility and interestingly, lowered VFT despite metoprolol at a dose that blocked the pro-arrhythmic effect of perfused noradrenaline. This residual pro-arrhythmic effect could be abolished by co-perfusion of metoprolol and BIBO3304, providing pharmacological evidence to support the fibrillatory influence of NPY. Direct stellate ganglia stimulation also increased the NPY levels in the coronary effluent in keeping with the observation above.

Clinical studies have demonstrated that plasma NPY levels increase in the context of acute coronary syndromes [296], and the post-infarct period can be complicated by

ventricular arrhythmia. Experimentally this association can be studied by ischaemia-reperfusion, and I was able to demonstrate that perfusion of NPY significantly increased ventricular arrhythmia compared to control.

These data provide a basis for on going experimental and potential clinical study in order to further elucidate the pathways involved in NPY-Y_1 receptor mediated arrhythmogenesis and subsequent clinical and therapeutic implications. The natural progression would be to investigate the effect of NPY by optical mapping of voltage and calcium to determine the temporo-spatial relationship of these parameters during NPY perfusion. The effects on calcium noted by previous studies and these data showing an increase in contractility indicate the probable role of changes in calcium dynamics in mediating this effect. This imaging modality would also be appropriate for the study of stellate ganglia stimulation in the presence of β-blockade with and without Y_1 receptor inhibition. Undertaking this approach in a post-infarct or coronary ligation model may also yield clinically relevant data.

There is no literature detailing the downstream signalling cascades following Y_1 receptor stimulation. A potential approach to this question may to be undertake a target discovery approach with Ingenuity® pathway analysis. This would allow analysis of NPY stimulated tissue or tissue from disease models to undergo micro-array or mass spectrometry and pathway analysis to identify associations for detailed mechanistic evaluation.

Undertaking clinical studies would allow the study of NPY in patients with normal hearts and those with structural heart disease. NPY is a potent vasoconstrictor and has

been used safely in human vascular studies [509] and the study of restitution by monophasic action potential recording [510] during infusion may provide insight on local electrophysiological changes in the human heart. A more global assessment of ventricular electrophysiology is technically feasible with the use of non-contact mapping arrays [511], although these are not used frequently in routine clinical practice due to increased size of vascular access, intracavity restriction to catheter manipulation and cost. Nevertheless, this approach may be feasible for the study of global electrophysiology in a large animal model where direct sympathetic stimulation could also be undertaken. The secondary prevention implantable cardiovertor defibrillator population may also provide a relevant disease model for study. These patients will have sympatho-vagal imbalance and often undergo induction of VF for defibrillation safety margin testing. The ease of VF induction may be correlated to plasma NPY levels or determined during NPY infusion. Lastly, it would be interesting to determine the time course of plasma NPY levels in patients presenting with ventricular arrhythmia storm, but this is likely to require a multi-centre approach to achieve a large sample size.

In summary, these data demonstrate that NPY is an independent, pro-arrhythmic trigger in the setting of maximal β-blockade. The clinical relevance of this observation may relate to emerging evidence of stellate ganglia interventions for the management of refractory ventricular arrhythmia in patients on maximal medical therapy. Patients with ischaemic VT/VF storm have been successfully managed with stellate ganglia block or stellectomy [476, 477] and patients with catecholaminergic polymorphic VT have been made arrhythmia free with left stellectomy [481]. These small case series may indicate that stellectomy not only reduces noradrenaline release

but also NPY, and this could be studied by molecular analysis of stellate tissue from patients. It may be reasonable to envisage that future anti-arrhythmic strategies may combine β-blockade with NPY receptor inhibition, with Y_1 blockade at the myocyte and Y_2 blockade to attenuate the reduction in parasympathetic neurotransmission by NPY.

6.4 Tetrahydrobiopterin and autonomic cardiovascular control

Tetrahydrobiopterin (BH4) is a critical cofactor for the generation of NO and catecholamines by the NO synthases (NOS) and tyrosine hydroxylase (TH) respectively. Nitric oxide and noradrenaline have been shown to modulate both ion channel activity and calcium dynamics, both also under autonomic control. The potential role for BH4 in influencing autonomic function was suggested by Zhang *et al.* [358] in a genome wide association study that identified a single nucleotide polymorphism (SNP) C+234T, associated with increased blood pressure, reduced urinary catecholamine excretion, reduced NO production and decreased baroreflex sensitivity and heart rate variability. This study along with observations of increased heart rate and low plasma catecholamines in patients with a variety of *GCH1* mutations in the context of dopa-responsive dystonia (DRD) [360] provided the basis of my hypothesis to investigate the role of BH4 in autonomic function.

Experimental approaches to date investigating the role of BH4 in physiological systems have been limited by the absence of effective pharmacological inhibitors [319, 512]. Work from the Channon laboratory has recently published data utilising tissue specific *Gch1* gene (murine GCH1 gene) deletion to successfully identify the cell autonomous requirement of BH4 in endothelial cells in the maintenance of vascular tone in the context of blood pressure regulation [325]. In addition, a myocyte specific

Gch1 knockout model has been generated and continues to undergo investigation (unpublished data). Therefore, I aimed to utilise this system to generate a sympathetic neuron specific *Gch1* knockout model to investigate the autonomic modulation of cardiovascular physiology by BH4. The tissue specific promoter chosen was TH, and by targeting cardiac sympathetic innervation. The confounding effect of uncoupling nNOS was not significant, as it has been shown to have minimal expression in murine cardiac sympathetic tissue [208].

The first series of experiments with cre-recombinase under the control of a TH promoter yielded a viable mouse model with genomic deletion of *Gch1* but no biochemical or physiologic phenotype. The critical experiment was to determine the excision efficiency of cre-recombinase which was shown to be less than 10%. Therefore, a further breeding program was undertaken with an alternative cre-recombinase system utilising an internal ribosome entry site (IRES) to improve gene excision. Once again, a viable mouse model was generated but this time demonstrated a marked neuro-motor phenotype with confirmed significant reduction in BH4 and biopterin in midbrain and adrenal tissue compared to controls. The specificity of excision effect was also confirmed by demonstrating normal BH4 and biopterin levels in non-TH expressing tissue such as liver and lung. The overall phenotype mimicked other models of gene knockout targeting enzymes in the biochemical synthesis of BH4 or catecholamines, and due to a failure to thrive required elective culling at day 21. This model is likely to represent an advanced Parkinson's disease (PD) phenotype and may be relevant for the study of either PD or DRD as loss of function variants in the *GCH1* gene are associated with both conditions.

This line of investigation would be feasible if a biochemical rescue of this model is possible, either by maternal supplementation of sepiapterin and L-DOPA or direct supplementation of knockout animals following birth. These experimental pathways are underway, and preliminary data appears to show a promising response in the knockout animals with supplementation with carbidopa and sepiapterin. Whether this approach allows sufficient ageing of the animals to allow cardiovascular phenotyping remains to be established. An alternative neurological investigative strategy would be to study the heterozygote animal by determining the acute biochemical effect of single allele deletion and potentially the effect of ageing.

The original hypothesis however was to establish the role of BH4 in cardiovascular autonomic control and this has not been achieved by these data. It is interesting to speculate with the benefit of these observations which modifications in experimental methodology could have answered the scientific question. Tissue specific gene knockout remains the most elegant method to determine this, but may require either an alternative promoter driving gene excision or an inducible gene silencing system. Coupling cre-recombinase activity to a PRS promoter [185] may allow specific targeting of sympathetic neurons for *Gch1* excision however embryonic loss of catecholamines may lead to failure of normal development [486]. Therefore an ideal model system may be a tamoxifen-regulated cre-recombinase to induce *GCH1* excision in adult animals to allow cardiovascular phenotyping with and without the presence of a disease state.

6.5 Concluding summary

Cardiovascular disease is associated with sympatho-vagal imbalance and results in adaptations at different levels of the autonomic hierarchy [373, 464]. Stress induced changes in electrical stability lead to arrhythmia and there are short and long-term

interactions at all levels of autonomic hierarchy and the neural-myocyte interface [12]. The data presented in this thesis focus on the neural-myocyte axis and add to the mechanistic evidence on cholinergic anti-arrhythmic signalling and identified neuropeptide Y as a novel, direct pro-arrhythmic trigger. The role of BH4 in autonomic control remains an interesting target indicated by population studies, and modification to the experimental strategy may allow this link to be explored mechanistically. Future studies will aim to add to this knowledge base, and in the long-term aim to investigate the autonomic nervous system in an integrated approach to develop novel, mechanism-based, neuromodulation therapies.

References

1. National institute of clinical excellence: Implantable cardioverter defibrillators and cardiac resynchronisation therapy for arrhythmias and heart failure. 2014
2. The heart rhythm foundation: Sudden cardiac arrest key facts. 2012
3. A comparison of antiarrhythmic-drug therapy with implantable defibrillators in patients resuscitated from near-fatal ventricular arrhythmias. The antiarrhythmics versus implantable defibrillators (avid) investigators. *The New England Journal of Medicine*1997;337:1576-1583
4. Bardy GH, Lee KL, Mark DB, Poole JE, Packer DL, Boineau R, Domanski M, Troutman C, Anderson J, Johnson G, McNulty SE, Clapp-Channing N, Davidson-Ray LD, Fraulo ES, Fishbein DP, Luceri RM, Ip JH. Amiodarone or an implantable cardioverter-defibrillator for congestive heart failure. *The New England Journal of Medicine*2005;352:225-237
5. Moss AJ, Zareba W, Hall WJ, Klein H, Wilber DJ, Cannom DS, Daubert JP, Higgins SL, Brown MW, Andrews ML. Prophylactic implantation of a defibrillator in patients with myocardial infarction and reduced ejection fraction. *The New England Journal of Medicine*2002;346:877-883
6. Floras JS. Sympathetic activation in human heart failure: Diverse mechanisms, therapeutic opportunities. *Acta Physiol Scand*. 2003;177:391-398
7. Ishise H, Asanoi H, Ishizaka S, Joho S, Kameyama T, Umeno K, Inoue H. Time course of sympathovagal imbalance and left ventricular dysfunction in conscious dogs with heart failure. *J Appl Physiol (1985)*. 1998;84:1234-1241
8. Motte S, Mathieu M, Brimioulle S, Pensis A, Ray L, Ketelslegers JM, Montano N, Naeije R, van de Borne P, Entee KM. Respiratory-related heart rate variability in progressive experimental heart failure. *American Journal of Physiology. Heart and Circulatory Physiology.* 2005;289:H1729-1735
9. Grassi G, Seravalle G, Bertinieri G, Turri C, Stella ML, Scopelliti F, Mancia G. Sympathetic and reflex abnormalities in heart failure secondary to ischaemic or idiopathic dilated cardiomyopathy. *Clinical Science*. 2001;101:141-146
10. Sun SY, Wang W, Zucker IH, Schultz HD. Enhanced activity of carotid body chemoreceptors in rabbits with heart failure: Role of nitric oxide. *J Appl Physiol (1985)*. 1999;86:1273-1282
11. Ma R, Zucker IH, Wang W. Central gain of the cardiac sympathetic afferent reflex in dogs with heart failure. *The American Journal of Physiology*. 1997;273:H2664-2671
12. Fukuda K, Kanazawa H, Aizawa Y, Ardell JL, Shivkumar K. Cardiac innervation and sudden cardiac death. *Circulation Research*. 2015;116:2005-2019
13. Schwartz PJ. The autonomic nervous system and sudden death. *European Heart Journal.* 1998;19 Suppl F:F72-80
14. La Rovere MT, Specchia G, Mortara A, Schwartz PJ. Baroreflex sensitivity, clinical correlates, and cardiovascular mortality among patients with a first myocardial infarction. A prospective study. *Circulation*. 1988;78:816-824
15. La Rovere MT, Bigger JT, Jr., Marcus FI, Mortara A, Schwartz PJ. Baroreflex sensitivity and heart-rate variability in prediction of total cardiac mortality after myocardial infarction. Atrami (autonomic tone and reflexes after myocardial infarction) investigators. *Lancet*. 1998;351:478-484

16. Nolan J, Batin PD, Andrews R, Lindsay SJ, Brooksby P, Mullen M, Baig W, Flapan AD, Cowley A, Prescott RJ, Neilson JM, Fox KA. Prospective study of heart rate variability and mortality in chronic heart failure: Results of the united kingdom heart failure evaluation and assessment of risk trial (uk-heart). *Circulation*. 1998;98:1510-1516
17. El-Omar M, Kardos A, Casadei B. Mechanisms of respiratory sinus arrhythmia in patients with mild heart failure. *American Journal of Physiology. Heart and Circulatory Physiology.* 2001;280:H125-131
18. Effects of enalapril on mortality in severe congestive heart failure. Results of the cooperative north scandinavian enalapril survival study (consensus). The consensus trial study group. *The New England Journal of Medicine*1987;316:1429-1435
19. Effect of enalapril on survival in patients with reduced left ventricular ejection fractions and congestive heart failure. The solvd investigators. *The New England Journal of Medicine*1991;325:293-302
20. Effect of ramipril on mortality and morbidity of survivors of acute myocardial infarction with clinical evidence of heart failure. The acute infarction ramipril efficacy (aire) study investigators. *Lancet*. 1993;342:821-828
21. The cardiac insufficiency bisoprolol study ii (cibis-ii): A randomised trial. *Lancet*. 1999;353:9-13
22. Effect of metoprolol cr/xl in chronic heart failure: Metoprolol cr/xl randomised intervention trial in congestive heart failure (merit-hf). *Lancet*. 1999;353:2001-2007
23. Pitt B, Zannad F, Remme WJ, Cody R, Castaigne A, Perez A, Palensky J, Wittes J. The effect of spironolactone on morbidity and mortality in patients with severe heart failure. Randomized aldactone evaluation study investigators. *The New England Journal of Medicine*1999;341:709-717
24. Zhang W, Qu X, Chen B, Snyder M, Wang M, Li B, Tang Y, Chen H, Zhu W, Zhan L, Yin N, Li D, Xie L, Liu Y, Zhang JJ, Fu XY, Rubart M, Song LS, Huang XY, Shou W. Critical roles of stat3 in beta-adrenergic functions in the heart. *Circulation*. 2016;133:48-61
25. Packer M, Coats AJ, Fowler MB, Katus HA, Krum H, Mohacsi P, Rouleau JL, Tendera M, Castaigne A, Roecker EB, Schultz MK, DeMets DL. Effect of carvedilol on survival in severe chronic heart failure. *The New England Journal of Medicine*2001;344:1651-1658
26. Brown NJ, Vaughan DE. Angiotensin-converting enzyme inhibitors. *Circulation*. 1998;97:1411-1420
27. Folkow B, Johansson B, Mellander S. The comparative effects of angiotensin and noradrenaline on consecutive vascular sections. *Acta Physiologica Scandinavica.* 1961;53:99-104
28. Eichhorn EJ, Bristow MR. Medical therapy can improve the biological properties of the chronically failing heart. A new era in the treatment of heart failure. *Circulation*. 1996;94:2285-2296
29. Zimmerman BG, Sybertz EJ, Wong PC. Interaction between sympathetic and renin-angiotensin system. *Journal of Hypertension*. 1984;2:581-587
30. Bell L, Madri JA. Influence of the angiotensin system on endothelial and smooth muscle cell migration. *Am J Pathol*. 1990;137:7-12
31. Daemen MJ, Lombardi DM, Bosman FT, Schwartz SM. Angiotensin ii induces smooth muscle cell proliferation in the normal and injured rat arterial wall. *Circulation Research*. 1991;68:450-456

32. Itoh H, Mukoyama M, Pratt RE, Gibbons GH, Dzau VJ. Multiple autocrine growth factors modulate vascular smooth muscle cell growth response to angiotensin ii. *The Journal of Clinical Investigation.* 1993;91:2268-2274
33. Dostal DE, Booz GW, Baker KM. Angiotensin ii signalling pathways in cardiac fibroblasts: Conventional versus novel mechanisms in mediating cardiac growth and function. *Molecular and Cellular Biochemistry.* 1996;157:15-21
34. Huckle WR, Earp HS. Regulation of cell proliferation and growth by angiotensin ii. *Prog Growth Factor Res*. 1994;5:177-194
35. Curtiss C, Cohn JN, Vrobel T, Franciosa JA. Role of the renin-angiotensin system in the systemic vasoconstriction of chronic congestive heart failure. *Circulation*. 1978;58:763-770
36. Gavras H, Faxon DP, Berkoben J, Brunner HR, Ryan TJ. Angiotensin converting enzyme inhibition in patients with congestive heart failure. *Circulation*. 1978;58:770-776
37. Turini GA, Brunner HR, Gribic M, Waeber B, Gavras H. Improvement of chronic congestive heart-failure by oral captopril. *Lancet*. 1979;1:1213-1215
38. Davis R, Ribner HS, Keung E, Sonnenblick EH, LeJemtel TH. Treatment of chronic congestive heart failure with captopril, an oral inhibitor of angiotensin-converting enzyme. *The New England Journal of Medicine*1979;301:117-121
39. Tarazi RC, Fouad FM, Ceimo JK, Bravo EL. Renin, aldosterone and cardiac decompensation: Studies with an oral converting enzyme inhibitor in heart failure. *Am J Cardiol*. 1979;44:1013-1018
40. Dzau VJ, Colucci WS, Williams GH, Curfman G, Meggs L, Hollenberg NK. Sustained effectiveness of converting-enzyme inhibition in patients with severe congestive heart failure. *The New England Journal of Medicine*1980;302:1373-1379
41. Levine TB, Franciosa JA, Cohn JN. Acute and long-term response to an oral converting-enzyme inhibitor, captopril, in congestive heart failure. *Circulation*. 1980;62:35-41
42. Sharpe DN, Douglas JE, Coxon RJ, Long B. Low-dose captopril in chronic heart failure: Acute haemodynamic effects and long-term treatment. *Lancet*. 1980;2:1154-1157
43. Maslowski AH, Ikram H, Nicholls MG, Espiner EA. Haemodynamic, hormonal, and electrolyte responses to captopril in resistant heart failure. *Lancet*. 1981;1:71-74
44. Cody RJ, Covit A, Schaer G, Williams G. Captopril pharmacokinetics and the acute hemodynamic and hormonal response in patients with severe chronic congestive heart failure. *Am Heart J*. 1982;104:1180-1183
45. Cohn JN, Johnson G, Ziesche S, Cobb F, Francis G, Tristani F, Smith R, Dunkman WB, Loeb H, Wong M, et al. A comparison of enalapril with hydralazine-isosorbide dinitrate in the treatment of chronic congestive heart failure. *The New England Journal of Medicine*1991;325:303-310
46. Kober L, Torp-Pedersen C, Carlsen JE, Bagger H, Eliasen P, Lyngborg K, Videbaek J, Cole DS, Auclert L, Pauly NC. A clinical trial of the angiotensin-converting-enzyme inhibitor trandolapril in patients with left ventricular dysfunction after myocardial infarction. Trandolapril cardiac evaluation (trace) study group. *The New England Journal of Medicine*1995;333:1670-1676

47. Armour JA. Potential clinical relevance of the 'little brain' on the mammalian heart. *Exp Physiol*. 2008;93:165-176
48. De Ferrari GM, Crijns HJ, Borggrefe M, Milasinovic G, Smid J, Zabel M, Gavazzi A, Sanzo A, Dennert R, Kuschyk J, Raspopovic S, Klein H, Swedberg K, Schwartz PJ. Chronic vagus nerve stimulation: A new and promising therapeutic approach for chronic heart failure. *European Heart Journal.* 2011;32:847-855
49. Premchand RK, Sharma K, Mittal S, Monteiro R, Dixit S, Libbus I, DiCarlo LA, Ardell JL, Rector TS, Amurthur B, KenKnight BH, Anand IS. Autonomic regulation therapy via left or right cervical vagus nerve stimulation in patients with chronic heart failure: Results of the anthem-hf trial. *J Card Fail*. 2014;20:808-816
50. Zannad F, De Ferrari GM, Tuinenburg AE, Wright D, Brugada J, Butter C, Klein H, Stolen C, Meyer S, Stein KM, Ramuzat A, Schubert B, Daum D, Neuzil P, Botman C, Castel MA, D'Onofrio A, Solomon SD, Wold N, Ruble SB. Chronic vagal stimulation for the treatment of low ejection fraction heart failure: Results of the neural cardiac therapy for heart failure (nectar-hf) randomized controlled trial. *European Heart Journal.* 2015;36:425-433
51. Hauptman PJ, Schwartz PJ, Gold MR, Borggrefe M, Van Veldhuisen DJ, Starling RC, Mann DL. Rationale and study design of the increase of vagal tone in heart failure study: Inovate-hf. *Am Heart J*. 2012;163:954-962 e951
52. Huang J, Qian J, Yao W, Wang N, Zhang Z, Cao C, Song B. Vagus nerve stimulation reverses ventricular electrophysiological changes induced by hypersympathetic nerve activity. *Experimental Physiology.* 2015;100:239-248
53. Einbrodt. Ueberherzreizungundihrverhaeltniszum blutdruck. Akademie der wissenschaften (vienna). *Sitzungsberichte* 1859;38:345
54. Scherlag BJ, Helfant RH, Haft JI, Damato AN. Electrophysiology underlying ventricular arrhythmias due to coronary ligation. *The American Journal of Physiology*. 1970;219:1665-1671
55. Goldstein RE, Karsh RB, Smith ER, Orlando M, Norman D, Farnham G, Redwood DR, Epstein SE. Influence of atropine and of vagally mediated bradycardia on the occurrence of ventricular arrhythmias following acute coronary occlusion in closed-chest dogs. *Circulation*. 1973;47:1180-1190
56. Myers RW, Pearlman AS, Hyman RM, Goldstein RA, Kent KM, Goldstein RE, Epstein SE. Beneficial effects of vagal stimulation and bradycardia during experimental acute myocardial ischemia. *Circulation*. 1974;49:943-947
57. Waxman HL, Cain ME, Greenspan AM, Josephson ME. Termination of ventricular tachycardia with ventricular stimulation: Salutary effect of increased current strength. *Circulation*. 1982;65:800-804
58. Kolman BS, Verrier RL, Lown B. The effect of vagus nerve stimulation upon vulnerability of the canine ventricle: Role of sympathetic-parasympathetic interactions. *Circulation*. 1975;52:578-585
59. Yoon MS, Han J, Tse WW, Rogers R. Effects of vagal stimulation, atropine, and propranolol on fibrillation threshold of normal and ischemic ventricles. *Am Heart J*. 1977;93:60-65
60. Kent KM, Smith ER, Redwood DR, Epstein SE. Electrical stability of acutely ischemic myocardium. Influences of heart rate and vagal stimulation. *Circulation*. 1973;47:291-298
61. Corr PB, Gillis RA. Role of the vagus nerves in the cardiovascular changes induced by coronary occlusion. *Circulation*. 1974;49:86-97

62. Zuanetti G, De Ferrari GM, Priori SG, Schwartz PJ. Protective effect of vagal stimulation on reperfusion arrhythmias in cats. *Circulation Research*. 1987;61:429-435
63. Schwartz PJ, Vanoli E, Stramba-Badiale M, De Ferrari GM, Billman GE, Foreman RD. Autonomic mechanisms and sudden death. New insights from analysis of baroreceptor reflexes in conscious dogs with and without a myocardial infarction. *Circulation*. 1988;78:969-979
64. Schwartz PJ, Billman GE, Stone HL. Autonomic mechanisms in ventricular fibrillation induced by myocardial ischemia during exercise in dogs with healed myocardial infarction. An experimental preparation for sudden cardiac death. *Circulation*. 1984;69:790-800
65. De Ferrari GM, Vanoli E, Stramba-Badiale M, Hull SS, Jr., Foreman RD, Schwartz PJ. Vagal reflexes and survival during acute myocardial ischemia in conscious dogs with healed myocardial infarction. *Am J Physiol*. 1991;261:H63-69
66. Vanoli E, De Ferrari GM, Stramba-Badiale M, Hull SS, Jr., Foreman RD, Schwartz PJ. Vagal stimulation and prevention of sudden death in conscious dogs with a healed myocardial infarction. *Circulation Research*. 1991;68:1471-1481
67. Coote JH. Myths and realities of the cardiac vagus. *The Journal of Physiology*. 2013;591:4073-4085
68. Weiss JN, Chen PS, Qu Z, Karagueuzian HS, Garfinkel A. Ventricular fibrillation: How do we stop the waves from breaking? *Circulation Research.* 2000;87:1103-1107
69. Weiss JN, Nivala M, Garfinkel A, Qu Z. Alternans and arrhythmias: From cell to heart. *Circulation Research*. 2011;108:98-112
70. Garfinkel A, Kim YH, Voroshilovsky O, Qu Z, Kil JR, Lee MH, Karagueuzian HS, Weiss JN, Chen PS. Preventing ventricular fibrillation by flattening cardiac restitution. *Proc Natl Acad Sci U S A*. 2000;97:6061-6066
71. Cabo C, Pertsov AM, Baxter WT, Davidenko JM, Gray RA, Jalife J. Wave-front curvature as a cause of slow conduction and block in isolated cardiac muscle. *Circulation Research*. 1994;75:1014-1028
72. Allessie MA, Bonke FI, Schopman FJ. Circus movement in rabbit atrial muscle as a mechanism of trachycardia. *Circulation Research*. 1973;33:54-62
73. Davidenko JM, Pertsov AV, Salomonsz R, Baxter W, Jalife J. Stationary and drifting spiral waves of excitation in isolated cardiac muscle. *Nature*. 1992;355:349-351
74. Moe GK, Rheinboldt WC, Abildskov JA. A computer model of atrial fibrillation. *Am Heart J*. 1964;67:200-220
75. Zaitsev AV, Berenfeld O, Mironov SF, Jalife J, Pertsov AM. Distribution of excitation frequencies on the epicardial and endocardial surfaces of fibrillating ventricular wall of the sheep heart. *Circulation Research*. 2000;86:408-417
76. Cabo C, Boyden PA. Electrical remodeling of the epicardial border zone in the canine infarcted heart: A computational analysis. *American Journal of Physiology. Heart and Circulatory Physiology.* 2003;284:H372-384
77. Kim YH, Xie F, Yashima M, Wu TJ, Valderrabano M, Lee MH, Ohara T, Voroshilovsky O, Doshi RN, Fishbein MC, Qu Z, Garfinkel A, Weiss JN, Karagueuzian HS, Chen PS. Role of papillary muscle in the generation and maintenance of reentry during ventricular tachycardia and fibrillation in isolated swine right ventricle. *Circulation*. 1999;100:1450-1459

78. Karma A. Electrical alternans and spiral wave breakup in cardiac tissue. *Chaos*. 1994;4:461-472
79. Qu Z, Weiss JN, Garfinkel A. Cardiac electrical restitution properties and stability of reentrant spiral waves: A simulation study. *The American Journal of Physiology*. 1999;276:H269-283
80. Qu Z, Kil J, Xie F, Garfinkel A, Weiss JN. Scroll wave dynamics in a three-dimensional cardiac tissue model: Roles of restitution, thickness, and fiber rotation. *Biophys J*. 2000;78:2761-2775
81. Koller ML, Riccio ML, Gilmour RF, Jr. Dynamic restitution of action potential duration during electrical alternans and ventricular fibrillation. *The American Journal of Physiology*. 1998;275:H1635-1642
82. Riccio ML, Koller ML, Gilmour RF, Jr. Electrical restitution and spatiotemporal organization during ventricular fibrillation. *Circulation Research*. 1999;84:955-963
83. Garfinkel A, Kim YH, Voroshilovsky O, Qu Z, Kil JR, Lee MH, Karagueuzian HS, Weiss JN, Chen PS. Preventing ventricular fibrillation by flattening cardiac restitution. *Proceedings of the National Academy of Sciences of the United States of America*. 2000;97:6061-6066
84. Lee MH, Lin SF, Ohara T, Omichi C, Okuyama Y, Chudin E, Garfinkel A, Weiss JN, Karagueuzian HS, Chen PS. Effects of diacetyl monoxime and cytochalasin d on ventricular fibrillation in swine right ventricles. *American Journal of Physiology. Heart and Circulatory Physiology.* 2001;280:H2689-2696
85. Omichi C, Zhou S, Lee MH, Naik A, Chang CM, Garfinkel A, Weiss JN, Lin SF, Karagueuzian HS, Chen PS. Effects of amiodarone on wave front dynamics during ventricular fibrillation in isolated swine right ventricle. *American Journal of Physiology. Heart and Circulatory Physiology.* 2002;282:H1063-1070
86. Wu TJ, Lin SF, Weiss JN, Ting CT, Chen PS. Two types of ventricular fibrillation in isolated rabbit hearts: Importance of excitability and action potential duration restitution. *Circulation*. 2002;106:1859-1866
87. Samie FH, Berenfeld O, Anumonwo J, Mironov SF, Udassi S, Beaumont J, Taffet S, Pertsov AM, Jalife J. Rectification of the background potassium current: A determinant of rotor dynamics in ventricular fibrillation. *Circulation Research*. 2001;89:1216-1223
88. Chudin E, Goldhaber J, Garfinkel A, Weiss J, Kogan B. Intracellular ca(2+) dynamics and the stability of ventricular tachycardia. *Biophys J*. 1999;77:2930-2941
89. Koller ML, Riccio ML, Gilmour RF, Jr. Dynamic restitution of action potential duration during electrical alternans and ventricular fibrillation. *Am J Physiol*. 1998;275:H1635-1642
90. Bers DM. *Excitation-contraction coupling and cardiac contractile force*. Boston: Kluwer Academic Publishers; 2001.
91. Hwang C, Fan W, Chen PS. Recurrent appearance of protective zones after an unsuccessful defibrillation shock. *The American Journal of Physiology*. 1996;271:H1491-1497
92. Brodsky M, Wu D, Denes P, Kanakis C, Rosen KM. Arrhythmias documented by 24 hour continuous electrocardiographic monitoring in 50 male medical students without apparent heart disease. *Am J Cardiol*. 1977;39:390-395

93. Franz MR. The electrical restitution curve revisited: Steep or flat slope--which is better? *J Cardiovasc Electrophysiol*. 2003;14:S140-147
94. Ng GA, Brack KE, Patel VH, Coote JH. Autonomic modulation of electrical restitution, alternans and ventricular fibrillation initiation in the isolated heart. *Cardiovascular Research.* 2007;73:750-760
95. Kuo CS, Munakata K, Reddy CP, Surawicz B. Characteristics and possible mechanism of ventricular arrhythmia dependent on the dispersion of action potential durations. *Circulation*. 1983;67:1356-1367
96. Winter J, Tanko AS, Brack KE, Coote JH, Ng GA. Differential cardiac responses to unilateral sympathetic nerve stimulation in the isolated innervated rabbit heart. *Auton Neurosci*. 2012;166:4-14
97. Wang X, Li F, Gerdes AM. Chronic pressure overload cardiac hypertrophy and failure in guinea pigs: I. Regional hemodynamics and myocyte remodeling. *Journal of Molecular and Cellular Cardiology.* 1999;31:307-317
98. Martin PJ, Levy MN, Zieske H. Analysis and simulation of the left ventricular response to autonomic nervous activity. *Cardiovascular research*. 1969;3:396-410
99. Levy MN, Zieske H. Effect of enhanced contractility on the left ventricular response to vagus nerve stimulation in dogs. *Circulation Research*. 1969;24:303-311
100. Brack KE, Coote JH, Ng GA. Vagus nerve stimulation protects against ventricular fibrillation independent of muscarinic receptor activation. *Cardiovascular Research.* 2011;91:437-446
101. Sabbah HN. Electrical vagus nerve stimulation for the treatment of chronic heart failure. *Cleve Clin J Med*. 2011;78 Suppl 1:S24-29
102. Ando M, Katare RG, Kakinuma Y, Zhang D, Yamasaki F, Muramoto K, Sato T. Efferent vagal nerve stimulation protects heart against ischemia-induced arrhythmias by preserving connexin43 protein. *Circulation*. 2005;112:164-170
103. Levy MN, Blattberg B. Effect of vagal stimulation on the overflow of norepinephrine into the coronary sinus during cardiac sympathetic nerve stimulation in the dog. *Circulation Research*. 1976;38:81-84
104. Brack KE, Winter J, Ng GA. Mechanisms underlying the autonomic modulation of ventricular fibrillation initiation-tentative prophylactic properties of vagus nerve stimulation on malignant arrhythmias in heart failure. *Heart Fail Rev*. 2012
105. Samaan A. The antagonistic cardiac nerves and heart rate. *The Journal of Physiology.* 1935;83:332-340
106. Brack KE, Coote JH, Ng GA. Interaction between direct sympathetic and vagus nerve stimulation on heart rate in the isolated rabbit heart. *Experimental Physiology.* 2004;89:128-139
107. Murad F, Chi YM, Rall TW, Sutherland EW. Adenyl cyclase. Iii. The effect of catecholamines and choline esters on the formation of adenosine 3',5'-phosphate by preparations from cardiac muscle and liver. *The Journal of Biological Chemistry.* 1962;237:1233-1238
108. Muscholl E. Peripheral muscarinic control of norepinephrine release in the cardiovascular system. *The American Journal of Physiology*. 1980;239:H713-720
109. Stiles GL, Caron MG, Lefkowitz RJ. Beta-adrenergic receptors: Biochemical mechanisms of physiological regulation. *Physiol Rev*. 1984;64:661-743

110. Vincent NH, Ellis S. Inhibitory effect of acetylcholine on glycogenolysis in the isolated guinea-pig heart. *J Pharmacol Exp Ther*. 1963;139:60-68
111. De Ferrari GM, Vanoli E, Curcuruto P, Tommasini G, Schwartz PJ. Prevention of life-threatening arrhythmias by pharmacologic stimulation of the muscarinic receptors with oxotremorine. *Am Heart J*. 1992;124:883-890
112. De Ferrari GM, Salvati P, Grossoni M, Ukmar G, Vaga L, Patrono C, Schwartz PJ. Pharmacologic modulation of the autonomic nervous system in the prevention of sudden cardiac death. A study with propranolol, methacholine and oxotremorine in conscious dogs with a healed myocardial infarction. *Journal of the American College of Cardiology*. 1993;22:283-290
113. Nicoletti A, Michel JB. Cardiac fibrosis and inflammation: Interaction with hemodynamic and hormonal factors. *Cardiovascular Research.* 1999;41:532-543
114. Tracey KJ. The inflammatory reflex. *Nature*. 2002;420:853-859
115. Sloan RP, McCreath H, Tracey KJ, Sidney S, Liu K, Seeman T. Rr interval variability is inversely related to inflammatory markers: The cardia study. *Mol Med*. 2007;13:178-184
116. Corrado D, Basso C, Thiene G. Sudden cardiac death in young people with apparently normal heart. *Cardiovascular Research.* 2001;50:399-408
117. Basso C, Calabrese F, Corrado D, Thiene G. Postmortem diagnosis in sudden cardiac death victims: Macroscopic, microscopic and molecular findings. *Cardiovascular Research.* 2001;50:290-300
118. Klein RM, Vester EG, Brehm MU, Dees H, Picard F, Niederacher D, Beckmann MW, Strauer BE. [inflammation of the myocardium as an arrhythmia trigger]. *Z Kardiol*. 2000;89 Suppl 3:24-35
119. Petkova-Kirova PS, Gursoy E, Mehdi H, McTiernan CF, London B, Salama G. Electrical remodeling of cardiac myocytes from mice with heart failure due to the overexpression of tumor necrosis factor-alpha. *American Journal of Physiology. Heart and Circulatory Physiology.* 2006;290:H2098-2107
120. Wang H, Yu M, Ochani M, Amella CA, Tanovic M, Susarla S, Li JH, Yang H, Ulloa L, Al-Abed Y, Czura CJ, Tracey KJ. Nicotinic acetylcholine receptor alpha7 subunit is an essential regulator of inflammation. *Nature*. 2003;421:384-388
121. Zhang Y, Popovic ZB, Bibevski S, Fakhry I, Sica DA, Van Wagoner DR, Mazgalev TN. Chronic vagus nerve stimulation improves autonomic control and attenuates systemic inflammation and heart failure progression in a canine high-rate pacing model. *Circ Heart Fail*. 2009;2:692-699
122. Hamann JJ, Ruble SB, Stolen C, Wang M, Gupta RC, Rastogi S, Sabbah HN. Vagus nerve stimulation improves left ventricular function in a canine model of chronic heart failure. *Eur J Heart Fail*. 2013;15:1319-1326
123. Vegh A, Gonczi M, Miskolczi G, Kovacs M. Regulation of gap junctions by nitric oxide influences the generation of arrhythmias resulting from acute ischemia and reperfusion in vivo. *Front Pharmacol*. 2013;4:76
124. Del Rio CL, Dawson TA, Clymer BD, Paterson DJ, Billman GE. Effects of acute vagal nerve stimulation on the early passive electrical changes induced by myocardial ischaemia in dogs: Heart rate-mediated attenuation. *Experimental Physiology.* 2008;93:931-944
125. Herring N, Danson EJ, Paterson DJ. Cholinergic control of heart rate by nitric oxide is site specific. *News Physiol Sci*. 2002;17:202-206

126. Loewi O. Über humorale übertragbarkeit der herznervenwirkung. *Pflüger's Archiv*. 1924;204
127. Dale HH, Feldberg W. The chemical transmission of secretory impulses to the sweat glands of the cat. *The Journal of Physiology.* 1934;82:121-128
128. Schulz R, Rassaf T, Massion PB, Kelm M, Balligand JL. Recent advances in the understanding of the role of nitric oxide in cardiovascular homeostasis. *Pharmacology & Therapeutics*. 2005;108:225-256
129. Balligand JL, Kelly RA, Marsden PA, Smith TW, Michel T. Control of cardiac muscle cell function by an endogenous nitric oxide signaling system. *Proceedings of the National Academy of Sciences of the United States of America*. 1993;90:347-351
130. Han X, Shimoni Y, Giles WR. A cellular mechanism for nitric oxide-mediated cholinergic control of mammalian heart rate. *J Gen Physiol*. 1995;106:45-65
131. Vandecasteele G, Eschenhagen T, Scholz H, Stein B, Verde I, Fischmeister R. Muscarinic and beta-adrenergic regulation of heart rate, force of contraction and calcium current is preserved in mice lacking endothelial nitric oxide synthase. *Nat Med*. 1999;5:331-334
132. Herring N, Paterson DJ. Nitric oxide-cgmp pathway facilitates acetylcholine release and bradycardia during vagal nerve stimulation in the guinea-pig in vitro. *J Physiol*. 2001;535:507-518
133. Sears CE, Choate JK, Paterson DJ. Inhibition of nitric oxide synthase slows heart rate recovery from cholinergic activation. *J Appl Physiol (1985)*. 1998;84:1596-1603
134. Sears CE, Choate JK, Paterson DJ. No-cgmp pathway accentuates the decrease in heart rate caused by cardiac vagal nerve stimulation. *J Appl Physiol (1985)*. 1999;86:510-516
135. Herring N, Golding S, Paterson DJ. Pre-synaptic no-cgmp pathway modulates vagal control of heart rate in isolated adult guinea pig atria. *J Mol Cell Cardiol*. 2000;32:1795-1804
136. Jumrussirikul P, Dinerman J, Dawson TM, Dawson VL, Ekelund U, Georgakopoulos D, Schramm LP, Calkins H, Snyder SH, Hare JM, Berger RD. Interaction between neuronal nitric oxide synthase and inhibitory g protein activity in heart rate regulation in conscious mice. *The Journal of Clinical Investigation.* 1998;102:1279-1285
137. Choate JK, Danson EJ, Morris JF, Paterson DJ. Peripheral vagal control of heart rate is impaired in neuronal nos knockout mice. *Am J Physiol Heart Circ Physiol*. 2001;281:H2310-2317
138. Swedberg K, Komajda M, Bohm M, Borer JS, Ford I, Dubost-Brama A, Lerebours G, Tavazzi L. Ivabradine and outcomes in chronic heart failure (shift): A randomised placebo-controlled study. *Lancet*. 2010;376:875-885
139. Ng GA, Brack KE, Coote JH. Effects of direct sympathetic and vagus nerve stimulation on the physiology of the whole heart--a novel model of isolated langendorff perfused rabbit heart with intact dual autonomic innervation. *Exp Physiol*. 2001;86:319-329
140. Brack KE, Patel VH, Coote JH, Ng GA. Nitric oxide mediates the vagal protective effect on ventricular fibrillation via effects on action potential duration restitution in the rabbit heart. *J Physiol*. 2007;583:695-704
141. Weidmann S. The electrical constants of purkinje fibres. *The Journal of Physiology.* 1952;118:348-360

142. Martins JB, Zipes DP. Effects of sympathetic and vagal nerves on recovery properties of the endocardium and epicardium of the canine left ventricle. *Circulation Research*. 1980;46:100-110
143. Mantravadi R, Gabris B, Liu T, Choi BR, de Groat WC, Ng GA, Salama G. Autonomic nerve stimulation reverses ventricular repolarization sequence in rabbit hearts. *Circulation Research*. 2007;100:e72-80
144. Zipes DP, Jalife, J. *Cardiac electrophysiology: From cell to bedside*. Philadelphia, PA: Saunders, Elsevier; 2009.
145. Nash MP, Thornton JM, Sears CE, Varghese A, O'Neill M, Paterson DJ. Ventricular activation during sympathetic imbalance and its computational reconstruction. *J Appl Physiol (1985)*. 2001;90:287-298
146. Kawano H, Okada R, Yano K. Histological study on the distribution of autonomic nerves in the human heart. *Heart Vessels*. 2003;18:32-39
147. Han X, Kubota I, Feron O, Opel DJ, Arstall MA, Zhao YY, Huang P, Fishman MC, Michel T, Kelly RA. Muscarinic cholinergic regulation of cardiac myocyte ica-l is absent in mice with targeted disruption of endothelial nitric oxide synthase. *Proceedings of the National Academy of Sciences of the United States of America*. 1998;95:6510-6515
148. Martin SR, Emanuel K, Sears CE, Zhang YH, Casadei B. Are myocardial enos and nnos involved in the beta-adrenergic and muscarinic regulation of inotropy? A systematic investigation. *Cardiovascular Research.* 2006;70:97-106
149. Mesirca P, Marger L, Toyoda F, Rizzetto R, Audoubert M, Dubel S, Torrente AG, Difrancesco ML, Muller JC, Leoni AL, Couette B, Nargeot J, Clapham DE, Wickman K, Mangoni ME. The g-protein-gated k+ channel, ikach, is required for regulation of pacemaker activity and recovery of resting heart rate after sympathetic stimulation. *J Gen Physiol*. 2013;142:113-126
150. Rathel TR, Leikert JJ, Vollmar AM, Dirsch VM. Application of 4,5-diaminofluorescein to reliably measure nitric oxide released from endothelial cells in vitro. *Biol Proced Online*. 2003;5:136-142
151. Zhang X, Kim WS, Hatcher N, Potgieter K, Moroz LL, Gillette R, Sweedler JV. Interfering with nitric oxide measurements. 4,5-diaminofluorescein reacts with dehydroascorbic acid and ascorbic acid. *The Journal of Biological Chemistry.* 2002;277:48472-48478
152. Handy RL, Harb HL, Wallace P, Gaffen Z, Whitehead KJ, Moore PK. Inhibition of nitric oxide synthase by 1-(2-trifluoromethylphenyl) imidazole (trim) in vitro: Antinociceptive and cardiovascular effects. *Br J Pharmacol*. 1996;119:423-431
153. Handy RL, Moore PK. Mechanism of the inhibition of neuronal nitric oxide synthase by 1-(2-trifluoromethylphenyl) imidazole (trim). *Life Sci*. 1997;60:PL389-394
154. Matsumura N, Kikuchi-Utsumi K, Nakaki T. Activities of 7-nitroindazole and 1-(2-(trifluoromethylphenyl)-imidazole independent of neuronal nitric-oxide synthase inhibition. *J Pharmacol Exp Ther*. 2008;325:357-362
155. Brack KE, Winter J, Ng GA. Mechanisms underlying the autonomic modulation of ventricular fibrillation initiation-tentative prophylactic properties of vagus nerve stimulation on malignant arrhythmias in heart failure. *Heart failure reviews*. 2012
156. Randall W. *Nervous control of cardiovascular function*. New York: OUP; 1984.

157. Levy MNM, P.J. Autonomic control of cardiac conduction and automaticity. In: Shephered JTV, S.F., ed. *Nervous control of the heart*. Amsterdam: HAP; 1996:201-225.
158. Singh S, Johnson PI, Lee RE, Orfei E, Lonchyna VA, Sullivan HJ, Montoya A, Tran H, Wehrmacher WH, Wurster RD. Topography of cardiac ganglia in the adult human heart. *J Thorac Cardiovasc Surg*. 1996;112:943-953
159. Gatti PJ, Johnson TA, McKenzie J, Lauenstein JM, Gray A, Massari VJ. Vagal control of left ventricular contractility is selectively mediated by a cranioventricular intracardiac ganglion in the cat. *Journal of the Autonomic Nervous System.* 1997;66:138-144
160. Dickerson LW, Rodak DJ, Fleming TJ, Gatti PJ, Massari VJ, McKenzie JC, Gillis RA. Parasympathetic neurons in the cranial medial ventricular fat pad on the dog heart selectively decrease ventricular contractility. *Journal of the Autonomic Nervous System.* 1998;70:129-141
161. Cullis W, Tribe EM. Distribution of nerves in the heart. *The Journal of Physiology.* 1913;46:141-150
162. Pauza DH, Saburkina I, Rysevaite K, Inokaitis H, Jokubauskas M, Jalife J, Pauziene N. Neuroanatomy of the murine cardiac conduction system: A combined stereomicroscopic and fluorescence immunohistochemical study. *Auton Neurosci*. 2013;176:32-47
163. Rysevaite K, Saburkina I, Pauziene N, Vaitkevicius R, Noujaim SF, Jalife J, Pauza DH. Immunohistochemical characterization of the intrinsic cardiac neural plexus in whole-mount mouse heart preparations. *Heart Rhythm*. 2011;8:731-738
164. Zang WJ, Chen LN, Yu XJ. Progress in the study of vagal control of cardiac ventricles. *Sheng Li Xue Bao*. 2005;57:659-672
165. Batulevicius D, Pauziene N, Pauza DH. Architecture and age-related analysis of the neuronal number of the guinea pig intrinsic cardiac nerve plexus. *Ann Anat*. 2005;187:225-243
166. Blomquist TM, Priola DV, Romero AM. Source of intrinsic innervation of canine ventricles: A functional study. *The American Journal of Physiology*. 1987;252:H638-644
167. Ulphani JS, Cain JH, Inderyas F, Gordon D, Gikas PV, Shade G, Mayor D, Arora R, Kadish AH, Goldberger JJ. Quantitative analysis of parasympathetic innervation of the porcine heart. *Heart Rhythm*. 2010;7:1113-1119
168. Pauza DH, Pauziene N, Pakeltyte G, Stropus R. Comparative quantitative study of the intrinsic cardiac ganglia and neurons in the rat, guinea pig, dog and human as revealed by histochemical staining for acetylcholinesterase. *Ann Anat*. 2002;184:125-136
169. Pardini BJ, Patel KP, Schmid PG, Lund DD. Location, distribution and projections of intracardiac ganglion cells in the rat. *Journal of the Autonomic Nervous System.* 1987;20:91-101
170. Fields JZ, Roeske WR, Morkin E, Yamamura HI. Cardiac muscarinic cholinergic receptors. Biochemical identification and characterization. *The Journal of Biological Chemistry.* 1978;253:3251-3258
171. Yamada S, Yamamura HI, Roeske WR. The regulation of cardiac alpha 1-adrenergic receptors by guanine nucleotides and by muscarinic cholinergic agonists. *European Journal of Pharmacology.* 1980;63:239-241
172. Mittmann C, Pinkepank G, Stamatelopoulou S, Wieland T, Nurnberg B, Hirt S, Eschenhagen T. Differential coupling of m-cholinoceptors to gi/go-proteins

in failing human myocardium. *Journal of Molecular and Cellular Cardiology.* 2003;35:1241-1249
173. Crick SJ, Anderson RH, Ho SY, Sheppard MN. Localisation and quantitation of autonomic innervation in the porcine heart ii: Endocardium, myocardium and epicardium. *J Anat*. 1999;195 (Pt 3):359-373
174. Akiyama T, Yamazaki T, Ninomiya I. In vivo detection of endogenous acetylcholine release in cat ventricles. *The American Journal of Physiology*. 1994;266:H854-860
175. Shimizu S, Akiyama T, Kawada T, Shishido T, Yamazaki T, Kamiya A, Mizuno M, Sano S, Sugimachi M. In vivo direct monitoring of vagal acetylcholine release to the sinoatrial node. *Auton Neurosci*. 2009;148:44-49
176. Nalivaiko E, Antunes VR, Paton JF. Control of cardiac contractility in the rat working heart-brainstem preparation. *Experimental Physiology.* 2010;95:107-119
177. Brack KE, Coote JH, Ng GA. The effect of direct autonomic nerve stimulation on left ventricular force in the isolated innervated langendorff perfused rabbit heart. *Auton Neurosci*. 2006;124:69-80
178. Lewis ME, Al-Khalidi AH, Bonser RS, Clutton-Brock T, Morton D, Paterson D, Townend JN, Coote JH. Vagus nerve stimulation decreases left ventricular contractility in vivo in the human and pig heart. *The Journal of Physiology.* 2001;534:547-552
179. Sears CE, Choate JK, Paterson DJ. Effect of nitric oxide synthase inhibition on the sympatho-vagal contol of heart rate. *Journal of the Autonomic Nervous System.* 1998;73:63-73
180. Conlon K, Collins T, Kidd C. Modulation of vagal actions on heart rate produced by inhibition of nitric oxide synthase in the anaesthetized ferret. *Experimental Physiology.* 1996;81:547-550
181. Conlon K, Kidd C. Neuronal nitric oxide facilitates vagal chronotropic and dromotropic actions on the heart. *Journal of the Autonomic Nervous System.* 1999;75:136-146
182. Mohan RM, Heaton DA, Danson EJ, Krishnan SP, Cai S, Channon KM, Paterson DJ. Neuronal nitric oxide synthase gene transfer promotes cardiac vagal gain of function. *Circulation Research*. 2002;91:1089-1091
183. Paton JF, Kasparov S, Paterson DJ. Nitric oxide and autonomic control of heart rate: A question of specificity. *Trends Neurosci*. 2002;25:626-631
184. Li D, Wang L, Lee CW, Dawson TA, Paterson DJ. Noradrenergic cell specific gene transfer with neuronal nitric oxide synthase reduces cardiac sympathetic neurotransmission in hypertensive rats. *Hypertension*. 2007;50:69-74
185. Wang L, Henrich M, Buckler KJ, McMenamin M, Mee CJ, Sattelle DB, Paterson DJ. Neuronal nitric oxide synthase gene transfer decreases [ca2+]i in cardiac sympathetic neurons. *Journal of Molecular and Cellular Cardiology.* 2007;43:717-725
186. Higgins CB, Vatner SF, Braunwald E. Parasympathetic control of the heart. *Pharmacol Rev*. 1973;25:119-155
187. Sarnoff SJ, Brockman SK, Gilmore JP, Linden RJ, Mitchell JH. Regulation of ventricular contraction. Influence of cardiac sympathetic and vagal nerve stimulation on atrial and ventricular dynamics. *Circulation Research*. 1960;8:1108-1122

188. Garcia Perez M, Jordan D. Effect of stimulating non-myelinated vagal axons on atrio-ventricular conduction and left ventricular function in anaesthetized rabbits. *Auton Neurosci*. 2001;86:183-191
189. Kent KM, Smith ER, Redwood DR, Epstein SE. Beneficial electrophysiologic effects of nitroglycerin during acute myocardial infarction. *Am J Cardiol*. 1974;33:513-516
190. Borer JS, Kent KM, Goldstein RE, Epstein SE. Nitroglycerin-induced reduction in the incidence of spontaneous ventricular fibrillation during coronary occlusion in dogs. *Am J Cardiol*. 1974;33:517-520
191. Knoebel SB, Rasmussen S, Noble RJ, Mihalick MJ. Nitroglycerin and premature ventricular complexes in myocardial infarction. *Br Heart J*. 1975;37:1064-1068
192. Gagnon RM, Lemire J, Beaudet R. Intravenous use of nitroglycerin to control severe ventricular arrhythmias in unstable angina. *Can Med Assoc J*. 1980;123:1131-1133
193. Lascano EC, Valle HF, Negroni JA. Nitroglycerin induces late preconditioning against arrhythmias but not stunning in conscious sheep. *Scand Cardiovasc J*. 2007;41:160-166
194. Rickover O, Zinman T, Kaplan D, Shainberg A. Exogenous nitric oxide triggers classic ischemic preconditioning by preventing intracellular ca2+ overload in cardiomyocytes. *Cell Calcium*. 2008;43:324-333
195. Vegh A, Szekeres L, Parratt J. Preconditioning of the ischaemic myocardium; involvement of the l-arginine nitric oxide pathway. *Br J Pharmacol*. 1992;107:648-652
196. Pabla R, Curtis MJ. Effects of no modulation on cardiac arrhythmias in the rat isolated heart. *Circulation Research*. 1995;77:984-992
197. Kim YD, Chen B, Beauregard J, Kouretas P, Thomas G, Farhat MY, Myers AK, Lees DE. 17 beta-estradiol prevents dysfunction of canine coronary endothelium and myocardium and reperfusion arrhythmias after brief ischemia/reperfusion. *Circulation*. 1996;94:2901-2908
198. Chen CC, Lin CC, Lee TM. 17beta-estradiol decreases vulnerability to ventricular arrhythmias by preserving connexin43 protein in infarcted rats. *European Journal of Pharmacology*. 2010;629:73-81
199. Burger DE, Xiang FL, Hammoud L, Jones DL, Feng Q. Erythropoietin protects the heart from ventricular arrhythmia during ischemia and reperfusion via neuronal nitric-oxide synthase. *J Pharmacol Exp Ther*. 2009;329:900-907
200. Barnes CS, Coker SJ. Failure of nitric oxide donors to alter arrhythmias induced by acute myocardial ischaemia or reperfusion in anaesthetized rats. *Br J Pharmacol*. 1995;114:349-356
201. Pabla R, Curtis MJ. Nitric oxide fails to confer endogenous antiarrhythmic cardioprotection in the primate heart in vitro. *Br J Pharmacol*. 2007;150:893-898
202. Kubota I, Han X, Opel DJ, Zhao YY, Baliga R, Huang P, Fishman MC, Shannon RP, Michel T, Kelly RA. Increased susceptibility to development of triggered activity in myocytes from mice with targeted disruption of endothelial nitric oxide synthase. *Journal of Molecular and Cellular Cardiology*. 2000;32:1239-1248
203. Rakhit A, Maguire CT, Wakimoto H, Gehrmann J, Li GK, Kelly RA, Michel T, Berul CI. In vivo electrophysiologic studies in endothelial nitric oxide

synthase (enos)-deficient mice. *J Cardiovasc Electrophysiol*. 2001;12:1295-1301
204. Massion PB, Dessy C, Desjardins F, Pelat M, Havaux X, Belge C, Moulin P, Guiot Y, Feron O, Janssens S, Balligand JL. Cardiomyocyte-restricted overexpression of endothelial nitric oxide synthase (nos3) attenuates beta-adrenergic stimulation and reinforces vagal inhibition of cardiac contraction. *Circulation*. 2004;110:2666-2672
205. Gonzalez DR, Beigi F, Treuer AV, Hare JM. Deficient ryanodine receptor s-nitrosylation increases sarcoplasmic reticulum calcium leak and arrhythmogenesis in cardiomyocytes. *Proceedings of the National Academy of Sciences of the United States of America*. 2007;104:20612-20617
206. Burger DE, Lu X, Lei M, Xiang FL, Hammoud L, Jiang M, Wang H, Jones DL, Sims SM, Feng Q. Neuronal nitric oxide synthase protects against myocardial infarction-induced ventricular arrhythmia and mortality in mice. *Circulation*. 2009;120:1345-1354
207. Mohan RM, Choate JK, Golding S, Herring N, Casadei B, Paterson DJ. Peripheral pre-synaptic pathway reduces the heart rate response to sympathetic activation following exercise training: Role of no. *Cardiovascular Research.* 2000;47:90-98
208. Sears CE, Bryant SM, Ashley EA, Lygate CA, Rakovic S, Wallis HL, Neubauer S, Terrar DA, Casadei B. Cardiac neuronal nitric oxide synthase isoform regulates myocardial contraction and calcium handling. *Circulation Research*. 2003;92:e52-59
209. Casadei B. The emerging role of neuronal nitric oxide synthase in the regulation of myocardial function. *Experimental Physiology.* 2006;91:943-955
210. Burkard N, Rokita AG, Kaufmann SG, Hallhuber M, Wu R, Hu K, Hofmann U, Bonz A, Frantz S, Cartwright EJ, Neyses L, Maier LS, Maier SK, Renne T, Schuh K, Ritter O. Conditional neuronal nitric oxide synthase overexpression impairs myocardial contractility. *Circulation Research*. 2007;100:e32-44
211. Mungrue IN, Gros R, You X, Pirani A, Azad A, Csont T, Schulz R, Butany J, Stewart DJ, Husain M. Cardiomyocyte overexpression of inos in mice results in peroxynitrite generation, heart block, and sudden death. *The Journal of Clinical Investigation.* 2002;109:735-743
212. Kim YM, Kattach H, Ratnatunga C, Pillai R, Channon KM, Casadei B. Association of atrial nicotinamide adenine dinucleotide phosphate oxidase activity with the development of atrial fibrillation after cardiac surgery. *Journal of the American College of Cardiology*. 2008;51:68-74
213. Morita N, Sovari AA, Xie Y, Fishbein MC, Mandel WJ, Garfinkel A, Lin SF, Chen PS, Xie LH, Chen F, Qu Z, Weiss JN, Karagueuzian HS. Increased susceptibility of aged hearts to ventricular fibrillation during oxidative stress. *American Journal of Physiology. Heart and Circulatory Physiology.* 2009;297:H1594-1605
214. Lin YK, Lin FZ, Chen YC, Cheng CC, Lin CI, Chen YJ, Chen SA. Oxidative stress on pulmonary vein and left atrium arrhythmogenesis. *Circ J.* 2010;74:1547-1556
215. Massion PB, Feron O, Dessy C, Balligand JL. Nitric oxide and cardiac function: Ten years after, and continuing. *Circulation Research*. 2003;93:388-398
216. Seddon M, Shah AM, Casadei B. Cardiomyocytes as effectors of nitric oxide signalling. *Cardiovascular Research.* 2007;75:315-326

217. Barouch LA, Harrison RW, Skaf MW, Rosas GO, Cappola TP, Kobeissi ZA, Hobai IA, Lemmon CA, Burnett AL, O'Rourke B, Rodriguez ER, Huang PL, Lima JA, Berkowitz DE, Hare JM. Nitric oxide regulates the heart by spatial confinement of nitric oxide synthase isoforms. *Nature*. 2002;416:337-339
218. Ziolo MT, Kohr MJ, Wang H. Nitric oxide signaling and the regulation of myocardial function. *Journal of Molecular and Cellular Cardiology.* 2008;45:625-632
219. Lohmann SM, Fischmeister R, Walter U. Signal transduction by cgmp in heart. *Basic Research in Cardiology*. 1991;86:503-514
220. Tamargo J, Caballero R, Gomez R, Delpon E. Cardiac electrophysiological effects of nitric oxide. *Cardiovascular Research.* 2010;87:593-600
221. Gonzalez DR, Treuer A, Sun QA, Stamler JS, Hare JM. S-nitrosylation of cardiac ion channels. *J Cardiovasc Pharmacol*. 2009;54:188-195
222. Wang Y, Wagner MB, Joyner RW, Kumar R. Cgmp-dependent protein kinase mediates stimulation of l-type calcium current by cgmp in rabbit atrial cells. *Cardiovascular Research.* 2000;48:310-322
223. Mery PF, Pavoine C, Belhassen L, Pecker F, Fischmeister R. Nitric oxide regulates cardiac ca2+ current. Involvement of cgmp-inhibited and cgmp-stimulated phosphodiesterases through guanylyl cyclase activation. *The Journal of Biological Chemistry.* 1993;268:26286-26295
224. Wahler GM, Dollinger SJ. Nitric oxide donor sin-1 inhibits mammalian cardiac calcium current through cgmp-dependent protein kinase. *The American Journal of Physiology*. 1995;268:C45-54
225. Sun J, Morgan M, Shen RF, Steenbergen C, Murphy E. Preconditioning results in s-nitrosylation of proteins involved in regulation of mitochondrial energetics and calcium transport. *Circulation Research*. 2007;101:1155-1163
226. Sun J, Picht E, Ginsburg KS, Bers DM, Steenbergen C, Murphy E. Hypercontractile female hearts exhibit increased s-nitrosylation of the l-type ca2+ channel alpha1 subunit and reduced ischemia/reperfusion injury. *Circulation Research*. 2006;98:403-411
227. Han X, Shimoni Y, Giles WR. An obligatory role for nitric oxide in autonomic control of mammalian heart rate. *The Journal of Physiology.* 1994;476:309-314
228. Abi-Gerges N, Fischmeister R, Mery PF. G protein-mediated inhibitory effect of a nitric oxide donor on the l-type ca2+ current in rat ventricular myocytes. *The Journal of Physiology.* 2001;531:117-130
229. Vandecasteele G, Eschenhagen T, Fischmeister R. Role of the no-cgmp pathway in the muscarinic regulation of the l-type ca2+ current in human atrial myocytes. *The Journal of Physiology.* 1998;506 (Pt 3):653-663
230. Taglialatela M, Pannaccione A, Iossa S, Castaldo P, Annunziato L. Modulation of the k(+) channels encoded by the human ether-a-gogo-related gene-1 (herg1) by nitric oxide. *Mol Pharmacol*. 1999;56:1298-1308
231. Tamargo J, Caballero R, Gomez R, Valenzuela C, Delpon E. Pharmacology of cardiac potassium channels. *Cardiovascular Research.* 2004;62:9-33
232. Bai CX, Takahashi K, Masumiya H, Sawanobori T, Furukawa T. Nitric oxide-dependent modulation of the delayed rectifier k+ current and the l-type ca2+ current by ginsenoside re, an ingredient of panax ginseng, in guinea-pig cardiomyocytes. *Br J Pharmacol*. 2004;142:567-575

233. Bai CX, Namekata I, Kurokawa J, Tanaka H, Shigenobu K, Furukawa T. Role of nitric oxide in ca2+ sensitivity of the slowly activating delayed rectifier k+ current in cardiac myocytes. *Circulation Research*. 2005;96:64-72
234. Gomez R, Caballero R, Barana A, Amoros I, Calvo E, Lopez JA, Klein H, Vaquero M, Osuna L, Atienza F, Almendral J, Pinto A, Tamargo J, Delpon E. Nitric oxide increases cardiac ik1 by nitrosylation of cysteine 76 of kir2.1 channels. *Circulation Research*. 2009;105:383-392
235. Michael G, Xiao L, Qi XY, Dobrev D, Nattel S. Remodelling of cardiac repolarization: How homeostatic responses can lead to arrhythmogenesis. *Cardiovascular Research.* 2009;81:491-499
236. Abi-Gerges N, Szabo G, Otero AS, Fischmeister R, Mery PF. No donors potentiate the beta-adrenergic stimulation of i(ca,l) and the muscarinic activation of i(k,ach) in rat cardiac myocytes. *The Journal of Physiology.* 2002;540:411-424
237. Shinbo A, Iijima T. Potentiation by nitric oxide of the atp-sensitive k+ current induced by k+ channel openers in guinea-pig ventricular cells. *Br J Pharmacol*. 1997;120:1568-1574
238. Han J, Kim N, Joo H, Kim E, Earm YE. Atp-sensitive k(+) channel activation by nitric oxide and protein kinase g in rabbit ventricular myocytes. *American Journal of Physiology. Heart and Circulatory Physiology.* 2002;283:H1545-1554
239. Cuong DV, Kim N, Youm JB, Joo H, Warda M, Lee JW, Park WS, Kim T, Kang S, Kim H, Han J. Nitric oxide-cgmp-protein kinase g signaling pathway induces anoxic preconditioning through activation of atp-sensitive k+ channels in rat hearts. *American Journal of Physiology. Heart and Circulatory Physiology.* 2006;290:H1808-1817
240. Ziolo MT, Harshbarger CH, Roycroft KE, Smith JM, Romano FD, Sondgeroth KL, Wahler GM. Myocytes isolated from rejecting transplanted rat hearts exhibit a nitric oxide-mediated reduction in the calcium current. *Journal of Molecular and Cellular Cardiology.* 2001;33:1691-1699
241. Danik SB, Rosner G, Lader J, Gutstein DE, Fishman GI, Morley GE. Electrical remodeling contributes to complex tachyarrhythmias in connexin43-deficient mouse hearts. *Faseb J*. 2008;22:1204-1212
242. Gutstein DE, Morley GE, Tamaddon H, Vaidya D, Schneider MD, Chen J, Chien KR, Stuhlmann H, Fishman GI. Conduction slowing and sudden arrhythmic death in mice with cardiac-restricted inactivation of connexin43. *Circulation Research*. 2001;88:333-339
243. Danik SB, Liu F, Zhang J, Suk HJ, Morley GE, Fishman GI, Gutstein DE. Modulation of cardiac gap junction expression and arrhythmic susceptibility. *Circulation Research*. 2004;95:1035-1041
244. Gonczi M, Papp R, Kovacs M, Seprenyi G, Vegh A. Modulation of gap junctions by nitric oxide contributes to the anti-arrhythmic effect of sodium nitroprusside? *Br J Pharmacol*. 2009;156:786-793
245. Rodenas J, Mitjavila MT, Carbonell T. Nitric oxide inhibits superoxide production by inflammatory polymorphonuclear leukocytes. *The American Journal of Physiology*. 1998;274:C827-830
246. Clancy RM, Leszczynska-Piziak J, Abramson SB. Nitric oxide, an endothelial cell relaxation factor, inhibits neutrophil superoxide anion production via a direct action on the nadph oxidase. *The Journal of Clinical Investigation.* 1992;90:1116-1121

247. Sohn HY, Krotz F, Gloe T, Keller M, Theisen K, Klauss V, Pohl U. Differential regulation of xanthine and nad(p)h oxidase by hypoxia in human umbilical vein endothelial cells. Role of nitric oxide and adenosine. *Cardiovascular Research.* 2003;58:638-646
248. Rodrigo R, Vinay J, Castillo R, Cereceda M, Asenjo R, Zamorano J, Araya J, Castillo-Koch R, Espinoza J, Larrain E. Use of vitamins c and e as a prophylactic therapy to prevent postoperative atrial fibrillation. *Int J Cardiol*. 2010;138:221-228
249. Kiss A, Juhasz L, Seprenyi G, Kupai K, Kaszaki J, Vegh A. The role of nitric oxide, superoxide and peroxynitrite in the anti-arrhythmic effects of preconditioning and peroxynitrite infusion in anaesthetized dogs. *Br J Pharmacol*. 2010;160:1263-1272
250. Burger D, Lei M, Geoghegan-Morphet N, Lu X, Xenocostas A, Feng Q. Erythropoietin protects cardiomyocytes from apoptosis via up-regulation of endothelial nitric oxide synthase. *Cardiovascular Research.* 2006;72:51-59
251. Feuerstein GZ. Apoptosis in cardiac diseases--new opportunities for novel therapeutics for heart diseases. *Cardiovasc Drugs Ther*. 1999;13:289-294
252. Dawson TA, Li D, Woodward T, Barber Z, Wang L, Paterson DJ. Cardiac cholinergic no-cgmp signaling following acute myocardial infarction and nnos gene transfer. *Am J Physiol Heart Circ Physiol*. 2008;295:H990-H998
253. Heaton DA, Li D, Almond SC, Dawson TA, Wang L, Channon KM, Paterson DJ. Gene transfer of neuronal nitric oxide synthase into intracardiac ganglia reverses vagal impairment in hypertensive rats. *Hypertension*. 2007;49:380-388
254. Heaton DA, Lei M, Li D, Golding S, Dawson TA, Mohan RM, Paterson DJ. Remodeling of the cardiac pacemaker l-type calcium current and its beta-adrenergic responsiveness in hypertension after neuronal no synthase gene transfer. *Hypertension*. 2006;48:443-452
255. Kleiger RE, Miller JP, Bigger JT, Jr., Moss AJ. Decreased heart rate variability and its association with increased mortality after acute myocardial infarction. *Am J Cardiol*. 1987;59:256-262
256. Cohn PF. When is concern about silent myocardial ischemia justified? *Ann Intern Med*. 1984;100:597-599
257. Schlaich MP, Kaye DM, Lambert E, Sommerville M, Socratous F, Esler MD. Relation between cardiac sympathetic activity and hypertensive left ventricular hypertrophy. *Circulation*. 2003;108:560-565
258. Levy D, Garrison RJ, Savage DD, Kannel WB, Castelli WP. Prognostic implications of echocardiographically determined left ventricular mass in the framingham heart study. *The New England Journal of Medicine*1990;322:1561-1566
259. De Ferrari GM, Vanoli E, Stramba-Badiale M, Hull SS, Jr., Foreman RD, Schwartz PJ. Vagal reflexes and survival during acute myocardial ischemia in conscious dogs with healed myocardial infarction. *The American Journal of Physiology*. 1991;261:H63-69
260. Danson EJ, Paterson DJ. Enhanced neuronal nitric oxide synthase expression is central to cardiac vagal phenotype in exercise-trained mice. *The Journal of Physiology.* 2003;546:225-232
261. Langewitz W, Ruddel H, Schachinger H. Reduced parasympathetic cardiac control in patients with hypertension at rest and under mental stress. *Am Heart J*. 1994;127:122-128

262. Randomised trial of intravenous atenolol among 16 027 cases of suspected acute myocardial infarction: Isis-1. First international study of infarct survival collaborative group. *Lancet*. 1986;2:57-66
263. Pfeffer MA, Braunwald E, Moye LA, Basta L, Brown EJ, Jr., Cuddy TE, Davis BR, Geltman EM, Goldman S, Flaker GC, et al. Effect of captopril on mortality and morbidity in patients with left ventricular dysfunction after myocardial infarction. Results of the survival and ventricular enlargement trial. The save investigators. *The New England Journal of Medicine*1992;327:669-677
264. Association AS. National out of hospital cardiac arrest project. 2006
265. Herring N, Lokale MN, Danson EJ, Heaton DA, Paterson DJ. Neuropeptide y reduces acetylcholine release and vagal bradycardia via a y2 receptor-mediated, protein kinase c-dependent pathway. *Journal of Molecular and Cellular Cardiology.* 2008;44:477-485
266. Herring N, Cranley J, Lokale MN, Li D, Shanks J, Alston EN, Girard BM, Carter E, Parsons RL, Habecker BA, Paterson DJ. The cardiac sympathetic co-transmitter galanin reduces acetylcholine release and vagal bradycardia: Implications for neural control of cardiac excitability. *Journal of Molecular and Cellular Cardiology.* 2012;52:667-676
267. Burnstock G. Do some nerve cells release more than one transmitter? *Neuroscience*. 1976;1:239-248
268. Strata P, Harvey R. Dale's principle. *Brain Res Bull*. 1999;50:349-350
269. Eccles J. From electrical to chemical transmission in the central nervous system. *Notes Rec R Soc Lond*. 1976;30:219-230
270. Burnstock G. Autonomic neurotransmission: 60 years since sir henry dale. *Annu Rev Pharmacol Toxicol*. 2009;49:1-30
271. Burnstock G. Cotransmission. *Curr Opin Pharmacol*. 2004;4:47-52
272. Labrakakis C, Tong CK, Weissman T, Torsney C, MacDermott AB. Localization and function of atp and gabaa receptors expressed by nociceptors and other postnatal sensory neurons in rat. *The Journal of Physiology.* 2003;549:131-142
273. Merighi A. Costorage and coexistence of neuropeptides in the mammalian cns. *Prog Neurobiol*. 2002;66:161-190
274. Wu LJ, Li Y, Xu TL. Co-release and interaction of two inhibitory co-transmitters in rat sacral dorsal commissural neurons. *Neuroreport*. 2002;13:977-981
275. Potter EK. Peripheral inhibition of the parasympathetic nervous system by angiotensin. *Clin Exp Pharmacol Physiol Suppl*. 1982;7:51-55
276. Lindh B, Staines W, Hokfelt T, Terenius L, Salvaterra PM. Immunohistochemical demonstration of choline acetyltransferase-immunoreactive preganglionic nerve fibers in guinea pig autonomic ganglia. *Proceedings of the National Academy of Sciences of the United States of America*. 1986;83:5316-5320
277. Kummer W. Galanin- and neuropeptide y-like immunoreactivities coexist in paravertebral sympathetic neurones of the cat. *Neurosci Lett*. 1987;78:127-131
278. Warner MR, Levy MN. Sinus and atrioventricular nodal distribution of sympathetic fibers that contain neuropeptide y. *Circulation Research*. 1990;67:713-721
279. Manabe N, Foldes FF, Torocsik A, Nagashima H, Goldiner PL, Vizi ES. Presynaptic interaction between vagal and sympathetic innervation in the

heart: Modulation of acetylcholine and noradrenaline release. *Journal of the Autonomic Nervous System.* 1991;32:233-242
280. Schwertfeger E, Klein T, Vonend O, Oberhauser V, Stegbauer J, Rump LC. Neuropeptide y inhibits acetylcholine release in human heart atrium by activation of y2-receptors. *Naunyn Schmiedebergs Arch Pharmacol*. 2004;369:455-461
281. Tatemoto K, Rokaeus A, Jornvall H, McDonald TJ, Mutt V. Galanin - a novel biologically active peptide from porcine intestine. *FEBS Lett*. 1983;164:124-128
282. Jacobowitz DM, Kresse A, Skofitsch G. Galanin in the brain: Chemoarchitectonics and brain cartography--a historical review. *Peptides*. 2004;25:433-464
283. Walton KM, Chin JE, Duplantier AJ, Mather RJ. Galanin function in the central nervous system. *Curr Opin Drug Discov Devel*. 2006;9:560-570
284. Diaz-Cabiale Z, Parrado C, Narvaez M, Millon C, Puigcerver A, Fuxe K, Narvaez JA. Neurochemical modulation of central cardiovascular control: The integrative role of galanin. *Exs*. 2010;102:113-131
285. Potter EK, Smith-White MA. Galanin modulates cholinergic neurotransmission in the heart. *Neuropeptides*. 2005;39:345-348
286. Boudaka A, Worl J, Shiina T, Shimizu Y, Takewaki T, Neuhuber WL. Galanin modulates vagally induced contractions in the mouse oesophagus. *Neurogastroenterol Motil*. 2009;21:180-188
287. Kowalyk S, Veith R, Boyle M, Taborsky GJ, Jr. Liver releases galanin during sympathetic nerve stimulation. *The American Journal of Physiology*. 1992;262:E671-678
288. Tatemoto K, Carlquist M, Mutt V. Neuropeptide y--a novel brain peptide with structural similarities to peptide yy and pancreatic polypeptide. *Nature*. 1982;296:659-660
289. Adrian TE, Gu J, Allen JM, Tatemoto K, Polak JM, Bloom SR. Neuropeptide y in the human male genital tract. *Life Sci*. 1984;35:2643-2648
290. McDermott BJ, Bell D. Npy and cardiac diseases. *Curr Top Med Chem*. 2007;7:1692-1703
291. Westfall TC. Neuropeptide y and sympathetic control of vascular tone in hypertension. *Exs*. 2006:89-103
292. Shah SH, Freedman NJ, Zhang L, Crosslin DR, Stone DH, Haynes C, Johnson J, Nelson S, Wang L, Connelly JJ, Muehlbauer M, Ginsburg GS, Crossman DC, Jones CJ, Vance J, Sketch MH, Granger CB, Newgard CB, Gregory SG, Goldschmidt-Clermont PJ, Kraus WE, Hauser ER. Neuropeptide y gene polymorphisms confer risk of early-onset atherosclerosis. *PLoS Genet*. 2009;5:e1000318
293. Han C, Wang XA, Fiscus RR, Gu J, McDonald JK. Changes in cardiac neuropeptide y after experimental myocardial infarction in rat. *Neurosci Lett*. 1989;104:141-146
294. Hulting J, Sollevi A, Ullman B, Franco-Cereceda A, Lundberg JM. Plasma neuropeptide y on admission to a coronary care unit: Raised levels in patients with left heart failure. *Cardiovascular Research.* 1990;24:102-108
295. Ullman B, Hulting J, Lundberg JM. Prognostic value of plasma neuropeptide-y in coronary care unit patients with and without acute myocardial infarction. *European Heart Journal.* 1994;15:454-461

296. Cuculi F, Herring N, De Caterina AR, Banning AP, Prendergast BD, Forfar JC, Choudhury RP, Channon KM, Kharbanda RK. Relationship of plasma neuropeptide y with angiographic, electrocardiographic and coronary physiology indices of reperfusion during st elevation myocardial infarction. *Heart*. 2013;99:1198-1203
297. Warner MR, Senanayake PD, Ferrario CM, Levy MN. Sympathetic stimulation-evoked overflow of norepinephrine and neuropeptide y from the heart. *Circulation Research*. 1991;69:455-465
298. Smith-White MA, Herzog H, Potter EK. Role of neuropeptide y y(2) receptors in modulation of cardiac parasympathetic neurotransmission. *Regul Pept*. 2002;103:105-111
299. Chottova Dvorakova M, Wiegand S, Pesta M, Slavikova J, Grau V, Reischig J, Kuncova J, Kummer W. Expression of neuropeptide y and its receptors y1 and y2 in the rat heart and its supplying autonomic and spinal sensory ganglia in experimentally induced diabetes. *Neuroscience*. 2008;151:1016-1028
300. Jonsson-Rylander AC, Nordlander M, Svindland A, Ilebekk A. Distribution of neuropeptide y y1 and y2 receptors in the postmortem human heart. *Peptides*. 2003;24:255-262
301. Potter E. Presynaptic inhibition of cardiac vagal postganglionic nerves by neuropeptide y. *Neurosci Lett*. 1987;83:101-106
302. Warner MR, Levy MN. Inhibition of cardiac vagal effects by neurally released and exogenous neuropeptide y. *Circulation Research*. 1989;65:1536-1546
303. Potter EK. Cardiac vagal action and plasma levels of neuropeptide y following intravenous injection in the dog. *Neurosci Lett*. 1987;77:243-247
304. Zhao HC, Liu ZB, Feng QL, Cui XL, Zhang CM, Wu BW. [effects of neuropeptide y on ion channels in ventricular myocytes]. *Sheng Li Xue Bao*. 2006;58:225-231
305. Heredia MP, Fernandez-Velasco M, Benito G, Delgado C. Neuropeptide y increases 4-aminopyridine-sensitive transient outward potassium current in rat ventricular myocytes. *Br J Pharmacol*. 2002;135:1701-1706
306. Bryant SM, Hart G. Effects of neuropeptide y on l-type calcium current in guinea-pig ventricular myocytes. *Br J Pharmacol*. 1996;118:1455-1460
307. Millar BC, Weis T, Piper HM, Weber M, Borchard U, McDermott BJ, Balasubramaniam A. Positive and negative contractile effects of neuropeptide y on ventricular cardiomyocytes. *The American Journal of Physiology*. 1991;261:H1727-1733
308. Heredia Mdel P, Delgado C, Pereira L, Perrier R, Richard S, Vassort G, Benitah JP, Gomez AM. Neuropeptide y rapidly enhances [ca2+]i transients and ca2+ sparks in adult rat ventricular myocytes through y1 receptor and plc activation. *Journal of Molecular and Cellular Cardiology*. 2005;38:205-212
309. Gross SS JC, Hattori Y and Raman CS. Tetrahydrobiopterin: An essential cofactor of nitric oxide synthesis with an elusive role. In: LJ I, ed. *Nitric oxide: Biology and pathobiology*. Portland, OR: Academic Press; 2000:167-185.
310. Klatt P, Schmidt K, Lehner D, Glatter O, Bachinger HP, Mayer B. Structural analysis of porcine brain nitric oxide synthase reveals a role for tetrahydrobiopterin and l-arginine in the formation of an sds-resistant dimer. *Embo J*. 1995;14:3687-3695
311. Liu Q, Gross SS. Binding sites of nitric oxide synthases. *Methods Enzymol*. 1996;268:311-324

312. Lee CK, Han JS, Won KJ, Jung SH, Park HJ, Lee HM, Kim J, Park YS, Kim HJ, Park PJ, Park TK, Kim B. Diminished expression of dihydropteridine reductase is a potent biomarker for hypertensive vessels. *Proteomics*. 2009;9:4851-4858
313. Feletou M, Vanhoutte PM. Endothelial dysfunction: A multifaceted disorder (the wiggers award lecture). *American Journal of Physiology. Heart and Circulatory Physiology*. 2006;291:H985-1002
314. Crabtree MJ, Tatham AL, Al-Wakeel Y, Warrick N, Hale AB, Cai S, Channon KM, Alp NJ. Quantitative regulation of intracellular endothelial nitric-oxide synthase (enos) coupling by both tetrahydrobiopterin-enos stoichiometry and biopterin redox status: Insights from cells with tet-regulated gtp cyclohydrolase i expression. *J Biol Chem*. 2009;284:1136-1144
315. Tatham AL, Crabtree MJ, Warrick N, Cai S, Alp NJ, Channon KM. Gtp cyclohydrolase i expression, protein, and activity determine intracellular tetrahydrobiopterin levels, independent of gtp cyclohydrolase feedback regulatory protein expression. *The Journal of Biological Chemistry*. 2009;284:13660-13668
316. Khoo JP, Zhao L, Alp NJ, Bendall JK, Nicoli T, Rockett K, Wilkins MR, Channon KM. Pivotal role for endothelial tetrahydrobiopterin in pulmonary hypertension. *Circulation*. 2005;111:2126-2133
317. Alp NJ, Mussa S, Khoo J, Cai S, Guzik T, Jefferson A, Goh N, Rockett KA, Channon KM. Tetrahydrobiopterin-dependent preservation of nitric oxide-mediated endothelial function in diabetes by targeted transgenic gtp-cyclohydrolase i overexpression. *The Journal of Clinical Investigation*. 2003;112:725-735
318. Alp NJ, McAteer MA, Khoo J, Choudhury RP, Channon KM. Increased endothelial tetrahydrobiopterin synthesis by targeted transgenic gtp-cyclohydrolase i overexpression reduces endothelial dysfunction and atherosclerosis in apoe-knockout mice. *Arteriosclerosis, Thrombosis, and Vascular Biology*. 2004;24:445-450
319. Bendall JK, Douglas G, McNeill E, Channon KM, Crabtree MJ. Tetrahydrobiopterin in cardiovascular health and disease. *Antioxid Redox Signal*. 2014;20:3040-3077
320. Antoniades C, Shirodaria C, Van Assche T, Cunnington C, Tegeder I, Lotsch J, Guzik TJ, Leeson P, Diesch J, Tousoulis D, Stefanadis C, Costigan M, Woolf CJ, Alp NJ, Channon KM. Gch1 haplotype determines vascular and plasma biopterin availability in coronary artery disease effects on vascular superoxide production and endothelial function. *Journal of the American College of Cardiology*. 2008;52:158-165
321. Mitchell BM, Dorrance AM, Webb RC. Gtp cyclohydrolase 1 inhibition attenuates vasodilation and increases blood pressure in rats. *American Journal of Physiology. Heart and Circulatory Physiology*. 2003;285:H2165-2170
322. Cosentino F, Katusic ZS. Tetrahydrobiopterin and dysfunction of endothelial nitric oxide synthase in coronary arteries. *Circulation*. 1995;91:139-144
323. Xie HH, Zhou S, Chen DD, Channon KM, Su DF, Chen AF. Gtp cyclohydrolase i/bh4 pathway protects epcs via suppressing oxidative stress and thrombospondin-1 in salt-sensitive hypertension. *Hypertension*. 2010;56:1137-1144
324. Douglas G, Van Kampen E, Hale AB, McNeill E, Patel J, Crabtree MJ, Ali Z, Hoerr RA, Alp NJ, Channon KM. Endothelial cell repopulation after stenting

determines in-stent neointima formation: Effects of bare-metal vs. Drug-eluting stents and genetic endothelial cell modification. *European Heart Journal.* 2013;34:3378-3388
325. Chuaiphichai S, McNeill E, Douglas G, Crabtree MJ, Bendall JK, Hale AB, Alp NJ, Channon KM. Cell-autonomous role of endothelial gtp cyclohydrolase 1 and tetrahydrobiopterin in blood pressure regulation. *Hypertension*. 2014;64:530-540
326. Kang KT, Sullivan JC, Spradley FT, d'Uscio LV, Katusic ZS, Pollock JS. Antihypertensive therapy increases tetrahydrobiopterin levels and no/cgmp signaling in small arteries of angiotensin ii-infused hypertensive rats. *American Journal of Physiology. Heart and Circulatory Physiology.* 2011;300:H718-724
327. Kase H, Hashikabe Y, Uchida K, Nakanishi N, Hattori Y. Supplementation with tetrahydrobiopterin prevents the cardiovascular effects of angiotensin ii-induced oxidative and nitrosative stress. *Journal of Hypertension*. 2005;23:1375-1382
328. Hong HJ, Hsiao G, Cheng TH, Yen MH. Supplemention with tetrahydrobiopterin suppresses the development of hypertension in spontaneously hypertensive rats. *Hypertension*. 2001;38:1044-1048
329. Schmidt TS, McNeill E, Douglas G, Crabtree MJ, Hale AB, Khoo J, O'Neill CA, Cheng A, Channon KM, Alp NJ. Tetrahydrobiopterin supplementation reduces atherosclerosis and vascular inflammation in apolipoprotein e-knockout mice. *Clinical Science*. 2010;119:131-142
330. Eskurza I, Myerburgh LA, Kahn ZD, Seals DR. Tetrahydrobiopterin augments endothelium-dependent dilatation in sedentary but not in habitually exercising older adults. *The Journal of Physiology.* 2005;568:1057-1065
331. Heitzer T, Brockhoff C, Mayer B, Warnholtz A, Mollnau H, Henne S, Meinertz T, Munzel T. Tetrahydrobiopterin improves endothelium-dependent vasodilation in chronic smokers : Evidence for a dysfunctional nitric oxide synthase. *Circulation Research*. 2000;86:E36-41
332. Higashi Y, Sasaki S, Nakagawa K, Fukuda Y, Matsuura H, Oshima T, Chayama K. Tetrahydrobiopterin enhances forearm vascular response to acetylcholine in both normotensive and hypertensive individuals. *Am J Hypertens*. 2002;15:326-332
333. Higashi Y, Sasaki S, Nakagawa K, Kimura M, Noma K, Hara K, Jitsuiki D, Goto C, Oshima T, Chayama K, Yoshizumi M. Tetrahydrobiopterin improves aging-related impairment of endothelium-dependent vasodilation through increase in nitric oxide production. *Atherosclerosis*. 2006;186:390-395
334. Ihlemann N, Rask-Madsen C, Perner A, Dominguez H, Hermann T, Kober L, Torp-Pedersen C. Tetrahydrobiopterin restores endothelial dysfunction induced by an oral glucose challenge in healthy subjects. *American Journal of Physiology. Heart and Circulatory Physiology.* 2003;285:H875-882
335. Pierce GL, Jablonski KL, Walker AE, Seibert SM, DeVan AE, Black SM, Sharma S, Seals DR. Tetrahydrobiopterin supplementation enhances carotid artery compliance in healthy older men: A pilot study. *Am J Hypertens*. 2012;25:1050-1054
336. Stroes E, Kastelein J, Cosentino F, Erkelens W, Wever R, Koomans H, Luscher T, Rabelink T. Tetrahydrobiopterin restores endothelial function in hypercholesterolemia. *The Journal of Clinical Investigation.* 1997;99:41-46

337. Ueda S, Matsuoka H, Miyazaki H, Usui M, Okuda S, Imaizumi T. Tetrahydrobiopterin restores endothelial function in long-term smokers. *Journal of the American College of Cardiology*. 2000;35:71-75
338. Fukuda M, Chayama K, Tsubota A, Kobayashi M, Hashimoto M, Miyano Y, Koike H, Koida I, Arase Y, Saitoh S, Murashima N, Ikeda K, Kumada H. Predictive factors in eradicating hepatitis c virus using a relatively small dose of interferon. *J Gastroenterol Hepatol*. 1998;13:412-418
339. Maier W, Cosentino F, Lutolf RB, Fleisch M, Seiler C, Hess OM, Meier B, Luscher TF. Tetrahydrobiopterin improves endothelial function in patients with coronary artery disease. *J Cardiovasc Pharmacol*. 2000;35:173-178
340. Setoguchi S, Mohri M, Shimokawa H, Takeshita A. Tetrahydrobiopterin improves endothelial dysfunction in coronary microcirculation in patients without epicardial coronary artery disease. *Journal of the American College of Cardiology*. 2001;38:493-498
341. Porkert M, Sher S, Reddy U, Cheema F, Niessner C, Kolm P, Jones DP, Hooper C, Taylor WR, Harrison D, Quyyumi AA. Tetrahydrobiopterin: A novel antihypertensive therapy. *J Hum Hypertens*. 2008;22:401-407
342. Cosentino F, Barker JE, Brand MP, Heales SJ, Werner ER, Tippins JR, West N, Channon KM, Volpe M, Luscher TF. Reactive oxygen species mediate endothelium-dependent relaxations in tetrahydrobiopterin-deficient mice. *Arteriosclerosis, thrombosis, and vascular biology*. 2001;21:496-502
343. Cunnington C, Van Assche T, Shirodaria C, Kylintireas I, Lindsay AC, Lee JM, Antoniades C, Margaritis M, Lee R, Cerrato R, Crabtree MJ, Francis JM, Sayeed R, Ratnatunga C, Pillai R, Choudhury RP, Neubauer S, Channon KM. Systemic and vascular oxidation limits the efficacy of oral tetrahydrobiopterin treatment in patients with coronary artery disease. *Circulation*. 2012;125:1356-1366
344. Feron O, Belhassen L, Kobzik L, Smith TW, Kelly RA, Michel T. Endothelial nitric oxide synthase targeting to caveolae. Specific interactions with caveolin isoforms in cardiac myocytes and endothelial cells. *The Journal of Biological Chemistry*. 1996;271:22810-22814
345. Danson EJ, Choate JK, Paterson DJ. Cardiac nitric oxide: Emerging role for nnos in regulating physiological function. *Pharmacol Ther*. 2005;106:57-74
346. Stoodley M, Weihl CC, Zhang ZD, Lin G, Johns LM, Kowalczuk A, Ghadge G, Roos RP, Macdonald RL. Effect of adenovirus-mediated nitric oxide synthase gene transfer on vasospasm after experimental subarachnoid hemorrhage. *Neurosurgery*. 2000;46:1193-1202; discussion 1202-1193
347. Shah AM, MacCarthy PA. Paracrine and autocrine effects of nitric oxide on myocardial function. *Pharmacology & therapeutics*. 2000;86:49-86
348. Seddon MD, Chowienczyk PJ, Brett SE, Casadei B, Shah AM. Neuronal nitric oxide synthase regulates basal microvascular tone in humans in vivo. *Circulation*. 2008;117:1991-1996
349. Hammond J, Balligand JL. Nitric oxide synthase and cyclic gmp signaling in cardiac myocytes: From contractility to remodeling. *Journal of Molecular and Cellular Cardiology*. 2012;52:330-340
350. Fiedler B, Lohmann SM, Smolenski A, Linnemuller S, Pieske B, Schroder F, Molkentin JD, Drexler H, Wollert KC. Inhibition of calcineurin-nfat hypertrophy signaling by cgmp-dependent protein kinase type i in cardiac myocytes. *Proceedings of the National Academy of Sciences of the United States of America*. 2002;99:11363-11368

351. Schroder F, Klein G, Fiedler B, Bastein M, Schnasse N, Hillmer A, Ames S, Gambaryan S, Drexler H, Walter U, Lohmann SM, Wollert KC. Single l-type ca(2+) channel regulation by cgmp-dependent protein kinase type i in adult cardiomyocytes from pkg i transgenic mice. *Cardiovascular Research.* 2003;60:268-277
352. Sun J, Yamaguchi N, Xu L, Eu JP, Stamler JS, Meissner G. Regulation of the cardiac muscle ryanodine receptor by o(2) tension and s-nitrosoglutathione. *Biochemistry*. 2008;47:13985-13990
353. Gonzalez DR, Treuer AV, Castellanos J, Dulce RA, Hare JM. Impaired s-nitrosylation of the ryanodine receptor caused by xanthine oxidase activity contributes to calcium leak in heart failure. *The Journal of Biological Chemistry*. 2010;285:28938-28945
354. Campbell DL, Stamler JS, Strauss HC. Redox modulation of l-type calcium channels in ferret ventricular myocytes. Dual mechanism regulation by nitric oxide and s-nitrosothiols. *J Gen Physiol*. 1996;108:277-293
355. Chowdhary S, Townend JN. Role of nitric oxide in the regulation of cardiovascular autonomic control. *Clinical Science*. 1999;97:5-17
356. Danson EJ, Li D, Wang L, Dawson TA, Paterson DJ. Targeting cardiac sympatho-vagal imbalance using gene transfer of nitric oxide synthase. *J Mol Cell Cardiol*. 2009;46:482-489
357. Choate JK, Paterson DJ. Nitric oxide inhibits the positive chronotropic and inotropic responses to sympathetic nerve stimulation in the isolated guinea-pig atria. *J Auton Nerv Syst*. 1999;75:100-108
358. Zhang L, Rao F, Zhang K, Khandrika S, Das M, Vaingankar SM, Bao X, Rana BK, Smith DW, Wessel J, Salem RM, Rodriguez-Flores JL, Mahata SK, Schork NJ, Ziegler MG, O'Connor DT. Discovery of common human genetic variants of gtp cyclohydrolase 1 (gch1) governing nitric oxide, autonomic activity, and cardiovascular risk. *J Clin Invest*. 2007;117:2658-2671
359. Ichinose H, Ohye T, Takahashi E, Seki N, Hori T, Segawa M, Nomura Y, Endo K, Tanaka H, Tsuji S, et al. Hereditary progressive dystonia with marked diurnal fluctuation caused by mutations in the gtp cyclohydrolase i gene. *Nat Genet*. 1994;8:236-242
360. Mayahi L, Mason L, Bleasdale-Barr K, Donald A, Trender-Gerhard I, Sweeney MG, Davis MB, Wood N, Mathias CJ, Watson L, Pellerin D, Heales S, Deanfield JE, Bhatia K, Murray-Rust J, Hingorani AD. Endothelial, sympathetic, and cardiac function in inherited (6r)-l-erythro-5,6,7,8-tetrahydro-l-biopterin deficiency. *Circ Cardiovasc Genet*. 2010;3:513-522
361. Adlam D, Herring N, Douglas G, De Bono JP, Li D, Danson EJ, Tatham A, Lu CJ, Jennings KA, Cragg SJ, Casadei B, Paterson DJ, Channon KM. Regulation of beta-adrenergic control of heart rate by gtp-cyclohydrolase 1 (gch1) and tetrahydrobiopterin. *Cardiovascular Research.* 2012;93:694-701
362. Douglas G, Hale AB, Crabtree MJ, Ryan BJ, Hansler A, Watschinger K, Gross SS, Lygate CA, Alp NJ, Channon KM. A requirement for gch1 and tetrahydrobiopterin in embryonic development. *Dev Biol*. 2015;399:129-138
363. Yang S, Lee YJ, Kim JM, Park S, Peris J, Laipis P, Park YS, Chung JH, Oh SP. A murine model for human sepiapterin-reductase deficiency. *American journal of human genetics*. 2006;78:575-587
364. Sumi-Ichinose C, Urano F, Kuroda R, Ohye T, Kojima M, Tazawa M, Shiraishi H, Hagino Y, Nagatsu T, Nomura T, Ichinose H. Catecholamines and serotonin are differently regulated by tetrahydrobiopterin. A study from 6-

pyruvoyltetrahydropterin synthase knockout mice. *The Journal of Biological Chemistry*. 2001;276:41150-41160
365. Kobayashi K, Morita S, Sawada H, Mizuguchi T, Yamada K, Nagatsu I, Hata T, Watanabe Y, Fujita K, Nagatsu T. Targeted disruption of the tyrosine hydroxylase locus results in severe catecholamine depletion and perinatal lethality in mice. *The Journal of Biological Chemistry*. 1995;270:27235-27243
366. Choate JK, Murphy SM, Feldman R, Anderson CR. Sympathetic control of heart rate in nnos knockout mice. *Am J Physiol Heart Circ Physiol*. 2008;294:H354-361
367. Kember G, Armour JA, Zamir M. Neural control of heart rate: The role of neuronal networking. *J Theor Biol*. 2011;277:41-47
368. Harper RM, Kumar R, Ogren JA, Macey PM. Sleep-disordered breathing: Effects on brain structure and function. *Respir Physiol Neurobiol*. 2013;188:383-391
369. McAllen RM, Salo LM, Paton JF, Pickering AE. Processing of central and reflex vagal drives by rat cardiac ganglion neurones: An intracellular analysis. *The Journal of Physiology*. 2011;589:5801-5818
370. Ardell JL, Cardinal R, Vermeulen M, Armour JA. Dorsal spinal cord stimulation obtunds the capacity of intrathoracic extracardiac neurons to transduce myocardial ischemia. *Am J Physiol Regul Integr Comp Physiol*. 2009;297:R470-477
371. Armour JA. Activity of in situ stellate ganglion neurons of dogs recorded extracellularly. *Can J Physiol Pharmacol*. 1986;64:101-111
372. Armour JA. Neuronal activity recorded extracellularly in chronically decentralized in situ canine middle cervical ganglia. *Can J Physiol Pharmacol*. 1986;64:1038-1046
373. Zucker IH, Patel KP, Schultz HD. Neurohumoral stimulation. *Heart Fail Clin*. 2012;8:87-99
374. Gebber GL, Zhong S, Paitel Y. Bispectral analysis of complex patterns of sympathetic nerve discharge. *The American Journal of Physiology*. 1996;271:R1173-1185
375. Hopkins DA, Armour JA. Ganglionic distribution of afferent neurons innervating the canine heart and cardiopulmonary nerves. *Journal of the Autonomic Nervous System*. 1989;26:213-222
376. Brown AM. Excitation of afferent cardiac sympathetic nerve fibres during myocardial ischaemia. *The Journal of Physiology*. 1967;190:35-53
377. Horackova M, Armour JA, Byczko Z. Distribution of intrinsic cardiac neurons in whole-mount guinea pig atria identified by multiple neurochemical coding. A confocal microscope study. *Cell Tissue Res*. 1999;297:409-421
378. Moravec J, Moravec M. Intrinsic nerve plexus of mammalian heart: Morphological basis of cardiac rhythmical activity? *Int Rev Cytol*. 1987;106:89-148
379. Hopkins DA, Armour JA. Localization of sympathetic postganglionic and parasympathetic preganglionic neurons which innervate different regions of the dog heart. *J Comp Neurol*. 1984;229:186-198
380. Plecha DM, Randall WC, Geis GS, Wurster RD. Localization of vagal preganglionic somata controlling sinoatrial and atrioventricular nodes. *The American Journal of Physiology*. 1988;255:R703-708

381. Norris JE, Randall WC. Responses of the canine myocardium to stimulation of thoracic cardiac nerves. *The American Journal of Physiology*. 1977;232:H485-494
382. Forsgren S, Moravec M, Moravec J. Catecholamine-synthesizing enzymes and neuropeptides in rat heart epicardial ganglia; an immunohistochemical study. *Histochem J*. 1990;22:667-676
383. Cheng Z, Powley TL, Schwaber JS, Doyle FJ, 3rd. Vagal afferent innervation of the atria of the rat heart reconstructed with confocal microscopy. *J Comp Neurol*. 1997;381:1-17
384. Burwash IG, Morgan DE, Koilpillai CJ, Blackmore GL, Johnstone DE, Armour JA. Sympathetic stimulation alters left ventricular relaxation and chamber size. *The American Journal of Physiology*. 1993;264:R1-7
385. Armour JA, Collier K, Kember G, Ardell JL. Differential selectivity of cardiac neurons in separate intrathoracic autonomic ganglia. *The American Journal of Physiology*. 1998;274:R939-949
386. Paton JF, Boscan P, Pickering AE, Nalivaiko E. The yin and yang of cardiac autonomic control: Vago-sympathetic interactions revisited. *Brain Res Brain Res Rev*. 2005;49:555-565
387. Hopkins DA, Macdonald SE, Murphy DA, Armour JA. Pathology of intrinsic cardiac neurons from ischemic human hearts. *Anat Rec*. 2000;259:424-436
388. Pappone C, Santinelli V, Manguso F, Vicedomini G, Gugliotta F, Augello G, Mazzone P, Tortoriello V, Landoni G, Zangrillo A, Lang C, Tomita T, Mesas C, Mastella E, Alfieri O. Pulmonary vein denervation enhances long-term benefit after circumferential ablation for paroxysmal atrial fibrillation. *Circulation*. 2004;109:327-334
389. Takahashi Y, Jais P, Hocini M, Sanders P, Rotter M, Rostock T, Hsu LF, Sacher F, Clementy J, Haissaguerre M. Shortening of fibrillatory cycle length in the pulmonary vein during vagal excitation. *Journal of the American College of Cardiology*. 2006;47:774-780
390. Mittal S, Lerman BB. The atrioventricular nodal fat pad in humans: Fat or fiction? *J Cardiovasc Electrophysiol*. 2002;13:740-741
391. Murphy DA, Thompson GW, Ardell JL, McCraty R, Stevenson RS, Sangalang VE, Cardinal R, Wilkinson M, Craig S, Smith FM, Kingma JG, Armour JA. The heart reinnervates after transplantation. *Ann Thorac Surg*. 2000;69:1769-1781
392. Tanguay M, Blaise G, Dumont L, Beique G, Hollmann C. Beneficial effects of volatile anesthetics on decrease in coronary flow and myocardial contractility induced by oxygen-derived free radicals in isolated rabbit hearts. *J Cardiovasc Pharmacol*. 1991;18:863-870
393. Jin C, Sonoda S, Fan L, Watanabe M, Kugimiya T, Okada T. Sevoflurane and nitrous oxide exert cardioprotective effects against hypoxia-reoxygenation injury in the isolated rat heart. *J Physiol Sci*. 2009;59:123-129
394. Maxwell MP, Hearse DJ, Yellon DM. Species variation in the coronary collateral circulation during regional myocardial ischaemia: A critical determinant of the rate of evolution and extent of myocardial infarction. *Cardiovascular Research.* 1987;21:737-746
395. Laurita KR, Girouard SD, Rosenbaum DS. Modulation of ventricular repolarization by a premature stimulus. Role of epicardial dispersion of repolarization kinetics demonstrated by optical mapping of the intact guinea pig heart. *Circulation Research*. 1996;79:493-503

396. Lubbe WF, Podzuweit T, Daries PS, Opie LH. The role of cyclic adenosine monophosphate in adrenergic effects on ventricular vulnerability to fibrillation in the isolated perfused rat heart. *The Journal of Clinical Investigation.* 1978;61:1260-1269
397. Walker MJ, Curtis MJ, Hearse DJ, Campbell RW, Janse MJ, Yellon DM, Cobbe SM, Coker SJ, Harness JB, Harron DW, et al. The lambeth conventions: Guidelines for the study of arrhythmias in ischaemia infarction, and reperfusion. *Cardiovascular Research.* 1988;22:447-455
398. Franz MR. Method and theory of monophasic action potential recording. *Prog Cardiovasc Dis*. 1991;33:347-368
399. Herron TJ, Lee P, Jalife J. Optical imaging of voltage and calcium in cardiac cells & tissues. *Circulation Research*. 2012;110:609-623
400. Salzberg BM, Davila HV, Cohen LB. Optical recording of impulses in individual neurones of an invertebrate central nervous system. *Nature*. 1973;246:508-509
401. Vaquero M, Calvo D, Jalife J. Cardiac fibrillation: From ion channels to rotors in the human heart. *Heart Rhythm*. 2008;5:872-879
402. Omichi C, Lamp ST, Lin SF, Yang J, Baher A, Zhou S, Attin M, Lee MH, Karagueuzian HS, Kogan B, Qu Z, Garfinkel A, Chen PS, Weiss JN. Intracellular ca dynamics in ventricular fibrillation. *American Journal of Physiology. Heart and Circulatory Physiology.* 2004;286:H1836-1844
403. Rogers KL, Martin JR, Renaud O, Karplus E, Nicola MA, Nguyen M, Picaud S, Shorte SL, Brulet P. Electron-multiplying charge-coupled detector-based bioluminescence recording of single-cell ca2+. *J Biomed Opt*. 2008;13:031211
404. Entcheva E, Kostov Y, Tchernev E, Tung L. Fluorescence imaging of electrical activity in cardiac cells using an all-solid-state system. *IEEE Trans Biomed Eng*. 2004;51:333-341
405. Entcheva E, Bien H. Macroscopic optical mapping of excitation in cardiac cell networks with ultra-high spatiotemporal resolution. *Prog Biophys Mol Biol*. 2006;92:232-257
406. Salama G, Hwang SM. Simultaneous optical mapping of intracellular free calcium and action potentials from langendorff perfused hearts. *Curr Protoc Cytom*. 2009;Chapter 12:Unit 12 17
407. Davila HV, Salzberg BM, Cohen LB, Waggoner AS. A large change in axon fluorescence that provides a promising method for measuring membrane potential. *Nat New Biol*. 1973;241:159-160
408. Salama G, Morad M. Merocyanine 540 as an optical probe of transmembrane electrical activity in the heart. *Science*. 1976;191:485-487
409. Di Lisa F, Blank PS, Colonna R, Gambassi G, Silverman HS, Stern MD, Hansford RG. Mitochondrial membrane potential in single living adult rat cardiac myocytes exposed to anoxia or metabolic inhibition. *The Journal of Physiology.* 1995;486 (Pt 1):1-13
410. Hou L, Deo M, Furspan P, Pandit SV, Mironov S, Auerbach DS, Gong Q, Zhou Z, Berenfeld O, Jalife J. A major role for herg in determining frequency of reentry in neonatal rat ventricular myocyte monolayer. *Circulation Research*. 2010;107:1503-1511
411. Cohen LB, Salzberg BM. Optical measurement of membrane potential. *Rev Physiol Biochem Pharmacol*. 1978;83:35-88

412. Fluhler E, Burnham VG, Loew LM. Spectra, membrane binding, and potentiometric responses of new charge shift probes. *Biochemistry*. 1985;24:5749-5755
413. Schaffer P, Ahammer H, Muller W, Koidl B, Windisch H. Di-4-anepps causes photodynamic damage to isolated cardiomyocytes. *Pflugers Arch*. 1994;426:548-551
414. Salama G, Choi BR, Azour G, Lavasani M, Tumbev V, Salzberg BM, Patrick MJ, Ernst LA, Waggoner AS. Properties of new, long-wavelength, voltage-sensitive dyes in the heart. *J Membr Biol*. 2005;208:125-140
415. Baker LC, Wolk R, Choi BR, Watkins S, Plan P, Shah A, Salama G. Effects of mechanical uncouplers, diacetyl monoxime, and cytochalasin-d on the electrophysiology of perfused mouse hearts. *American Journal of Physiology. Heart and Circulatory Physiology*. 2004;287:H1771-1779
416. Cheng Y, Li L, Nikolski V, Wallick DW, Efimov IR. Shock-induced arrhythmogenesis is enhanced by 2,3-butanedione monoxime compared with cytochalasin d. *American Journal of Physiology. Heart and Circulatory Physiology*. 2004;286:H310-318
417. Jalife J, Morley GE, Tallini NY, Vaidya D. A fungal metabolite that eliminates motion artifacts. *J Cardiovasc Electrophysiol*. 1998;9:1358-1362
418. Undrovinas AI, Shander GS, Makielski JC. Cytoskeleton modulates gating of voltage-dependent sodium channel in heart. *The American Journal of Physiology*. 1995;269:H203-214
419. Mazzanti M, Assandri R, Ferroni A, DiFrancesco D. Cytoskeletal control of rectification and expression of four substates in cardiac inward rectifier k+ channels. *Faseb J*. 1996;10:357-361
420. Straight AF, Cheung A, Limouze J, Chen I, Westwood NJ, Sellers JR, Mitchison TJ. Dissecting temporal and spatial control of cytokinesis with a myosin ii inhibitor. *Science*. 2003;299:1743-1747
421. Fedorov VV, Lozinsky IT, Sosunov EA, Anyukhovsky EP, Rosen MR, Balke CW, Efimov IR. Application of blebbistatin as an excitation-contraction uncoupler for electrophysiologic study of rat and rabbit hearts. *Heart Rhythm*. 2007;4:619-626
422. Brack KE, Narang R, Winter J, Ng GA. The mechanical uncoupler blebbistatin is associated with significant electrophysiological effects in the isolated rabbit heart. *Experimental Physiology*. 2013;98:1009-1027
423. Hwang SM, Yea KH, Lee KJ. Regular and alternant spiral waves of contractile motion on rat ventricle cell cultures. *Phys Rev Lett*. 2004;92:198103
424. Pinder AG, Rogers SC, Khalatbari A, Ingram TE, James PE. The measurement of nitric oxide and its metabolites in biological samples by ozone-based chemiluminescence. *Methods Mol Biol*. 2008;476:11-28
425. Sauer B, Henderson N. Site-specific DNA recombination in mammalian cells by the cre recombinase of bacteriophage p1. *Proceedings of the National Academy of Sciences of the United States of America*. 1988;85:5166-5170
426. Orban PC, Chui D, Marth JD. Tissue- and site-specific DNA recombination in transgenic mice. *Proceedings of the National Academy of Sciences of the United States of America*. 1992;89:6861-6865
427. Lindeberg J, Usoskin D, Bengtsson H, Gustafsson A, Kylberg A, Soderstrom S, Ebendal T. Transgenic expression of cre recombinase from the tyrosine hydroxylase locus. *Genesis*. 2004;40:67-73

428. Lindeberg J, Ebendal T. Use of an internal ribosome entry site for bicistronic expression of cre recombinase or rtta transactivator. *Nucleic Acids Res*. 1999;27:1552-1554
429. McNeill E, Crabtree MJ, Sahgal N, Patel J, Chuaiphichai S, Iqbal AJ, Hale AB, Greaves DR, Channon KM. Regulation of inos function and cellular redox state by macrophage gch1 reveals specific requirements for tetrahydrobiopterin in nrf2 activation. *Free Radic Biol Med*. 2015;79:206-216
430. Williams RL, Risau W, Zerwes HG, Drexler H, Aguzzi A, Wagner EF. Endothelioma cells expressing the polyoma middle t oncogene induce hemangiomas by host cell recruitment. *Cell*. 1989;57:1053-1063
431. Howells DW, Smith I, Hyland K. Estimation of tetrahydrobiopterin and other pterins in cerebrospinal fluid using reversed-phase high-performance liquid chromatography with electrochemical and fluorescence detection. *J Chromatogr*. 1986;381:285-294
432. Heales S, Hyland K. Determination of quinonoid dihydrobiopterin by high-performance liquid chromatography and electrochemical detection. *J Chromatogr*. 1989;494:77-85
433. Ryan BJ, Lourenco-Venda LL, Crabtree MJ, Hale AB, Channon KM, Wade-Martins R. Alpha-synuclein and mitochondrial bioenergetics regulate tetrahydrobiopterin levels in a human dopaminergic model of parkinson disease. *Free Radic Biol Med*. 2014;67:58-68
434. Fisher SP, Godinho SI, Pothecary CA, Hankins MW, Foster RG, Peirson SN. Rapid assessment of sleep-wake behavior in mice. *J Biol Rhythms*. 2012;27:48-58
435. Martins JB, Zipes DP. Epicardial phenol interrupts refractory period responses to sympathetic but not vagal stimulation in canine left ventricular epicardium and endocardium. *Circulation Research*. 1980;47:33-40
436. Ito M, Zipes DP. Efferent sympathetic and vagal innervation of the canine right ventricle. *Circulation*. 1994;90:1459-1468
437. Brack KE, Coote JH, Ng GA. Vagus nerve stimulation inhibits the increase in ca2+ transient and left ventricular force caused by sympathetic nerve stimulation but has no direct effects alone--epicardial ca2+ fluorescence studies using fura-2 am in the isolated innervated beating rabbit heart. *Exp Physiol*. 2010;95:80-92
438. Efimov IR, Nikolski VP, Salama G. Optical imaging of the heart. *Circulation Research*. 2004;95:21-33
439. Choi BR, Salama G. Simultaneous maps of optical action potentials and calcium transients in guinea-pig hearts: Mechanisms underlying concordant alternans. *The Journal of Physiology*. 2000;529 Pt 1:171-188
440. Beker F, Weber M, Fink RH, Adams DJ. Muscarinic and nicotinic ach receptor activation differentially mobilize ca2+ in rat intracardiac ganglion neurons. *J Neurophysiol*. 2003;90:1956-1964
441. Musialek P, Lei M, Brown HF, Paterson DJ, Casadei B. Nitric oxide can increase heart rate by stimulating the hyperpolarization-activated inward current, i(f). *Circulation Research*. 1997;81:60-68
442. Wang L, Li D, Dawson TA, Paterson DJ. Long-term effect of neuronal nitric oxide synthase over-expression on cardiac neurotransmission mediated by a lentiviral vector. *The Journal of Physiology*. 2009;587:3629-3637
443. Balligand JL, Kobzik L, Han X, Kaye DM, Belhassen L, O'Hara DS, Kelly RA, Smith TW, Michel T. Nitric oxide-dependent parasympathetic signaling

is due to activation of constitutive endothelial (type iii) nitric oxide synthase in cardiac myocytes. *The Journal of Biological Chemistry*. 1995;270:14582-14586
444. Sears CE, Ashley EA, Casadei B. Nitric oxide control of cardiac function: Is neuronal nitric oxide synthase a key component? *Philos Trans R Soc Lond B Biol Sci*. 2004;359:1021-1044
445. Berthoud HR, Neuhuber WL. Functional and chemical anatomy of the afferent vagal system. *Auton Neurosci*. 2000;85:1-17
446. Xu KY, Huso DL, Dawson TM, Bredt DS, Becker LC. Nitric oxide synthase in cardiac sarcoplasmic reticulum. *Proceedings of the National Academy of Sciences of the United States of America*. 1999;96:657-662
447. Eglen RM, Michel AD, Cornett CM, Kunysz EA, Whiting RL. The interaction of hexamethonium with muscarinic receptor subtypes in vitro. *Br J Pharmacol*. 1989;98:499-506
448. Shinlapawittayatorn K, Chinda K, Palee S, Surinkaew S, Kumfu S, Kumphune S, Chattipakorn S, KenKnight BH, Chattipakorn N. Vagus nerve stimulation initiated late during ischemia, but not reperfusion, exerts cardioprotection via amelioration of cardiac mitochondrial dysfunction. *Heart Rhythm*. 2014;11:2278-2287
449. Shorofsky SR, January CT. L- and t-type ca2+ channels in canine cardiac purkinje cells. Single-channel demonstration of l-type ca2+ window current. *Circulation Research*. 1992;70:456-464
450. Zeng J, Rudy Y. Early afterdepolarizations in cardiac myocytes: Mechanism and rate dependence. *Biophys J*. 1995;68:949-964
451. Wickenden AD, Kaprielian R, Kassiri Z, Tsoporis JN, Tsushima R, Fishman GI, Backx PH. The role of action potential prolongation and altered intracellular calcium handling in the pathogenesis of heart failure. *Cardiovascular Research.* 1998;37:312-323
452. Maltsev VA, Sabbah HN, Higgins RS, Silverman N, Lesch M, Undrovinas AI. Novel, ultraslow inactivating sodium current in human ventricular cardiomyocytes. *Circulation*. 1998;98:2545-2552
453. Pogwizd SM, Schlotthauer K, Li L, Yuan W, Bers DM. Arrhythmogenesis and contractile dysfunction in heart failure: Roles of sodium-calcium exchange, inward rectifier potassium current, and residual beta-adrenergic responsiveness. *Circulation Research*. 2001;88:1159-1167
454. Pogwizd SM, McKenzie JP, Cain ME. Mechanisms underlying spontaneous and induced ventricular arrhythmias in patients with idiopathic dilated cardiomyopathy. *Circulation*. 1998;98:2404-2414
455. Akar FG, Spragg DD, Tunin RS, Kass DA, Tomaselli GF. Mechanisms underlying conduction slowing and arrhythmogenesis in nonischemic dilated cardiomyopathy. *Circulation Research*. 2004;95:717-725
456. Kostin S, Dammer S, Hein S, Klovekorn WP, Bauer EP, Schaper J. Connexin 43 expression and distribution in compensated and decompensated cardiac hypertrophy in patients with aortic stenosis. *Cardiovascular Research.* 2004;62:426-436
457. Akar FG, Rosenbaum DS. Transmural electrophysiological heterogeneities underlying arrhythmogenesis in heart failure. *Circulation Research*. 2003;93:638-645
458. Yan GX, Rials SJ, Wu Y, Liu T, Xu X, Marinchak RA, Kowey PR. Ventricular hypertrophy amplifies transmural repolarization dispersion and

induces early afterdepolarization. *American Journal of Physiology. Heart and Circulatory Physiology*. 2001;281:H1968-1975
459. Levy MN. Sympathetic-parasympathetic interactions in the heart. *Circulation Research*. 1971;29:437-445
460. Sunahara RK, Dessauer CW, Gilman AG. Complexity and diversity of mammalian adenylyl cyclases. *Annu Rev Pharmacol Toxicol*. 1996;36:461-480
461. Smit MJ, Iyengar R. Mammalian adenylyl cyclases. *Adv Second Messenger Phosphoprotein Res*. 1998;32:1-21
462. Han X, Kobzik L, Balligand JL, Kelly RA, Smith TW. Nitric oxide synthase (nos3)-mediated cholinergic modulation of ca2+ current in adult rabbit atrioventricular nodal cells. *Circulation Research*. 1996;78:998-1008
463. Ardell JL, Rajendran PS, Nier HA, KenKnight BH, Armour JA. Central-peripheral neural network interactions evoked by vagus nerve stimulation: Functional consequences on control of cardiac function. *American Journal of Physiology. Heart and Circulatory Physiology*. 2015;309:H1740-1752
464. Shen MJ, Zipes DP. Role of the autonomic nervous system in modulating cardiac arrhythmias. *Circulation Research*. 2014;114:1004-1021
465. Schwartz PJ, De Ferrari GM, Sanzo A, Landolina M, Rordorf R, Raineri C, Campana C, Revera M, Ajmone-Marsan N, Tavazzi L, Odero A. Long term vagal stimulation in patients with advanced heart failure: First experience in man. *Eur J Heart Fail*. 2008;10:884-891
466. Lubbe WF, Podzuweit T, Opie LH. Potential arrhythmogenic role of cyclic adenosine monophosphate (amp) and cytosolic calcium overload: Implications for prophylactic effects of beta-blockers in myocardial infarction and proarrhythmic effects of phosphodiesterase inhibitors. *J Am Coll Cardiol*. 1992;19:1622-1633
467. Opie LH, Clusin WT. Cellular mechanism for ischemic ventricular arrhythmias. *Annu Rev Med*. 1990;41:231-238
468. Zipes DP, Barber MJ, Takahashi N, Gilmour RF, Jr. Influence of the autonomic nervous system on the genesis of cardiac arrhythmias. *Pacing Clin Electrophysiol*. 1983;6:1210-1220
469. Vaseghi M, Shivkumar K. The role of the autonomic nervous system in sudden cardiac death. *Progress in cardiovascular diseases*. 2008;50:404-419
470. van der Werf C, Zwinderman AH, Wilde AA. Therapeutic approach for patients with catecholaminergic polymorphic ventricular tachycardia: State of the art and future developments. *Europace*. 2012;14:175-183
471. Schwartz PJ, Spazzolini C, Priori SG, Crotti L, Vicentini A, Landolina M, Gasparini M, Wilde AA, Knops RE, Denjoy I, Toivonen L, Monnig G, Al-Fayyadh M, Jordaens L, Borggrefe M, Holmgren C, Brugada P, De Roy L, Hohnloser SH, Brink PA. Who are the long-qt syndrome patients who receive an implantable cardioverter-defibrillator and what happens to them?: Data from the european long-qt syndrome implantable cardioverter-defibrillator (lqts icd) registry. *Circulation*. 2010;122:1272-1282
472. Pedersen CT, Kay GN, Kalman J, Borggrefe M, Della-Bella P, Dickfeld T, Dorian P, Huikuri H, Kim YH, Knight B, Marchlinski F, Ross D, Sacher F, Sapp J, Shivkumar K, Soejima K, Tada H, Alexander ME, Triedman JK, Yamada T, Kirchhof P, Lip GY, Kuck KH, Mont L, Haines D, Indik J, Dimarco J, Exner D, Iesaka Y, Savelieva I. Ehra/hrs/aphrs expert consensus on ventricular arrhythmias. *Heart Rhythm*. 2014;11:e166-196

473. Tung R, Vaseghi M, Frankel DS, Vergara P, Di Biase L, Nagashima K, Yu R, Vangala S, Tseng CH, Choi EK, Khurshid S, Patel M, Mathuria N, Nakahara S, Tzou WS, Sauer WH, Vakil K, Tedrow U, Burkhardt JD, Tholakanahalli VN, Saliaris A, Dickfeld T, Weiss JP, Bunch TJ, Reddy M, Kanmanthareddy A, Callans DJ, Lakkireddy D, Natale A, Marchlinski F, Stevenson WG, Della Bella P, Shivkumar K. Freedom from recurrent ventricular tachycardia after catheter ablation is associated with improved survival in patients with structural heart disease: An international vt ablation center collaborative group study. *Heart Rhythm*. 2015;12:1997-2007
474. Ajijola OA, Lellouche N, Bourke T, Tung R, Ahn S, Mahajan A, Shivkumar K. Bilateral cardiac sympathetic denervation for the management of electrical storm. *Journal of the American College of Cardiology*. 2012;59:91-92
475. Bourke T, Vaseghi M, Michowitz Y, Sankhla V, Shah M, Swapna N, Boyle NG, Mahajan A, Narasimhan C, Lokhandwala Y, Shivkumar K. Neuraxial modulation for refractory ventricular arrhythmias: Value of thoracic epidural anesthesia and surgical left cardiac sympathetic denervation. *Circulation*. 2010;121:2255-2262
476. Mahajan A, Moore J, Cesario DA, Shivkumar K. Use of thoracic epidural anesthesia for management of electrical storm: A case report. *Heart Rhythm*. 2005;2:1359-1362
477. Vaseghi M, Gima J, Kanaan C, Ajijola OA, Marmureanu A, Mahajan A, Shivkumar K. Cardiac sympathetic denervation in patients with refractory ventricular arrhythmias or electrical storm: Intermediate and long-term follow-up. *Heart Rhythm*. 2014;11:360-366
478. Moss AJ, McDonald J. Unilateral cervicothoracic sympathetic ganglionectomy for the treatment of long qt interval syndrome. *The New England Journal of Medicine*1971;285:903-904
479. Schwartz PJ, Locati EH, Moss AJ, Crampton RS, Trazzi R, Ruberti U. Left cardiac sympathetic denervation in the therapy of congenital long qt syndrome. A worldwide report. *Circulation*. 1991;84:503-511
480. Collura CA, Johnson JN, Moir C, Ackerman MJ. Left cardiac sympathetic denervation for the treatment of long qt syndrome and catecholaminergic polymorphic ventricular tachycardia using video-assisted thoracic surgery. *Heart Rhythm*. 2009;6:752-759
481. Olde Nordkamp LR, Driessen AH, Odero A, Blom NA, Koolbergen DR, Schwartz PJ, Wilde AA. Left cardiac sympathetic denervation in the netherlands for the treatment of inherited arrhythmia syndromes. *Neth Heart J*. 2014;22:160-166
482. Remo BF, Preminger M, Bradfield J, Mittal S, Boyle N, Gupta A, Shivkumar K, Steinberg JS, Dickfeld T. Safety and efficacy of renal denervation as a novel treatment of ventricular tachycardia storm in patients with cardiomyopathy. *Heart Rhythm*. 2014;11:541-546
483. Cotton RG. A model for hyperphenylalaninaemia due to tetrahydrobiopterin deficiency. *J Inherit Metab Dis*. 1986;9:4-14
484. Savitt JM, Jang SS, Mu W, Dawson VL, Dawson TM. Bcl-x is required for proper development of the mouse substantia nigra. *J Neurosci*. 2005;25:6721-6728
485. Daher JP, Ying M, Banerjee R, McDonald RS, Hahn MD, Yang L, Flint Beal M, Thomas B, Dawson VL, Dawson TM, Moore DJ. Conditional transgenic mice expressing c-terminally truncated human alpha-synuclein (alphasyn119)

exhibit reduced striatal dopamine without loss of nigrostriatal pathway dopaminergic neurons. *Mol Neurodegener*. 2009;4:34
486. Zhou QY, Quaife CJ, Palmiter RD. Targeted disruption of the tyrosine hydroxylase gene reveals that catecholamines are required for mouse fetal development. *Nature*. 1995;374:640-643
487. Thomas SA, Matsumoto AM, Palmiter RD. Noradrenaline is essential for mouse fetal development. *Nature*. 1995;374:643-646
488. Palmiter RD. Dopamine signaling in the dorsal striatum is essential for motivated behaviors: Lessons from dopamine-deficient mice. *Ann N Y Acad Sci*. 2008;1129:35-46
489. Mencacci NE, Isaias IU, Reich MM, Ganos C, Plagnol V, Polke JM, Bras J, Hersheson J, Stamelou M, Pittman AM, Noyce AJ, Mok KY, Opladen T, Kunstmann E, Hodecker S, Munchau A, Volkmann J, Samnick S, Sidle K, Nanji T, Sweeney MG, Houlden H, Batla A, Zecchinelli AL, Pezzoli G, Marotta G, Lees A, Alegria P, Krack P, Cormier-Dequaire F, Lesage S, Brice A, Heutink P, Gasser T, Lubbe SJ, Morris HR, Taba P, Koks S, Majounie E, Raphael Gibbs J, Singleton A, Hardy J, Klebe S, Bhatia KP, Wood NW. Parkinson's disease in gtp cyclohydrolase 1 mutation carriers. *Brain*. 2014;137:2480-2492
490. Jain S. Multi-organ autonomic dysfunction in parkinson disease. *Parkinsonism Relat Disord*. 2011;17:77-83
491. Nalls MA, Pankratz N, Lill CM, Do CB, Hernandez DG, Saad M, DeStefano AL, Kara E, Bras J, Sharma M, Schulte C, Keller MF, Arepalli S, Letson C, Edsall C, Stefansson H, Liu X, Pliner H, Lee JH, Cheng R, Ikram MA, Ioannidis JP, Hadjigeorgiou GM, Bis JC, Martinez M, Perlmutter JS, Goate A, Marder K, Fiske B, Sutherland M, Xiromerisiou G, Myers RH, Clark LN, Stefansson K, Hardy JA, Heutink P, Chen H, Wood NW, Houlden H, Payami H, Brice A, Scott WK, Gasser T, Bertram L, Eriksson N, Foroud T, Singleton AB. Large-scale meta-analysis of genome-wide association data identifies six new risk loci for parkinson's disease. *Nat Genet*. 2014;46:989-993
492. Nagatsu T, Yamaguchi T, Kato T, Sugimoto T, Matsuura S, Akino M, Nagatsu I, Iizuka R, Narabayashi H. Biopterin in human brain and urine from controls and parkinsonian patients: Application of a new radioimmunoassay. *Clin Chim Acta*. 1981;109:305-311
493. Dissing IC, Guttler F, Pakkenberg H, Lou H, Gerdes AM, Lykkelund C, Rasmussen V. Tetrahydrobiopterin and parkinson's disease. *Acta Neurol Scand*. 1989;79:493-499
494. Schwartz PJ. Cardiac sympathetic denervation to prevent life-threatening arrhythmias. *Nat Rev Cardiol*. 2014;11:346-353
495. Mastitskaya S, Marina N, Gourine A, Gilbey MP, Spyer KM, Teschemacher AG, Kasparov S, Trapp S, Ackland GL, Gourine AV. Cardioprotection evoked by remote ischaemic preconditioning is critically dependent on the activity of vagal pre-ganglionic neurones. *Cardiovascular Research.* 2012;95:487-494
496. Ashton JL, Paton JF, Trew ML, LeGrice IJ, Smaill BH. A working heart-brainstem preparation of the rat for the study of reflex mediated autonomic influences on atrial arrhythmia development. *Conf Proc IEEE Eng Med Biol Soc*. 2013;2013:3785-3788
497. Post W, Shen H, Damcott C, Arking DE, Kao WH, Sack PA, Ryan KA, Chakravarti A, Mitchell BD, Shuldiner AR. Associations between genetic

variants in the nos1ap (capon) gene and cardiac repolarization in the old order amish. *Hum Hered*. 2007;64:214-219
498. Aarnoudse AJ, Newton-Cheh C, de Bakker PI, Straus SM, Kors JA, Hofman A, Uitterlinden AG, Witteman JC, Stricker BH. Common nos1ap variants are associated with a prolonged qtc interval in the rotterdam study. *Circulation*. 2007;116:10-16
499. Jaffrey SR, Snowman AM, Eliasson MJ, Cohen NA, Snyder SH. Capon: A protein associated with neuronal nitric oxide synthase that regulates its interactions with psd95. *Neuron*. 1998;20:115-124
500. Chang KC, Barth AS, Sasano T, Kizana E, Kashiwakura Y, Zhang Y, Foster DB, Marban E. Capon modulates cardiac repolarization via neuronal nitric oxide synthase signaling in the heart. *Proceedings of the National Academy of Sciences of the United States of America*. 2008;105:4477-4482
501. Cui Z, Lv Q, Yan M, Cheng C, Guo Z, Yang J, Chen M, Xia Y, Zhang L, Shen A. Elevated expression of capon and neuronal nitric oxide synthase in the sciatic nerve of rats following constriction injury. *Vet J*. 2011;187:374-380
502. Shen A, Chen M, Niu S, Sun L, Gao S, Shi S, Li X, Lv Q, Guo Z, Cheng C. Changes in mrna for capon and dexras1 in adult rat following sciatic nerve transection. *J Chem Neuroanat*. 2008;35:85-93
503. Lu CJ, Hao G, Nikiforova N, Larsen HE, Liu K, Crabtree MJ, Li D, Herring N, Paterson DJ. Capon modulates neuronal calcium handling and cardiac sympathetic neurotransmission during dysautonomia in hypertension. *Hypertension*. 2015;65:1288-1297
504. Treuer AV, Gonzalez DR. Nos1ap modulates intracellular ca(2+) in cardiac myocytes and is up-regulated in dystrophic cardiomyopathy. *Int J Physiol Pathophysiol Pharmacol*. 2014;6:37-46
505. Kapoor A, Sekar RB, Hansen NF, Fox-Talbot K, Morley M, Pihur V, Chatterjee S, Brandimarto J, Moravec CS, Pulit SL, Pfeufer A, Mullikin J, Ross M, Green ED, Bentley D, Newton-Cheh C, Boerwinkle E, Tomaselli GF, Cappola TP, Arking DE, Halushka MK, Chakravarti A. An enhancer polymorphism at the cardiomyocyte intercalated disc protein nos1ap locus is a major regulator of the qt interval. *American journal of human genetics*. 2014;94:854-869
506. Schwartz PJ. Vagal stimulation for the treatment of heart failure: A translational success story. *Heart*. 2012;98:1687-1689
507. Hayward C, Banner NR, Morley-Smith A, Lyon AR, Harding SE. The current and future landscape of serca gene therapy for heart failure: A clinical perspective. *Hum Gene Ther*. 2015;26:293-304
508. Ullman B, Franco-Cereceda A, Hulting J, Lundberg JM, Sollevi A. Elevation of plasma neuropeptide y-like immunoreactivity and noradrenaline during myocardial ischaemia in man. *J Intern Med*. 1990;228:583-589
509. Awad SJ, Einstein R, Potter EK, Richardson DP. The effects of neuropeptide y on myocardial contractility and coronary blood flow. *Br J Pharmacol*. 1991;104:195-201
510. Taggart P, Sutton P, Chalabi Z, Boyett MR, Simon R, Elliott D, Gill JS. Effect of adrenergic stimulation on action potential duration restitution in humans. *Circulation*. 2003;107:285-289
511. Yue AM, Betts TR, Roberts PR, Morgan JM. Global dynamic coupling of activation and repolarization in the human ventricle. *Circulation*. 2005;112:2592-2601

512. Cunnington C, Channon KM. Tetrahydrobiopterin: Pleiotropic roles in cardiovascular pathophysiology. *Heart*. 2010;96:1872-1877